UC San Diego

UC San Diego Electronic Theses and Dissertations

Title

Climate change in the Pacific North America region over the past millennium : development and application of novel geochemical tracers

Permalink

https://escholarship.org/uc/item/04t4q36f

Author

Roach, Lydia Darcy

Publication Date

2010

Peer reviewed|Thesis/dissertation

eScholarship.org Powered by the California Digital Library
University of California

UNIVERSITY OF CALIFORNIA, SAN DIEGO

Climate Change in the Pacific North America Region Over the Past Millenium: Development and Application of Novel Geochemical Tracers

A dissertation submitted in partial satisfaction of the requirements for the degree of

Doctor of Philosophy

in

Oceanography

by

Lydia Darcy Roach

Committee in charge:

Christopher D. Charles, Chair
Daniel R. Cayan, Co-Chair
Ellen R. M. Druffel
Alex L. Sessions
Jeffrey P. Severinghaus
Nolan R. Wallach

2010

Copyright

Lydia Darcy Roach, 2010

All rights reserved.

The Dissertation of Lydia Darcy Roach is approved, and it is acceptable in quality and form for publication on microfilm and electronically:

_____

_____

_____

_____

_____
Co-Chair

_____
Chair

University of California, San Diego

2010

EPIGRAPH

What are men to rocks and mountains?

Jane Austen

TABLE OF CONTENTS

Signature Page ……..iii

Epigraph ……iv

Table of Contents ……..……...v

List of Abbreviations ……viii

List of Tables ……... ix

List of Figures ……...x

Acknowledgements ……xiv

Vita ……xvii

Abstract of the Dissertation ……xviii

Preface ……...1
References ……...10

Chapter 1. Radiocarbon as a tracer for decadal scale sub-thermocline variability along the southern California margin…… 18

Abstract ……... 18
1.1 Introduction ……19
1.2 Oceanographic setting ……21
1.3 Methods ……...23
1.3.1 Core collections and sub-sampling ……...23
1.3.2 Stable isotope measurement …… 24
1.3.3 Benthic foraminiferal species assemblages …….. 24
1.3.4 Calcite $\Delta^{14}C$ measurement ……... 25
1.3.5 Seawater collection and $\Delta^{14}C$ measurement …… 26
1.4 Results ……26
1.4.1 Benthic foraminiferal stable isotopes ……26
1.4.2 Seawater $\Delta^{14}C$ ……28
1.4.3 Benthic foraminiferal $\Delta^{14}C$ ……28
1.4.4 Species-specific $\Delta^{14}C$ …… 29
1.4.5 Consideration of diagenetic processes …… 30
1.4.6 Consideration of hydrographic processes ……33
1.5 Discussion ……... 36

1.6 Conclusions ……42
1.7 References ……..59

Chapter 2. Benthic foraminiferal community distribution in the bathyal Santa Barbara Basin ……66

Abstract ……..…….. 66
2.1 Introduction ……..…… 67
2.2 Study area ……..……...68
2.3 Background ……..……70
2.4 Methods ……..……..71
2.5 Results ……..…… 76
2.6 Discussion ……..…….. 80
2.7 Conclusions ……..……... .88
2.8 References ……..…….. 97

Chapter 3. High-resolution measurements of sedimentary leaf wax lipid hydrogen isotope ratios capture interannual to decadal scale variability in wintertime precipitation and snowmelt in the Sierra Nevada Mountains……...103

Abstract …… 103
3.1 Introduction ……..…….. 105
3.2 Background ……... 107
3.2.1 δD of environmental water in the Sierra Nevada Mountains ……. 107
3.2.2 Plant lipid δD ……..110
3.3 Study location ……... 113
3.3.1 Regional climatology …… 113
3.3.2 Annual lake level cycle ……..…… 115
3.3.3 Swamp Lake plant species diversity …….. 117
3.4 Methods …… 118
3.4.1 Sample collection and processes …… 118
3.4.2 Core logging and imaging ……..…… 119
3.4.3 Water sample δD analysis …….. 120
3.4.4 Sediment and plant sample preparation and lipid identification ….120
3.4.5 δD analysis of plant and sediment samples …… 122
3.5 Determination of Chronology ……... 123
3.6 Results ……... 123
3.6.1 Sediment and plant *n*-acid distributions …… 123
3.6.2 Storm event, lake water and plant δD …… 125
3.6.3 Sediment *n*-acid δD ……..…….. 127
3.6.4 Comparison of modern δD to instrumental records ……128

3.7 Discussion 136
3.8 Conclusions 143
3.9 References 167

Chapter 4. Hydroclimate of the Sierra Nevada Mountains during the late medieval period (1160-1432 A.D.) as captured by sedimentary leaf wax lipid hydrogen isotope ratios 174

Abstract 174
4.1 Introduction 176
4.2 Study Site 179
4.3 Methods 180
4.4 Determination of Chronology..... 181
4.5 Results 183
4.6 Discussion 188
4.7 Conclusions 193
4.8 References 201

Appendix A. Benthic Foraminiferal Faunal Reference List 206

Appendix B. Swamp Lake Core Descriptions and Metadata 207

Appendix C. The Varve Selection Program: A Computerized Technique for Identifying Sub-millimeter Varves in Digital Images of Swamp Lake Freeze Cores 217

Appendix D. Supplementary Text and Figures 230

LIST OF ABBREVIATIONS

CalCOFI	California Cooperative Fisheries Investigation
C_{ox}	Carbon Oxidation Rate
DIC	Dissolved Inorganic Carbon
ENSO	El Nino Southern Oscillation
NPGO	North Pacific Gyre Oscillation
NPIW	North Pacific Intermediate Water
PDO	Pacific Decadal Oscillation
PDSI	Palmer Drought Severity Index
PNA	Pacific North America
SBB	Santa Barbara Basin
SBBC	Santa Barbara Basin Box Core
SCB	Southern California Bight
SCM	Southern California Margin
SSHa	Sea Surface Height Anomalies
SST/SSTa	Sea Surface Temperature/Sea Surface Temperature Anomalies
SWE	Snow Water Equivalence
WOCE:	World Ocean Circulation Experiment

LIST OF TABLES

Table 1.1 SBB Benthic Foraminifera Species Specific $\delta^{13}C$ Averages ……45

Table 1.2 Water sample $\Delta^{14}C$ from center Santa Barbara Basin and western sill …….. 46

Table 1.3 $\Delta\Delta^{14}C$ Corresponding to three strongest SBB flushing events …….. 47
since 1986

Table 2.1 Coefficients of correlation between annual flux of individual benthic foraminiferal species and total annual benthic foraminiferal flux with annually averaged values of the PDO (Mantua *et al*., 1997; Zhang *et al*., 1997) and NPGO (Di Lorenzo *et al*., 2008) climate indices ……90

Table 3.1 List of plant species collected at Swamp Lake ……147

Table 3.2 δD of Plant collected at Swamp Lake, July 2009 and snow samples collected at Hodgdon Meadow, winter 2010 ……... 148

Table 3.3 Correlation coefficients of C24 δD with instrumental records at 0 to -3 years lag. Instrumental records smoothed with a 2-year running average ……149

Table 3.4 Correlation coefficients between instrumental records …… 150

Table 4.1 Correlation of annually interpolated C24 δD with reconstructed PDSI records from the five most proximal grid squares in the NADA (Cook & Krusic 2004; NOAA National Climatic Data Center, 2008a) to the location of ……196
Swamp Lake

Table B1 Locations and information of Swamp Lake sediment Freeze and Bolivia cores ……..209

LIST OF FIGURES

Figure 1.1 Profile of $\Delta^{14}C$ versus potential density for three WOCE stations near the Santa Barbara Basin and specific depths in the SBB and at the western sill measured in this study 48

Figure 1.2 North Pacific distribution of $\Delta^{14}C$ on the σ_Θ = 26.88 kgm-3 (a) and σ_Θ=26.95 kgm^{-3} (b) isopycnal surfaces measured at WOCE stations 49

Figure 1.3 Map of the Santa Barbara Basin depicting sampling locations as well as CalCOFI stations and WOCE stations discussed in this study 50

Figure 1.4 Potential density measurements from CalCOFI surveys at station 82 47 (central SBB) 1986-2005. Time evolution of the potential density profile (a) and bottom water potential density (b). 51

Figure 1.5 $\delta^{18}O$ (a) and $\delta^{13}C$ (b) from the Santa Barbara Basin spanning 1744-2001 measured from the tests of benthic foraminifera *Cassidulinoides cornuta*. 52

Figure 1.6 (a) Records of Santa Barbara Basin benthic foraminiferal $\Delta^{14}C$ measured from two box cores spanning 1827-2006. 53

Figure 1.7 Results of modeling exercises investigating the influence of remineralization on pore water $\Delta^{14}C$ in the top 3.1 cm of the central SBB sediments 54

Figure 1.8 (a) Modeled evolution of upper SBB pore water $\Delta^{14}C$ 1940-2001, (b) Raw and bomb-corrected benthic $\Delta^{14}C$ records between 1940 and 2001. 55

Figure 1.9 Comparison of bomb-corrected $\Delta^{14}C$ (black line) with April-July averaged SSTa from the 32.5ºN 112.5ºW grid square of the Kaplan OS SSTa record (bars) 56

Figure 1.10 (a) The first difference ($\Delta\Delta^{14}C$) of SBB benthic Δ14C record 1857-2001, (b) Composite of April–July monthly SSTas for years corresponding the lowest 25% of $\Delta\Delta^{14}C$ values, (c) same as (b) but for years corresponding to the highest 25% $\Delta\Delta^{14}C$ values. 58

Figure 2.1 (Modified from Bernhard *et al*. (1997), Figure 3) Percent abundance of benthic foraminiferal species at 9 stations across a depth and $[O_2]$ gradient in the SBB. 91

Figure 2.2 (Modified and updated version of Bograd *et al*. (2002), Figure 3) Time series of bottom-most physical and chemical measurements from the Santa Barbara Basin at CalCOFI station 82 47 (central SBB) ……92

Figure 2.3 Flux of benthic foraminiferal species from SBBC 0110-3001 and SBBC 080621-02 ……93

Figure 2.4 Comparison of annually averaged monthly values of NPGO (a) and PDO (b) with total benthic foraminiferal flux from SBBC 0110-3001 (c) ……94

Figure 2.5 Overlapping benthic foraminiferal relative abundances from SBBC 0110-3001 (dark lines) and SBBC 080621-02 (light lines) between 1975 and 2001 … 95

Figure 2.6 Relative abundances of *N. stella* (purple), *S. eckisi* (blue), *C. cornuta* (yellow) and *L. pseudobeyrichi* (red). ……96

Figure 3.1 Map showing location of the Swamp Lake basin (a), bathymetric map of Swamp Lake indicating locations of Bolivia cores and Freeze cores collected in October 2006 and September 2007. Bathymetric map modified from Smith & Anderson (1992). ……151

Figure 3.2 Daily meteorological and stream flow variability from stations and gauges near Swamp Lake for water years 2006-2009, Swamp Lake surface water temperature for water years 2006-2008 and lake level for water year 2006-2007 ……152

Figure 3.3 Temperature (blue), dissolved oxygen (pink) and specific conductance (red) profiles from the center of Swamp Lake, measured July 2009 ……..153

Figure 3.4 Age-depth model for SL0601T (a) and digital image of SL0601T (b) …...154

Figure 3.5 *n*-acid distribution from 15 plant species collected from in and around Swamp Lake July 2009. (S), (F), (E) and (T) refer to plant groups submerged, floating, emergent and terrestrial respectively. X-axis labels refer to carbon number. …155

Figure 3.6 Average *n*-acid distribution for floating/submergent (blue), emergent (green) and terrestrial (orange) plants from the 15 individual species. Error bars represent 1σ. X-axis labels refer to carbon number ……...156

Figure 3.7 Average *n*-acid distribution from SL0601T sediment samples. Error bars represent 1σ. Axis labels as in figures 3.5 and 3.6 ……157

Figure 3.8 Lake water δD profile from the center of Swamp Lake, July 2009. Error bars represent 1σ of 3 replicate measurements ……..158

Figure 3.9 SL0601T *n*-acid δD for C22 (yellow), C24 (solid black), C26 (green) and C28 (cyan). Dashed black line is C24 δD from SL0606T ……159

Figure 3.10 Comparison of C24 δD with instrumental records of regional hydrology and tropical Pacific SSTa ……..160

Figure 3.11 20-year low pass filtered C24 δD (black), BHV April 1st SWE (pink), gs59 PDSI (ref) and PDO (blue) (Mantua *et al*., 1997) ……..161

Figure 3.12 Correlation of C24 δD with April 1st SWE for CDEC and SNOTEL stations in the Sierra Nevada and throughout the West ……...162

Figure 3.13 Correlation of C24 δD with gridded instrumental PDSI from the NADA 1901-2003. PDSI records have been smoothed with a two-year running mean. Large symbols indicate significance at the 95% confidence interval ……163

Figure 3.14 Gridded composites of instrumental NADA PDSI for the high δD subset (δD < 3rd quartile) (a) and low δD subset (δD < 1st quartile) (b) ……...164

Figure 3.15 Difference in spring pulse timing in days for the low δD subset minus the high δD subset …… 165

Figure 3.16 Composited NCEP Reanalysis I 700mb height anomalies from the high δD (a) and low δD (b) subsets. Figures generated using the Earth System Research Laboratory Monthly/Seasonal Climate Composites page (http:www.esrl.noaa.gov/psd/cgi-gin/data/composites/printpage.pl) ……166

Figure 4.1 Age model for freeze core SL0708 …… 197

Figure 4.2 Measured δD for *n*-acids C22 (yellow), C24 (black), C26 (green) and C28 (blue) …….. 198

Figure 4.3 Comparison of late medieval δD record with reconstructed PDSI (Cook *et al*., 2004; Cook & Krusic, 2004), the DAI (Cook *et al*., 2004) and reconstructed PDO (MacDonald & Case, 2005) ……199

Figure 4.4 Comparison of late medieval and modern leaf wax lipid δD and with concomitant hydrologic proxy reconstructions from previous studies ……..200

Figure B1 Lithological core descriptions of freeze cores SL0601T T and B), SL0604 (T and B), SL0606 (T and B), SL0605 and SL0708 (T and B) …… 211

Figure B2 Digital images and initial core descriptions of Bolivia cores SL0701 (a), SL0702 (b), SL0703 (c), SL0704 (d) and SL0706 (e) ……... 212

Figure C1 Digital image SL0708b1 (the upper subimage from the image for freeze core SL0708b). The two 50-pixel wide swaths from which the lightness curve was generated are marked by the parallel white lines ……... 225

Figure C2 Lightness curve for image SL0708b1 created in the rgb2lab script ……... 226

Figure C3 Identification of lightness curve inflections points using the v_spline script ……... 227

Figure C4 Periodograms for freeze core images SL0708b1 (a) and SL0708b1 (b), SL0601b (unlaminated sediment from the Owens Valley earthquake slump) (c) and randomly assigned lightness values (d) created using the v_chron script. …….. 228

Figure D1 Location and perimeter of grid squares 46, 47, 47, 59 and 60 (a) and location of individual tree ring chronologies for used in PDSI reconstructions from grid squares 46 (b), 47 (c), 48 (d), 59 (e) and 60 (f) that begin before 1450 A.D …. 232

Figure D2 Number of individual tree ring chronologies incorporated into the NADA PDSI reconstructions (Cook *et al*., 2004; Cook & Krusic, 2004) for grid squares 46 (a), 47 (b), 48 (c), 59 (d) and 60 (e) between 1150 and 1450 A.D ……233

Figure D3 Spatial pattern of DAI (Cook *et al*., 2004) correlation, r, with gridded NADA PDSI reconstructions (Cook *et al*., 2004; Cook & Krusic, 2004) over the last millennium (800-2003 A.D.) (a) and from 1150-1450 A.D. (b) …… 234

Figure D4 Average *n*-acid distribution from SL0708b sediment samples ……235

ACKNOWLEDGEMENTS

I am grateful for the financial support of an Achievement Rewards for College Scientists (ARCS) scholarship (2007-2010) and the Scripps Institution of Oceanography Wyer Family Fellowship (2004-2005).

Many, many people provided support without which I would not have been able to successfully carry out my thesis research. Chris Charles, my adviser, has been a constant source of intellectual guidance; always helping me target interesting academic questions and synthesize the big picture. In addition to this intellectual guidance, Chris always seemed to, at least from my perspective, believe in my scientific abilities even as I often doubted them myself, a belief that helped me navigate the inevitable difficulties of being a graduate student. I also thank my co-advisor, Dan Cayan, for taking me on in my second year, and providing academic, financial and manpower (two field trips to Swamp Lake!) support and guidance for the Swamp Lake project. Through Dan, I was able to stretch my project beyond the boundaries of pure paleoclimatology and gained an exposure to California meteorology. I must also thank Alex Sessions, a committee member, for opening up his lab, resources, and mass spec to me on so many occasions, allowing me to carry out numerous Swamp Lake isotopic measurements. From Alex I learned a great deal not only about organic geochemistry but also about how to be a good scientist. I thank the members of the Sessions Lab, particularly Lichun, for their help and hospitality. I also thank my committee members, Ellen Druffel, Jeff Severinghaus and Nolan Wallach for sharing their expertise and advice along the way. I also thank Martin

Wahlen for offering the invaluable use of freezer for so many years, which allowed me to carefully store and sample numerous frozen sediment cores.

The help of many other scientists outside of SIO was also invaluable as I carried out my thesis research. Tom Guilderson at LLNL patiently guided me through the carbon graphitization process and analysis of my radiocarbon samples (in addition to providing long distance running advice that helped me complete two marathons). Jan Van Wagdendonk, Alison Colwell and Jim Roche of the Yosemite National Park Service provided immense help with fieldwork in Yosemite National Park. The two Swamp Lake field expeditions required significant manpower, and I am grateful to the many volunteers who literally carried my thesis materials on their backs over the rough Yosemite backcountry. I am also grateful to those that helped me plan and carry out my marine expeditions to Santa Barbara Basin, including Dave Field, Vicente, Pat Rafter, Neal Driscoll and others. I thank my undergraduate mentor, Elizabeth Kujawinski, who encouraged my pursuit of a graduate career and guided me through my first steps as a researcher.

Friends and family have also been immensely supportive. I thank my parents for the endless love and support and for providing the outdoor and academic opportunities that lead me to be a graduate student at SIO. Thank you to Pat Rafter, my office mate of five years, for, well, being such a great office mate. I thank Travis, Roman and Roberta for welcoming me when I was just a perspective and being great friends throughout my time at SIO. Melissa has been such an amazing friend and inspiration. Jim, thank you for being a fantastic res tech and roommate.

Chapter 1:, in part, will be submitted for publication to the Journal of Geophysical Research-Oceans. Roach, L.D.; Field, D.B; Guilderson, T.P; Charles, C.D. The dissertation author was the primary investigator and author of this paper.

Chapter 2:, in part, is being prepared for submission for publication. Roach, L.D., Field, D.B., Charles, C.D. The dissertation author was the primary investigator and author of this paper.

Chapter 3:, in part, is being prepared for submission for publication. Roach, L.D., Sessions, A.L., Cayan D.R., Charles, C.D., R.S. Anderson. The dissertation author was the primary investigator and author of this paper.

Chapter 4:, in part, is being prepared for submission for publication Roach, L.D., Sessions, A.L., Cayan D.R., Charles, C.D., R. S Anderson. The dissertation author was the primary investigator and author of this material.

VITA

2004 B.A. Environmental Chemistry, Columbia University

2010 Ph.D. Oceanography, Scripps Institution of Oceanography, University of California, San Diego

ABSTRACT OF THE DISSERTATION

Climate Change in the Pacific North America Region Over the Past Millennium: Development and Application of Novel Geochemical Tracers

by

Lydia Darcy Roach

Doctor of Philosophy in Oceanography

University of California, San Diego, 2010

Christopher D. Charles, Chair
Daniel R. Cayan, Co-Chair

Decadal climate variability in the Pacific North America (PNA) region largely determines the fresh-water supply of the western United States and fisheries production of the northeast Pacific Ocean through tightly coupled ocean-atmosphere interactions. Documenting the historical manifestations of these interactions, over at least the past

millennium, is an essential step towards anticipating the ramifications of future climate change on these resources. This dissertation aims to extend efforts at PNA paleoclimate reconstruction through the development of interannually resolved geochemical proxy records from annually laminated marine and lacustrine sediments. Comparison with instrumental climate measurements provides constraint on the driving mechanisms for observed geochemical variability in each record. The radiocarbon content ($\Delta^{14}C$) of benthic foraminiferal tests in the Santa Barbara Basin (SBB) proves a sensitive tracer for decadal fluctuations in vertical density structure along the southern California margin that are forced by north Pacific ocean-atmosphere interactions and tropical-midlatitude teleconnections. Enumeration of cosmopolitan benthic foraminifera in the SBB over the past ~250 years suggests that, on decadal time scales, the overall size and distribution of the SBB benthic foraminiferal community is largely a function of benthic carbon oxidation rate—a property previously linked to regional surface productivity. In the terrestrial realm, stable hydrogen isotope ratios (δD) of plant lipid biomarkers preserved in the sediments of Swamp Lake, Yosemite National Park, were measured over the 20th century and late medieval period (1160-1432 A.D). Plant lipid δD exhibits a complex relationship with environmental parameters but nevertheless reflects interannual to multidecadal changes in amount of wintertime precipitation in the Sierra Nevada Mountains over the 20th century. Consistent with this observation, multidecadal δD variability during the late medieval generally follows that of concomitant tree ring-derived hydrologic reconstructions and captures droughts of greater severity than any witnessed in the Sierra Nevada over the past 100 years. Comparison of the two isotopic records in terms of medieval vs. modern drought severity, however, requires further

constraint on the driving mechanisms for long-term shifts in plant lipid δD. Overall, this dissertation documents the novel application of benthic foraminiferal $\Delta^{14}C$ and plant lipid δD as a means for reconstructing decadal scale PNA climate from high-resolution sedimentary archives.

Preface

Climate warming over the coming decades to centuries poses major risks for marine ecosystems and continental water resources in the Pacific North American (PNA) region (e.g. McGowan *et al*., 1998; Bograd *et al*., 2008; Seager *et al*., 2007; Barnett *et al*., 2008; Overpeck & Udall, 2010). Anticipation and mitigation of these risks requires our understanding the physical driving mechanisms of decadal scale marine and terrestrial PNA climate variability. Although we possess over a century's worth of instrumental climatic measurements, we still depend on high-resolution proxy reconstructions of prehistoric climate (i.e. paleoclimate) to capture the multiple cycles of decadal variability necessary to investigate these driving mechanisms (Wunsch, 1999; Alverson *et al*., 2001; Mestas-Nuñez & Miller, 2006). While proxy archives such as tree rings (e.g. Cook *et al*., 1999, 2004a, 2010; Jones & Mann, 2004; Biondi *et al*., 2001; MacDonald & Case, 2005; Stahle *et al*., 2007; Treydte *et al*., 2006), corals (e.g. Cobb *et al*., 2003; Seager *et al*., 2008; Urban *et al*., 2000; Felis *et al*., 2010), ice cores (e.g. Moore *et al*., 2002; Vimeux *et al*., 2009; Thompson, 1979; Kobashi *et al*., 2010) and speleothems (Asmerom *et al*., 2007) capture climatic information at the annual to interannual resolutions necessary to realize decadal scale variability over the past millennium, these archives are unevenly distributed, rare or nonexistent in the PNA region. Marine and lacustrine lake sediments are abundant and house numerous geochemical indicators that provide continuous records of past environmental change, yet their utility in decadal scale climate reconstruction is often limited by low sedimentation rates and homogenization that preclude measurement at the necessary temporal resolution. This dissertation exploits two high-sedimentation

rate, annually laminated (varved) sedimentary archives from the PNA region to generate novel geochemical paleoclimate proxy records with implications for the circulation of the Northeast Pacific Ocean, benthic environment along the southern California margin and hydrology of the western United States over the past millennium. Below I introduce the motivation and background supporting these records, and briefly describe the geochemical tracers used in their creation.

The first two chapters of the dissertation consider climate variability and environmental change along the northeast Pacific margin (NEPM). The prevailing northerly winds along the NEPM drive the upwelling of nutrients to the euphotic zone that supports highly productive marine ecosystems. Understanding the influence of climate variability on these upwelling dynamics is therefore an important factor in managing these ecosystems. While well-documented patterns of anomalous surface properties along the northeast Pacific margin have been linked to dominant modes of climate variability such as the Pacific Decadal Oscillation (PDO, Mantua *et al*., 1997), the El Nino Southern Oscillation (ENSO, Ropelewski & Halpert, 1987), and the North Pacific Gyre Oscillation (NPGO, Di Lorenzo *et al*., 2008), the accompanying subsurface dynamics remain poorly understand outside of a sparse set of instrumental observations over the past few decades (Mestas-Nuñez & Miller, 2006; Auad 2003; Auad *et al*, 2003; Bograd *et al*. 2002; Schneider *et al*. 1999; Deser *et al*. 1996; Banks *et al*. 2000; Wong *et al*. 1999; Miller *et al*., 1997). In Chapter 1, I use the radiocarbon concentration ($\Delta^{14}C$) of benthic foraminiferal microfossils preserved in the annually laminated sediments of the Santa Barbara Basin to trace decadal scale sub-surface circulation along the SCM over the past two centuries.

Radiocarbon (^{14}C), the radioactive isotope of carbon, is naturally produced in the atmosphere by the reaction of atomic ^{14}N with neutrons during cosmic radiation. ^{14}C is rare, with a natural abundance approximately 10^{-12} percent that of ^{12}C (Libby, 1946; Libby *et al*., 1949). Atmospheric ^{14}C reacts with oxygen in the atmosphere to form $^{14}CO_2$ (MacKay *et al*., 1963), and becomes incorporated into the marine dissolved inorganic carbon (DIC) reservoir through air-sea gas exchange. Once isolated from the atmosphere, the radiocarbon content of this reservoir decays with a 5730±40 year half-life (Godwin, 1962) and therefore lends itself as a useful tracer for basin scale water mass geometry, ventilation (i.e. time since exposure to the atmosphere), and deep water formation on millennial timescales (Broecker *et al*. 1990; Edwards *et al*., 1993; Bard *et al*., 1994; Adkins & Boyle, 1997). In this study, we present radiocarbon measurements as $\Delta^{14}C$, which represents the deviation, in parts per thousand, of a sample $^{14}C/^{12}C$ ratio from that in the reference material known as Oxalic Acid I. $\Delta^{14}C$ is corrected for 1) mass dependent fractionation, based on measurements of the sample's stable carbon isotope ratio, $\delta^{13}C$ and 2) the ^{14}C decay that has occurred between the time the sample was isolated from the atmosphere and the time of analysis. Benthic foraminifera, ubiquitous bottom dwelling macrofuana, capture the $\Delta^{14}C$-DIC signature of the surrounding water through the secretion of their calcite tests. Several studies have reported $\Delta^{14}C$ of foraminiferal tests preserved in marine sedimentary archives to reconstruct water mass characteristics in the northeast Pacific on millennial time scales during the last glacial and deglacial periods (e.g. Kennett & Ingraham 1996; Marchitto *et al* 2007; Galbraith *et al*., 2007).

In addition to serving as a tracer for basin scale horizontal water mass geometry, $\Delta^{14}C$ gradients in the upper ocean can also be used to investigate vertical mixing (e.g.

Druffel *et al*., 2007; Druffel & Griffin, 1993; Druffel 1997). Above ground nuclear weapons testing in the late 1950s and early 1960s elevated atmospheric $\Delta^{14}C$ by nearly a factor of two above natural levels. Penetration of the surface ocean by this newly released radiocarbon transient, or "bomb carbon," has increased the already pronounced natural $\Delta^{14}C$ gradients in the upper ocean, rendering $\Delta^{14}C$ even more sensitive to decadal scale fluctuations in vertical mixing (Quay, 1983; Guilderson & Schrag, 1998; Hinger *et al*., 2010). Vertical mixing studies often measure $\Delta^{14}C$ variability using coral, an archive that supports radio-isotopic measurement at higher resolution than marine sediments but is absent, with the exception of deep-sea corals, in the northeast Pacific. The high accumulation rate and annual laminations of the Santa Barbara Basin (SBB) sediment, however, lends itself to biennial $\Delta^{14}C$ measurement in benthic foraminiferal tests. In Chapter 1, I apply these $\Delta^{14}C$ measurements to capture decadal scale fluctuations of the vertical density structure along the southern California Margin (SCM) since 1827 A.D. Comparison of measured $\Delta^{14}C$ variability with instrumental observations indicates that these fluctuations are driven by documented modes of interannual and decadal tropical and north Pacific climate variability.

Preserved benthic foraminifera can reflect changing bottom water conditions in their abundance and species distribution. The benthic foraminiferal community of the bathyal Santa Barbara Basin consists of a handful of opportunistic species tolerant of microxic (oxygen concentration, $[O_2]$, < 0.2 ml/l; Bernhard & SenGupta, 2000). The relative distribution of species within this community can change dramatically over months in response to slight changes in bottom water $[O_2]$ and flux of organic material from above (Corliss & Silva, 1996; Silva *et al*., 1993; Bernhard & Reimers, 1991).

Species distributions have also been found to shift on millennial time scales in response to fluctuations in the ventilation of basin source water and location of the regional oxygen minimum zone (OMZ) (Kennett & Ingram 1995; Cannariato & Kennett, 1999; Cannariato *et al*., 1999; Behl & Kennett, 1996). However, little is known of the nature of decadal scale variability in the benthic foraminiferal species abundances in the SBB, and the extent that this variability may reflect changes in bottom water properties. In Chapter 2, I present biennial records of the flux and relative abundance of the ten cosmopolitan SBB benthic foraminiferal species from 1744-2008. I observe significant decadal scale as well as two dramatic shifts in community distribution over this time. One of these shifts coincides with previously documented changes in benthic carbon oxidation rate and $[O_2]$ along the SCM (Stott *et al*., 2002; Holsten *et al*., 2004; Berelson & Stott, 2003; Hagadorn *et al*., 1995; Christensen *et al*., 1994) potentially linked to coeval changes in surface productivity and North Pacific climate (Berelson & Stott, 2003; Holsten *et al*., 2004; Stott *et al*., 2000). The other involves the explosion since 1950 of a previously rare or absent species that possess unique physiological adaptations (Bernhard & Bowser, 1999; Grzymski *et al*., 2001), including possibly the ability to use nitrate as a terminal electron acceptor (Risgaard-Petersen *et al*., 2006).

Although the bathyal SCM inhabited by this benthic foraminiferal community may seem geographically isolated from the continental western United States (henceforth "the West"), environmental conditions in these regions are linked through tightly coupled North Pacific ocean-atmosphere interactions and atmospheric teleconnections (e.g. Namias, 1974; Namias, 1979; Wallace & Gutzler, 1981; Cayan & Namias, 1981; Cayan & Namias, 1982; Namias, 1989) active on interannual to decadal time scales (e.g.

Trenberth & Hurrell, 1994; Cayan *et al*., 1998). In Chapters 3 and 4 the focus of this dissertation shifts to tracing hydrologic variability in the naturally drought-prone West, where these ocean-atmosphere interactions drive fluctuations between wet and dry conditions that can pose major challenges for water resource management. These challenges are exacerbated in the West by rising human population, growing fresh water demand (e.g. National Research Council, 2007; California Department of Water Resources, 2006) and projections of increased water stress with climate warming over the coming decades to centuries (Seager *et al*., 2007; Barnett *et al*., 2008). The ability to anticipate and mitigate negative impacts on water resources is in large part a function of our grasp on the nature and driving mechanisms of decadal scale hydrologic variability in the West that in turn relies on the compilation of multiple independent paleohydrologic proxy records. In Chapters 3 and 4 I use the hydrogen isotope ratios (δD) of specific plant photosynthetic products (biomarkers) to reconstruct hydrologic variability in the Sierra Nevada Mountains at interannual to multidecadal resolution. The resulting isotopic records represent initial attempts to apply plant biomarker hydrogen isotope ratios towards high-resolution paleohydrologic reconstruction in the West.

Deuterium, ^{2}H or D, is a naturally occurring stable isotope of hydrogen, which occurs at a natural abundance of ~0.015%. Protium, ^{1}H or simply H, is the commonly occurring hydrogen isotope. D/H ratios are typically reported in delta (δ) notation, such that δD represents the deviation in parts per thousand of the D/H ratio in a sample from that in a standard normalized relative to the D/H ratio in the international standard Vienna Standard Mean Ocean Water (VSMOW) (Craig, 1961). Samples with negative δD values have a D/H ratio less than that of VSMOW (155.76×10^{-6}). Deuterium becomes

incorporated in plant photosynthetic products, or biomarkers, through the uptake of the DHO isotopolouge during photosynthesis.

Hydrogen and oxygen isotope ratios (δD and $\delta^{18}O$ respectively) in plant biomarkers, particularly cellulose, have long been used in paleoclimate studies (e.g. Gray & Thompson, 1976; Epstein & Yapp, 1976; Burk & Stuiver, 1981; Andersen *et al*., 2001; Huang *et al*., 2002; Treydte *et al*., 2006) because they are in part a function of the isotopic ratios of environmental water (precipitation, surface water and shallow ground water) from which the plants draw on to support metabolic functioning (Epstein *et al*., 1976; Sternberg, 1988). The δD and $\delta^{18}O$ of environmental water is in turn controlled by physical processes within the hydrologic cycle such as evaporation and storm trajectory (Craig, 1961; Dansgaard, 1964; Ehhalt *et al*., 1963; Friedman *et al*., 1964; Gat 1996), such that proxies that capture the isotopic signature of environmental water can be diagnostic of these processes. Plant lipids, a type of biomarker, are refractory compounds that remain well-preserved in lacustrine sediments (Meyers & Ishiwatari 1993) for up to millions of years (Huang *et al*., 1995). At ambient temperatures the carbon bound lipid hydrogens do not exchange with the surrounding environment (Schimmelman *et al*., 1999) and thus retain their δD value through time. Environmental water is the only source of hydrogen for plant lipid biosynthesis. The incorporation of this water into plant lipid compounds results in biological fractionation that is primarily determined by the metabolic pathway or biosynthetic precursor; in other words, it is not a function of environmental factors such as temperature (Sessions, 1999).

The δD values of long carbon chain epicuticular leaf wax lipids have recently been shown to track those of environmental water across a wide variety of humidity,

vegetative and temperature gradients (Sachse *et al*., 2004, 2006, Hou *et al*., 2008; Feakins & Sessions, 2010), suggesting that leaf wax lipid δD may be a promising paleohydrologic tracer. The research presented in Chapters 3 and 4 serves to both further investigate the utility of sedimentary leaf wax lipid δD as a paleohydrologic proxy and elucidate past hydrologic conditions in the Sierra Nevada Mountains over the past millennium. As with the marine records described above, comparison of modern δD with instrumental climate records in Chapter 3 facilitates investigation of the physical driving mechanisms for observed δD variability. This comparison reveals Swamp Lake leaf wax lipid δD is sensitive to catchment water balance on interannual to multidecadal time scales and therefore reflects the amount of wintertime precipitation and snowpack. This observed relationship is used to interpret the hydrologic implications of the wax lipid δD record presented in Chapter 4 that spans 1160-1432 AD, a period of tumultuous hydroclimate in The Sierra Nevada Mountains (Meko *et al*., 2001; Graumlich, 1993) and across the West (Cook *et al*., 2004; Herweijer *et al*., 2007; Stahle *et al*., 2007).

In summary, Chapters 1 and 2 of this dissertation present the use of $\Delta^{14}C$ values and benthic foraminiferal species abundances from the SBB to trace circulation and benthic conditions along the SCM. These records respectively document decadal scale fluctuations in the vertical density structure of the water column along the SCM, and decadal shifts benthic of abundances community distributions possibly linked to North Pacific climate. In Chapters 3 and 4 the focus shifts to the terrestrial realm of the PNA region with δD measurements of leaf wax lipids preserved in lake sediments applied towards reconstructing hydrologic variability in the Sierra Nevada Mountains. Chapter 3 describes the qualitative calibration of a 20th century plant lipid δD record with

instrumental climate records that reveals the sensitivity of the proxy to moisture availability on interannual to multidecadal time scales. Chapter 4 extends these findings toward determining the implications of down core δD variability for hydrologic conditions in the Sierra Nevada over the period 1160-1432 AD. As a whole, this dissertation provides new insight into the development and use of high-resolution geochemical paleoclimate tracers from sedimentary archives to examine critical aspects of PNA climate variability over the past millennium.

References

Adkins, J.F. and Boyle, E.A. (1997) Changing atmospheric $\Delta^{14}C$ and the record of deep water paleoventilation ages. *Paleoceanography* 12:337-344.

Alverson, K. Bradley, R. Briffa, K. Cole, J. Hughes, M. Larocque, I. Pedersen, T. Thompson, L. and Tudhope, S. (2001) A global paleoclimate observing system. *Science* 293:47-48.

Andersen, N. Paul, H.A., Bernasconi, S.M., McKenzie, J.A., Behrens, A., Schaeffer, P. and Albrecht, P. (2001) Large and rapid climate variability during the Messinian salinity crisis: Evidence from deuterium concentrations of individual biomarkers. *Geology* 29:799-802.

Asmerom, Y., Polyak, V., Burns, S., and Rassmussen, J. (2007) Solar forcing of Holocene climate: New insights from a speleothems record, southwestern United States. *Geology* 35:1-4.

Auad, G. (2003) Interdecadal dynamics of the North Pacific Ocean. *J. Phys. Oceanogr.* 33:2483-2503.

Auad, G., Kennett, J.P., and Miller, A.J. (2003) North Pacific intermediate water response to a modern climate shift. *J. Geophys. Res.* 108:doi:10.1029/2003JC001987.

Banks, H.T., Wood, R.A., Gregory, J.M., Johns, T.C., and Jones, G.S (2000) Are observed decadal changes in intermediate water masses a signature of anthropogenic climate change? *Geophys. Res. Lett.* 27:2961-2964.

Bard, E., Arnold, J., Mangerud, J., Paterne, M., Labeyrie, L., Duprat, J., Mélières, M.-A., Sønsstegaard, E. and Duplessy, J.-C. (1994) The North Atlantic atmosphere-sea surface ^{14}C gradient during the Younger Dryas climate event. *Earth Planet. Sci. Lett.* 126:275-287.

Barnett, T. P., Pierce, D. W., Hidalgo, H. G., Bonfils, C., Santer, B. D., *et al.* (2008) Human-induced changes in the hydrology of the western United States. *Science* 319:1080-1083.

Behl, R.J. and Kennett, J.P. (1996) Brief interstadial events in the Santa Barbara Basin, NE Pacific, during the past 60 kyr. , *Nature* 379, p. 243-246

Berelson, W. and Stott, L.D. (2003) Productivity and organic carbon rain to the California margin seafloor: Modern and paleoceanographic perspectives. *Paleoceanography* 18:doi:10.1029/2001PA000672.

Bernhard, J.M. and Bowser, S.S. (1999) Benthic foraminifera of dysoxic sediments: chloroplast sequestration and functional morphology. *Earth-Science Reviews* 46:149-165.

Bernhard, J.M. and Reimers, C.E. (1991) Benthic foraminiferal population fluctuations related to anoxia: Santa Barbara Basin. *Biogeochemistry* 15:127-149.

Bernhard, J.M. and Sen Gupta, B.K. (1999) Foraminifera of oxygen-depleted environments. In: *Modern Foraminifera* (Ed. B. K. Sen Gupta). Kluwer Academic, Dordrecht, 201-217 pp.

Biondi, F. Gershunov, A. and Cayan, D.R. (2001) North Pacific decadal climate variability since 1661. *J. Climate* 14:5-10.

Bograd, S.J., Castro, C.G., Di Lorenzo, E., Palacios, D.M., Bailey, H., Gilly, W. and Chavez, F.P. (2008) Oxygen declines and the shoaling of the hypoxic boundary in the California Current. *Geophys Res. Lett.* 35:doi:10.1029/208GL034185.

Bograd, S.J., Schwing, F.B., Castro, C., and Timothy, D.A. (2002) Bottom water renewal in the Santa Barbara Basin, *J. Geophys. Res.* 107, doi:1029/2001JC001291

Broecker, W.S., Peng, T.H., Trumbore, S., Bonani, G. and Wolfli, W. (1990) The glacial distribution of radiocarbon in the glacial ocean. *Global Biogeochem. Cycles* 4:103-117.

California Climate Change Center (2006) Our Changing Climate Assessing Risks to California 16 pp. [Available online at meteora.ucsd.edu/cap/pdffiles/CA_climate_Scenarios.pdf]

Cannariato, K.G. and Kennett, J.P. (1999) Climatically related millennial-scale fluctuations in strength of California margin oxygen-minimum zone during the past 60 k.y. *Geology* 27:975-978.

Cannariato, K.G., Kennett, J.P. and Behl, R.J. (1999) Biotic response to late Quaternary rapid climate switches in Santa Barbara Basin: ecological and evolutionary implications, *Geology*, 27, 63-66

Cayan, D. R., Dettinger, M. D., Diaz, H. F., and Graham, N. E. (1998) Decadal variability of precipitation over western North America. *J. Climate* 11:3148-3166.

Cayan, D.R. and Namias, J. (1981) Large-scale air-sea interactions and short-period climatic fluctuations. *Science* 214:869-876.

Cayan, D.R. and Namias, J. (1982) Large-scale changes in north Pacific and North-American weather patterns in recent decades. *Mon. Weather Rev.* 12:1851-1862

Christensen, C.J., Gorsline, D.S., Hammond, D.E., and Lund, S.P. (1994) Non-annual laminations and expansion of anoxic basin-floor conditions in Santa Monica Basin, California Borderland, over the past four centuries. *Mar Geol.* 116:399-418.

Cobb, K.M., Charles, C.D., Cheng, H. and Edwards, R.L. (2003) El Niño/Southern Oscillation and tropical Pacific climate during the last millennium. *Nature* 407:271-276.

Cook, E. R., Woodhouse, C.A., Eakin, C.M., Meko, D.M., and Stahle, D.W. (2004) Long-term aridity changes in the western United States. *Science* 306:1015-1018.

Cook, E. R., Meko, D.M., Stahle, D.W. and Cleaveland, M.K. (1999) Drought reconstructions for the continental United States. *J. Climate* 12:1145-1162.

Corliss, B. and Silva, K.A. (1993) Rapid Growth of deep-sea benthic foraminifera. *Geology* 21:991-994.

Craig, H., (1961) Isotopic variations in meteoric waters. *Science* 133:1702-1703.

Dansgaard, W., (1964) Stable isotopes in precipitation. *Tellus* 16:436-468.

Deser, C., Alexander, M.A., and Timlin, M.S. (1996) Upper-ocean thermal variations in the North Pacific during 1970-1991, *J. Climate*, 9:1840-1855.

Di Lorenzo, E., Schneider, N., Cobb, K.M., Franks, P.J.S., Chhak, K., Miller, A.J., *et al*. (2008) North Pacific Gyre Oscillation links ocean climate and ecosystem change. *Geophys. Res. Lett*. 35:doi:10.1029/2007GL032838.

Druffel, E.R.M, Griffin, S., Beaupre, S.R., and Dunbar, R.B. (2007) Oceanic climate and circulation changes during the past four centuries from radiocarbon in corals. *Geophys. Res. Lett*. 34:doi:10.1029/2006GL028681.

Druffel, E.R.M (1997) Pulses of rapid ventilation in the north Atlantic surface ocean during the past century. *Science* 275:1454-1457.

Druffel, E.R.M. and Griffin, S. (1993) Large variations of surface ocean radiocarbon: evidence of circulation changes in the southwestern Pacific. *J Geophys. Res*. 98:20,249-20,259.

Edwards, R.L., Beck, J.W., Burr, G.S., Donahue, D.J., Chappell, J.M.A., Bloom, A.L., Druffle, E.R.M. and Taylor, F.W. (1993) A large drop in atmospheric $^{14}C/^{12}C$ and reduced melting in the Yonger Dryas documented with ^{230}Th of corals. *Science* 260:962-968.

Ehhalt, D., Knott, K., Nagel, J.F. and Vogel, J.C. (1963) Deuterium and oxygen-18 in rain water. *J. Geophys. Res*. 68:3774-3780.

Epstein, S. and Yapp, C.J. (1976) Climatic implications of D-H ratio hydrogen in C-H groups in tree cellulose. *Earth Planet. Sc. Lett*. 30:252-261.

Epstein, S., Yapp, C.J. and Hall, J.H. (1976) Determination of D-H ratio of non-exchangeable hydrogen in cellulose extracted from aquatic and land plants. *Earth Planet. Sc. Lett*. 30: 241-251.

Feakins, S.J. and Sessions, A.L. (2010) Controls on the D/H ratios of plant leaf waxes in an arid ecosystem. *Geochim. Cosmochim. Acta* 74:2128-2141.

Friedman I., Redfield, A.C., Schoen, B. and Harris, J. (1964) The Variation of the Deuterium Content of Natural Waters in the Hydrologic Cycle. *Rev. Geophys.* 2:177-224.

Galbraith, E.D., Jaccard, S.L., Pedersen, T.F., Signam, D.M., Haug, G.H., Cook, M., Southon J.R., and Francois, R. (2007) Carbon dioxide release from the North Pacific abyss during the last deglaciation. *Nature* 449:890-894.

Gat, J. R., (1996) Oxygen and hydrogen in the hydrologic cycle. *Ann. Rev. Earth Pl. Sc.* 24:225-262.

Godwin, H. (1962) Half-life of radiocarbon. *Nature* 195:984.

Graumlich L. J. (1993) A 1000-year record of temperature and precipitation in the Sierra Nevada. *Quat. Res.* 39:249-255.

Gray, J. and Thompson, P. (1976) Climatic information from 18O/16O ratios of cellulose in tree rings. *Nature* 262:481-482.

Grzymski, J., Schofield, O.M., Falkowski, P.G., and Bernhard, J.M. (2002) The function of plastids in the deep-sea benthic foraminifer, *Nonionella stella*. *Limnol Oceanogr* 6:1569-1580.

Guilderson, T.P. and Schrag, D.P. (1998) Abrubpt shift in subsurface temperatures in the tropical Pacific associated with Changes in El Nino. *Science* 281:240-243.

Hagadorn, J.W., Stott, L.D., Sinha, A., and Rincon, M. (1995) Geochemical and sedimentologic variations in inter-annually laminated sediments from Santa Monica Basin. *Mar. Geol.* 125:111-131.

Herweijer, C., Cook, E.R., and Emile-Geay, J. (2007) North American droughts of the last millennium from a gridded network of tree-ring data. *J. Climate* 20:1353-1376.

Hinger, E.N., Santos, G.M., Druffel, E.R.M. and Griffin, S. (2010) Carbon measurements of surface seawater from a time-series site off southern California. *Radiocarbon* 52:69-89.

Høgslund, S., Revsbech, N.P., Cedhagen, T., Nielsen, L.P., and Gallardo, V.A. (2008) Denitrification, nitrate turnover, and aerobic respiration by benthic foraminiferans in the oxygen minimum zone off Chile. *J. Exp. Mar. Biol. Ecol.* 359:85-91.

Holsten, J., Stott, L. and Berelson, W. (2004) Reconstructing benthic carbon oxidation rates using d13C of benthic foraminifers. *Marine Micropaleontology* 53:117-132.

Hou, J., D'Andrea, W.J., and Huang, Y. (2008) Can sedimentary leaf waxes record D/H ratios of continental precipitation? Field, model and experimental assessments. *Geochim. Cosmochim. Acta* 72:3503-3517.

Huang , Y.S., Lockheart, M.J., Collister, J.W. and Eglington, G. (1995) Molecular and isotopic biogeochemistry of the Miocene Clarkia Formation: hydrocarbons and alcohols. *Org. Geochem.* 23:785-801.

Huang, J. H. Shuman, B., Wang, Y. and Webb III, T. (2002) Hydrogen isotope ratios of palmitic acid in lacustrine sediments record late Quaternary climate variations. *Geology* 30:1103-1106.

Jones, P.D. and Mann, M.E. (2004) Climate over past millennia. *Rev Geophys* 42:2003RG000143.

Kennett, J.P. and Ingram, B.L. (1995), A 20,000-year record of ocean circulation and climate change from the Santa Barbara Basin, *Nature*, 377, 510-514.

Kobashi, T., Severinghaus, J.P., Barnola, J., Kawamura, K., Carter, T. and Nakaegawa, T. (2010) Persistent multi-decadal Greenland temperature fluctuation through the last millennium. *Climatic Change* 100:733-756.

Libby, W. (1946) Atmospheric helium three and radiocarbon from cosmic radiation. *Phys. Rev.* 69:671-672.

Libby, W., Anderson, E. and Arnold, J. (1949) Age determination by radiocarbon content: World-wide assay of natural radiocarbon. *Science* 109:227-228.

MacDonald, G.M. and Case, R.A. (2005) Variations in the Pacific Decadal Oscillation over the past millennium. *Geophys. Res. Lett.* 32:doi:10.1029/2005GL022478.

MacKay, C., Pandow, M. and Wolfgang, R. (1963) On the chemistry of natural radiocarbon. *J. Geophys. Res.* 68:3929-3931.

Mantua, N.J., Hare, S.R., Zhang, Y., Wallace, J.M., and Francis, R.C. (1997) A Pacific interdecadal climate oscillation with impacts on salmon productions. *Bull. Amer. Met. Soc.* 78:1069-1079.

Marchitto, T.M., Lehman, S.J., Ortiz, J.D., Fluckiger, J., and van Geen, A. (2007) Marine radiocarbon evidence for the mechanism of deglacial atmospheric CO_2 rise. *Science* 316:1456-1459.

McGowan, J.A., Cayan, D.R. and Dorman, L.M. (1998) Climate-ocean variability and ecosystem response in the northeast Pacific. *Science* 281:210-217.

Meko, D. M., Therrell, M. D., Baisan, C. H., and Hughes, M. K. (2001) Sacramento River flow reconstructed to A.D. 869 from tree rings. *J. Amer. Water Res. Assoc.* 37: 1029-1039.

Mestas-Nuñez, A.M. and Miller, A.J. (2006) Interdecadal variability and climate change in the eastern tropical Pacific: A review. *Prog. Oceanogr.* 69:267-284.

Meyers, P. A. and R. Ishiwatari, 1993. Lacustrine organic geochemistry—An overview of indicators of organic matter sources and diagenesis in lake sediments. *Org. Geochem.* 20:867-900.

Miller, A.J., White, W.B., and Cayan, D.R. (1997) North Pacific thermocline variations on ENSO timescales. *J. Phys. Oceanogr.* 27:2023-2093.

Moore, G.W.K., Holdsworth, G. and Alverson, K. (2002) Climate change in the North Pacific region over the past three centuries. *Nature* 420:401-403.

Namias, J. (1974) Longevity of a coupled air-sea-continent system. *Mon. Weather Rev.* 102:638-648.

Namias, J. (1978) Multiple causes of North-American abnormal winter 1976-77. *Mon. Weather Rev.* 106:279-295.

Namias, J. (1989) Cold waters and hot summers. *Nature* 338:15-16.

National Research Council (2007) Colorado River Basin Water Management: Evaluating and Adjusting to Hydroclimate Variability. National Academies Press, 222 pp.

Overpeck, J., Udall, B. (2010) Dry Times Ahead. *Science* 328:1624-1643.

Quay, P.D., Stuiver, M. and Broecker, W.S. (1983) Upwelling rates for the equatorial Pacific-Ocean derived from the bomb C-14 distribution. *J. Mar. Res.* 41:769-792.

Risgaard-Petersen, N. Langezaal, A.M., Ingvardsen, S., Schmid, M.C., Jetten, M.S.M, Op den Camp, H.J.M, *et al.* (2006) Evidence for complete denitrification in a benthic foraminifer. *Nature* 443:93-96.

Ropelewski, C.F. and Halpert, M.S. (1987) Global and regional scale precipitation patterns associated with the El Niño/Southern Oscillation. *Mon. Weather Rev.* 111:1606-1626.

Sachse, D., Radke, J. and Gleixner, G. (2004) Hydrogen isotope ratios of recent lacustrine sedimentary *n*-alkanes record modern climate variability. *Geochim. Cosmochim. Acta* 68:4877-4889.

Sachse, D., Radke, J. and Gleixner, G. (2006) δD values of individual n-alkanes from terrestrial plants along a climatic gradient—Implications for the sedimentary biomarker record. *Org. Geochem.* 37:469-483.

Schimmelman A. Sessions, A.L. and Mastalerz, M. (2006) Hydrogen isotopic (D/H) composition of organic material during diagenesis and thermal maturation. *Annu. Rev. Earth Pl. Sc.* 34:501-533.

Schneider, N. Miller, A.J., Alexander, M.A. and Deser, C. (1999) Subduction of decadal North Pacific temperature anomalies: Observations and dynamics. *J. Phys. Oceanogr*. 29:1056-1070.

Seager, R. Burgman, R., Kushnir, Y., Clement, A., Cook, E., Naik, N., and Miller, J. (2008) Tropical Pacific forcing of North American Medieval Megadroughts: Testing the concept with an atmospheric model forced by coral-reconstructed SSTs. *J. Climate* 21:6175-6190.

Seager R. and coauthors (2007) Model projections of an imminent transitions to a more arid climate in southwestern North America. *Science* 312:1181-1184.

Sessions, A.L., Burgoyne, T.W., Schimmelmann, A., and Hayes, J.M. (1999). Fractionation of hydrogen isotopes in lipid biosynthesis. *Org. Geochem*. 30:1193-1200.

Silva, K.A., Corliss, B.H., Rathburn, A.E. and Thunell, R.C. (1996) Seasonality of living benthic foraminifera from the San Pedro Basin, California Borderland. *J. Foram Res*. 26:71-93.

Stahle, D.W., Fye, F.K., Cook, E.R. and Griffin, R.D. (2007) Tree-ring reconstructed megadroughts over North America since A.D. 1300. *Climatic Change* 83:133-149.

Sternberg, L.D.L. (1988) D/H ratios of environmental water recorded by D/H ratios of plant lipids. *Nature* 333:59-61.

Stott, L.D., Berelson, W., Douglas, R. and Gorsline, D. (2000) Increased dissolved oxygen in Pacific intermediate waters due to lower rates of carbon oxidation in sediments. *Nature* 407:367-370.

Stott, L.D., Bunn, T., Prokopenko, M., Mahn, C., Gieskes, J. and Bernhard, J.M. (2002) Does the oxidation of methane leave an isotopic fingerprint in the geologic record? *Geochem Geophys Geosys* 3:doi:10.1029/2001GC000196.

Burk, R.L. and Stuiver, M. (1981) Oxygen isotope ratios in trees reflect mean annual temperature and humidity. *Science* 211:1417-1419.

Thompson, L.G., Hastenrath, S. and Arnao, B.M. (1979) Climatic ice core records from the tropical Quelccaya ice cap. *Science* 203:1240-1243.

Trenberth, K.E. and Hurrell, J.W. (1994) Decadal atmosphere-ocean variations in the Pacific. *Climate Dyn*. 9:303-319.

Treydte, K.S., Schleser, G.H., Helle, G., Frank, D.C., Winiger, M., Haug, G.H., and Esper, J. (2006) The twentieth century was the wettest period in northern Pakistan over the past millennium. *Nature* 440:1179-1182.

Urban, F.E., Cole, J.E. and Overpeck, J.T. (2000) Influence of mean climate change on climate variability from a 155-year tropical Pacific coral record. *Nature* 407:989-993.

Vimeux, F. and coauthors (2009) Climate variability during the last 1000 years inferred from Andean ice cores: A review of methodology and recent results. *Paleaogeogr. Palaeclimatol. Palaeoceol.* 281:229-241.

Wallace, J.M. and Gutzler, D.S. (1981) Teleconnections in the geopotential height field during the Northern Hemisphere winter. *Mon. Weather Rev.* 109:784-812.

Wong, A.P.S., Bindoff, N.L., and Church, J.A. (1999) Large-scale freshening of intermediate waters in the Pacific and Indian oceans. *Nature* 400:440-443.

Wunsch, C. (1999) The interpretation of short climate records, with comments on the North Atlantic and Southern Oscillations. *Bull.*

Chapter 1. Radiocarbon as a tracer for decadal scale sub-thermocline variability along the southern California margin

Abstract

The sub-thermocline, decadal scale dynamics of the northeast Pacific Ocean remain largely inaccessible beyond sparse instrumental observations spanning the last twenty years. However, horizontal and vertical gradients in the radiocarbon concentration ($\Delta^{14}C$) of dissolved inorganic carbon (DIC) at intermediate depths in the northeast Pacific can be exploited to capture these dynamics. $\Delta^{14}C$ of benthic foraminifera extracted from the annually laminated sediments at the Santa Barbara Basin (SBB) depocenter (~600 m) was measured at biennial resolution from 1827-2006. Comparison of core top $\Delta^{14}C$ values with instrumental measurements reveals that benthic foraminifera faithfully capture the $\Delta^{14}C$ values of surrounding DIC. We observe substantial $\Delta^{14}C$ variability on decadal timescales with excursions on the order of 40‰. Intervals displaying a significantly lower $\Delta^{14}C$ trend correspond to periods of enhanced upwelling and subsurface equatorward flow along the SCM. Although pore-water chemistry and source water properties cannot be definitively ruled out, our results implicate interannual to decadal scale ocean-atmospheric interactions in the north and tropical Pacific as the primary drivers of SBB bottom $\Delta^{14}C$ variability through their manipulation of the vertical density structure along the Southern California Margin (SCM). These results suggest that on decadal timescales local isopycnal geometry dominates basin-scale water mass geometry in determining the $\Delta^{14}C$ value recorded in SCM sediment.

1.1 Introduction

Synoptic-scale atmospheric circulation is known to influence patterns of surface ocean properties in the north Pacific on interannual to decadal time scales, such as the spatial distribution of sea surface temperature and pressure anomalies associated with the El Nino Southern Oscillation (ENSO) and other documented modes of tropical and north Pacific climate variability. The persistence and propagation of these patterns must involve aspects of the interior ocean, yet the extent and nature of the sub-surface north Pacific's involvement in the surface expression of climate variability remains unclear outside a limited set of short-term investigations carried out over the last few decades (e.g. Auad 2003; Auad *et al*, 2003; Bograd *et al*. 2002; Schneider *et al*. 1999; Deser *et al*. 1996; Banks *et al*. 2000; Wong *et al*. 1999; Miller *et al*., 1997; Mestas-Nuñez & Miller, 2006). The California Cooperative Fisheries Investigation (CalCOFI) time series of Southern California Bight (SCB) chemistry and hydrography reveals significant interannual variability in the physical and chemical properties of intermediate waters along the southern California margin (SCM) Bograd *et al*. (2002). Although results from these studies indicate that the sub-surface North Pacific is dynamic on decadal and interannual time scales, we must rely on high-resolution proxy records to capture multiple realizations of decadal-scale hydrographic variability along the SCM that extend beyond the period of instrumental measurement.

The high-resolution sediments of the Santa Barbara Basin (SBB) offer a unique archive from which to extract proxy information that can capture multiple realizations of decadal scale intermediate water variability. Benthic foraminifera, ubiquitous in the top one centimeter of SBB sediments (Harman, 1964; Phleger & Soutar 1973; Bernhard &

Reimers 1991; Bernhard *et al*., 1997; Bernhard *et al*., 2003), present a suite of geochemical indicators from which to reconstruct SBB bottom water properties. Of these indicators, radiocarbon, reported here as $\Delta^{14}C$ (the per mil offset from the $^{12}C/^{14}C$ ratio in mid 19th century wood, corrected as per Stuiver and Polach, (1977)) exhibits pronounced horizontal and vertical gradients in the intermediate waters of the northeast Pacific (Figures 2.1 and 2.2 respectively), as documented by the World Ocean Circulation Experiment (WOCE) surveys in the 1990s. These gradients make $\Delta^{14}C$ a sensitive tracer for vertical mixing (Druffel, 1981; Druffel & Griffin, 1993; Druffel, 1997; Guilderson & Schrag, 1998; Druffel *et al*., 2007), including in the SCB (Hinger *et al*., 2010), and horizontal advection of end-member water mass sources (Kennett & Ingram 1995; Roark *et al*., 2003; Marchitto *et al*., 2007; Galbraith *et al*., 2007). Interannual to decadal scale fluctuations in these processes can be driven by anomalies in local Ekman dynamics, regional atmospheric dynamics and forcing through remote atmospheric or oceanic teleconnections (Bograd *et al*., 2001) that are often associated with documented modes climate variability including ENSO (e.g. Bograd *et al*., 2001; Lynn & Bograd, 2002; Lynn *et al*., 1998, 1995; Chelton & Davis, 1982; Clarke & Van Gorder 1994; Enfield & Allen 1980; Schwing *et al*., 2000, 2001), the Pacific Decadal Oscillation (PDO) (Di Lorenzo *et al*., 2007; Auad *et al*., 2003; Mantua *et al*., 1997) and the North Pacific Gyre Oscillation (NPGO) (Di Lorenzo *et al*., 2008). In this study, we use $\Delta^{14}C$, measured at biennial resolution from benthic foraminiferal tests in the central SBB as a tracer for decadal scale hydrographic fluctuations along the SCM over the past two centuries. Through comparisons of $\Delta^{14}C$ values with instrumental records we aim to identify the

role of North Pacific climate in driving $\Delta^{14}C$ in the deep SBB and examine the relationship between decadal scale surface and subsurface variability along the SCM.

1.2 Oceanographic setting

As the northernmost California Borderland Basin, the SBB, situated within the SCB, is bound by mainland California to the north and the Channel Islands to the south (Figure 1.3). The pattern of wind driven circulation in the SCB can be generally characterized by three components: the California Current (CC), the California Undercurrent and the Inshore Current. The equatorward CC, typically centered 100-200 km off Point Conception (Lynn & Simpson 1987, 1990), transports relatively oxygenated, cool, low salinity water from the Subarctic Gyre (Reid *et al*., 1958; Hikey, 1979; Simpson *et al*., 1984). Organization and intensification of the CC, along with the onset of coastal upwelling, offshore Ekman transport and reduction of coastal sea surface height (SSH), typically begins in the spring and extends through the early summer driven by enhanced northerly wind stress that stem from the strengthening and northward migration of the North Pacific high (Bograd *et al*., 2001; Lynn *et al*. 2003; Lynn and Simpson, 1987). Stronger northerly, upwelling favorable, wind also sets up positive wind stress curl in the SCB, which drives open ocean Ekman pumping (Di Lorenzo, 2003). These seasonal conditions are associated with pronounced springtime isopycnal shoaling in the SBC (Figure 1.4a) and the associated fluctuation in bottom water potential density (Figure 1.4b). This instrumentally-recorded variability in bottom water potential density along with other physical and chemical parameters is believed to be driven by periodic "flushing events" (Bograd *et al*., 2002)—displacement of deep basin water with denser water spilling over the basin's western sill (Berelson, 1991; Reimers *et al*., 1990;

Sholkovitz & Gieskes, 1971). The sub-surface California Undercurrent (CU) situated along the continental margin usually between 100 and 250 m depth (Bray *et al*., 1999; Lynn & Simpson, 1987, 1990) transports relatively warm, saline and oxygen-depleted waters poleward from the eastern equatorial Pacific (Sverdrup & Flemming, 1941; Reid *et al*., 1958; Reid, 1962). During winter months, the Undercurrent occasionally surfaces in the SCB to form the Inshore Countercurrent (IC, Lynn & Simpson, 1987; Hickey, 1979) that typically reverses direction in spring to join the main equatorward flow of the CC. Depression of isopycnals occurs during the fall and winter (Figure 1.4a) when the CU and IC experience peak strength (Bray *et al*., 1999; Lynn and Simpson 1987; Lynn *et al*., 2003).

Source waters to the deep SBB, ~600 m at its deepest point, derive from a mixture of young, relatively oxygen rich North Pacific intermediate water (NPIW), recently ventilated in the Sea of Okhotsk (Talley, 1991, 1993), the Bering Sea (Takahashi, 1998) and the Gulf of Alaska (Van Scoy *et al*., 1991) and older, poorly ventilated relatively oxygen-depleted water advected from the northern eastern tropical Pacific (Behl & Kennett 1996; Hendy & Kennett, 2003). This mixture enters the basin from the northwest by spilling over its western sill at ~475 m (Emery, 1954), which intersects with the local oxygen minimum zone. Decomposition of organic detritus raining out of the highly productive euphotic zone further depletes oxygen levels, resulting in concentrations typically < 0.1 ml L^{-1} (Emery & Hulsemann, 1961). Oxygen renewal can occur during flushing events, when denser water spills over the western sill, displacing stagnant water within the basin (Sholkovitz & Gieskes, 1971; Reimers *et al*., 1990; Bograd *et al*., 2002) over the course of 1 to 2 months (Liu, 1979; Bograd *et al*. 2002). Strong equatorward

flow and the presence of denser water outside the basin at sill depth than within the deep basin are thought to be the two prerequisites for basin flushing, supplying the necessary kinetic and potential energy respectively (Bograd *et al*., 2002).

The oxygen-starved environment at the SBB bottom is inhospitable to bioturbating benthic macrofuana and thus ideal for the preservation of annually laminated (varved) sediments. Formation of dark and light varve couplets has been attributed to the winter input of terrigenous material followed by spring and summer deposition of diatomaceous autochthonous material (Emery & Hulsemann, 1962) as well as seasonal cycles in the replenishment of basin oxygen and the formation of *Beggoatia* bacterial mats during periods of oxygen depletion (Reimers *et al*., 1990). This varved sedimentology provides an independent age chronology upon which to measure benthic foraminiferal $\Delta^{14}C$, thereby reducing the additional error imposed by the use of coexisting benthic-planktonic age pairs (Broecker *et al*., 2004).

1.3 Methods

1.3.1 Core collection and sub sampling

Benthic foraminifera were obtained from Soutar box cores SBBC 080621-02 collected June 2008 and SBBC 0110-3001 collected November 2001, both from the *R/V Robert Gordon Sproul*. SBBC 080621-02 was taken at 34º13.73'N, 120º02.11'W from a depth of 589 m and SBBC 0110-3001 at approximately the same location (Field *et al*., 2006) (Figure 1.1). Core collection, preservation, subsampling, determination of varve chronology and preparation of foraminiferal samples were carried out as described in Field *et al* (2006). Briefly, X-radiographs of core ~0.5 cm thick core slabs were used to identify individual varves and create detailed chronologies. Following these

chronologies, slabs from SBBC 0110-3001 were subsampled at 2-year intervals from the 2001 to 1744 AD and SBBC 080621-02 subsampled at 1-year intervals from 2007 to 2002 and two year intervals from 2001-1980. Error due to sample excision from both cores is approximately 0.5 to 1 year, which may increase down core in SBBC 0110-3001 due to diminished varve clarity. Samples were then washed, dry-sieved and divided into five size fractions (120-150 μm, 150-180 μm, 180-212 μm, 212-250 μm, 250-300 μm and 300-500 μm) for SBBC 0110-3001 and three to four size fractions (300-425 μm, 212-250 μm, 150-212 μm or 180-212 μm and 150-180 μm) for SBBC 080621-02.

1.3.2 Stable isotope measurement

Stable carbon and oxygen isotope measurements were made on the tests of *Cassidulinoides cornuta*, a benthic foraminiferal species abundant throughout the record. Individuals from mixed size fractions were used in order to achieve adequate mass (~100 μg), with an average of 80 specimens picked for each sample. Stable isotope values were measured on a Finnigan MAT 252 mass spectrometer equipped with a carbonate device at an analytical precision of 0.09‰ and 0.08‰ for $\delta^{18}O$ and $\delta^{13}C$ respectively and determined relative to the Pee Dee belemnite (PDB) standard. Two to five replicate measurements were made for the majority of intervals. Species-specific measurements were also made for *Bolivina tenuata*, *Bolivina semiduda*, *Nonionella stella*, *Chilostomella ovoidea*, *Seggrunda eckisi*, and *Loxostomum pseudobeyrichi* (Table 1.1).

1.3.3 Benthic foraminiferal species assemblages

The ten most abundant benthic foraminiferal species observed in the SBB sediment samples were identified and counted, namely: *Bolivina argentea, B. seminuda, B. tenuata, Bolivina sp., C. cornuta, C. ovoidea, L. pseudobeyrichi, N. stella, Nonionella*

sp. and *S. eckisi*. Quantification was carried out for every two year interval by evenly distributing the sample on a 10 x 18 or 11 x 19 gridded tray and counting individuals in grid square splits as representatives of the entire row of squares. Approximately 100-600 specimens were counted for each interval and assemblages from every two year interval between 2001 and 1736 were counted except for the intervals beginning in 1824 and 1848, which were lost. A detailed discussion of observed assemblage variability in the SBB is presented in Chapter 2.

1.3.4 Calcite $\Delta^{14}C$ measurement

Radiocarbon samples were compiled from a mixture of five cosmopolitan species, *B. seminuda, B. tenuata, S. eckisi, N. stella* and *C. cornuta* picked from dry-sieved sediments. No single species existed in adequate abundance to achieve the carbon mass necessary for measurements with reasonable instrumental error. Sample masses ranged from 1 to 10 mg calcite (0.1-1.0 mg C). The relative abundance of species in each sample reflected the assemblage distribution of each interval. *C. ovoidea* was not included due to the unusually low $\delta^{13}C$ values obtained for its tests. Eight species-specific samples of *S. eckisi* and *N. stella* were also assembled to cross check against the mixed assemblages. Samples were acidified and graphitized following standard procedures (McNichol *et al*., 1994) and measured at the Center for Accelerated Mass Spectrometry, Lawrence Livermore National Laboratory (CAMS). Age corrected $\Delta^{14}C$ values are reported following conventions described by Stuiver and Pollach (1977), using $\delta^{13}C$ value based on stable isotope measurements of representative species mixtures. Radiocarbon measurements from SBBC 0110-3001 were made for every two-year interval between 2001 and 1827 with the exception those beginning in 1979, 1977, 1965, 1947, 1935,

1878, 1876, 1858 and 1848, due to insufficient calcite weight during these intervals; they were not extended earlier than 1827 because of to the decreasing overall numbers of benthic foraminiferal individuals after this date. Measurements from SBBC 080621-02 were made every one year between 2001 and 2005 and every two years from 2000-1984.

1.3.5 Seawater collection and $\Delta^{14}C$ measurement

Two sets of water column samples were collected using a Niskin-CTD array from over the deepest portion of the Santa Barbara Basin and just outside the western sill during the 2008 cruise (Table 1.2). Five hundred mL glass bottles were filled from the bottom using Tygon tubing and over-flowed one and one-half times their volume. Each sample was treated with 100 μl $HgCl_2$ and sealed with a glass stopper using vacuum grease following protocols from the National Ocean Sciences Accelerator Mass Spectrometry Facility (NOSAMS) (http://www.nosams.whoi.edu/clients/submissions_sample_prep.html#dic) at Woods Hole Oceanographic Institution and the Marine Physical Laboratory (http://132.239.122.17/co2qc/handbook/sop01.pdf) at the Scripps Institution of Oceanography (SIO). Carbon dioxide gas was quantitatively extracted from each sample and cryogenically purified at SIO. The CO_2 gas was isolated in a flame sealed glass tube for subsequent AMS analysis at CAMS.

1.4 Results

1.4.1 Benthic foraminiferal stable isotopes

The $\delta^{13}C$ values of *C. cornuta* (Figure 1.5a) fall between –0.5 ‰ and –1.1 ‰ for the entire record spanning 1744 to 2001. The average standard deviation of 48 triplicate measurements was 0.049‰. Values peak around 1780, and then decrease in two phases,

the first between 1800 and 1870 at a rate of ~0.04‰ per decade and the second between 1920 and 2001 at a rate of ~0.03‰ per decade. The latter decrease in $\delta^{13}C$ values is approximately 13-16% that observed in global surface waters due to the ^{13}C Suess effect (Gruber *et al*., 1999; Sonnerup *et al*., 1999), roughly consistent with the 5-20% contribution from remineralized photosynthate organic carbon to the pore water dissolved inorganic carbon (DIC) pool between 0-1cm derived from the SBB DIC profile of Berelson *et al* (2005).

Species specific and mixed assemblage δ13C values are listed in Table 1.1. For the individual species, *B. argentea* displayed the highest $\delta^{13}C$ with an average of -0.813‰ and *C. ovoidea* the lowest with an average of -3.74‰. The average of eight mixed assemblage samples from a range of time intervals between 1999 and 1937 was -1.46‰, with a standard deviation of 0.32‰ and no temporal trend observed. When compared to the SBB upper pore water $\delta^{13}C$ profile of Stott *et al*. (2002), the species specific values indicate that the sampled benthic foraminifera calcified their tests between 0.1 and 0.5 cm in the sediment column, consistent with the depth preference of living SBB benthic foraminifera investigated in previous studies (Bernhard & Reimers 1991; Stott *et al*., 2002; Holsten *et al*., 2004).

$\delta^{18}O$ of *C. cornuta* (Figure 1.5b) shows little variability and no monotonic trends throughout the record, with values fluctuating between 1.9 and 2.4‰. The average standard deviation of 48 triplicate measurements was 0.09‰. SBB bottom exhibits minimal temperature variability, typically ranging between 6.2 and 6.4ºC (Talley *et al*., 2007). Although flushing events can result in measureable temperature decreases (Bograd *et al*., 2002) the magnitude of these changes (0.1-0.5ºC) corresponds to a theoretical 0.02-

0.11‰ increase in $\delta^{18}O$ of calcite benthic foraminiferal tests. As this ranges falls almost entirely within analytical noise of $\delta^{18}O$ measured here, an alternative tracer, such as $\Delta^{14}C$, must be employed to investigate decadal scale variability in the physical properties of SBB bottom water.

1.4.2 Seawater $\Delta^{14}C$

We measured $\Delta^{14}C$ of five seawater samples, two from the SBB center at 579 m and 475 m and three from the western sill at 500 m, 475 m and 450 m (Figure 1.3, Table 1.2). The deep SBB DIC was the lowest in ^{14}C ($\Delta^{14}C$ = -111‰) while that from the shallowest sample at the western sill was the highest ($\Delta^{14}C$ = -97‰). $\Delta^{14}C$ values of seawater samples are close to those of corresponding depths measured at nearby WOCE stations in the 1990s (Figure 1.2), and also match those recorded in the tests of core top benthic foraminifera from this study (Figure 1.6b).

1.4.3 Benthic foraminiferal $\Delta^{14}C$

The time series of benthic foraminiferal $\Delta^{14}C$ is shown in Figure 1.6. Values of age corrected benthic foraminiferal $\Delta^{14}C$ from SBBC 0110-3001 range between –118‰ and –160‰ with an average of –141‰ over the period 1844 to 2001 (Figure 1.6a). Between 1860 and 1910 $\Delta^{14}C$ values undergo repeated fluctuations on the order of 30‰, well outside the analytical uncertainty of 3 to 5‰. In terms of ^{14}C age, this range of variability, ~240 ^{14}C years, is similar to that documented by Kennett & Ingram (1995) between the Bolling Allerod warm period (~15-13 kyr bp) and the Younger Dryas (13-11 kyr bp) cooling during the last deglacial. The onset of an approximately 30‰ trend towards heavier values in 1965 corresponds to the injection of "bomb ^{14}C" into the atmosphere by mid-century above ground nuclear weapons testing and subsequent

penetration into the surface ocean through air-sea gas exchange. There is little variability during the periods 1844-1860, and 1910-1960 with the exception of a 10‰ excursion towards lower $\Delta^{14}C$ during the two-year interval 1932-1933. Other similar excursions in SBBC 0110-3001 occur at the 1862-1863, 1874-1875 and 1990-1991 intervals with magnitudes between 7 and 30‰. In SBBC 080621-02 we observe 5-11‰ decreases in $\Delta^{14}C$ for the intervals 1987-1988, 1999-2000, 2004 and 2006. Based on the fraction of surface water ^{13}C Suess effect observed in the *C. cornuta* $\delta^{13}C$ record, we estimate that the $\Delta^{14}C$ value recorded by benthic foraminifera in the SBB would experience a 3.4‰ decrease over the industrial period (1890-2001)—a trend that is within analytical uncertainty. Thus, we assume that any diagenetic translation of the surface $\Delta^{14}C$ Suess effect is negligible and therefore not considered further as a potential driver of $\Delta^{14}C$ variability.

The $\Delta^{14}C$ time series from SBBC 080621-02 spanning 1985 to 2006 exhibits excursions towards lower $\Delta^{14}C$ values in 1989, 2001 and possibly 2005 with samples from 1997 and 2001-2004 having values of around -110‰. Extending the SBBC 0110-3001 time series with these newer measurements, we observe the continuation of the enrichment trend, now apparently peaking at 1995. The SBBC 080621-02 values are about 5‰ elevated relative to the SBBC 0110-3001 record.

1.4.4 Species-specific $\Delta^{14}C$

Five $\Delta^{14}C$ values were measured for *N. Stella* and three for *S. eckisi* (Figure 1.6b). Large error-bars for many of these measurements are due to the low sample sizes. All species-specific $\Delta^{14}C$ values are equal to or below the corresponding value from the mixed sample, with some pairs recording $\Delta^{14}C$ values significantly lower than those of

the mixed samples. This incongruity may reflect migration of individual benthic species from the depth horizon where they calcified at a shallower depth than that where they died. The offset in species specific versus mixed $\Delta^{14}C$ values for a given interval may also reflect the relatively short (i.e. months-long) benthic foraminiferal reproductive cycle and variation in the seasonal timing of peak abundance among different species (Bernhard & Reimers, 1991; Corliss & Silva 1993). However, by using a mixture of species integrated over a two-year period, we average out the effects of vertical migration and seasonal biases that might appear in the $\Delta^{14}C$ of individual species.

1.4.5 Consideration of diagenetic processes

In order to use $\Delta^{14}C$ as a hydrographic tracer, we must consider the possible influence of pore-water chemistry on observed $\Delta^{14}C$ variability. Sharp [DIC] (Stott *et al*., 2002; Berelson *et al*., 2005) and $\delta^{13}C$ (Stott *et al*., 2002) gradients reflect the influence of organic carbon (orgC) remineralization on the inorganic carbon chemistry of pore waters in the top 3 cm of the SBB sediment column. In order to estimate the upper limit pre-bomb (i.e. before the release of bomb ^{14}C) impact of remineralization on the $\Delta^{14}C$ of these pore waters, we employ the mass balance model posed by Bauer *et al*. (1995) (equation 1). Assuming negligible bioturbation (Bauer *et al*. 1995; Stott *et al*. 2002), this equation produces an estimate of $\Delta^{14}C$ of pore water at a given depth horizon (z).

$$\Delta^{14}C_{pw}(z) = \left(\frac{[DIC_{olw}]}{[DIC_{pw}](z)}\right)\Delta^{14}C_{olw} + \left(\frac{\left([DIC_{pw}](z) - [DIC_{olw}]\right)}{[DIC_{pw}](z)}\right)\Delta^{14}C_{source} \qquad (2.1)$$

Where the olw subscript denotes bottom water overlying the sediment water interface, the pw subscript denotes pore water values at a given sediment depth, and $\Delta^{14}C_{source}$ represents

the assigned $\Delta^{14}C$ value of respired photosynthate carbon. A detailed description of the model can be found in the supplementary materials. Below we describe the results of our upper-limit estimates for the influence of orgC remineralization on $\Delta^{14}C_{pw}$ in the upper 3 cm, which disqualify organic carbon remineralization as the dominant contributor to the observed $\Delta^{14}C$ variability.

Figure 1.7a shows pre-bomb, steady state change in $\Delta^{14}C_{pw}$, $\Delta\Delta^{14}C_{pw}$, due to orgC remineralization at discrete sedimentary depth horizons as calculated from equation 2.1. As $\Delta^{14}C_{pw}$ is partly a function of $\Delta^{14}C_{olw}$, we calculate $\Delta^{14}C_{pw}$ within an envelope of $\Delta^{14}C_{olw}$ values with the lowest value being the most depleted value recorded by benthic foraminifera, -160‰, and the highest value being that which we measured directly from the water column in 2008, -111‰ (Table 1.2). $\Delta^{14}C_{source}$ is set to the pre-bomb surface water $\Delta^{14}C$ value of -81‰ (Ingram & Southon, 1996; Pearson *et al*. 2000), the upper limit for this variable, and $[DIC_{pw}]$ is set according to the SBB profile measured by Berelson *et al*., (2005). We find that remineralization of orgC increases $\Delta^{14}C_{pw}$ by 3 - 11‰ at 0.7 cm and between 1 - 5‰ at 0.3 cm for the high and low and high end members of $\Delta^{14}C_{olw}$ respectively. These results suggest that the majority of benthic foraminifera below 0.7cm incur a 10‰ increase due to remineralization, whereas various lines of evidence, including $\delta^{13}C$ from this study, indicate that the majority of benthic foraminiferal calcification occurs above 0.5 cm.

The results above provide an estimate for the influence of remineralization assuming a constant oxidation rate of orgC (C_{ox}). However, studies from the Southern California Borderland Basins indicate that this rate has varied by as much as a factor of 2 over the last few centuries (Berelson & Stott 2003; Holsten *et al*., 2004; Stott *et al*., 2002;

Stott *et al*., 2000). In order to test whether an increase in C_{ox} would significantly affect the upper pore water $\Delta^{14}C$, we quantify the impact of an instantaneous doubling of C_{ox} on $\Delta^{14}C_{pw}$. We integrate under a best fit linear curve to the [DIC] profile of Berelson *et al*. (2005) (Figure 1.7b), double the area under the curve, and reevaluate the $\Delta^{14}C_{pw}$ profile from equation (1), assuming $[DIC_{olw}]$ remains constant (Figure 1.7c). For a $\Delta^{14}C_{olw}$ of -111.4‰ at 0.5 cm, $\Delta^{14}C_{pw}$ increases 2.80‰ from -107.5‰ to -104.7‰ and at 1.0 cm increases 4.2‰ from –104.4‰ to -100.2‰. The presence of lower $\Delta^{14}C$ bottom water enhances the sensitivity of upper pore water $\Delta^{14}C$ values to the products of C_{ox}-such that an instantaneous doubling of C_{ox} rate increases $\Delta^{14}C_{pw}$ by 7.2‰ and 10.9‰ at 0.5 and 1.0 cm, respectively, when $\Delta^{14}C_{olw}$ is set to -160‰.

An assumption of constant $\Delta^{14}C_{source}$ is only valid until the release of bomb ^{14}C in the mid 20th century. Surface $\Delta^{14}C$ values in the SCB peaked in the mid-1970s at nearly 300‰ above pre-bomb concentrations, lagging the peak in atmospheric concentrations by about a decade (Levin *et al*., 1985, Levin & Kromer, 1997) and has since reached ~30‰ in 2008 (Hinger *et al*., 2010). To generate a continuous, upper limit, record of post-bomb $\Delta^{14}C_{source}$, we annually interpolate documented values of SCB surface $\Delta^{14}C$ spanning the latter half of the 20th century with a cubic spline following Pearson *et al*. (2000). We assign $\Delta^{14}C_{olw}$ to be -143‰, the average pre-bomb $\Delta^{14}C$ value in our benthic record. Figure 1.8 shows the post-bomb evolution of upper pore water $\Delta^{14}C$ at depth horizons of 0.3 and 1.7 cm in the sediment as calculated from equation 2.1. We calculate that remineralization of bomb-enriched photosynthate material increases $\Delta^{14}C_{pw}$ by an upper limit of ~15‰ at 0.3 cm in the mid 1970s. By subtracting the calculated theoretical increase in pore water $\Delta^{14}C$ at this depth horizon, we can create a "bomb-corrected" $\Delta^{14}C$

record. We find that subtracting this increase does not fully eliminate the rising $\Delta^{14}C$ trend we observe after 1960 (Figure 1.8). As the calculated change in $\Delta^{14}C_{pw}$ due to the remineralization of bomb-enriched organic carbon is only an approximation subject to numerous assumptions and is dependant on the benthic $\Delta^{14}C$ data, the bomb-corrected record does not serve as a reconstruction of bottom water $\Delta^{14}C$ after 1960 but it does allow us to isolate the influence of hydrographic processes on observed $\Delta^{14}C$ variability in both the pre- and post-bomb portions of the record.

1.4.6 Consideration of hydrographic processes

Variability in the relative contribution of the two end-member water mass contributors to SBB source water has the potential to drive bottom water $\Delta^{14}C$ variability in the SBB. Figure 1.2 illustrates the spatial distribution of $\Delta^{14}C$ on the 26.88 kgm^{-3} and 26.95 kgm^{-3} isopycnal surfaces, which represent the extremes of SBB bottom σ_Θ recorded by the CalCOFI time series (Figure 1.4b). On the 26.88 kgm^{-3} isopycnal, water in the eastern tropical Pacific is depleted in $\Delta^{14}C$ by approximately 30‰ relative to the younger NPIW. This N/S gradient drops to approximately 20‰ on the 26.95 kgm^{-3} isopycnal. While these end-member horizontal $\Delta^{14}C$ gradients are on the order of variability observed in the benthic record, realization of their full 20-30‰ magnitude would require wholesale shifts in the contribution of these water masses to the deep SBB source water or a significant change in the ventilation state of either water mass to occur over one to two years.

Vertical mixing also has the potential to drive interannual to decadal scale $\Delta^{14}C$ variability in SBB bottom waters. The vertical $\Delta^{14}C$ gradient near the SBB is greatest at the depth of the western sill, as seen in the DIC $\Delta^{14}C$ profiles from stations 1, 5 and 10

along WOCE line P17C (Figure 1.1). Water above ~400m in these profiles is heavily enriched in ^{14}C by the presence of bomb ^{14}C and it is difficult to judge the extent to which this bomb transient has penetrated below this depth to date. Nevertheless, below the thermocline, a gradient of roughly 30 to 40 ‰ per 100 meters water depth should always have existed, assuming pre-bomb surface water values of –81 ± 5‰ (Robinson, 1981; Pearson *et al*., 2000).

We fit a smoothing spline to these profiles and evaluate the first derivative $d\Delta^{14}C/d\sigma_\Theta$, at every 0.01kgm^{-3} in order to calculate the theoretical change in $\Delta^{14}C$ that would occur in the SBB following the three strongest flushing events in the CalCOFI record at station 82 47 between 1986 and 2005. We define strength of flushing by the magnitude of potential density increase between two consecutive CalCOFI occupations. The change in $\Delta^{14}C$, or $\Delta\Delta^{14}C$, for stations 5 and 10 is determined by multiplying the observed rise in potential density by the calculated $d\Delta^{14}C/d\sigma_\Theta$ value corresponding to the average of potential density measured before and after the flushing event. For station 1, the shallowest of the three stations, we select the $d\Delta14C/ d\sigma_\Theta$ from the deepest potential density value recorded. We find that the decrease in $\Delta^{14}C$ associated with the three strongest flushing events is between 8 and 27‰, on the order of variability observed in the benthic radiocarbon record. While flushing events occur over a period of one to two months (Bograd *et al*., 2002; Liu 1979), each benthic sample represents $\Delta^{14}C$ integrated over 2 years. However, SBB bottom water σ_Θ tends to remain elevated following a flushing event and only gradually decreases over the next 2-3 years (Figure 1.1b) (Bograd *et al*., 2002). Therefore, the biennial resolution of the benthic $\Delta^{14}C$ record should be capable of capturing the $\Delta^{14}C$ impact of documented flushing events, particularly those

that leave a long-lived physical and chemical imprint. Although these calculations are based on both $\Delta^{14}C$ profiles and σ_Θ measurements representing a snap shot in time and not necessarily the mean chemical or physical state, they nevertheless demonstrate the possibility that relatively small changes in σ_Θ driven by vertical mixing could drive significant changes in $\Delta^{14}C$ at the depth of the SBB sill. Based on these results, we hypothesize that decreases in $\Delta^{14}C$ values correspond to periods of relatively strong upwelling along the SCM, when the isopycnal shoaling and vigorous equatorward flow necessary for basin flushing prevail.

In order to test this hypothesis, we first compare the bomb-corrected $\Delta^{14}C$ record from SBBC 0110-3001 to a time series of annually averaged monthly sea surface temperature anomalies (SSTa), between 1856 and 2001, for the 5º x 5º grid square of the Kaplan *et al*. (1998) data set centered on 32.5ºN, 122.5ºW. SSTa data were obtained from http://ingrid.ldgo.columbia.edu/SOURCES/.KAPLAN/.EXTENDED/.v2/.ssta/ (Reynold & Smith 1994; Kaplan *et al*., 1998) (Figure 1.9). We find a moderate yet significant positive correlation between these records ($r = 0.28$ $p < 0.001$) , such that low $\Delta^{14}C$ values correspond to negative SSTa, as expected during periods of enhanced upwelling. While this result is consistent with a potential link between upwelling and value of bottom water $\Delta^{14}C$, it is not diagnostic of regional or basin-scale processes responsible for this relationship. To uncover such processes, we must examine broader patterns of SSTa in relation to temporal $\Delta^{14}C$ variability. We therefore create two SSTa composites: one for intervals corresponding to the lowest 25% $\Delta\Delta^{14}C$ (i.e. the first difference between consecutive $\Delta^{14}C$ values in the raw $\Delta^{14}C$ record) values and one for intervals corresponding to the highest 25% $\Delta\Delta^{14}C$ values (Figure 1.10). The assignment of the

25% threshold is arbitrary, but allows for the objective selection of temporal subsets containing the same number of years, in this case 10, that reflect extremes in $\Delta\Delta^{14}C$. We choose to measure $\Delta\Delta^{14}C$ for two reasons: first, by capturing the local derivative, it eliminates the need to correct for the influence of bomb ^{14}C and second, $\Delta\Delta^{14}C$, as opposed to absolute value, should more accurately represent the change in $\Delta^{14}C$ that would be induced during a flushing event. Two coherent patterns of SSTa variability emerge: Years associated with a decrease in $\Delta^{14}C$ exhibit a horseshoe of strongly negative SSTa in the eastern subtropics, along the SCM and in the Gulf of Alaska, a patch positive SSTa in the central North Pacific and little variability in the tropical North Pacific (Figure 1.10b). This pattern closely resembles that generated by regressing North Pacific SSTa onto the NPGO climate index (Di Lorenzo *et al*., 2008). Years associated with an increase in $\Delta^{14}C$ exhibit positive SSTa along the western coast of North America and strongly positive SSTa in the central tropical Pacific with negative SSTa predominant the central North Pacific-a pattern similar to that associated with the PDO index (Mantua *et al*., 2007) but with greater tropical expression. The SSTa patterns generated by these $\Delta^{14}C$ composites suggest that the correspondence between $\Delta^{14}C$ fluctuations and local SSTa in driven by basin-scale mechanisms associated with modes of decadal North Pacific climate variability.

1.5 Discussion

Based on upper limit estimations, we find that pre-bomb orgC remineralization invokes an insufficient mass-balance isotopic effect on $\Delta^{14}C_{pw}$ to be the sole or dominant process responsible for driving SBB benthic $\Delta^{14}C$ variability. However, diagenesis may contribute to the $\Delta^{14}C$ offset between SBBC 0110-3001 and SBBC 080621-02. In a study

of molecularly uncharacterized organic carbon (MUC) in the Santa Barbara Basin, Roland *et al*. (2008) present resuspended slope sediments as the primary contributor to MUC in the bathyal SBB. Patchy distribution of these sediments in the deep SBB could lead to post-bomb inter-core $\Delta^{14}C$ offsets on the order observed between SBBC 0110-3001 and SBBC 080621-02. For example, remineralization of organic carbon fixed in the 1970s will have a greater impact on pore water $\Delta^{14}C$ than that of organic carbon fixed in the 1990s. Significant resuspension, however, is unlikely, as species of benthic foraminifera such as *Uvigerina juncea*, abundant on SBB slopes (Bernhard *et al*., 1997) are absent in both cores.

Second, post-bomb $\Delta^{14}C$ enrichment could be advected to the deep SBB as a preformed characteristic of NPIW. A $\Delta^{14}C$ record from deep-sea corals at 630-720 m in the Gulf of Alaska exhibits a ~30‰ increasing trend between 1960 and 1980, thought to be caused by entrainment of bomb ^{14}C to the interior North Pacific (Roark *et al*., 2005; Guilderson *et al*., 2006). The timing and magnitude of the trend observed in our record is consistent with advection of this entrained bomb ^{14}C to the SCM (Watanabe *et al*., 1994). Lacking further constraint on the impact of this advection on intermediate depth $\Delta^{14}C$ along the SCM, we cannot rule it out as a contributing factor to the trend we observe after 1960. However, we must still account for pre-bomb variability and interannual excursions within the post bomb portion of the record. We therefore determine that the 20-30‰ interannual variability in the $\Delta^{14}C$ record likely reflects changes in SBB bottom water $\Delta^{14}C$, unrelated to diagenesis or entrainment of bomb carbon.

If fluctuations in the ventilation of SBB source water were the primary driver of bottom water $\Delta^{14}C$ variability, we would expect periods with greater contribution from

old, poorly ventilated water from the tropical and subtropical North Pacific to be associated with lower $\Delta^{14}C$ values, and the reverse to be true for periods with greater contribution from well-ventilated water originating in the sub-polar North Pacific. This relationship between intermediate water $\Delta^{14}C$ along the SCM and Northeast Pacific water mass geometry is manifested over centuries to millennia during the Holocene (Roark *et al*., 2004) and last deglacial period (Kennett & Ingram, 1995; Galbraith *et al*., 2007; Marchitto *et al*., 2007). Kennett & Ingram (1995) cite lower ^{14}C age difference between concurrent benthic and planktonic foraminiferal pairs in the SBB as evidence for increased ventilation of SBB source water during the Last Glacial Maximum (LGM) (~18 kyr bp) and Younger Dryas (~13-11 kyr bp). The authors attribute this increased ventilation to Northern Hemisphere cooling, which resulted in a greater contribution of well-ventilated NPIW to the SCM. Using the $\Delta^{14}C$ values of benthic foraminifera, Marchitto *et al*. (2007) record two periods during which extremely old, poorly ventilated intermediate water that they suggest originated in the Southern Ocean, encroached upon the Baja California margin during Heinrich Event 1 (~18-14.5 kyr bp) and the Younger Dryas in accompaniment of diminishing Southern Hemisphere sea ice and increased Southern Ocean overturning.

Over shorter (interannual to decadal) timescales, enhanced poleward transport of poorly ventilated water by the California Undercurrent occurs during El Niño events (Lynn & Bograd, 2002; Bograd *et al*., 2001; Lynn *et al*., 1998) and the positive phase of PDO (Auad *et al*., 2003) when ocean-atmosphere interactions repress upwelling along the SCM. Therefore, warmer SSTa along the margin and possibly in the eastern tropical Pacific should accompany lower Δ14C values, which is opposite to the relationship we

observe in figures 1.9 and 1.10. Due to the 20-30‰ magnitude of the N/S $\Delta^{14}C$ gradient in the Northeast Pacific, wholesale shifts in end-member water mass contribution would be necessary to drive the $\Delta^{14}C$ variability observed in Figure 1.6. Our findings suggest that on shorter timescales, shifts in the ventilation of SBB source water analogous to those observed during the last deglacial result in subtle changes in $\Delta^{14}C$ that are overprinted by the competing influence of fluctuations in the vertical density structure.

We determine that flushing of the sub-sill SBB with relatively dense water could significantly decrease SBB bottom water $\Delta^{14}C$ (Table 1.3) due to the sharp vertical $\Delta^{14}C$ versus potential density gradient along the SCM (Figure 1.1). If vertical mixing along this gradient exerts the primary control on $\Delta^{14}C$ variability, then based on the arguments of Reimers *et al*. (1990) and Bograd *et al*. (2002) we would expect decreases in $\Delta^{14}C$ values to correspond to periods of stronger upwelling and equatorward transport, when isopycnals are shoaled along the SCM (Chaak & Di Lorenzo, 2007; Di Lorenzo, 2003;) and conditions are favorable for basin flushing. A comparison of the timing low $\Delta^{14}C$ excursions with documented flushing events is generally consistent with this proposed relationship. Sharp decreases in $\Delta^{14}C$ values obtained for the 1987-88 (SBBC 080621-02) and 1990-91 (SBBC 0100 3001) intervals occur during or directly following a strong 1988 flushing event. The $\Delta^{14}C$ decrease in SBBC 080621-02 corresponding to the 1999-2001 interval is coincident with the peak in bottom water density in 1999 following a strong flushing event in 1998. However not all documented flushing events appear to result in $\Delta^{14}C$ decreases. Weaker flushing events, such as those documented in 1993 and 1995 (Bograd *et al*., 2002) may result in only partial displacement of basin water, diminishing the mass balance impact of the low $\Delta^{14}C$ water entering the basin.

Furthermore, bottom water density does not remain elevated for the same amount of time following all flushing events. Densities remained high for two years following the 1988 and 1998 events (Figure 1.4), which may have allowed the low $\Delta^{14}C$ signal to be captured by the two-year integrated $\Delta^{14}C$ measurements. Signals of shorter duration, however, may be suppressed by the biennial sampling resolution. Nevertheless, comparison with the CalCOFI record of bottom water potential density suggests that $\Delta^{14}C$ can record strong basin flushing events.

Prior to the start of the seasonally resolved CalCOFI SBB time series in 1986, sub-surface dynamics along the SCM must be inferred from sea surface observations. The weakly positive correlation of $\Delta^{14}C$ with local SSTa (Figure 1.9) is consistent with $\Delta^{14}C$ being a tracer for vertical density structure and basin flushing. The correspondence of sharp decreases in $\Delta^{14}C$ in the 1870s and around 1900 with transitions from positive to negative SSTas indicate that vigorous upwelling and equatorward flow may have resulted in strong SBB flushing events during these times. Similar drops in $\Delta^{14}C$ corresponding to negative SSTa are suggestive of strong flushing events around 1910 and 1933. Upwelling will also reduce the $\Delta^{14}C$ of surface waters along the SCM (Masiello *et al*., 1998; Hinger *et al*., 2010) and therefore the $\Delta^{14}C$ of newly produced organic. However, we have shown that, particularly in the pre-bomb ocean, the influence of remineralization on pore water $\Delta^{14}C$ is insufficient to explain the full range of variability observed in Figure 1.6a.

The SSTa composites in Figure 1.10b and 10c provide additional insight into the ability of $\Delta^{14}C$ to trace modulations in vertical density structure. The composite in Figure 1.10b resembles a pattern similar to that derived by regressing North Pacific SSTa onto the NPGO climate index (Di Lorenzo *et al*., 2008). NPGO climate index is defined

spatially and temporally as the second empirical orthogonal function (EOF) and principle component (PC), respectively, of North Pacific sea surface height anomalies (SSHa) (Di Lorenzo *et al*., 2008). The NPGO index is strongly correlated to the second PC of North Pacific SSTa, and therefore uncorrelated to PDO. NPGO exerts a dominant influence on upwelling between 30ºN and 38ºN along the Northeast Pacific margin, as exhibited by its strong correlations with salinity, nutrients and upwelling in this region. Patterns of atmospheric circulation associated with the positive phase of NPGO drive a strengthening of the California Current (Di Lorenzo *et al*., 2008). The influence of NPGO on upwelling and equatorward transport is evident in the timing of SBB flushing events. The three strongest flushing events between 1986 and 2005 occur when NPGO is strongly positive. Although for two of these events PDO was also in its negative, upwelling-favorable phase, the strongest, documented between February and April 2003 (Figure 1.4b), occurred despite PDO being in its positive phase. The correspondence of decreasing $\Delta^{14}C$ with a SSTa pattern similar to that associated with the positive, upwelling-favorable, phase of NPGO is consistent with the hypothesis that periods of more frequent and vigorous flushing with dense water depleted in ^{14}C will facilitate decreases in $\Delta^{14}C$ of SBB bottom water that overprint horizontal transport of well ventilated water to the SCM.

The SSTa composite in Figure 1.10c, however, exhibits a pattern more closely resembling that associated with the positive phases of PDO and ENSO as opposed to the negative phase of NPGO as might be expected were its influence on $\Delta^{14}C$ symmetric. The presence of strong positive SSTa in the eastern and central tropical Pacific suggest that the atmospheric or oceanic forcing mechanisms associated with El Niño events play a

dominant role in elevating $\Delta^{14}C$ values in the deep SBB. Both of these forcing mechanisms are known to drive anomalous conditions in the surface and sub-thermocline CCS during El Niño events (Lynn & Bograd, 2002; Bograd *et al*., 2001; Lynn *et al*., 1998; Schwing *et al*., 2002). However, strong atmospheric teleconnections between the tropics and midlatitudes are absent during all El Niño events, even as positive SSHa are documented along the SCM (Lynn & Bograd, 2002). These SSH anomalies are attributed to the passage of coastally-trapped Kelvin waves propagating north from the eastern tropical Pacific (Lynn *et al*., 1995; Bograd *et al*., 2001; Lynn & Bograd, 2002; Lynn *et al*., 1998). The isopycnal compression that occurs during this passage could serve to increase $\Delta^{14}C$ in the deep SBB by pushing less dense water with higher $\Delta^{14}C$ values (Figure 1.2) towards to basin floor. This compression of the vertical density structure can be observed in the anomalous deepening of isopycnals over the SBB during the 1987 and 1998 El Niño events (Figure 1.1a). As the conditions that prevail during El Niño events tend to repress upwelling and weaken equatorward flow, we might expect $\Delta^{14}C$ values to remain unchanged during these periods due to lack of flushing. However, downwelling (compression of the vertical density structure) is the only mechanism we see that is capable of causing rapid increases in $\Delta^{14}C$ values on the order observed in the SBB benthic record.

1.6 Conclusions

We have measured $\Delta^{14}C$ of benthic foraminifera from the SBB at biennial resolution over the period 1827-2006, and assessed the role of orgC remineralization, source water partitioning and vertical density structure in driving observed $\Delta^{14}C$ variability. Using the mass-balance model of Bauer *et al*. (1995), we find that above the 1

cm depth horizon, where the majority SBB benthic foraminifera calcify (Holsten *et al*., 2004; Stott *et al*., 2002; Bernhard & Reimers, 1991), orgC remineralization and changes in Cox cannot invoke interannual $\Delta^{14}C_{pw}$ variability on the order observed in the benthic record. The moderate yet significant positive correlation between $\Delta^{14}C$ variability with local SSTa over the period 1856-2001 is in the opposite direction of that expected were shifts in the horizontal transport of end-member water masses to the SCM the primary driver of this variability. Negative SSTa are associated with lower values of $\Delta^{14}C$ despite the fact that during periods of increased upwelling, and anomalously cool SSTs along the SCM there is enhanced transport of younger, well ventilated NPIW relatively enriched in ^{14}C. We suggest that the N/S $\Delta^{14}C$ gradient in the Northeast Pacific is subtle enough that $\Delta^{14}C$ fluctuations generated by such shifts are overprinted by the competing effect of modulations in the local vertical density structure and their influence on basin flushing (Bograd *et al*., 2002). This hypothesis is consistent with the SSTa composite for intervals with the lowest $\Delta^{14}C$ tendencies resembling a pattern associated with the positive phase of NPGO (Di Lorenzo *et al*., 2008) and that for intervals with the highest $\Delta^{14}C$ tendencies containing similarities with the patterns associated with the positive phases of ENSO and PDO. Based on these findings, we propose that the isopycnal shoaling during periods of enhanced upwelling along the SCM draws up denser water with relatively low $\Delta^{14}C$ values to the depth of the SBB western sill. The presence of less dense water in the basin below sill depth can facilitate a flushing event (Bograd *et al*., 2002), resulting in the displacement of stagnant water and a decrease in $\Delta^{14}C$ values of DIC at the basin floor. The passage of oceanic Kelvin waves along the SCM during El Niño events compresses

isopycnals above the SBB, pushing water relatively enriched in ^{14}C to deeper depths within the basin.

Foraminiferal $\Delta^{14}C$ values from the SBB and elsewhere along the northeast Pacific margin have proven an important tracer for intermediate water mass geometry and transport during the Holocene and deglacial periods (Kennett & Ingram, 1995; Roark *et al*., 2004; Galbraith *et al*., 2007; Marchitto *et al*., 2007). These studies exploit the N/S horizontal $\Delta^{14}C$ gradients to detect centennial to millennial scale shifts in the contributions of end-member water masses with disparate ventilation states to the interior northeast Pacific. Although analogous shifts of smaller magnitude have been proposed to occur as result of decadal scale fluctuations in north Pacific climate (Auad *et al*., 2003) our findings suggest that, on these shorter time periods, $\Delta^{14}C$ values in the SBB is more sensitive to the changes in the vertical density structure invoked by these fluctuations, with subtle changes in potential density as small as 0.03 kgm^{-3} resulting in significant changes in $\Delta^{14}C$. This sensitivity may allow $\Delta^{14}C$ to trace sub-surface dynamics associated with the interannual and decadal scale atmospheric and oceanic processes that force documented patterns of anomalies at the sea surface. However, a more thorough understanding of the drivers of decadal scale $\Delta^{14}C$ variability and its ability to reflect these processes requires additional time series from within enclosed basins and at exposed marginal locations along the northeast Pacific margin over the past few centuries.

Chapter 1:, in part, will be submitted for publication to the Journal of Geophysical Research-Oceans. Roach, L.D.; Field, D.B; Guilderson, T.P; Charles, C.D. The dissertation author was the primary investigator and author of this paper.

Table 1.1 SBB Benthic Foraminifera Species Specific $\delta^{13}C$ Averages

Species	Mean $\delta^{13}C$	N
Bolivina argentea	-0.813	2
Cassidulinoides cornuta	-0.886	16
Seggrunda eckisi	-1.547	3
Loxostomum pseudobeyrichi	-1.722	1
Nonionella stella	-1.905	3
Bolivina seminuda	-2.013	3
Buliminella tenuata	-2.171	1
Chilostomella ovoidea	-3.736	9

Table 1.2 Water Sample $\Delta^{14}C$ from Center Santa Barbara Basin and Western Sill

Sample Name	Station Location	Latitude	Longitude	Depth (m)	Date Collected	$\Delta^{14}C$ (‰)	± (‰)
1A-579-1	Basin	34.226ºN	120.033ºW	579	June, 2008	-111.4	3.1
1A-475-3	Basin	34.226ºN	120.033ºW	475	June, 2008	-96.5	3.0
2-500-21	Sill	34.300ºN	120.800ºW	500	June, 2008	-109.6	3.0
2-475-2	Sill	34.300ºN	120.800ºW	475	June, 2008	-106.9	3.3
2-450-23	Sill	34.300ºN	120.800ºW	450	June, 2008	-96.4	3.0

Table 1.3 $\Delta\Delta^{14}C$ Corresponding to Three Strongest SBB Flushing Events Since 1986[a]

Year	Month 1[b]	Month 2	$\Delta\sigma_\Theta$ (kgm^{-3})	$\Delta\Delta^{14}C$ (‰)[c]		
				station 1[d]	station 5	station 10
2003	February	April	0.055	-26.64	-17.64	-18.03
1998	February	April	0.031	-10.16	-9.94	-15.01
1987/88	November	January	0.024	-9.87	-7.70	-11.62

[a] strength of flushing event determined by the change in SBB bottom σ_Θ (the deepest σ_Θ measurement of the cast) between two successive CalCOFI occupations of station 82 47.
[b] month 1 and Month 2 represent the two months CalCOFI visited station 82 47 between which the flushing event occurred.
[c] $\Delta\Delta^{14}C$ represents the change in $\Delta^{14}C$ associated with the corresponding change in σ_Θ during the flushing event. These values are derived from $\Delta^{14}C$ vs. σ_Θ profile from the respective WOCE stations.
[d] stations 1, 5 and 10 are stations along WOCE line P17C.

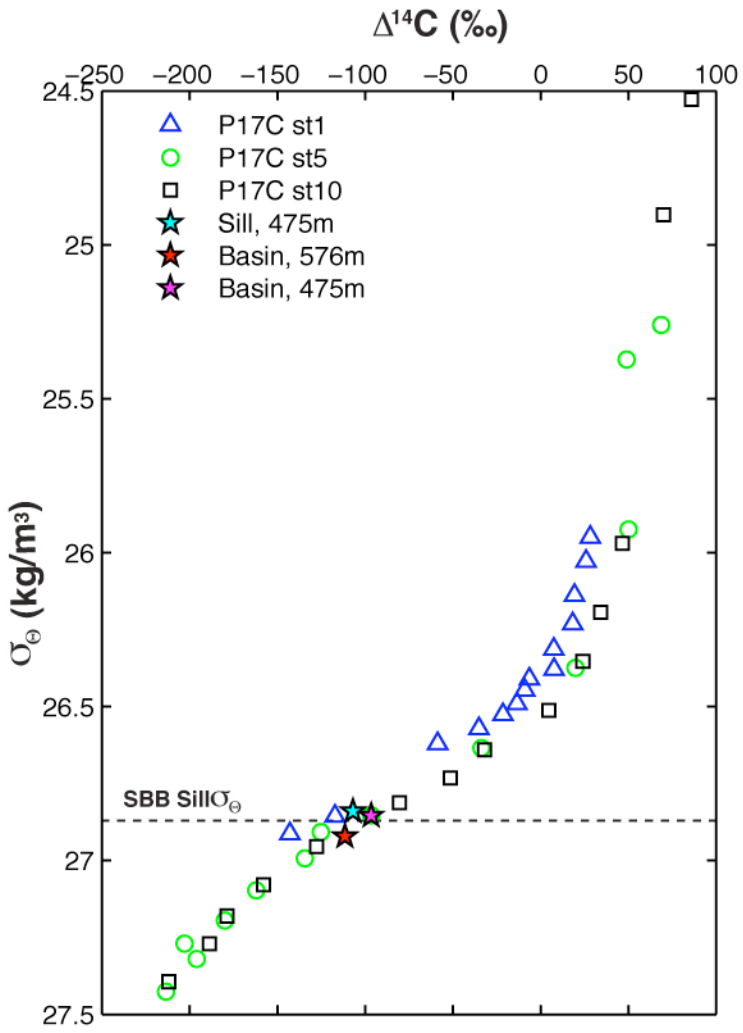


Figure 1.1 Profile of $\Delta^{14}C$ versus potential density for three WOCE stations near the Santa Barbara Basin and specific depths in the SBB and at the western sill measured in this study. WOCE stations correspond to stations along line PC17C (Figure 1.3). Sill and Basin values from samples collected approximately at CalCOFI stations 80 55 and 82 47 respectively in June 2008**.** Note that the $\Delta^{14}C$-σ_Θ gradient is greatest at ~26.9 kgm^{-3}, the isopycnal that baths the western sill of the Santa Barbara Basin at ~475 m (indicated by dashed line) as recorded by CalCOFI occupations of station 80 55 since 1986.

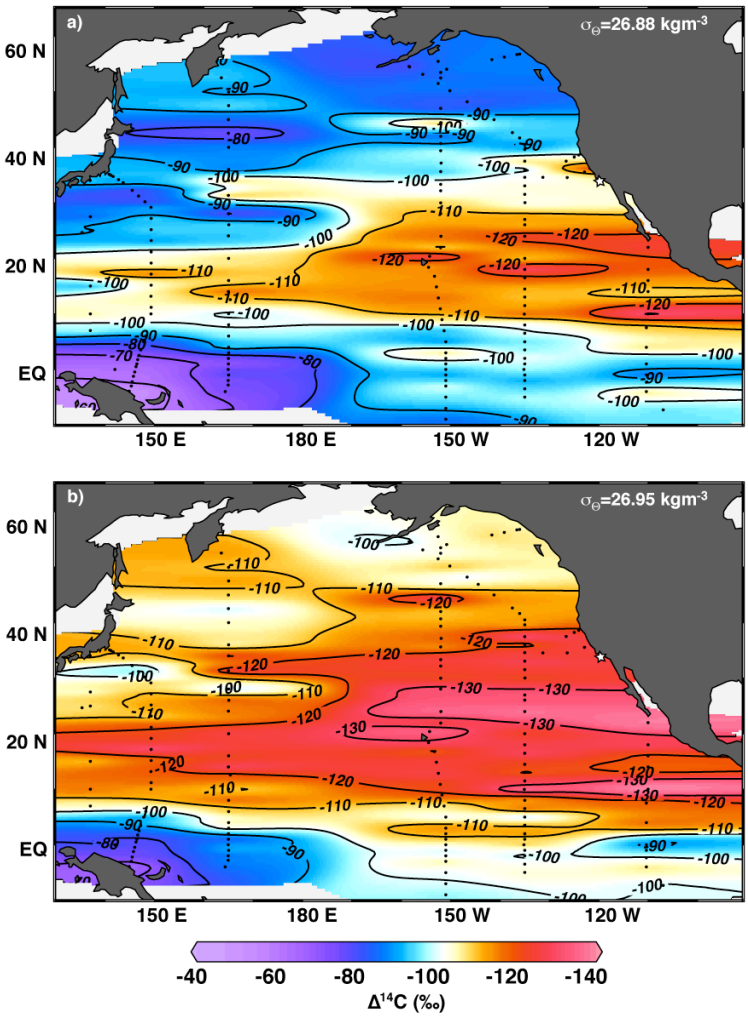


Figure 1.2 North Pacific distribution of $\Delta^{14}C$ on the σ_Θ = 26.88 kgm^{-3} (a) and σ_Θ = 26.95 kgm^{-3} (b) isopycnal surfaces measured at WOCE stations (shown in black dots) between 1991 and 1996. Latitudinal transects from west to east correspond to WOCE lines P08, P10, P13, P16, P17N, P17C, P18 respectively. These isopycnals represent the low and high extremes of potential density recorded by CalCOFI in the SBB bottom since 1986 (Figure 1.4b). The location of the SBB is indicated with a white star. The oldest waters, those most depleted in $\Delta^{14}C$, on both surfaces are found in the eastern subtropics. However, the N/S $\Delta^{14}C$ gradient along the eastern margin is ~20‰ greater on the 26.88 kgm^{-3} isopycnal than the denser isopycnal.

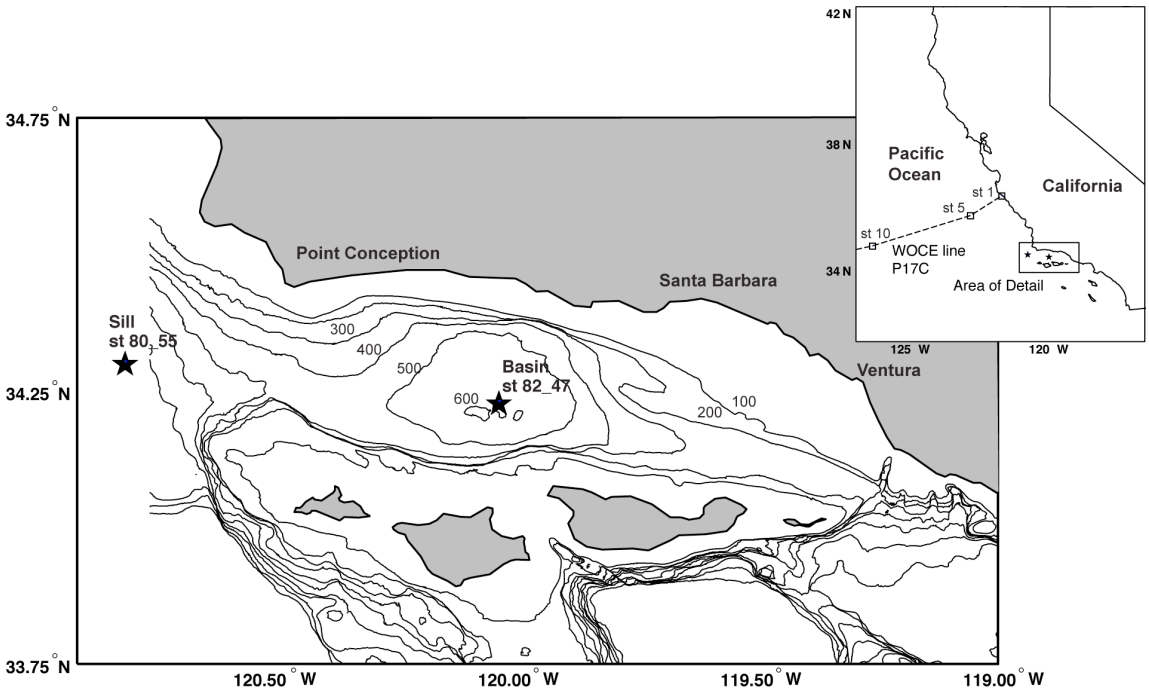


Figure 1.3 Map of Santa Barbara Basin depicting locations of CalCOFI stations 82 47 and 80 55 (stars). Soutar Box cores SBBC 0110-3001 and SBBC 080621-02 were collected at the location of station 82 47. Bathymetric contour interval is 100 meters. Inset map shows locations of three proximal WOCE stations from line P17C. Basin bottom water consists of a combination of relatively well ventilated North Pacific Intermediate Water (NPIW) and poorly ventilated water advected from the eastern equatorial Pacific, which enter the basin from the north and south, respectively, flowing over the western sill at ~475 m. Surface circulation in the Southern California Bight is dominated by the poleward flowing California Counter Current while the core of the equatorward California Current sits farther offshore.

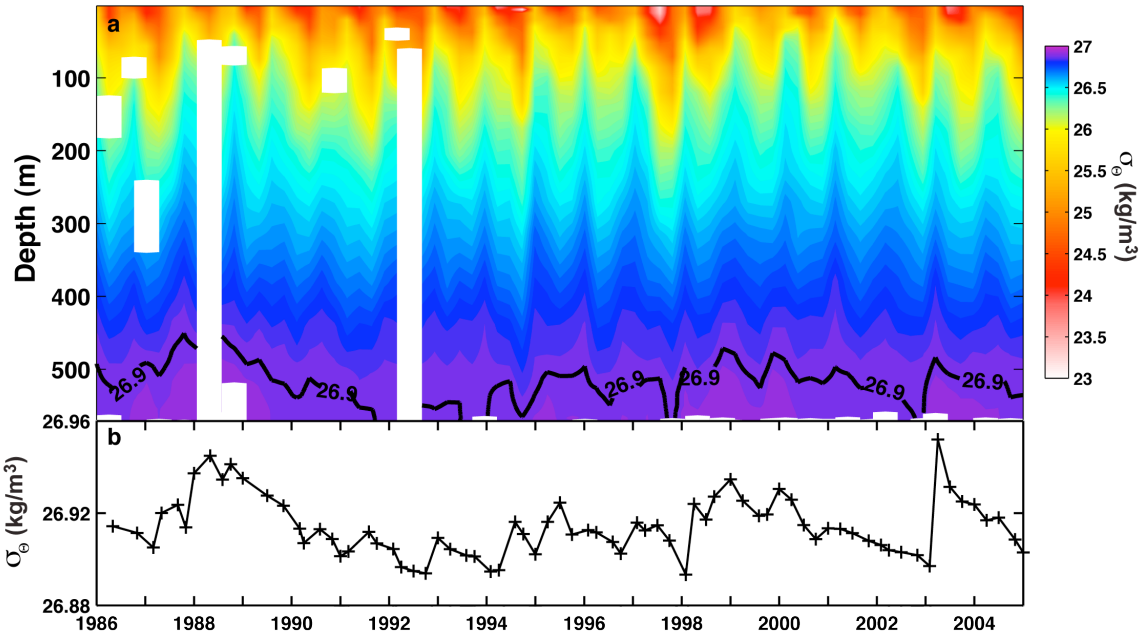


Figure 1.4 Potential density measurements from CalCOFI surveys at station 82 47 (central SBB) 1986-2005. Time evolution of the potential density profile with the depth of the 26.9 kgm^{-3} isopycnal contoured in the bold black line (a) and time series of SBB bottom water potential density (bottommost measurement from each cast) (b). Although it is most pronounced in the upper 200m, the seasonal pattern of isopycnal shoaling and deepening extends to bottom of the SBB, as evidenced by the fluctuations in the 26.9 kgm^{-3} isopycnal and the SBB bottom potential density.

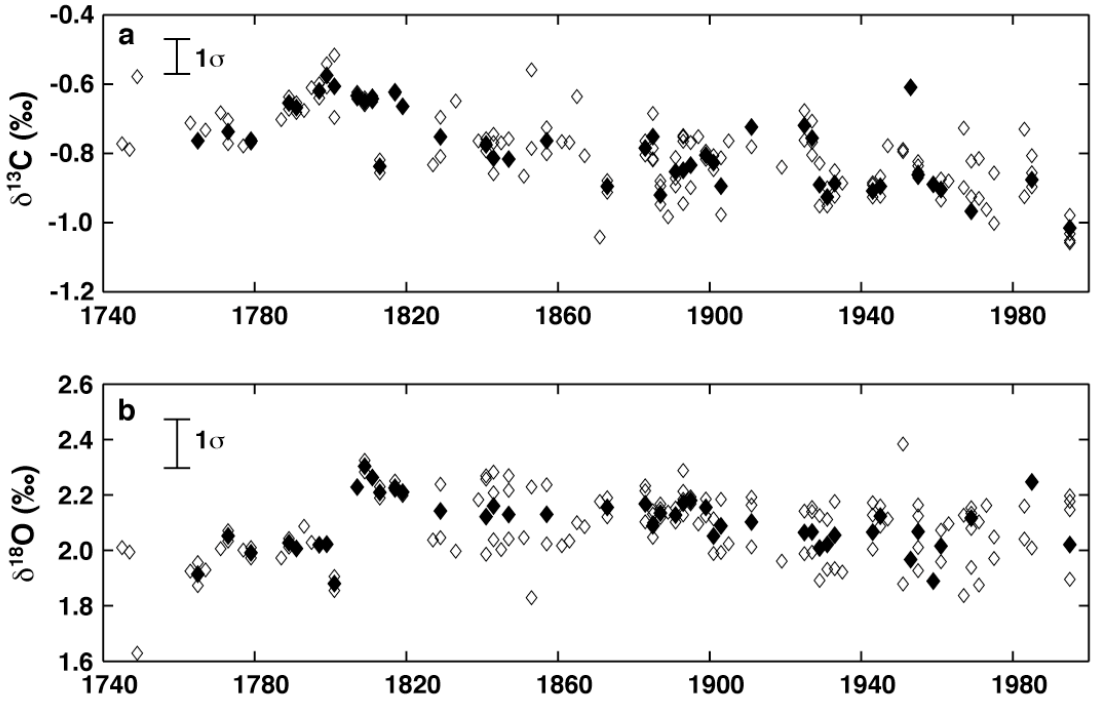


Figure 1.5 $\delta^{18}O$ (a) and $\delta^{13}C$ (b) from the Santa Barbara Basin spanning 1744-2001 measured from the tests of benthic foraminifera *Cassidulinoides cornuta*. Open symbols represent raw values and closed symbols represent averages of the first two of replicate measurements. 1σ bars from all replicate measurements (N = 48) are shown in the upper left corner of each graph.

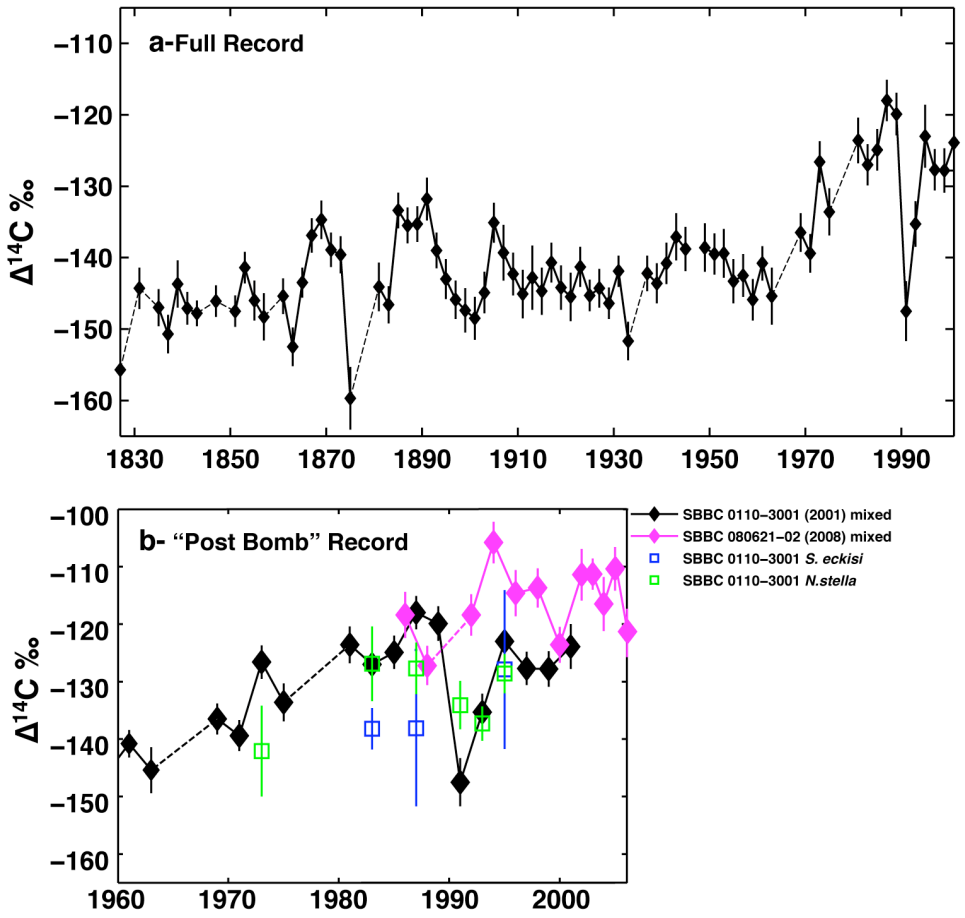


Figure 1.6 (a) Record of mixed benthic foraminiferal $\Delta^{14}C$ (see text for description of species used for $\Delta^{14}C$ samples) from box core SBBC 0110-3001 spanning 1827-2001. Values adjacent to missing values are connected with a dashed line. (b) The same record as above spanning 1960-2001 (black line) and the $\Delta^{14}C$ record from SBBC 080621-02 spanning 1994-2006 (pink line) with $\Delta^{14}C$ values from species-specific values shown in open symbols (blue-*S. eckisi*, green-*N. stella*).

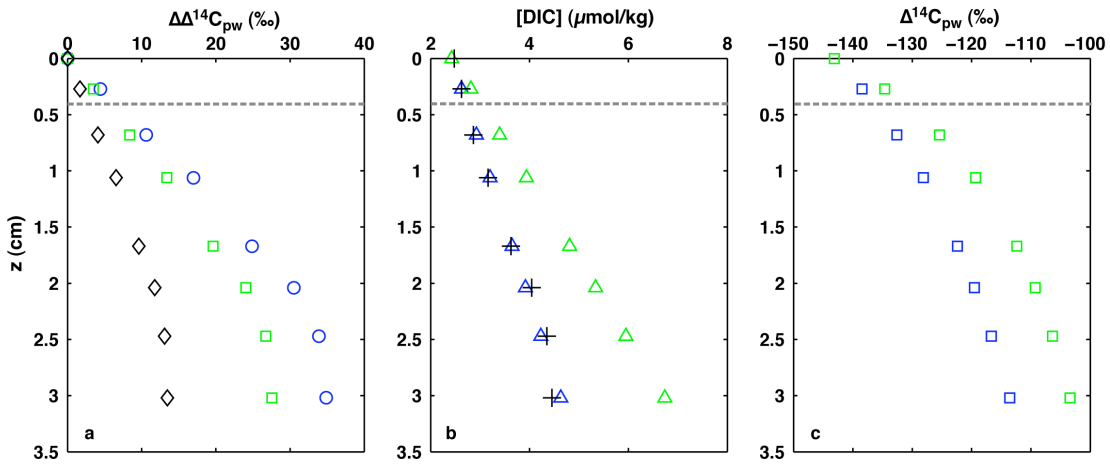


Figure 1.7 Results of modeling exercises investigating the influence of remineralization on $\Delta^{14}C_{pw}$ in the top 3.1 cm of central SBB sediments. The grey dashed line represents the 0.4 cm depth horizon above where 90% of benthic foraminifera in the central (deep) SBB are constrained to live (Bernhard & Reimers, 1991; Holsten *et al*., 2004 Berelson & Stott 2003) and the majority benthic foraminifera in this study calcified, as indicated by $\delta^{13}C$ values of their tests. (a) Modeled change in pore water $\Delta^{14}C$ ($\Delta\Delta^{14}C$pw) resulting from addition of respired DIC to the pore water DIC pool as a function of overlying water $\Delta^{14}C$ (i.e. $\Delta^{14}C$ at the sediment water interface, z=0). Different symbols refer to assigned bottom water values: diamonds, $\Delta^{14}C$olw = -160‰, the minimum value observed in the pre-bomb benthic record, squares, $\Delta^{14}C$ = 143‰, the mean value observed in the pre-bomb benthic record and circles, $\Delta^{14}C$ = -111‰, the modern value measured from the water column in 2008. (b) Increase of modeled [DIC] at discreet depth intervals as a result of an instantaneous doubling of carbon oxidation rate (Cox). Cross hatches are measured [DIC] from Berelson *et al*. (2005), blue triangles a linear fit to measured values, and green triangles [DIC] following Cox doubling. (c) The $\Delta^{14}C_{pw}$ at discrete depth horizons measured from equation (1) before (blue squares) and after (green squares) an instantaneous doubling of Cox, where $\Delta^{14}C_{olw}$ is assumed to be the mean value observed in pre-bomb benthic record.

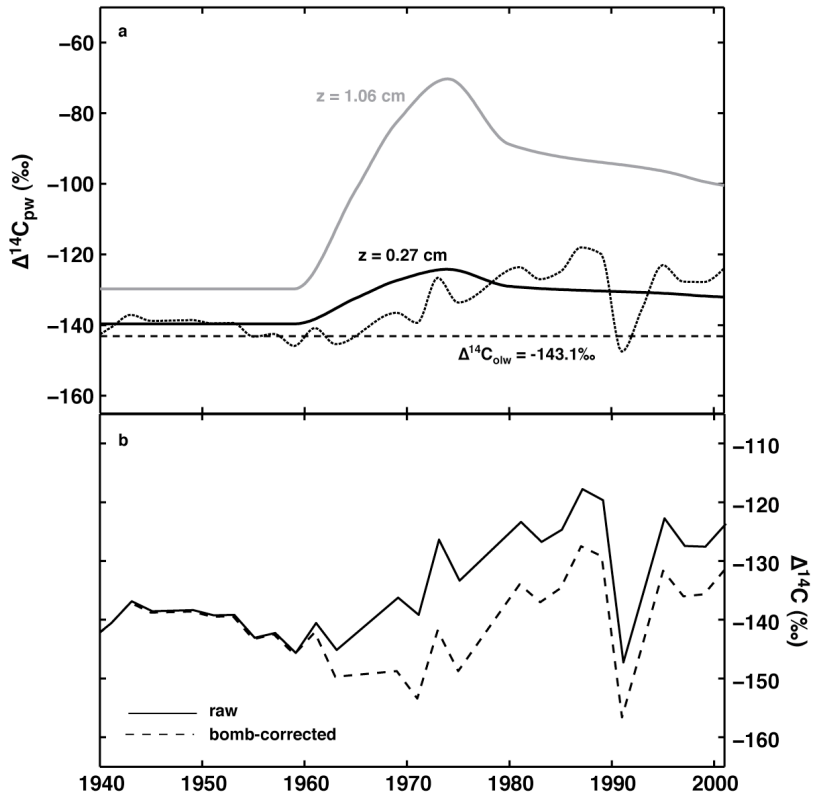


Figure 1.8 (a) Modeled evolution of upper SBB pore water $\Delta^{14}C$ at sedimentary depths of 0.27 cm (solid black line) and 1.06 cm (solid grey line) under the incorporation of bomb ^{14}C, assuming $\Delta^{14}Colw$ of -143.1‰, the mean value over the pre-bomb benthic record. [DIC] used in calculation from Berelson *et al*. (2005). Dotted line shows benthic $\Delta^{14}C$ record and dashed line $\Delta^{14}Colw$. Inset figure: Interpolated evolution of SCB surface water (dashed line), and atmospheric $\Delta^{14}C$-CO2 (solid line) both from Pearson *et al*. (2000) and refs therein. (b) Raw (solid line) and bomb-corrected (dashed line) benthic $\Delta^{14}C$ records between 1940 and 2001. Bomb correction was derived by subtracting the increase of modeled $\Delta^{14}C_{pw}$ values at 0.27cm shown in **a)** from the measured values.

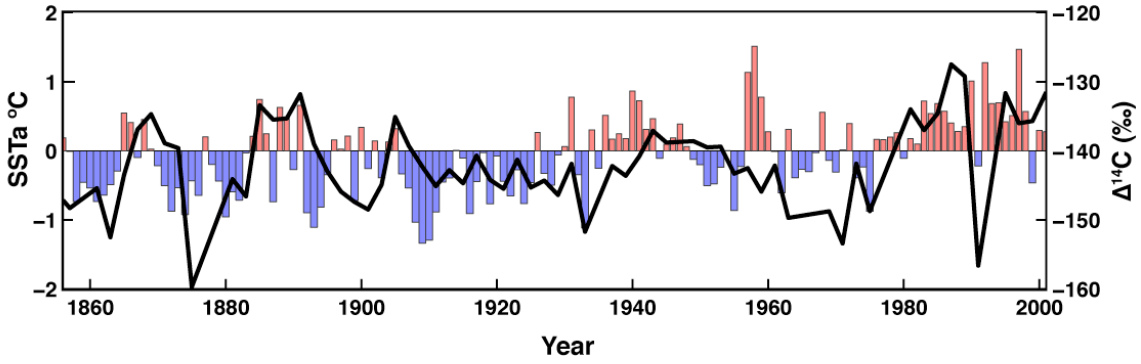
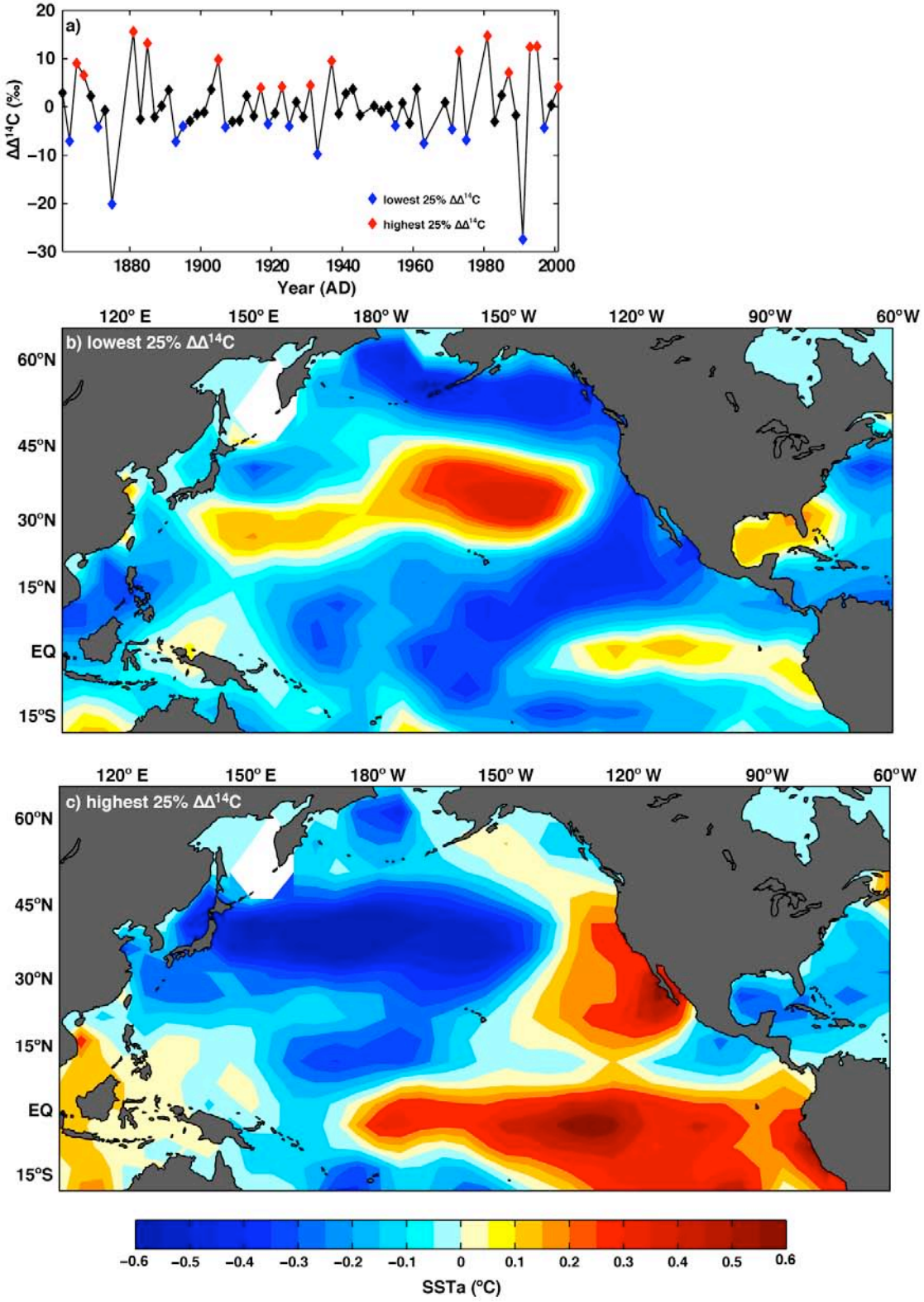


Figure 1.9 Comparison of bomb-corrected $\Delta^{14}C$ (thick black line) with April-July averaged SSTa from the 32.5ºN 122.5ºW grid square of the Kaplan OS SSTa record (bars).

Figure 1.10 (a) The first difference ($\Delta\Delta^{14}C$) of SBB benthic $\Delta^{14}C$ record 1857-2001. $\Delta\Delta^{14}C=\Delta^{14}C(t)-\Delta^{14}C(t-1)$ where t corresponds to the single "central year" selected to represent each biennial sampling interval. The lowest (highest) 25% (N=15) of $\Delta\Delta^{14}C$ values plotted in blue (red), representing intervals in which a significant decrease (increase) in $\Delta^{14}C$ relative to the previous interval was recorded by SBB benthic foraminifera. (b) Composite of April – July monthly SSTas (Kaplan *et al*., 1998; Reynold & Smith, 1994) from years corresponding to the lowest 25% of $\Delta\Delta^{14}C$ values. This composite exhibits anomalously cool SSTs along the eastern North Pacific Margin and Gulf of Alaska with anomalously warm SSTs in the eastern central North Pacific between 20ºN and 45ºN. This SSTa pattern resembles that associated with the positive phase of NPGO, and is indicative of increased strength of the California and Alaska Currents and enhanced upwelling along the SCM. Note the lack tropical SSTa expression. (c) Same as in (b) but for years corresponding to the highest 25% $\Delta\Delta^{14}C$ values. This composite exhibits strongly positive SSTas in the eastern and central tropical Pacific as well as along the Southern California and Baja California margins. Cool SSTas appear throughout the central North Pacific. This SSTa pattern is similar to that associated with the positive phases of ENSO and PDO, associated with a weakened California, strengthened Alaska current and diminished upwelling along the SCM. The tropical SSTa expression is suggestive of a remote forcing on the mechanisms that drive $\Delta^{14}C$ up in the SBB.


a)
20
10
0
−10
−20
−30
ΔΔ14C (‰)
1880
1900
1920
1940
1960
1980
2000
Year (AD)
lowest 25% ΔΔ14C
highest 25% ΔΔ14C
120° E
150° E
180° W
150° W
120° W
90°W
60°W
b) lowest 25% ΔΔ14C
60°N
45°N
30°N
15°N
EQ
15°S
c) highest 25% ΔΔ14C
−0.6
−0.5
−0.4
−0.3
−0.2
−0.1
0
0.1
0.2
0.3
0.4
0.5
0.6
SSTa (°C)

1.7 References

Auad, G. (2003) Interdecadal dynamics of the North Pacific Ocean. *J. Phys. Oceanogr.* 33:2483-2503.

Auad, G., Kennett, J.P., and Miller, A.J. (2003) North Pacific intermediate water response to a modern climate shift. *J. Geophys. Res.* 108:doi:10.1029/2003JC001987.

Banks, H.T., Wood, R.A., Gregory, J.M., Johns, T.C., and Jones, G.S (2000) Are observed decadal changes in intermediate water masses a signature of anthropogenic climate change? *Geophys. Res. Lett.* 27:2961-2964.

Bauer, J.E., Reimers, C.E., Druffel, E.R.M. and Williams, P.M. (1995) Isotopic constrains on carbon exchange between deep ocean sediments and sea water. *Nature.* 373:686-689

Behl, R.J. and Kennett, J.P. (1996) Brief interstadial events in the Santa Barbara Basin, NE Pacific, during the past 60 kyr. *Nature* 379:243-246

Berelson, W.M. (1991) The flushing of two deep-sea basins, southern California borderland, *Limnol. Oceanogr*. 36:1150-1166

Berelson, W.M., Prokopenko, M., Sansone, F.J., Graham, A.W., McManus, J. and Bernhard, J.M. (2005) Anaerobic diagenesis of silica and carbon in continental margin sediments: Discrete zones of TCO2 production. *Geochem. Cosmochim. Acta* 69:4611-4629.

Berelson, W.M., and Stott, L.D. (2003) Productivity and organic carbon rain to the California margin seafloor: Modern and paleoceanographic perspectives. *Paleoceaongraphy* 18:doi:10.1029/2001PA000672.

Bernhard, J.M., Buck, K.R., Farmer, M.A., and Bowser, S.S. (2000) The Santa Barbara Basin is a symbiosis oasis. *Nature* 404:77-80

Bernhard, J.M., Sen Gupta, B.K., and Borne, P.F. (1997) Benthic foraminiferal proxy to estimate dysoxic bottom-water oxygen concentrations: Santa Barbara Basin, U.S. Pacific continental margin. *J. Foram. Res*. 27:301-301.

Bograd, S.J., Schwing, F.B., Castro, C., and Timothy, D.A. (2002) Bottom water renewal in the Santa Barbara Basin, *J. Geophys. Res*. 107, doi:1029/2001JC001291

Bograd, S.J., Chereskin, T.K., and Roemmich, D. (2001) Transport of mass, heat, salt, and nutrients in the southern California Current System: Annual cycle and interannual variability. *J Geophys. Res.* 106:9255-9275.

Bray, N.A., Keyes, A. and Morawitz, W.M.L. (1999) The California Current system in the southern California Bight and the Santa Barbara Channel. *J. Geophys. Res.* 104:7695-7714.

Broecker, W.S., Clark, E., Hajdas, I, and Bonani, G., (2004) Glacial ventilation rates for the deep Pacific Ocean, *Paleoceanography* 19:doi 1029/2003PA000974

Cannariato, K.G., Kennett, J.P. and Behl, R.J. (1999) Biotic response to late Quaternary rapid climate switches in Santa Barbara Basin: ecological and evolutionary implications, *Geology* 27: 63-66

Chhak, K., Di Lorenzo, E. (2007) Decadal variations in the California Current upwelling cells. *Geophys. Res. Let.* 34:doi:10.1029/2007GL030203.

Chelton, D.B., and Davis, R.E. (1982) Monthly mean sea-level variability along the west coast of North America. *J. Phys Oceanogr.* 12:757-784.

Clarke, A. J., and Van Gorder, S. On ENSO coastal currents and sea levels. *J. Phys. Oceanogr.* 24:661-680.

Deser, C., Alexander, M.A., and Timlin, M.S. (1996) Upper-ocean thermal variations in the North Pacific during 1970-1991, *J. Climate*, 9:1840-1855.

Di Lorenzo, E. (2003) Seasonal dynamics of the surface circulation in the southern California Current System. *Deep-Sea Res. II* 50:2371-2388.

Di Lorenzo, E., Schneider, N., Cobb, K.M., Franks, P.J.S., Chhak, K., Miller, A.J., *et al.* (2008) North Pacific Gyre Oscillation links ocean climate and ecosystem change. *Geophys. Res. Lett.* 35:doi:10.1029/2007GL032838.

Druffel, E.R.M, Griffin, S., Beaupre, S.R., and Dunbar, R.B. (2007) Oceanic climate and circulation changes during the past four centuries from radiocarbon in corals. *Geophys. Res. Lett.* 34:doi:10.1029/2006GL028681.

Druffel, E.R.M (1997) Pulses of rapid ventilation in the north Atlantic surface ocean during the past century. *Science* 275:1454-1457.

Druffel, E.R.M. (1981) Radiocarbon in annual coral rings from the eastern tropical Pacific Ocean. *Geophys. Res. Lett.* 8:59-62.

Druffel, E.R.M. and Griffin, S. (1993) Large variations of surface ocean radiocarbon: evidence of circulation changes in the southwestern Pacific. *J Geophys. Res.* 98:20,249-20,259.

Emery, K.O. (1954) Source of water in basins off Southern California. *J. Marine Res.* 13:1-21.

Emery, K.O. and Hulsemann, J. (1962) The relationship of sediments, life, and water in a marine basin. *Deep-Sea Res.* 8:165-180.

Enfield, D.B., and Allen, J.S. (1980) On the structure and dynamics of monthly mean sea level anomalies along the Pacific coast of North and South America. *J. Phys. Oceanogr.* 10:557-578.

Field, D.B. and Baumgartner, T.R. (2000), A 900 year stable isotope record of interdecadal and centennial change from the California Current, *Paleoceanography*, 15, 695–708.

Field, D.B., Baumgartner, T.R., Charles, C.D., Ferriera, V., and Ohman, M.D. (2006) Planktonic foraminifera in the California Current reflect twentieth century warming, *Science* 311:63-66.

Galbraith, E.D., Jaccard, S.L., Pedersen, T.F., Signam, D.M., Haug, G.H., Cook, M., Southon J.R., and Francois, R. (2007) Carbon dioxide release from the North Pacific abyss during the last deglaciation. *Nature* 449:890-894.

Gruber, N., Keeling, C.D., Bacastow, R.B., Guenther, P.R., Lueker, T.J., Wahlen, M. *et al.* (1999) Spatiotemporal patterns of carbon-13 in the global surface oceans and the oceanic Suess effect. *Global Biogeochem. Cy.* 13:307-335.

Guilderson, T.P., Roark, E.B., Quay, P.D., Flood Page, S.R. and Moy, C. (2006) Seawater radiocarbon evolution in the Gulf of Alaska: 2002 observations. *Radiocarbon* 48:1-15.

Guilderson, T.P. and Schrag, D.P. (1998) Abrubpt shift in subsurface temperatures in the tropical Pacific associated with Changes in El Niño. *Science* 281:240-243.

Harman, R.A. (1964) Distribution of foraminifera in the Santa Barbara Basin, California. *Micropaleontology* 10:81-96.

Hendy, I.L., and Kennett, J.P. (2003) Tropical forcing of north Pacific intermediate water distribution during late Quaternary rapid climate change? *Quat Sci Rev.* 22:673-689.

Hickey, B.M. 1979. The California Current system—hypotheses and facts. *Prog. Oceanogr.* 8:191-279.

Hinger, E.N., Santos, G.M., Druffel, E.R.M. and Griffin, S. (2010) Carbon measurements of surface seawater from a time-series site off southern California. *Radiocarbon* 52:69-89.

Holsten, J., Stott, L. and Berelson, W. (2004) Reconstructing benthic carbon oxidation rates using d13C of benthic foraminifers. *Mar. Micropaleontol. 5*3:117-132.

Kaplan, A. Cane, M.A., Kushnir, Y. Clement, A.C., Blumenthal, M.B., and Rajagopalan, B. (1998) Analyses of global sea surface temperature 1856-1991. *J. Geophys. Res.* 103:18,567-18,589.

Kennett, J.P. and Ingram, B.L. (1995), A 20,000-year record of ocean circulation and climate change from the Santa Barbara Basin, *Nature*, 377, 510-514

Keigwin, L.D. and Jones, G.A., (1990) Deglacial climatic oscillations in the Gulf of California, *Paleoceanography*, 5, 1009-1023

Levin, I. and Kromer, B. (1997) Twenty years of atmospheric $^{14}CO2$ observations at Schauinsland. *Radiocarbon* 39:205-218.

Levin, I., Kromer, B., Schoch-Fischer, H., Bruns, M., Munnich, M., Berdau, D., Vogel, J.C., and Munnich, K.O. (1985) 25 years of tropospheric ^{14}C observations in central Europe. *Radiocarbon* 27:1-19.

Liu, K.-K. (1979) Geochemistry of inorganic nitrogen compounds in two marine environments: The Santa Barbara Basin and the ocean off Peru. Ph.D. thesis, 354 pp., Univ of Calif, Los Angeles.

Lynn, R.J., and Simpson, J.J. (1987) The California Current System: The seasonal variability of its physical characteristics. *J. Geophys. Res.* 92:12,947-12,966.

Lynn, R.J., and Simpson, J.J. (1990) The flow of the Undercurrent over the continental borderland off southern California. *J Geophys. Res.* 95:12,995-13,008.

Lynn R.J. *et al.* (1998) State of the California Current, 1997-1998: transition to El Niño conditions. CalCOFI Report, 39:25-49.

Lynn, R.J., Schwing, F.B., and Hayward, T.L. (1995) The effect of the 1991-1993 ENSO on the California Current System. CalCOFI Report 36:57-71.

Lynn, R.J. and Bograd, S.J. (2002) Dynamic evolution of the 1997-1999 El Niño-La Niña cycle in the southern California Current System. *Prog. Oceanog*r. 54:59-75.

Lynn, R.J., Bograd, S.J., Chereskin, T.K. and Huyer, A. (2003) Seasonal renewal of the California Current: The spring transition off California. *J. Geophys. Res.* 108:doi:10.1029/2003JC001787.

Masiello, C.A., Druffel, E.R.M., and Bauer, J.E. (1998) Physical controls on dissolved inorganic radiocarbon variability in the California Current. *Deep-Sea Res. II* 45:617-642.

Mantua, N.J., Hare, S.R., Zhang, Y., Wallance, J.M. and Francis, R.C. (1997) A Pacific interdecadal climate oscillation with impacts on salmon production. *Bull. Am. Meteorol. Soc.* 78:1069-1079.

Marchitto, T.M., Lehman, S.J., Ortiz, J.D., Fluckiger, J., and van Geen, A. (2007) Marine radiocarbon evidence for the mechanism of deglacial atmospheric CO_2 rise. *Science* 316:1456-1459.

Miller, A.J., White, W.B., and Cayan, D.R. (1997) North Pacific thermocline variations on ENSO timescales. *J. Phys. Oceanogr.* 27:2023-2093.

Osterman, L.E., Poore, R.Z., Swarzenski, P.W., and Turner, R.E. (2005) Reconstructing a 180 yr record of natural and anthropogenic induced low-oxygen conditions from Louisiana continental shelf sediments, *Geology*, 33, 329-332

Pearson, A., Eglinton, T.I. and McNichol, A.P. (2000) An organic tracer for surface ocean radiocarbon, *Paleoceanography*, 15, 541-550,

Phelger, F.B. and Soutar, A. (1973) Production of benthic foraminifera in three east Pacific oxygen minima. *Micropaleontology* 19:110-115.

Rathburn, A.E., Perez, M.E., and Lange, C.B. (2001) Benthic-pelagic coupling in the Southern California Bight: relationships between sinking organic material, diatoms and benthic foraminifera, *Mar. Micropaleontol.* 261-271

Reid, J.L., Roden, G.I., and Wyllie, J.G. (1958) Studies of the California Current system. CalCOFI Report. 6:27-56.

Reid, J.L. (1962) Measurements of the California Countercurrent at a depth of 250 m. *J. Mar. Res.* 20L134-137.

Reimers, C.E., Lange, C.B., Tabak, M., and Bernhard, J.M. (1990) Seasonal spillover and varve formation in the Santa Barbara Basin, California, *Limnol. Oceanogr.* 35:1577-1585

Reynolds, R.W. and Smith, T.M. (1994) Improved global sea-surface temperature analyses using optimum interpolation. *J. Climate* 7:929-948.

Roark, E.B., Guilderson, T.P., Flood-Page, S., Dunbar, R.B., Ingram, L.B., Fallon, S.J., McCulloch, M. (2005) Radiocarbon-based ages and growth rates of bamboo corals from the Gulf of Alaska. *Geophys. Res. Lett.* 32:doi:10.1029/2004GL021919.

Roark, E.B., Ingram, B.L, Southon, J., Kennett, J.P. (2003) Holocene foraminiferal radiocarbon record of paleocirculation in the Santa Barbara Basin, *Geology* 31:379-382

Robinson, S.W. (1981) Natural and man-made radiocarbon as a tracer for coastal upwelling processes, *Coastal Estuarine Sci.* 1:298-302.

Roland, L.A., McCarthy, M.D., and Guilderson, T. (2008) Sources of moleculary uncharacterized organic carbon in sinking particles from three ocean basins: A coupled $\Delta^{14}C$ and $\delta^{13}C$ approach. *Mar. Chem.* 111:199-213.

Schneider, N. Miller, A.J., Alexander, M.A. and Deser, C. (1999) Subduction of decadal North Pacific temperature anomalies: Observations and dynamics. *J. Phys. Oceanogr.* 29:1056-1070.

Schwing, F.B., Ralston, S. and Sakuma K.M. (2000) Record coastal upwelling in the California Current in 1999. CalCOFI Report 41:148-160.

Schwing, F.B., and coauthros (2001) The state of the California Current, 2000-2001: A third straight La Niña year. CalCOFI Report 42: 29-60.

Sholkovitz, E.R. and Gieskes, J. M. (1971) A physical-chemical study of the flushing of the Santa Barbara Basin, *Limnol. Oceanogr.* 16:479-489

Simpson, J.J., Dickey, T.D., and Koblinsky, C.J. (1984) An offshore eddy in the California Current system, I, interior dynamics. *Prog. Oceanogr.* 13:5-49.

Sonnerup, R.E., Quay, P.D., McNichol, A.P., Bullister, J.L., Westby, T.A. and Anderson, H.L. (1999) Reconstructing the oceanic 13C Suess effect. *Global Biogeochem. Cy.* 13:857-872.

Stott, L.D., Bunn, T., Prokopenko, M., Mahn, C., Gieskes, J. and Bernhard, J.M. (2002) Does the oxidation of methane leave an isotopic fingerprint in the geologic record? *Geochem Geophys. Geosys.* 3:doi:10.1029/2001GC000196.

Stuiver, M. and Polach, H.A. (1977) Discussion reporting of ^{14}C data. *Radiocarbon* 19:355-363.

Sverdrup, H.U., and Freming, R.H. (1941) The waters off the coast of southern California. *Scripps Institute of Ocreanography Bulletin* 4:261-387.

Takahashi, K. (1998) The Bering and Okhotsk Seas: modern and past paleoceanographic changes and gateway impact. *J. Asian Earth Sci*. 16:49-58.

Talley, L.D. (1991) An Okhotsk Sea water anomaly: implications for ventilation in the North Pacific. *Deep-Sea Res*. 38:S171-190.

Talley, L.D. (1993) Distribution and formation of North Pacific Intermediate Water. *J. Phys. Oceanogr*. 23:517-537.

Tallye, L.D. (2007) Hydrographic atlas of the World Ocean Circulation Experiment (WOCE). Volume 2: Pacific Ocean (Sparrow, M., Chapman, P., and Gould, J. eds), International WOCE Project Office, Southampton, U.K.

van Geen A., Fairbanks, R.G., Dartnell, P. et al. (1996) Ventilation changes in the northeast Pacific during the last deglaciation, *Paleoceanography*, 11, 519-528

Van Scoy, K.A., Olsen, D.B., and Fine, R.A. (1991) Ventilation of North Pacific Intermediate Waters: The role of the Alaskan Gyre. *J. Geophys. Res*. 96:16,801-16,810.

Wantanabe, Y.W., Harada, K. and Ishikawa, K. (1994) Chlorofluorocarbons in the central North Pacific and southward spreading time of North Pacific Intermediate Water. *J. Geophys. Res*. 99:25,195-25,213.

Wong, A.P.S., Bindoff, N.L., and Church, J.A. (1999) Large-scale freshening of intermediate waters in the Pacific and Indian oceans. *Nature* 400:440-443.

Zhao, M. X., Eglinton, G., Read, G., and Schimmelmann, A. (2000) An alkenone (U^{-} 37(K')) quasi-annual sea surface temperature record (AD 1440-1940) using varved sedim

Chapter 2. Benthic foraminiferal community distribution in the bathyal Santa Barbara Basin over the past 250 years

Abstract

The distribution of the opportunistic benthic foraminiferal species that inhabit the microxic ($[O_2] < 0.2$ ml/l) upper sediments of the bathyal Santa Barbara Basin (SBB) fluctuates on seasonal to millennial timescales. However, the temporal variability of this distribution over years to decades remains poorly documented, despite the fact that physio-chemical conditions of the benthic environment in the SBB are dynamic on these time scales. For example, it is not know to what extent decadal fluctuations in benthic foraminiferal assemblages are driven by large-scale changes in bottom water characteristics analogous to those responsible for the wholesale assemblage shifts observed over the last glacial and deglacial periods. In this study we quantify the abundance of the ten cosmopolitan benthic foraminiferal species from two Soutar box cores collected from the deep SBB (~600 m) at biennial resolution from 1744-2008 A.D. The resulting record reveals significant decadal scale fluctuations in absolute and relative abundances of SBB benthic foraminifera in part linked to well documented oscillatory modes of north Pacific climate variability. Large-scale shifts in community distribution are also observed, including the unprecedented growth in the latter half of the 20th century of the chloroplast-bearing species *Nonionella stella*. While the mechanism driving this growth and behavioral deviation from the other species remains unclear, the sensitivity of benthic foraminifera to their environment hints at subtle chemical and/or physical changes in the SBB benthos occurring over the last three decades

2.1 Introduction

Benthic foraminifera comprise the majority of benthic biomass in the bathyal Santa Barbara Basin (SBB) (Bernhard *et al*., 2000; Bernhard & Reimers 1991; Phleger & Soutar, 1973). The benthic foraminiferal species that inhabit this dysoxic (dissolved oxygen concentration, $[O_2]$, < 1.0 ml/l; Bernhard & Sen Gupta, 1999) environment, and those at the centers of surrounding California Borderland Basins, are opportunistic (Sen Gupta & Machain-Castillo, 1993) and capable to responding within months to slight changes in bottom water $[O_2]$ (Bernhard & Reimers, 1991) and flux of organic carbon (Corliss & Silva 1993; Silva *et al*., 1996, see also review by Gooday & Rathburn, 1999). One species, *Nonionella stella*, likely possesses unique physiological advantages that allow it to flourish under microxic ($[O_2]$ < 0.2 ml/l, Bernhard & Sen Gupta, 2000) conditions (Bernhard & Bowser, 1999; Grzymski *et al*., 2002). Wholesale shifts in benthic foraminiferal assemblages over millennial time scales are thought to reflect oscillations between oxic and dysoxic conditions driven by changes in bottom water ventilation (i.e. time since exposure to the atmosphere) during the last glacial and deglacial periods (Cannariato & Kennett 1999; Cannariato *et al*., 1999; Behl & Kennett, 1996). It has been suggested that the sensitivity of benthic foraminifera to $[O_2]$ could be also be exploited as a means to trace much subtler $[O_2]$ changes (i.e. the severity of dysoxia) in past SBB bottom water (Bernhard *et al*. 1997).

In addition to millennial scale fluctuations, the physical and chemical of the SBB benthos are also dynamic on decadal time scales as evidenced sediment morphology (Stott *et al*., 2000), sediment pore water chemistry (Stott *et al*., 2002; Berelson *et al*., 2005; Berelson & Stott 2003; Holsten *et al*., 2004) and instrumental measurements from

the California Cooperative Fisheries Investigation (CalCOFI) time series (Bograd *et al*., 2002, this study). For this reason it is important to document temporal variability of benthic foraminiferal community structure on the decadal time scales for which bottom water properties and other environmental controls might be changing. Here we quantify the absolute and relative abundances of the ten cosmopolitan benthic foraminiferal species in the SBB at biennial resolution from 1744-2008. The results of this study, as we will demonstrate, suggest not only decadal scale fluctuations, but also monotonic trends that pose interesting questions as to the environmental controls of benthic foraminiferal community distribution in the bathyal SBB.

2.2 Study area

A series of basins, sills and islands make up the California Borderland Province, located in the Southern California Bight (SCB) along the Southern California Margin (SCM). As the northernmost basin in this province, the ~600 m deep SBB is bounded by mainland California to the north and the Channel Islands to the south (Chapter 1, Figure 1.3). Wind driven circulation in the SCB reflects a complex organization of the California Current System (CCS), with the offshore, equatorward flowing California Current advecting relatively cool, fresh, oxygenated water from the Subarctic Gyre (Lynn & Simpson, 1987; Hikey, 1979; Bray *et al*., 1999) and the inshore, poleward flowing California Counter Current, advecting relatively warm, saline water from the subtropical Pacific (Lynn & Simpson, 1987; Hickey, 1979; Reid 1958). The California Undercurrent, which sits along the continental margin between 100 and 250 m depth (Bray *et al*., 1999; Lynn & Simpson, 1987, 1990) transports relatively warm, saline and oxygen depleted waters poleward from the eastern equatorial Pacific. This circulation

pattern undergoes significant seasonal modulation, with springtime intensification of the California occurring in response to the strengthening of northerly upwelling favorable winds and isopycnal shoaling along the SCM.

Source waters to the modern SBB derive from a mixture of young, well ventilated North Pacific intermediate water (NPIW) with origins in the high latitude western North Pacific (Talley, 1993) and older, poorly ventilated water advected from the tropical Pacific (Kennett & Ingram, 1995; Hendy & Kennett, 2003). This water enters the basin over its western sill, which, at 475 m, intersects the top of the regional oxygen minimum zone (OMZ). Seasonal upwelling drives high primary productivity and decomposition of the resulting organic detritus at depth and further depletes oxygen levels, resulting in [O2] typically < 0.2 ml/L (Emery, 1960; Emery & Hulsemann, 1962), and occasionally below detectable limits (Bernhard & Reimers 1991) at the basin bottom. These conditions are inhospitable to bioturbating benthic macrofuana and thus ideal for the preservation of annually laminated (varved) sediments (Hulsemann & Emery, 1962). This varved sedimentology provides an independent age model upon which to measure benthic foraminiferal species abundances.

Oxygen renewal to the bathyal SBB occurs during periodic flushing events when relatively dense water spills over the western sill and displaces stagnant water within the basin (Bograd *et al*., 2002; Reimers *et al*., 1990; Sholkovitz and Gieskes, 1971). In addition to elevating oxygen concentrations, these flushing events can cause pronounced increases in the potential density and decreases in the temperature and salinity of SBB bottom water (Bograd *et al*., 2002) over the course of 1 to 2 months (Liu, 1979; Bograd *et al*. 2002) as evident in the over two-decades long quarterly CalCOFI time series of

physio-chemical bottom water properties in the central SBB (Figure 2.1). In addition to providing evidence for flushing events, this time series highlights the dynamic nature of SBB bottom water characteristics on interannual to decadal time scales.

2.3 Background

Early studies of benthic foraminifera along the SCM documented distinct depth ranges inhabited by individual species, concluding that temperature was a dominant control on species habitat (Natland, 1933; Bandy, 1953, Resig, 1958; Zalesny, 1959). However these studies also noted that other environmental factors such as oxygen concentration and organic content of sediments must play a role when locations of similar temperature and depth along the SCM yield markedly different benthic communities (Bandy 1953). Species including *Buliminella tenuata* (Zalesny 1959) and *Chilostomella ovoidea* (Resig 1958) were found to inhabit the deepest portions of the Santa Monica Bay and Santa Cruz Basin respectively. Harman (1964), the first to study benthic foraminifera in the SBB, found that together *Suggrunda eckisi*, *Bolivina seminuda,* and *B. tenuata* made up 75% of the tests at basin center (550-589 m). Harman (1964) also identified "dwarfed" forms of *C. ovoidea*, *Globobulimina pacifica*, *B. seminuda, Bolivina pacifica*, *Nonionella stella*, and *Loxostomum pseudobeyrichi* in the deep SBB. The basin slope (400-550m) fauna were characterized by much greater percentages of *Bolivina argentea* and *Uvigerina peregina* than the bathyal communities. Harman (1964) suggests that a sharp oxygen gradient between slope and basin (Emery, 1960) may account for this differentiation of species distribution, with only the bathyal species tolerant of microxic conditions.

Later studies focused in greater detail on the role of chemical properties including oxygen concentration (Bernhard 1992; Bernhard *et al*. 1997) and food (organic carbon) availability (Phleger & Soutar, 1973; Rathburn *et al*., 2001) in determining the spatial distribution of benthic foraminiferal species in the southern California Borderland. Several of these studies collected sediment with a box corer, preserving the uppermost sedimentary layers and employed rose Bengal staining (Phleger & Soutar, 1973) and adenosine triphosphate (ATP) assay (Bernhard & Reimers, 1991; Bernhard *et al*., 1997) to identify living benthic foraminifera. Using these methods, Phleger & Soutar (1973) found *N. stella*, *B. seminuda,* and *Textularia* sp. to make up 80% of the living population in the deep SBB. Large standing stocks (2,100 per 20 cm^2 surface sediment) of living benthic foraminifera were identified in the deep SBB indicating these individuals were well adapted to the low oxygen environment. Bernhard *et al*. (1997) studied the spatial distribution of live individuals with respect to $[O_2]$ over a vertical oxygen gradient and found that individual species experienced maximal relative abundance over specific $[O_2]$ ranges along this gradient (Figure 2.2). The authors used this observation to rank species based on their tolerance for varying degrees of dysoxia and suggested that this ranking could be applied to fossilized assemblages as a means to reconstruct small-scale variability in basin oxygenation. Among the species found to be least tolerant of dysoxia were *B. argentea*, *Fursenkoina cornuta* and *L. pseudobeyrichi*. At the other extreme, *N. stella* was found to be the dominant species in the deepest and lowest oxygen habitats.

Recent studies over the past two decades reveal that *N. stella* possesses unique physiological properties. Bernhard & Reimers (1991) first suggested the possibility that *N. stella* could respire nitrate (NO_3^-) as an explanation for its survival in the presence of

anoxia. Later, Bernhard & Bowser (1999) discovered sequestered algal chloroplasts in *N. stella*, hypothesizing that, due to aphotic conditions, these chloroplasts were not providing oxygen through photosynthesis, but were instead involved in a yet to be identified biochemical pathway that facilitates inhabitance of dysoxic environments. Grzymski *et al*. (2002) investigated the role of these sequestered chloroplasts in greater depth, determining that they may help *N. stella* meet its metabolic nitrogen requirements through the assimilation of inorganic nitrogen. A more recent study discovered high concentrations of intracellular NO_3^- in the foraminifer *Nonionella* cf. *stella* collected from the Chilean margin and found that this species underwent complete denitrification reducing NO_3^- to dinitrogen (N_2) (Risgaard-Petersen *et al*., 2006). However, the authors suggest that the foraminifer's own organelles were responsible for a carrying out this denitrification as opposed to sequestered prokaryotic plastids. The findings of this study were replicated in a study by Høgslund *et al*. (2008), which also determined that the nitrogen assimilation pathways associated with sequestered organelles were unlikely to be involved in NO_3^- reduction. As a whole these studies indicate that *N. stella* likely possesses adaptations advantageous for survival in microxic environments that experience periodic depletion of nitrogen.

Several studies have captured seasonal fluctuations of benthic foraminiferal populations in the California Borderland Basins, documenting significant changes in species distributions over the course of several months that include pronounced changes in the abundance of *N. stella* (Bernhard & Reimers 1991; Corliss & Silva 1993; Silva *et al*., 1996). Bernhard & Reimers (1991) observed a complete die-off of the benthic community in the Santa Barbara Basin (SBB) between October 1988 and July 1989, an

event they attributed to a weak or non-existent springtime flushing event that resulted in anoxic conditions by July. *N. stella* comprised 83% of the rose-Bengal stained (i.e. recently living) individuals in the July sample. Corliss & Silva (1993) found that while total benthic foraminiferal abundances did not undergo substantial change over the period April-October 1988 in the central San Pedro Basin (SPB) (~720 m), the distribution of individual species exhibited significant variability, with increases in the abundance of two species, *B. tenuata* and *N. stella*, likely reflecting a reproduction or recruitment event in response to a pulse of phytodetritus from a spring surface bloom. In a related study, Silva *et al* (1996) suggest that a recruitment event for *B. tenuata* and *N. stella* occurred between July and October 1988 in the SPB, highlighting the rapid growth rate and opportunistic nature of these species. The authors found that the other dominant species in the SPB exhibit a maximum in abundance in July and not October, which they attribute to a more rapid response to the pulse of organic carbon than that displayed by *B. tenuata* and *N. stella*. Regardless of whether this seasonal dynamism is driven by [O_2] (Bernhard *et al*., 1997; Bernhard & Reimers 1991; Machain-Castillo, 1993; Loubere 1994; Kaiho, 1994) or food availability (Loubere, 1991; Gooday 1994; Loubere, 1994, 1996), factors difficult to discriminate, these studies highlight the sensitivity of overall abundance and species distribution of benthic foraminifera in the Borderland Basins to changes in physio-chemical benthi conditions.

This sensitivity has been exploited to trace variability in water mass geometry and surface productivity on millennial timescales. Qualitative analysis of benthic foraminiferal populations over the period of 0-60 kyr bp in ODP core 893 (central SBB) revealed dramatic assemblage shifts during marine isotope stages 2 and 3 that occurred in

concert with fluctuations in the ventilation of basin source water driven by north Pacific climate variability (Kennett *et al*., 1994; Kennett & Ingram 1995; Behl & Kennett, 1996). Concurrent fluctuations in bioturbation index offshore southern (Lyle *et al*., 1997) and central (van Geen *et al*., 1996) California and in the Gulf of California (Keigwin & Jones, 1990) indicate that these changes in ventilation were a basin-wide phenomenon. Cannariato *et al*. (1999) document wholesale shifts from dysoxic to oxic species across interstadial to stadial transitions during the last glacial period in response to expansion and contraction of the northeast Pacific OMZ (Cannariato & Kennett, 1999). In contrast, the Holocene community was found to be relatively invariant and dominated by dysoxic species, consistent with a stable Northern Hemisphere climate and primarily laminated sediments in the SBB during this time.

The studies described above indicate that benthic foraminiferal assemblage distributions are dynamic on timescales ranging from months to millennia. In this study, we consider to what extent, if any, shifts in taxonomic distribution occurring over decades are analogous, albeit at diminished magnitude, to those documented by Cannariato & Kennett (1999) occurring on millennial timescales in response to changes in water mass characteristics. Our results will therefore carry implications for the use of benthic foraminifera in the oxygen depleted depocenters of the California Borderland Basins as a tracer for bottom water properties on decadal time scales.

2.4 Methods

Benthic foraminifera were obtained from Soutar box cores SBBC 0110-3001, collected in November 2001, and SBBC 060821-02, collected June 2008, both from the *R/V Robert Gordon Sproul* (see Chapter 1, Figure 1.3 for core locations). Core collection,

preservation, subsampling and preparation of varve chronology and foraminiferal samples were carried out following Field *et al* (2006). Briefly, visual inspection of X-radiographs of core slabs was used to identify individual varves and create detailed chronologies. Following these chronologies, slabs from SBBC 0110-3001 were subsampled at 2-year intervals from the 2001 to 1744 AD and slabs from SBBC 080621-02 subsampled at 1-year intervals from 2008 to 2002 and two year intervals from 2001-1974. Error due to sample excision from both cores is approximately 0.5 to 1 year, which may increase down core in SBBC 0110-3001 due to diminished varve clarity. Samples were washed, dry-sieved and divided into five size fractions (120-150 μm, 150-180 μm, 180-212 μm, 212-250 μm, 250-300 μm and 300-500 μm) for SBBC 0110-3001 and three to four size fractions (300-425 μm, 212-250 μm, 150-212 μm or 180-212 μm and 150-180μm) for SBBC 080621-02.

Tests from the ten cosmopolitan benthic foraminiferal species were enumerated, namely: *Bolivina advena, Bolivina argentea, Bolivina seminuda, Bulumina tenuata, Cassidulinoides cornuta, C. ovoidea, L. pseudobrechi, Nonionella stella, Suggrunda eckisi, Nonionella* cf. *globosa* and an unidentified species of the genus *Bolivina*. Together these species comprise nearly 100% of the benthic foraminiferal population. *N.* cf. *globosa* was not counted between 1978 and 2001 in SBBC 3001-0110 but was counted over this period in SBBC 080621-02. All other species were counted over 1744-2001 in SBBC 3001-0110 and 1974-2008 in SBBC 080621-02. Tests from each size fraction were evenly distributed on a 10 x 18 or 11 x 19 gridded tray and individuals counted in one grid square split per row. Three samples from SBBC 080621-02 required the use of a splitter due to numerous individuals. Species from all size fractions > 150μm

were quantified. Typically >200 specimens counted per sample, with some samples numbering ~500 individual counts. Each two year interval between 1744 and 2008 was counted except for the intervals beginning in 1824, 1848 which were lost. Following the method of Field *et al*. (2006) for enumeration of planktonic foraminifera from box core SBBC 0110-3001, abundance totals for each two-year interval were converted to flux (number individuals / cm^2 / year) by dividing by the box core cross sectional area at the corresponding depth and dividing by 2. One-year intervals were simply divided by box core cross sectional area. Because we do not know when during the sampled interval the benthic foraminifera actually lived, these values are estimates, but provide a standardized means to compare abundances from different samples.

2.5 Results

Flux of the ten species enumerated in the > 150 μm size fraction from SBBC 3001-0110 and SBBC 080621-02 display significant decadal scale variability throughout the record (Figure 2.3). Although their flux varies considerably, *B. seminuda, C. cornuta, S. eckisi*, *C. ovoidea*, *N.* cf. *globosa* and *B. tenuata* are present throughout the record. Comparison of fluxes smoothed with a 10-year running mean reveals that the abundance of these species generally covaries on decadal time scales with peak fluxes observed at 1920-1930, 1870-1890, 1850 and 1820. *C. cornuta* and *S. eckisi* have the highest fluxes with record-long averages between 1744 and 2001 (SBBC 0110-3001) of 5.4 and 7.5/cm^2/yr respectively. *B seminuda* has an average flux of 3.5/cm^2/year, *C. ovoidea* of 1.5/cm^2/yr, *B. tenuata* of 1.7/cm^2/yr, *N. cf. globosa* of 1.6/cm^2/yr and *Bolivina* sp. of 0.7/cm^2/yr. Fluxes of *N. stella, L. pseudobeyrichi and B. argentea* appear decoupled from this group of ubiquitous species. *N. stella* is rare to absent before 1950 with the exception

of 1750-1762, but increases dramatically after 1950 with an average flux between 1950 and 2001 of 11.0/cm^2/yr, greater than any other species over this time period by more than a factor of 2. In 2004 flux of *N. stella* in SBBC 080621-02 peaks near 120/cm^2/year, again the highest observed for any of the ten species in either record. With the exception of 1760-1800, flux of *B. argentea* ranges between 3 and 8/cm^2/yr before 1880 when it drops to near zero for the remainder of the record. Similarly, *L. pseudobeyrichi* has an average flux of 6.5/cm^2/year, reaching as high as 37/cm^2/yr from 1780-1820, and is otherwise nearly absent from the population. Total benthic foraminiferal flux also displays decadal cyclicity over the entire record (Figure 2.3), with periods of peak flux generally corresponding to peaks in *S. eckisi*, *B. seminuda* and *C. cornuta* prior to ~1970 and *N. stella* after this time. Average total annual flux is 26 ± 18/cm^2.

In order to investigate the link between observed variability in absolute abundance (i.e. flux) and large-scale fluctuations in north Pacific climate, we correlate the raw and decadally smoothed abundances of individual species (Table 2.1) as well as total abundance (Table 2.1, Figure 2.4) with annual time series of the Pacific Decadal Oscillation (PDO, Mantua *et al*., 1997; Zhang *et al*., 1997) and the North Pacific Gyre Oscillation (NPGO, Di Lorenzo *et al*., 2008). These climate indices, defined as the first principle component (PC) of north Pacific sea surface temperature anomalies (SSTa) and the second PC of north Pacific sea surface height anomalies (SSHa) respectively, represent dominant modes of north Pacific climate variability and reflect oscillations in basin-scale ocean-atmosphere interactions (e.g. Di Lorenzo *et al*., 2008; Mantua *et al*., 1997; Chaak & Di Lorenzo, 2007; Di Lorenzo, 2003; Trenberth & Hurrell, 1994). Monthly PDO values were obtained from http://jisao.washington.edu/data_sets/pdo/ and

monthly NPGO values from http://www.o3d.org/npgo/. Table 2.1 lists the coefficients of correlation between benthic foraminiferal fluxes and these modes of climate variability. Decadally smoothed total flux exhibits a significant positive correlation to PDO ($r = 0.41$, $p < 0.001$) and significant negative correlation to NPGO ($r = -0.38$, $p < 0.01$). Significant correlations of the same sign (positive for PDO and negative for NPGO) are observed for raw flux although that for PDO is diminished in magnitude ($r = 0.20$, $p < 0.05$) while that for NPGO is identical. As observed in table 2.1, the correlation of raw and decadally smoothed fluxes of individual species to NPGO and PDO varies considerably, although more species exhibit a positive than negative correlation to PDO while the reverse is true for NPGO. Individual species correlation with NPGO is stronger for the raw fluxes than the smoothed, while the opposite is observed for PDO. Overall, the positive correlation with PDO is driven by variability in the fluxes of *N. stella*, *C. ovoidea*, *Nonionella* cf. *globosa* and *Bolivina* sp. while the negative correlation with NPGO is driven by variability in the fluxes of *N. stella*, *S. eckisi, C. cornuta* and *Nonionella* cf. *globosa*.

Determining species relative abundance allows us to examine shifts in community structure in the absence of absolute changes in total abundance. While fluxes in SBBC 080621-02 are generally higher than those in SBBC 0110-3001 overlapping relative abundances from these two cores over the period 1975-2001 shows good correspondence (Figure 2.5). *Bolivina* sp. and *N.* cf. *globosa* are not included in figure 2.5 because relative abundance of *Bolivina* sp. is negligible over this period and *N.* cf. *globosa* was not counted in SBBC 0110-3001 before 1975. Two-year intervals from SBBC 080621-02 begin on odd numbered years (e.g. 2003-2004) while those from SBBC 3001-0110 begin on even numbered years, resulting in a one year offset between measurements. Taking

this offset into account, specific features coincide in both cores such as the spike in relative abundance of *C. cornuta* in 1994 and peaks in relative abundance of *C. ovoidea* around 25% in the late 1980 and late 1990s. Based on the correspondence between relative abundances in SBBC 3001-0110 and SBBC 080621-02, we extend the relative abundance record of SBBC 0110-3001 to 2008 with measurements from SBBC 080621-02 to create a continuous time series from 1744 to 2008.

Principle components analysis (PCA) of this time series (not shown) reveals that variability in the relative abundance of four species, *N. stella, S. eckisi*, *C. cornuta* and *L. pseudobeyrichi* reflects the majority of variability in the overall benthic foraminiferal community distribution. These species have the strongest loadings in the first 3 principle components (PCs), which together make up 75% of the total variance in relative abundance. These species also have the strongest loadings when PCA is preformed on flux. In figure 2.6, which displays the abundance of these four species relative to their combined total absolute abundance, we observe 2 transitions in community distribution: one around 1870 and another after 1950. The first transition is marked by the decline in relative abundance of *L. pseudobeyrichi*. Over the periods 1744-1754 and 1779-1870 *L. pseudobeyrichi* and *B. argentea* together comprise on average 25 ± 20% of the total population, and reach > 60% in 1792, 1802 and 1835. These species are particularly dominant between 1744 and 1760 and again from 1790 to 1810 for *L. pseudobrechi*, with the dominance of *B. argentea* extending until 1850. After 1870 the cumulative relative abundance of these two species drops to 1 ± 2% and never exceeds 9%. The second transition is driven by the rise in relative abundance of *N. stella* in the latter half of the 20th century. With the exception of a brief period of prevalence from 1750-1762, *N. stella*

makes up 0-4% of the population until 1950, when its relative abundance begins to steadily rise before until peaking in 2004 at nearly 100%. Together *B. seminuda* and *S. eckisi* comprise on average 36 ± 19% population until 1960 when their relative abundance is dwarfed by the dominance of *N. stella* to an average of 20 ± 17% in SBBC 0110-3001 and 18 ± 13% in SBBC 080621-02 (1975-2008). The decrease in relative abundance of these species also corresponds to a decrease in their flux (Figure 2.3). *C. cornuta* has a consistently significant presence, making up 27 ± 20% of the population between 1744 and 2001, although its relative abundance is also somewhat diminished by the dominance of *N stella* at the turn of the 21st century.

2.6 Discussion

We observe pronounced decadal variability as well as long term directional trends over our ~2.5 century long record of SBB benthic foraminiferal abundances. Total annual flux of SBB benthic foraminifera > 150 μm varies on the order of 20/cm^2 at decadal time scales. Average total annual flux is approximately an order of magnitude smaller that that observed by Phleger & Soutar (1973) who counted 2,100 living and 1,600 dead benthic foraminifera per 20 cm^2 in the > 63 μm fraction of upper 1 cm of deep SBB sediment. The difference in these values is likely due in part to the fact a significant portion of total foraminifera in the Borderland Basins can be found in the 63-150μm size fraction (Rathburn *et al*., 2001; Sen Gupta & Machain-Castillo, 1993), which was not counted in this study due to the immense time required to accurately enumerate the minute specimens. While counting the > 63 μm size fraction appears necessary for investigating seasonal shifts in community distribution (Rathburn *et al*., 2001; Corliss & Silva, 1993; Silva *et al*., 1996), limiting our investigation to the >150 μm size fraction

still allows for direct comparison of decadal scale variability observed in this study with that occurring over longer timescales (e.g. Cannariato *et al*., 1999) and within the > 150 μm size fraction on seasonal timescales (e.g. Silva *et al*., 1996). In examining the possible environmental drivers for observed variability in absolute or relative species abundances, it must be noted that our record represent a two-year (or one year for the case of the most recent samples in SBBC 0806210-02) time averaged picture of seasonal fluctuations. The increase in two species during a given two-year sampling interval does not necessarily imply that these two species bloomed at the same time, or that they necessarily responded to the same set of favorable conditions. However, an increase in the frequency of favorable conditions for a given taxon over years to decades should drive an increase in its abundance measurable within our biennial sampling resolution.

Decadal fluctuations in the total abundance of benthic foraminifera in the bathyal SBB appears to be influenced by north Pacific climate variability associated with both the PDO and NGPO indices. The patterns of atmospheric circulation associated with the negative and positive phases of PDO and NPGO respectively result in stronger northerly, upwelling favorable winds along the SCM and consequently more vigorous coastal and offshore upwelling (Chaak & Di Lorenzo, 2007; Di Lorenzo, 2003; Di Lorenzo *et al*., 2008). The respective positive and negative correlation of total benthic foraminiferal abundance with PDO and NGPO indicate that cumulative abundance is greater during times of diminished upwelling and therefore reduced productivity along the SCM. Lower productivity results in decreased benthic flux of organic material (Berelson & Stott, 2003), which in turn is thought to reduce the rate of carbon oxidation (C_{ox}) in the upper sediments of the California Borderland Basins, thereby increasing [O_2] (Berelson & Stott,

2003). Our results therefore suggest that on decadal time scales, the benthic foraminiferal community as a whole is limited by $[O_2]$ rather than benthic flux of organic material, consistent with the findings of Bernhard & Reimers (1991) and the proposed behavior for benthic foraminiferal communities in extremely oxygen depleted ($[O_2] < 1.0$ ml/l) environments (e.g. Jorissen *et al*., 2007). The direction of correlation between total abundance and PDO and NPGO also indicates that on decadal time scales benthic foraminifera are more sensitive to the influence of regional productivity on upper pore water $[O_2]$ than that of periodic flushing events or ventilation of SBB source water--as enhanced upwelling should lead to a higher frequency of flushing events (Bograd *et al*., 2002; Chapter 1 of this dissertation) and greater contribution of well ventilated NPIW to SBB source waters (Lynn & Bograd, 2002; Bograd *et al*., 2001; Lynn *et al*., 1998). However, the wide range in correlation among the fluxes of individual species to PDO and NGPO reflects the fact that different taxa respond to specific combinations of environmental parameters of which $[O_2]$ is only a part.

In addition to absolute abundance, the species distribution of the SBB benthic foraminiferal community also fluctuates on decadal time scales (Figure 2.6). The correspondence in relative abundances between cores separated by at least 10s of meters indicates that fluctuations in community distribution are likely a basin-wide phenomenon and not due to spatial patchiness, consistent with the findings of Bernhard & Reimers (1991). Superimposed on decadal variability are the two large-scale assemblage shifts, the first of which marked by the decline of *L. pseudobrechi* and *B. argentea* between 1850 and 1900. The timing of this decline generally corresponds to an increase in the $\delta^{13}C$ gradient in the upper few centimeters of sediment in the Santa Monica Basin

indicative of increased C_{ox} (Stott *et al*., 2002; Berelson & Stott, 2003; Holsten *et al*., 2004). Berelson & Stott (2003) posit that this increase in C_{ox} likely driven by elevated organic carbon rain rate, which is strongly correlated to surface productivity. Based on this relationship between surface productivity and C_{ox}, Stott *et al*. (2000) link an increase in basin oxygenation since the late 1970s to a contemporaneous decrease upwelling along the SCM associated with the shift to the positive phase of PDO. An increase in surface productivity between 1850 and 1900 may therefore tied to the hypothesized coeval weakened Aleutian Low (D'Arrigo *et al*., 2005; Field *et al*., 2010) and the resultant strengthening of northerly, upwelling favorable, winds along the SCM. The expansion of laminated sediments in the borderland basins after 1850 (Hagadorn *et al*., 1995; Christensen *et al*., 1994) is also consistent with increased C_{ox} and the resultant decrease in $[O_2]$.

The decrease in relative and absolute abundance of *B. argentea* and *L. pseudobeyrichi* in response to increased surface productivity and benthic C_{ox} between 1850 and 1900 reflects the same sensitivity to local pore water chemistry evident in the negative correlations of total species abundance to upwelling strength over the 20th century. The decadally smoothed flux of *B. argentea* exhibits a significant positive correlation to PDO, consistent with the decline of this species during periods of enhanced upwelling. Lack of correlation between *L. pseudobeyrichi* and PDO and NPGO is difficult to interpret as the numbers of this species over the 20th century are negligible. The observed relationship of total foraminiferal abundance to PDO and NPGO over the 20th century and shift in dominance to species more tolerant extreme dysoxia between 1850 and 1900 indicate that on decadal timescales the benthic foraminiferal community

responds more strongly to local changes in pore water chemistry than it does to basin scale shifts in water mass properties analogous to those thought to be responsible for driving the wholesale community redistributions observed on millennial timescales (Cannariato *et al*., 1999; Cannariato & Kennett, 1999)

The demise of *B. argentea* and *L. pseudobeyrichi* between 1850 and 1900 is consistent with their classification by Bernhard *et al*., (1997) as relatively intolerant of severe dysoxia. However, we observe an increase in absolute abundance of *S. eckisi* over this interval despite its being ranked above *B. argentea* and *L. pseudobeyrichi* in intolerance for extreme oxygen depletion, second only to *Uvigerina juncea* (Figure 2.2). Yet while *U. juncea* is entirely absent from the deep parts of the basin, *S. eckisi* is present at least 5% relative abundance throughout the basin and exhibits > 20% abundance at the shallower depths sampled, indicating that this species, unlike *U. juncea*, can survive when [O2] < 5 μM (~0.05 ml/L). Our finds suggest that the relative paucity of *S. eckisi* in the deepest, most oxygen depleted regions of the SBB in Bernhard *et al*., (1997) may be due to environmental factors other than oxygen demand. Or, if this species does in fact thrive under relatively higher oxygen concentrations and that oxygen concentrations, its increase in the late 19th century must be in response to conditions besides [O_2], according to the evidence for decreasing [O_2] in the Borderland Basin benthos over this time described above. Therefore, the use benthic foraminiferal species distributions as proxy for subtle changes in oxygenation when conditions are consistently dysoxic may be complicated by other environmental factors. However, abundances of specific species, such as *B. argentea* may be diagnostic of these changes.

Bernhard *et al*. (1997) also conclude that, on the basis of its clear dominance at the deepest, most oxygen depleted, stations, *N. stella* should be considered in paleoclimate studies as a representative for the lowest [O_2] conditions. Our results suggest that the dominance of *N. stella* observed in figure 2.2 may be a relatively new feature of the benthic foraminiferal community in the central SBB. An explosion of this species over the latter half of the 20th century marks the second major shift in community distribution. The brief presence of this species in the mid 18th century suggests that the increasing trend in its abundance in the 20th does not herald the arrival of *N. stella* to the SBB for the first time. Instead, it suggests that conditions favorable to this species prevailed briefly in the mid 18th century and returned after 1950 with increased prevalence. These conditions likely offer *N. stella* an advantage over other species due to its sequestered chloroplasts and potential unique physiological characteristics (Bernhard & Bowser, 1999; Grzymski *et al*., 2001; Risgaard-Peterson *et al*, 2006; Høgslund *et al*., 2008). In light of these characteristics, and previously documented spatial and seasonal patterns in *N. stella* abundance (Bernhard & Reimers, 1991; Bernhard *et al*., 1997), the monotonic increasing trend in the relative and absolute abundance of this species over the last ~50 years invites speculation as to its environmental drivers.

Several studies indicate that, of the current benthic foraminiferal inhabitants of the SBB, *N. stella* is the most tolerant of dysoxia and the last to succumb to anoxia (Bernhard & Reimers, 1991; Bernhard *et al*., 1997). It is possible, therefore, that the increase in *N. stella* over the latter half of the 20th century reflects a gradual decrease in upper pore water [O_2]. There is no evidence in the CalCOFI record for decreasing bottom water oxygen over the last two decades (Figure 2.1) despite the continued rise of *N. stella* over

this time. [O_2] in the 1960s (Emery, 1960) was not significantly higher than the average [O_2] measured over the past 20 years. Furthermore, contraction in laminated sediments in the Santa Monica and Santa Barbara Basins since the late 1970s indicates increasing, not decreasing benthic [O_2] over this time (Stott *et al*., 2000). However, evidence has recently emerged for declining oxygen below the seasonal thermocline in the CCS over the past two decades, which may reflect an expansion of the northeast Pacific OMZ (Bograd *et al*., 2008). Although the significant decreasing trends are confined to depths above those of the SBB sill, it is possible that *N. stella* is responding to a deeper decline in [O_2] too subtle to be recorded instrumentally. Additional benthic foraminiferal time series along the northeast Pacific margin are necessary to further investigate this hypothesis. *N. stella* has been documented in abundance elsewhere along the SCM (Zalesny, 1959; Stott *et al*, 1996; Bandy, 1964; Corliss & Silva, 1993; Silva *et al*., 1996) and in a cursory examination of sediment deposited within the last decade along the northern Chilean margin (LDR, personal observation). Therefore either the absence of *N. stella* prior to 1950 was unique to the SBB or its increase in abundance was witnessed along the entire SCM and perhaps even the northeast and southeast Pacific margins. Studies from additional locations along these margins will help determine whether the rise in *N. stella* is a local, regional or basin-wide phenomenon. Widespread occurrence of this shift in benthic foraminiferal community could reflect a basin-scale change in intermediate water properties possibly related to an expanding and/or intensifying OMZ. Confinement of this shift to the SCB might instead reflect evolution in the flux or quality of organic carbon from the surface ocean, or as yet undocumented changes in additional environmental

parameters such as sediment composition, grain size, and bottom water velocity (Jorissen *et al*., 2007).

Another possibility is that a decrease in available nitrogen in the upper pore waters of the bathyal SBB sediments drove the increase in *N. stella* over the past several decades. Sedimentary denitrification is thought to be the dominant nitrogen sink in the deep SBB (Sigman *et al*., 2003) where the nitrate concentration ($[NO_3^-]$) often decreases with depth below the sill depth (Kuwabara *et al*., 1999; Bograd *et al*., 2002). Were the rate of sedimentary denitrification increasing over the latter half of the 20th century, we would expect to discern a decreasing trend in bottom water $[NO_3^-]$ in the CalCOFI time series (Figure 2.2e), where no such trend is observed. However, we do note that the peak in *N. stella* abundance in 2004 (Figure 2.3) corresponds to the dramatic denitrification episode between April 2004 and January 2005, evidenced by a rise and rapid decline in nitrite concentrations ($[NO_2^-]$) between April and November 2004 (Figure 2.2f) followed by undetectable $[NO_3^-]$ (Figure 2.2e) and $[O_2]$ (Figure 2.2d) in January 2005. Due to the disparate time scales between our enumerations and CalCOFI occupations of the SBB, we cannot directly ascribe this peak to the denitrification. However, lack of a sharp drop in the flux of *N. stella* in 2005 and 2006 is evidence against a massive die off following the denitrification episode, while abundances of every other species quantified drops to near zero (Figure 2.3). While these findings do not link decreasing nitrogen in the bathyal SBB to the rise in dominance of *N. stella*, they are consistent with the hypothesized role of its chloroplast symbionts in supporting nitrogen demand, and its ability to withstand temporary anoxia.

2.7 Conclusions

The flux and relative abundance of the ten cosmopolitan benthic foraminiferal species in the bathyal SBB fluctuate dramatically at decadal time scales over the period 1744-2008. Total abundance of benthic foraminifera is positively correlated with PDO and negatively correlated with NPGO over the periods 1900-2001 and 1950-2001 respectively, suggesting that as a whole the community grows under conditions of lower surface productivity (e.g. McGowan *et al*., 1998; Di Lorenzo *et al*., 2008) and decreased flux of organic carbon (Berelson & Stott, 2003) likely in response to the resulting lower C_{ox} and higher $[O_2]$ in the upper pore waters of SBB sediments (Stott *et al*., 2000, 2002; Berelson & Stott, 2003; Holsten *et al*., 2004). Flux of *S. eckisi, B. seminuda*, *C. ovoidea*, *N.* cf. *globosa*, *B. tenuata* and *C. cornuta* generally covary, with peak fluxes observed in the late 18th and early 19th centuries. Flux of *N. stella*, *L. pseudobeyrichi* and *B. argentea* are decoupled from this group. *L. pseudobeyrichi* and *B. argentea* comprise a significant portion of the benthic population before 1870, but are rare or absent after 1900. The decline in abundance of *B. argentea* and *L. pseudobeyrichi*, two species relatively intolerant of severe oxygen depletion (Bernhard & Reimers, 1991; Bernhard *et al*., 1997), between 1850 and 1900 is consistent with the hypothesized decrease in benthic $[O_2]$ in the California Borderland Basins over this time (Hagadorn *et al*., 1995; Christensen *et al*., 1994), resulting from higher C_{ox} (Stott *et al*., 2002; Berelson & Stott, 2003; Holsten *et al*., 2004) that may be linked to increased surface productivity (Berelson & Stott, 2003; Stott *et al*., 2000). These findings suggest that on decadal timescales the benthic foraminiferal community as a whole, and certain species such as *B. argentea*, are more sensitive to locally induced changes in pore water $[O_2]$ than those driven by variability in the ventilation of SBB source waters or in the frequency of flushing events. In other words,

decadal fluctuations in the benthic community distribution are not analogues of the millennial scale fluctuations documented by Cannariato *et al*. (1999).

A second shift in benthic foraminiferal community occurs when abundances of *N. stella* undergo a steady yet dramatic increase in the latter half of the 20th century. With the exception of a ~10 year period in the mid 1700s, this species comprises < 4% of the population prior to 1950, after which time its numbers explode until it comprises nearly 100% of the benthic foraminiferal community by 2004. Decreases in oxygen or nitrogen in the upper pore waters of the SBB could provide *N. stella* with a competitive advantage due to its tolerance of dysoxia (Bernhard & Reimers, 1991; Bernhard *et al*., 1997), sequestration of chloroplast symbionts (Bernhard & Bowser, 1999; Grzymski *et al*., 2001) and possible ability to use nitrate as a terminal electron acceptor (Risgaard-Peterson *et al*., 2006; Høgslund *et al*., 2008). The 20th century trend in *N. stella* abundance observed here warrants further investigation of temporal variability in benthic foraminiferal communities at additional locations along the eastern Pacific margin—investigations that will help constrain the driving mechanisms of this trend and capture its spatial extent. If discovered, widespread occurrence of this trend may signal that a basin-scale change in intermediate water properties has occurred over the last few decades.

Chapter 2:, in part, is being prepared for submission for publication. Roach, L.D., Field, D.B., Charles, C.D. The dissertation author was the primary investigator and author of this paper.

Table 2.1 Coefficients of correlation between annual flux of individual benthic foraminiferal species and total annual benthic foraminiferal flux with annually averaged values of the PDO (Mantua *et al*., 1997; Zhang *et al*., 1997) and NPGO (Di Lorenzo *et al*., 2008) climate indices. Bold coefficients indicate correlation significant at the 95% confidence interval.

Species flux	r			
	PDO		NPGO	
	raw	smoothed[a]	raw	smoothed[a]
N. stella	**0.24**	**0.23**	-0.15	-0.20
S. eckisi	0.10	0.14	**-0.35**	0.13
L. pseudobeyrichi	-0.08	-0.06	-0.03	-0.02
B. seminuda	-0.01	0.03	-0.20	0.08
C. ovoidea	0.15	**0.33**	0.15	-0.23
B. argentea	0.16	**0.21**	0.03	-0.06
C. cornuta	-0.01	0.17	**-0.30**	**-0.42**
B. tenuata	003	0.20	**0.28**	0.00
N. cf. *globosa*	**0.23**	**0.26**	-0.20	**-0.37**
Bolivina sp.	**0.25**	**0.26**	-0.03	0.00
Total	**0.20**	**0.41**	**-0.38**	**-0.38**

[a] Time series of flux smoothed with a 10 year running average.

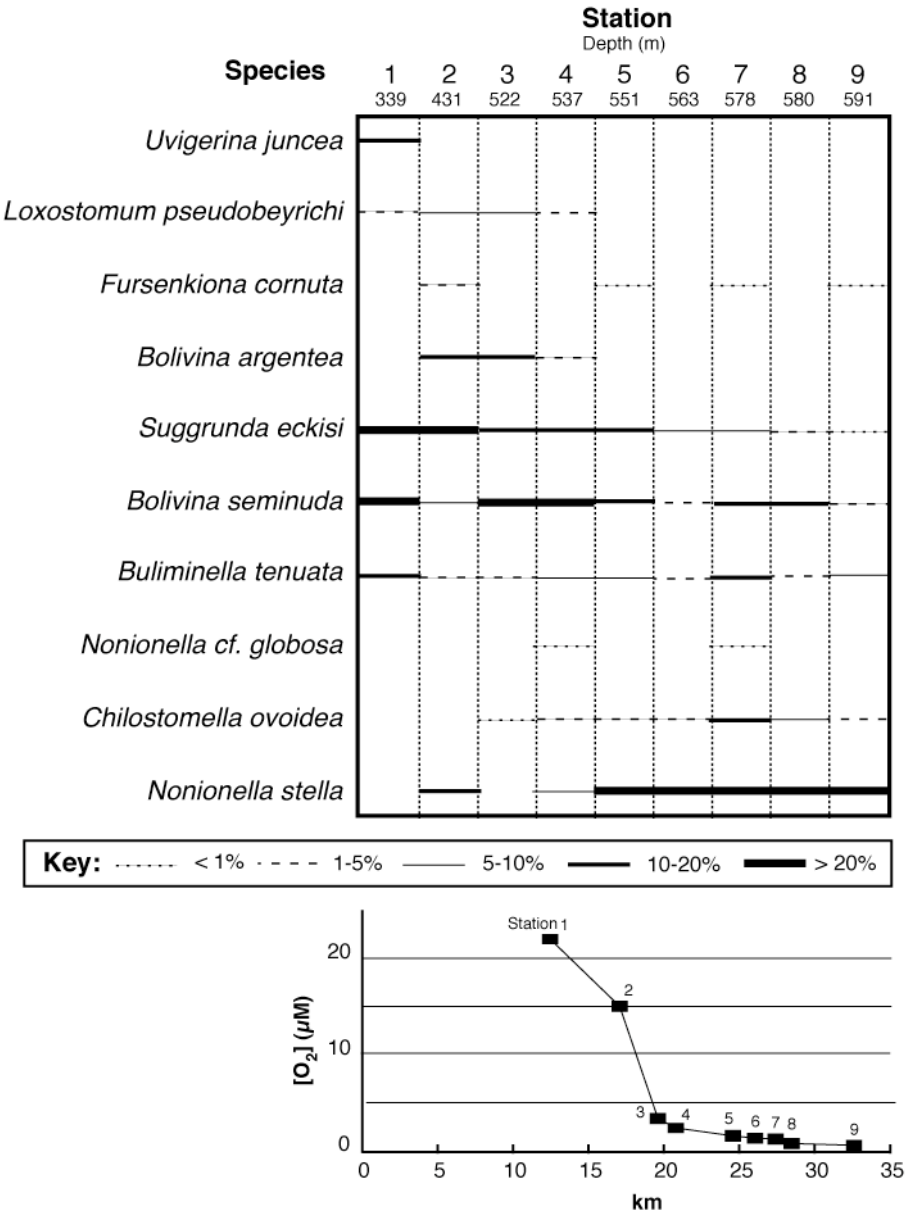


Figure 2.1 (Modified from Bernhard *et al*. (1997), Figure 3) Percent abundance of benthic foraminiferal species at 9 stations across a depth and $[O_2]$ gradient in the SBB.

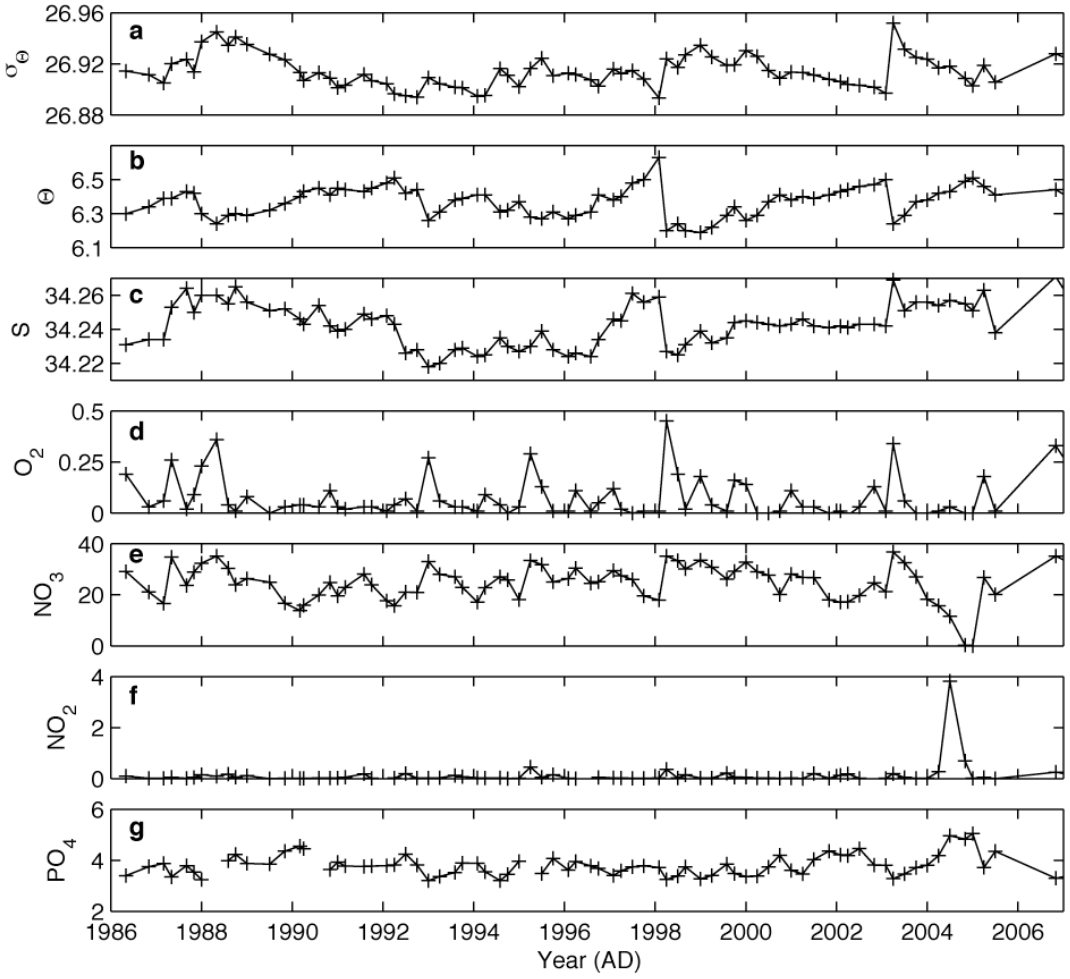


Figure 2.2 (Modified and updated version of Bograd *et al*. (2002), Figure 3) Time series of bottom-most measurements (a) potential density (kgm^{-3}), (b) potential temperature (ºC), (c) salinity (psu), (d) oxygen (ml/l), e) nitrate (μMol/kg), (f) nitrite (μMol/kg) and (g) phosphorous (μMol/kg) at CalCOFI station 82 47 (central SBB). Depth range 557-580 m.

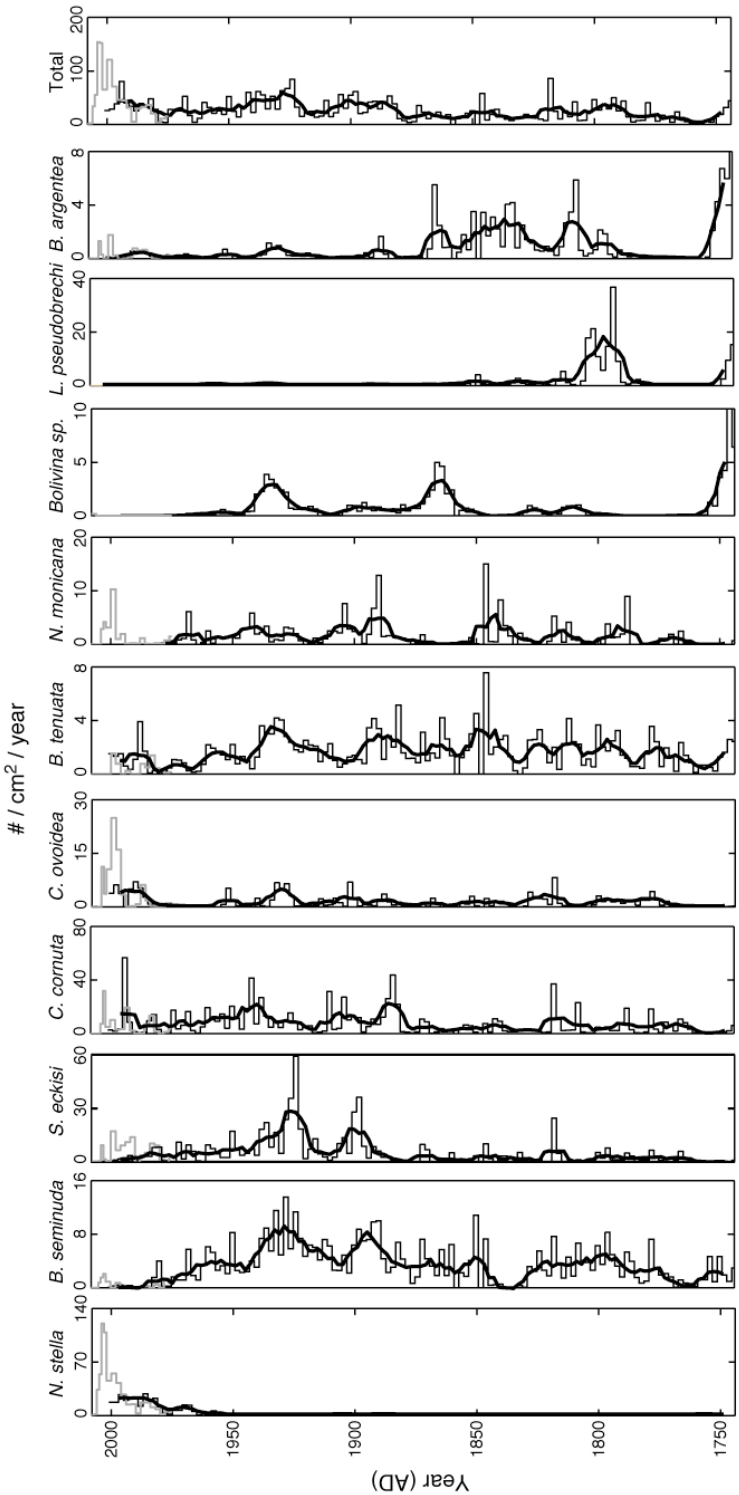


Figure 2.3 Flux of benthic foraminiferal species from SBBC 0110-3001 (dark line) and SBBC 080621-02 (light line). Thick black line depicts 10-year running mean of flux from SBBC 0110-3001. Note differing y-axis ranges.

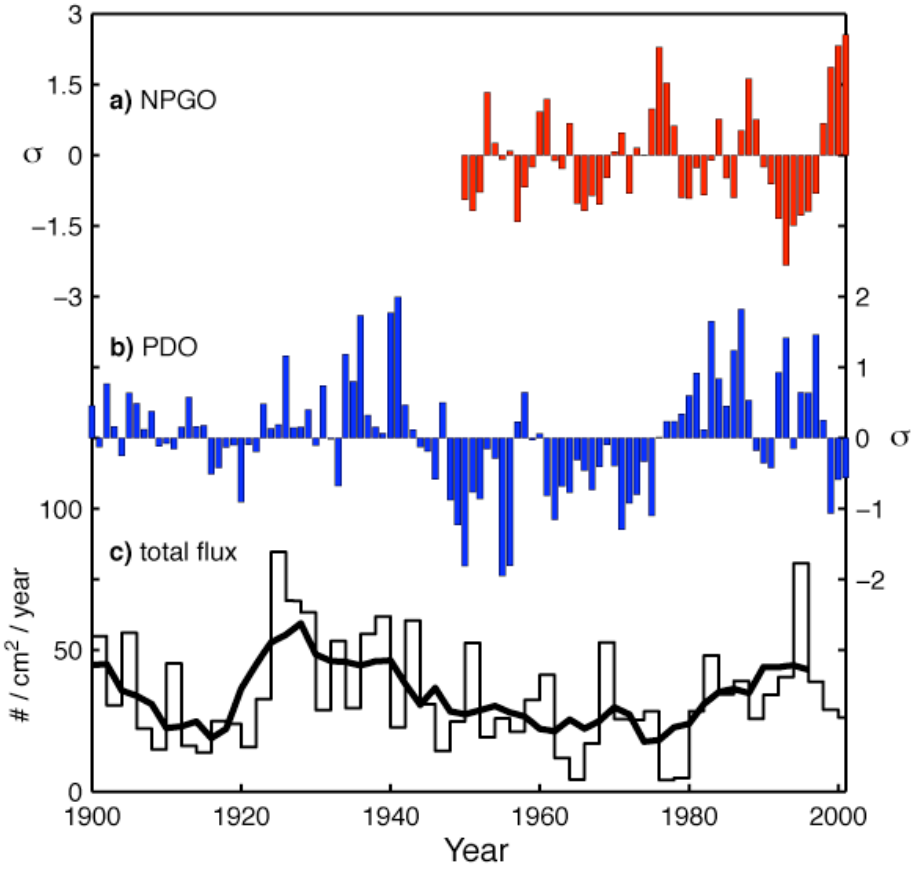


Figure 2.4 Comparison of annually averaged monthly values of NPGO (Di Lorenzo *et al*., 2008) (a) and PDO (Mantua *et al*., 1997; Zhang *et al*., 1997) (a) with total benthic foraminiferal flux from SBBC 0110-3001 (c). Thick black line represents 10-year running average of total flux.

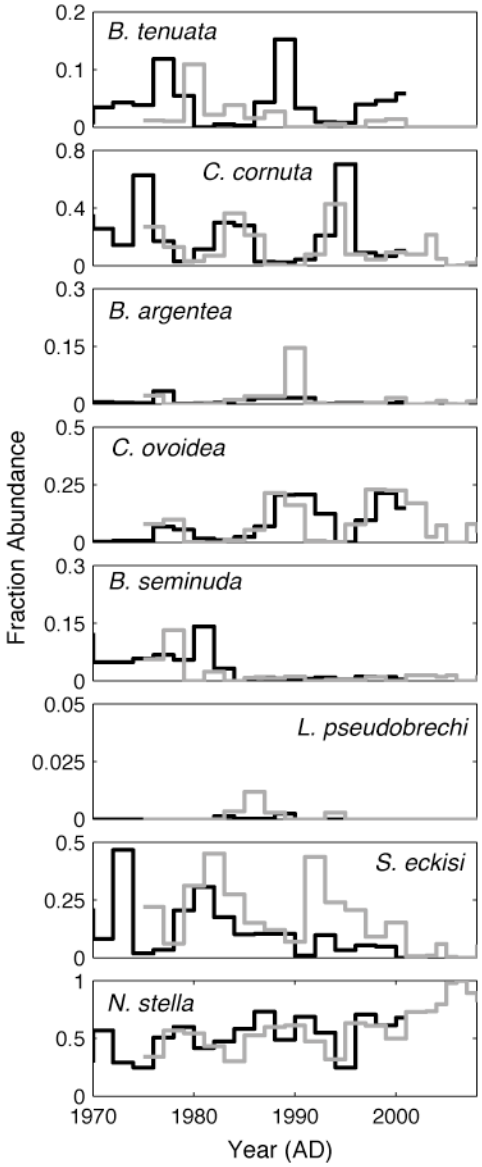


Figure 2.5 Overlapping benthic foraminiferal relative abundances from SBBC 0110-3001 (dark lines) and SBBC 080621-02 (light lines) between 1975 and 2001.

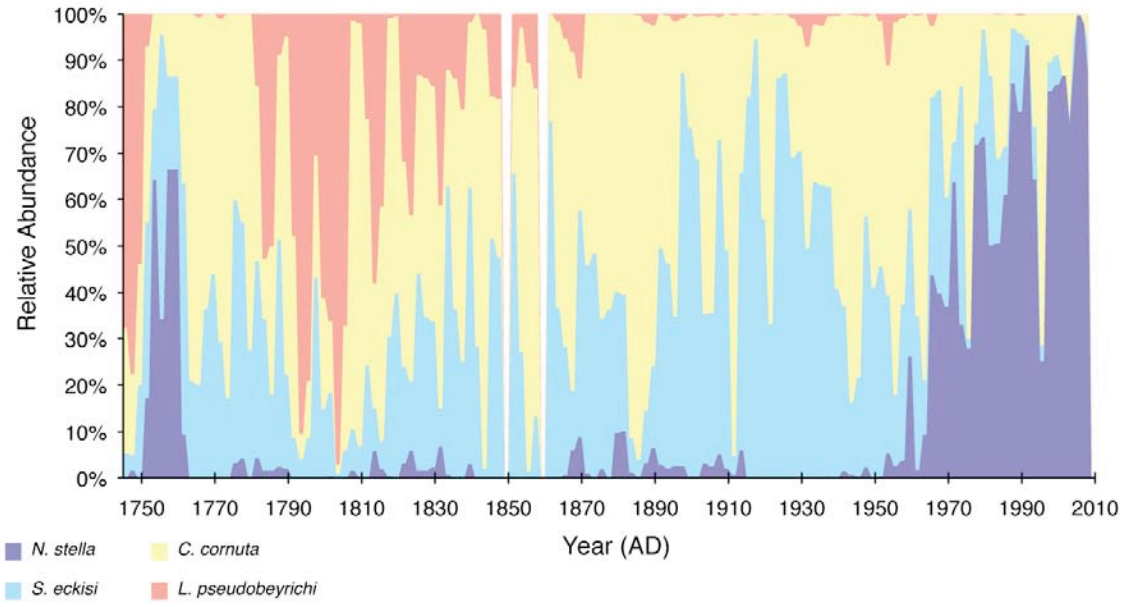


Figure 2.6 Relative abundances of *N. stella* (purple), *S. eckisi* (blue), *C. cornuta* (yellow) and *L. pseudobeyrichi* (red). White lines reflect missing intervals that were not counted.

2.7 References

Auad, G., Kennett, J.P., and Miller, A.J. (2003) North Pacific intermediate water response to a modern climate shift. *J Geophys. Res* 108:doi:10.1029/2003JC001987.

Bandy, O.L. (1953) Ecology and paleoecology of some California foraminifera; Part I – The frequency distribution of recent foraminifera off California. *J. Paleoecol.* 27:161-182.

Bandy, O.L., Ingle, J.C., and Resig, J.M. (1964) Foraminifera, Los Angeles County outfall area, California. *Limnol. Oceanogr.* 9:124-137.

Bandy, O.L. (1964) Foraminiferal trends associated with depp-water sands, San Pedro and Santa Monica Basins, California. *J. Paleontol.* 38:138-148.

Behl, R.J. and Kennett, J.P. (1996) Brief interstadial events in the Santa Barbara Basin, NE Pacific, during the past 60 kyr. , *Nature* 379, p. 243-246

Berelson, W.M., Prokopenko, M., Sansone, F.J., Graham, A.W., McManus, J. and Bernhard, J.M. (2005) Anaerobic diagenesis of silica and carbon in continental margin sediments: Discrete zones of TCO2 production. *Geochim. Cosmochim. Acta* 69:4611-4629.

Berelson, W. and Stott, L.D. (2003) Productivity and organic carbon rain to the California margin seafloor: Modern and paleoceanographic perspectives. *Paleoceanography* 18:doi:10.1029/2001PA000672.

Berkelhammer, M. B., Stott, L. D. (2008) Recent and dramatic changes in Pacific storm trajectories recorded in d18O from Bristlecone Pine tree ring cellulose. *Geochem. Geophys. Geosys.* 9:doi:10.1029/2007GC001803.

Bernhard, J.M. (1992) Benthic foraminifera distribution and biomass related to pore-water oxygen content: central California continental slope and rise. *Deep-Sea Res.* 39:585-605.

Bernhard, J.M. and Bowser, S.S. (1999) Benthic foraminifera of dysoxic sediments: chloroplast sequestration and functional morphology. *Earth-Science Reviews* 46:149-165.

Bernhard, J.M., Buck, K.R., Farmer, M.A. and Bowser, S.S. (2000) The Santa Barbara Basin is a symbiosis oasis. *Nature* 403:77-80.

Bernhard, J.M. and Reimers, C.E. (1991) Benthic foraminiferal population fluctuations related to anoxia: Santa Barbara Basin. *Biogeochemistry* 15:127-149.

Bernhard, J.M., Sen Gupta, B.K., and Borne, P.E. (1997) Benthic foraminiferal proxy to estimate dysoxic bottom-water oxygen concentrations: Santa Barbara Basin, U.S. Pacific continental margin. *J. Foram. Res.* 27:301-310.

Bernhard, J.M. and Sen Gupta, B.K. (1999) Foraminifera of oxygen-depleted environments. In: *Modern Foraminifera* (Ed. B. K. Sen Gupta). Kluwer Academic, Dordrecht, 201-217 pp.

Bograd, S.J., Castro, C.G., Di Lorenzo, E., Palacios, D.M., Bailey, H., Gilly, W. and Chavez, F.P. (2008) Oxygen declines and the shoaling of the hypoxic boundary in the California Current. *Geophys Res. Lett.* 35:doi:10.1029/208GL034185.

Bograd, S.J., Schwing, F.B., Castro, C., and Timothy, D.A. (2002) Bottom water renewal in the Santa Barbara Basin, *J. Geophysical Res.* 107, doi:1029/2001JC001291

Bray, N.A., Keyes, A. and Morawitz, W.M.L. (1999) The California Current system in the Southern California Bight and the Santa Barbara Channel. *J. Geophys. Res.* 104:7695-7714.

Cannariato, K.G. and Kennett, J.P. (1999) Climatically related millennial-scale fluctuations in strength of California margin oxygen-minimum zone during the past 60 k.y. *Geology* 27:975-978.

Cannariato, K.G., Kennett, J.P. and Behl, R.J. (1999) Biotic response to late Quaternary rapid climate switches in Santa Barbara Basin: ecological and evolutionary implications, *Geology*, 27, 63-66

Christensen, C.J., Gorsline, D.S., Hammond, D.E., and Lund, S.P. (1994) Non-annual laminations and expansion of anoxic basin-floor conditions in Santa Monica Basin, California Borderland, over the past four centuries. *Mar Geol.* 116:399-418.

Corliss, B. and Silva, K.A. (1993) Rapid Growth of deep-sea benthic foraminifera. *Geology* 21:991-994.

D'Arrigo, R. Cook, E.R., Wilson, R.J., Allen, R., and Mann, M.E. (2005) On the variability of ENSO over the past 6 centuries. *Geophys. Res. Lett.* 32:1-4.

Deser, C., Alexander, M.A., and Timlin, M.S. (1996) Upper-ocean thermal variations in the North Pacific during 1970-1991, *Journal of Climate*, 9, 1840-1855.

Di Lorenzo, E. (2003) Seasonal dynamics of the surface circulation in the southern California Current System. *Deep-Sea Res. II* 50:2371-2388.

Di Lorenzo, E., Schneider, N., Cobb, K.M., Franks, P.J.S., Chhak, K., Miller, A.J., *et al.* (2008) North Pacific Gyre Oscillation links ocean climate and ecosystem change. *Geophys. Res. Lett.* 35:doi:10.1029/2007GL032838.

Emery, K.O. (1960) The Sea off Southern California. Wiley, New York, 366 pp.

Emery, K.O. and Hulsemann, J. (1962) The relationship of sediments, life, and water in a marine basin. *Deep-Sea Res*. 8:165-180.

Field, D.B., Baumgartner, T.R., Charles, C.D., Ferriera, V., and Ohman, M.D. (2006) Planktonic foraminifera in the California Current reflect twentieth century warming, *Science* 311:63-66.

Field, R.D., Moore, G.W.D., Holdsworth, G. and Schmidt, G.A. (2010) A GCM-based analysis of circulation controls on d18O in the southwest Yukon, Canada: Implications for climate reconstructions in the region

Fisher, D. *et al*. (2004) Stable isotope records from Mt. Logan, Eclipse ice cores and nearby Jellybean Lake. Water cycle of the North Pacific over 2,000 years and over five vertical kilometers: Sudden shifts and tropical connections, *Geogr*. *Phys*. *Quat*. 58:337-352.

Hagadorn, J.W., Stott, L.D., Sinha, A., and Rincon, M. (1995) Geochemical and sedimentologic variations in inter-annually laminated sediments from Santa Monica Basin. *Mar*. *Geol*. 125:111-131.

Harman, R.A. (1964) Distribution of foraminifera in the Santa Barbara Basin, California. *Micropaleontology* 10:81-96.

Hendy, I.L., and Kennett, J.P. (2003) Tropical forcing of north Pacific intermediate water distribution during late Quaternary rapid climate change? *Quat*. *Sci*. *Rev*. 22:673-689.

Hickey, B.M. 1979. The California Current system—hypotheses and facts. *Prog*. *Oceanogr*. 8:191-279.

Høgslund, S., Revsbech, N.P., Cedhagen, T., Nielsen, L.P., and Gallardo, V.A. (2008) Denitrification, nitrate turnover, and aerobic respiration by benthic foraminiferans in the oxygen minimum zone off Chile. *J*. *Exp*. *Mar*. *Biol*. *Ecol*. 359:85-91.

Holsten, J., Stott, L. and Berelson, W. (2004) Reconstructing benthic carbon oxidation rates using d13C of benthic foraminifers. *Marine Micropaleontology* 53:117-132.

Gooday, A.J. (1994) The biology of deep-sea foraminifera: a review of some advance and their applications in paleoceanography. *Palaios* 9:14-31.

Gooday, A.J. and Rathburn, A.E. (1999) Temporal variability in living deep-sea benthic foraminifera: a review. *Earth Sci*. *Rev*. 46:187-212.

Grzymski, J., Schofield, O.M., Falkowski, P.G., and Bernhard, J.M. (2002) The function of plastids in the deep-sea benthic foraminifer, *Nonionella stella*. *Limnol Oceanogr* 6:1569-1580.

Jones, P.D. and Mann, M.E. (2004) Climate over past millennia. *Rev Geophys* 42:2003RG000143.

Jorissen, F.J., Fontanier, C. and Thomas, E. (2007) Paleoceanographic proxies based on deep-sea benthic foraminiferal assemblage characteristics. In: *Proxies in Late Cenozoic Paleoceanography* (Eds: Hillaire-Marcel C. and de Vernal, A.) Elsevier, Amsterdam, 263-326 pp.

Keigwin, L.D. and Jones, G.A., (1990) Deglacial climatic oscillations in the Gulf of California, *Paleoceanography*, 5, 1009-1023

Kuwabara, J., van Geen, A., McCorkle, D.C., and Bernhard, J.M. (1999) Dissolved sulfide distributions in the water column and sediment pore waters of the Santa Barbara Basin. *Geochim. Cosmochim. Acta* 63:2199-2209.

Levin, L.A. (2003) Oxygen minimum zone benthos: Adaptation and community response to hypoxia. *Oceanogr. Mar. Biol.* 41:1-45.

Liu, K.K. (1979) Geochemistry of inorganic nitrogen compounds in two marine environments: The Santa Barbara Basin and the ocean off Peru. Ph.D. thesis, 354 pp., Univ. of Calif., Los Angeles.

Loubere, P. (1991) Deep-sea benthic foraminiferal assemblage response to a surface ocean productivity gradient: a test. *Paleoceanography* 6:193-204.

Loubere, P. (1994) Quantitative estimation of surface ocean productivity and bottom water oxygen concentration using benthic foraminifera. *Paleoceanography* 9:727-737.

Loubere, P. (1996). The surface ocean productivity and bottom water oxygen signals in deep water benthic foraminiferal assemblages. *Mar. Micropaleontol.* 28:247-261.

Lyle, M. Koizumi, I. Richter, C. *et al.* (1997) Proceedings of the Ocean Drilling Program, Initial results, Volume 167: College Station, Texas, Ocean Drilling Program, 1376 p.

Lynn, R.J., and Simpson, J.J. (1987) The California Current System: The seasonal variability of its physical characteristics. *J. Geophys. Res.* 92:12,947-12,966.

Lynn, R.J., and Simpson, J.J. (1990) The flow of the Undercurrent over the continental borderland off southern California. *J. Geophys. Res.* 95:12,995-13,008.

Miller, A.J., White, W.B., and Cayan, D.R. (1997) North Pacific thermocline variations on ENSO timescales. *J Phys. Oceanogr.* 27:2023-2093.

Moore, G.W.K., Holdsworth, G. and Alverson, K. (2002) Climate change in the North Pacific region over the past three centuries. *Nature* 420:410-403.

Natland, M.L. (1933) The temperature and depth distribution of some recent and fossil foraminifera in the Southern California region. Scripps Institution of Oceanography, *Bull. Tech. Ser.* 3:225-230.

Phleger, F.B. and Soutar, A. (1973) Production of benthic foraminifera in three east Pacific oxygen minima. *Micropaleontology*. 19:110-115.

Piña-Ochoa, E., Høgslund, S., Geslin, E., Cedhagen, T., Revsbech, N.P., Nielsen, L.P. *et al*. (2010) Widespread occurrence of nitrate storage and denitrification among Foraminifera and *Gromiida*. *PNAS* 107:1148-1153.

Rathburn, A.E., Perez, M.E. and Lange, C.B. (2001) Benthic-pelagic coupling in the Southern California Bight: Relationships between sinking organic material, diatoms and benthic foraminifera. *Mar. Micropaleontol*. 43:261-271.

Reid, J.L., Roden, G.I., and Wyllie, J.G. (1958) Studies of the California Current system. *CalCOFI Rep*. 6:27-56.

Resig, J.M. (1958) Ecology of Foraminifera of the Santa Cruz Basin, California. *Micropaleontology* 4:287-308.

Risgaard-Petersen, N. Langezaal, A.M., Ingvardsen, S., Schmid, M.C., Jetten, M.S.M, Op den Camp, H.J.M, *et al*. (2006) Evidence for complete denitrification in a benthic foraminifer. *Nature* 443:93-96.

Sen Gupta, B.K. and Machain-Castillo, M.L. (1993) Benthic foraminifera in oxygen-poor habitats. *Mar Micropaleontol* 20:183-201.

Sholkovitz, E.R. and Gieskes, J.M. (1971) A physical-chemical study of the flushing of the Santa Barbara Basin, *Limnol. Oceanogr.*,16:479-489

Sigman, D.M., Robinson, R. and Knapp, A.N. (2003) Distinguishing between water column and sedimentary denitrification in the Santa Barbara Basin using the stable isotopes of nitrate. *Geochem. Geophys. Geosys.* 4:doi:10.1029/2002GC000384.

Silva, K.A., Corliss, B.H., Rathburn, A.E. and Thunell, R.C. (1996) Seasonality of living benthic foraminifera from the San Pedro Basin, California Borderland. *J. Foram Res*. 26:71-93.

Stott, L.D., Berelson, W., Douglas, R. and Gorsline, D. (2000) Increased dissolved oxygen in Pacific intermediate waters due to lower rates of carbon oxidation in sediments. *Nature* 407:367-370.

Stott, L.D., Bunn, T., Prokopenko, M., Mahn, C., Gieskes, J. and Bernhard, J.M. (2002) Does the oxidation of methane leave an isotopic fingerprint in the geologic record? *Geochem Geophys Geosys* 3:doi:10.1029/2001GC000196.

Stott, L.D., Hayden, T.P., and Griffith, J. (1996) Benthic foraminifera at the Los Angeles County White Point outfall revisited. *J Foram Res* 26:357-368.

Talley, L.D. (1993) Distribution and formation of North Pacific Intermediate Water. *J. Phys Oceanogr* 23:517-537.

Trenberth, K.E. and Hurrell, J.W. (1994) Decadal atmosphere-ocean variations in the Pacific. *Climate Dyn*. 9:303.

van Geen A., Fairbanks, R.G., Dartnell, P. et al. (1996) Ventilation changes in the northeast Pacific during the last deglaciation, *Paleoceanography*, 11, 519-528

Zalesny, E.R. (1959) Foraminiferal ecology of Santa Monica Bay, California. *Micropaleontology* 5:101-126.

Zhang, Y., Wallace, J.M. and Battisti, D.S. (1997) ENSO-like interdecadal variability: 1900-93. *J. Climate* 10:1004-1020.

Chapter 3. High-resolution measurements of sedimentary leaf wax lipid hydrogen isotope ratios capture interannual to decadal scale variability in wintertime precipitation and snowmelt in the Sierra Nevada Mountains

Abstract

Southern California derives much of its year-round freshwater supply from snowpack in the Sierra Nevada Mountains—a resource that is highly sensitive to climate warming. Understanding how snowpack and precipitation have varied in the Sierra Nevada Mountains over the past millennium is therefore crucial for the prediction and mitigation of future water shortages in this naturally drought-prone region. This task requires the development of numerous independent proxy records. In this study, we examine the utility of hydrogen isotope ratios (δD) of plant leaf wax lipids, preserved in lake sediments, as a high-resolution (interannual to multidecadal) proxy for past Sierra Nevada hydroclimate. Leaf wax lipid δD was measured over the 20th century at approximately biennial resolution from annually laminated lake sediments in Yosemite National Park. Comparison with local and regional instrumental records of precipitation, snow water equivalence (SWE) and Palmer Drought Severity Index (PDSI) reveals that leaf wax lipid δD faithfully traces hydrologic variability on interannual to multidecadal scales in the Sierra Nevada and throughout the western United States. The negative correlation observed between δD and moisture availability indicates that catchment water balance is the primary driver of isotopic variability. Although the results here show promise for the use of leaf wax lipid δD in paleohydrologic applications, they also emphasize the importance of local environmental factors, including the relative

contribution of aquatic and terrestrial plants to the sedimentary leaf wax lipid reservoir. Thus, adequate constraint of these local influences is a prerequisite for precise hydrologic interpretations of this proxy.

3.1 Introduction

Paleoclimate proxy reconstructions that capture multiple realizations of decadal scale hydrologic variability are an important tool for assessing the impacts of climate change on water resources. These reconstructions, which extend hydroclimate observations beyond the relatively short period of instrumental record, yield information about the climatological sensitivity and physical driving mechanisms of hydrologic variability over decades to centuries. Understanding these factors is particularly important for the naturally drought-prone semiarid regions of the American west (henceforth "the West") that face rising populations and growing demand for freshwater in the coming decades. Numerous studies indicate that climate warming will move this region towards enhanced water stress (Barnett *et al*., 2008; Overpeck & Udall, 2010; Seager *et al*., 2007). Heavy reliance on snowpack in the Sierra Nevada Mountains as a source of freshwater places southern California at particular risk for future drought, as alpine snow pack is highly sensitive to climate warming, and may already be exhibiting signs of demise at lower elevation catchments in the form of advances in spring snowmelt-driven runoff (Roos, 1991; Dettinger & Cayan, 1994; Cayan et al. 2001; Regonda et al. 2005; Stewart et al. 2005), and a diminished accumulation of spring snowpack (Barnett *et al*., 2008; Mote et al 2005; Howat and Tulaczyk 2005). Therefore, paleohydrologic proxies that capture fluctuations in Sierra Nevada snow pack should be particularly useful for assessing future changes in freshwater availability in southern California.

At present a handful of proxies exist that capture decadal scale hydrologic variability in the Sierra Nevada Mountains over the past millennium, including tree-ring

widths (Graumlich, 1993; Cook *et al*., 1999, 2004; Meko *et al*., 2001; Meko & Woodhouse, 2005; Stahle *et al*., 2007) and stable oxygen isotope ratios ($\delta^{18}O$) of calcareous lake sediment (Benson *et al*., 2003; Yuan *et al*., 2004) and tree-ring cellulose (Berkelhammer & Stott, 2008). Because these proxies rely on fundamentally different mechanisms to capture hydrologic information, each reveals a unique, yet potentially incomplete, aspect of the hydrologic cycle. For example, multi-decadal scale fluctuations of calcite $\delta^{18}O$ in Mono Lake sediments are driven by changes in evaporative enrichment related to lake level, while those of $\delta^{18}O$ in the cellulose of Bristlecone Pines in the White Mountains also just east of the Sierra Nevada, appear to reflect variation in the preformed $\delta^{18}O$ of regional precipitation (Berkelhammer & Stott, 2008) that derive from basin scale shifts in atmospheric circulation (Berkelhammer *et al*., submitted). The addition of proxy records from independent archives will help achieve a more comprehensive, mechanistic understanding of decadal scale hydrologic variability in this mountain range over the past millennium.

The hydrogen isotope ratios (δD) of specific plant lipid compounds (biomarkers) that are well preserved in lake sediments (Eglinton & Hamilton, 1967; Meyers & Ishiwatari, 1993; Huang *et al*., 1995) show promise in recent studies as capturing the hydrogen isotope ratios of the surrounding environmental water across a wide range of temperature and moisture gradients (Sauer *et al*., 2001; Sachse *et al*., 2004, 2006; Huang *et al*., 2002, 2004; Hou *et al*., 2006; Hou *et al*., 2008; Feakins & Sessions 2010). Despite these promising findings, the utility of plant lipid δD in decadal scale hydrologic reconstruction has yet to be tested, in part due to the difficulty of extracting sufficient lipid material at high temporal sampling resolution. In this study we have generated an

interannually resolved 20th century record of plant lipid δD from Sierra Nevada lake sediments. Through comparison with instrumental hydrologic observations, we assess the utility of leaf wax lipid δD as a proxy for decadal scale hydrologic variability in the Sierra Nevada Mountains, and attempt to unravel the physical mechanisms responsible for driving observed δD variability.

3.2 Background

3.2.1 δD of environmental water in the Sierra Nevada Mountains.

We follow the convention of using H to represent protium (1H), the commonly occurring hydrogen isotope, and D to represent deuterium (2H), which occurs at ~0.015% natural abundance. We present these ratios in delta notation such that

$$\delta D(‰) = \frac{(D/H)_{SA} - (D/H)_{STD}}{(D/H)_{STD}}(10^3) \quad (3.1)$$

where the subscripts SA and STD refer to the sample and standard respectively. δD values are relative to Vienna Standard Mean Ocean Water (VSMOW) (Craig, 1961). We use the words "higher" and "enriched" to refer to water or plant lipid δD values that are less negative and "lower" and "depleted" to refer to δD values that are more negative. For example, water enriched in deuterium will have δD values that are less negative than water depleted in deuterium.

The δD of environmental water is a function of physical processes within the hydrologic cycle such as temperature, evaporation, moisture source and storm track (Craig, 1961; Dansgaard, 1964; Ehhalt *et al*., 1963; Friedman *et al*., 1964; Gat 1996). Proxies that capture these isotope ratios can therefore provide a mechanistic perspective

on hydrologic variability. At midlatitudes the δD of precipitation is primarily determined by the fraction of original vapor that remains in the air mass when precipitation occurs and the fraction of that moisture that gets recycled back to the atmosphere through evapotranspiration (Ingraham & Taylor 1986, 1991). Precipitation in the Sierra Nevada Mountains is highly seasonal, with > 75% of annual totals falling during the winter (Markham, 1970) primary through the passage of frontal (November-March) storms originating over the Pacific Ocean. The moisture in these storms becomes progressively depleted in deuterium as the storms move inland due to the preferential loss, under equilibrium conditions, of the heavier HDO isotopolouge from the vapor to the denser phase (water or snow). The highly non-linear relationship between temperature and the saturation vapor pressure of water coupled with adiabatic cooling that occurs as the air mass travels east and rises over the Sierra Nevada crest results in a sharp elevational δD gradient with values decreasing ~35-40‰ per 1000 m along the western slope of the mountain range (Friedman & Smith 1969; Smith *et al*., 1979; Ingraham & Taylor, 1991). The precipitation along this slope is therefore depleted in deuterium by ~60-180‰ relative to the ocean water from which the moisture derived. Recycling of moisture back to the atmosphere through evapotranspiration influences the δD evolution of precipitation as moisture moves inland. In a study of precipitation, surface water and shallow ground waters along three zonal transects across California and Nevada Ingraham & Taylor (1991) document increasing contribution of evapotranspiration to moisture recycling and its influence on the δD of precipitation, surface water and shallow ground water with increasing distance inland. This recycling causes a relaxation in the inland δD gradient, deviating it from that expected in a completely open system where all precipitation is

removed through runoff. Using a simplified water balance model, the authors calculate upwind recycling by evapotranspiration contributes 22% of environmental water at the western Sierra Nevada crest.

There are several other factors that influence the δD of precipitation in the Sierra Nevada Mountains. The temperature at which moisture first evaporates and later condenses also contributes to meteoric δD composition. Varying patterns of atmospheric circulation influence the origins and trajectories of storms making land fall on the California coast, with relatively warm and cold storms transporting moisture from the central/subtropical and subpolar North Pacific respectively. Because fractionation between the vapor and water phases increases with decreasing temperature (Majzoub, 1971), the initial vapor in equilibrium with water at 10ºC, typical of midlatitudes north Pacific SSTs, will be depleted by ~18‰ relative to that in equilibrium with 25ºC water in the subtropics. Therefore, the partitioning of moisture derived from northerly or southerly sources can influence meteoric δD in the Sierra Nevada Mountains. Additional factors such as temperature of condensation and relative humidity of air through which precipitation falls can also influence meteoric δD values. Intra-storm precipitation measurements reveal the influence of air mass altitude on the δD of raindrops, with lower values from higher, colder portions of the cloud (Coplen *et al*., 2008). Evaporation off the surface of raindrops and snow that melts prior to deposition shifts δD towards less negative values as the heavier isotope becomes concentrated in the liquid phase. Partial or total requilibration with moisture at lower elevations and warmer temperatures can also increase the δD value of raindrops that formed higher up in the atmosphere (Friedman *et al*., 1962, 1964). Snow is typically depleted in δD relative to rain at a given location

because it precipitates from a colder air mass that has lost a greater fraction of its original moisture. Furthermore, due to slow rates of isotopic exchange between ice and vapor, snowflakes are not subject to these processes and preserve their original δD values as they fall. The combined influence of these processes generates inter storm δD differences > 100‰ (Smith *et al*., 1979; Berkelhammer *et al*., submitted) in the Sierra Nevada Mountains and throughout the American southwest (Friedman *et al*, 2002; Benson & Klieforth, 1989). However, Friedman *et al*. (1992) found that year-to-year variability in the δD of southern California precipitation was only on the order of ~30‰ due to the isotopic integration of many storms. Post-depositional processes will further influence the δD composition of environmental water. Evaporation of soil and lake water can have a disproportionately large isotopic enriching effect on these reservoirs despite limited overall contribution to the catchment's water budget (Kendall & McDonnell, 1998).

3.3.2 Plant lipid δD

Environmental water is the only source of hydrogen for plant lipid biosynthesis. Following uptake, biophysical and biochemical processes within the plant modify the δD signature of this water. Hydrogen isotopes do not undergo fractionation in the uptake of water by plant roots (Barnes & Turner, 1998; Feakins & Sessions, 2010), but are subject to the deuterium enriching effects of leaf water evapotranspiration (Roden *et al*., 2000; Feakins & Sessions, 2010) as well as evaporation of soil moisture prior to uptake (Krull *et al*., 2006; Sachse *et al*., 2006, 2009; Smith & Freeman 2006; but see also Feakins & Sessions, 2010). Feakins & Sessions (2010) found that transpiration in the arid ecosystems of southern California enriched leaf water by as much as 74‰ and that this signal was translated to the δD value of leaf wax lipids. The metabolic pathways

responsible for incorporating leaf water hydrogen into leaf epicuticular wax lipids involve a biochemical fractionation that discriminates against the heavier isotope (Sternberg, 1988; Sessions 2006; Sessions *et al*., 1999). Current studies suggest that this fractionation is constant and primarily determined by the metabolic pathway or biosynthetic precursor, in other words, it is not a function of environmental factors such as temperature (Sessions, 1999). Estimates from previous studies suggest that the magnitude of biosynthetic fractionation is typically around -150‰ (Yakir & Daniro, 1990; Sessions *et al*., 1999; Chikaraishi *et al*, 2004; Sachse *et al*., 2004; Feakins & Sessions, 2010). The combined effect of these biophysical and biochemical processes can be considered as the net biological fractionation (Sessions, 2006), which can differ significantly from the pure biosynthetic fractionation, primarily due to opposing enrichment imposed by evaporation of lake surface or soil water (Sachse *et al*., 2006) or transpiration of leaf water (Feakins & Sessions 2010). Net biological fractionations have been shown to vary significantly, on the order of parts per hundred, between and within individual plant species at the same location under a variety of climatic conditions (e.g. Chikaraishi & Naraoka, 2003; Liu & Huang, 2005; Sachse *et al*., 2006; Hou *et al*., 2007; Feakins & Sessions 2010), a fact that can complicate interpretation of lake sediment isotope records where multiple plant species contribute to the pool of sedimentary lipid compounds (Cranwell 1974; Meyers & Ishiwatari 1993; Fiken *et al*., 2000). Although previous studies identify offsets for particular plants groups, particularly for grasses (Liu *et al*., 2006; Hou *et al*., 2007) an analysis of leaf wax lipid δD from a variety of plants along an aridity gradient in southern California revealed that interspecies variability in net biological fractionation is randomly distributed among individual plants and is not a

function of plant type (Feakins & Sessions 2010). While the authors note that this finding requires further investigation it nevertheless suggests that the spatial and temporal variability of δD from leaf wax lipids preserved in lake sediments, which integrate randomly distributed biological fractionations of individual plants, may be primarily attributed to changes in the δD of environmental water.

Numerous studies to date have empirically demonstrated the ability of sedimentary plant lipid δD, including that of leaf wax lipids, to track δD of environmental water across numerous climatic gradients. Sauer *et al*. (2001) find a direct correlation between δD of algal and terrestrial lipids from lake surface sediments and the overlying lake water along a latitudinal gradient in the northeast United States and southern Canada. Similar studies by Sachse *et al*. (2004, 2006) and Huang *et al*. (2004) along a N/S transect of European and North American lakes respectively show that sedimentary *n*-alkanes of terrestrial and aquatic origins also track their source lake water. Hou *et al*. (2008) compare δD of sedimentary terrestrial leaf wax *n*-acids to δD of precipitation and lake water across an expansive humidity, annual precipitation and vegetative gradient in the American southwest. The authors find a significant correlation between lipid δD, and that of precipitation and lake water. Feakins & Sessions (2010) find that the δD of leaf waxes tracks that of environmental water across an aridity gradient in southern California, allowing for an enrichment factor due to transpiration of leaf water, which appears insensitive to the degree of aridity.

While noting the complex pathways through which δD signatures of environmental water are incorporated in plant lipids, the overall message of these studies is one of cautionary optimism for the utility of plant lipid δD as a paleohydrologic proxy.

Here we test the utility of this potential proxy in decadal scale hydrologic reconstruction. The organic-rich, undisturbed and annually laminated sediments of Swamp Lake, in the Sierra Nevada Mountains, provide the ideal archive from which to make high-resolution (annual to biennial) measurements of leaf-wax lipid δD over the 20th century. Direct comparison of the resulting δD time series with instrumental climate records reveals the extent of and mechanisms by which this proxy captures hydrologic variability on interannual to decadal time scales. Further δD measurements from lake water, regional precipitation and plant specimens are made to help constrain interpretation observed δD variability.

3.3 Study location

3.3.1 Regional climatology

The Sierra Nevada are a north-south trending mountain range spanning 34ºN to 41ºN and bounded by the San Joaquin valley to the west and the Basin and Range province to the east. The Sierra Nevada crest peaks at ~4,000 m in the southern portion of the range and drops off to the north. From west to east, the Sierra Nevada elevation profile rises gradually from the floor of the San Joaquin valley and drops off sharply east of the crest into Owens Valley. Swamp Lake (37º57'N, 119º46'W) is situated at 1535 m elevation along the western slope of the Sierra Nevada in the northwest corner of Yosemite National Park (Figure 3.1a), a location that receives the full brunt of land falling wintertime storms over the range. Protected within the confines of one of the country's oldest National Parks, Swamp Lake has received negligible human impact. The lake has a broad, approximately 20 m deep depocenter surrounded by steep banks (Figure 3.1b) and a surface area of about ~0.8 hectares. Swamp Lake drains a relatively small

catchment of ~160 hectares (Figure 3.1a). Mapped geologic features in Yosemite at 0.4-16 ha resolution were obtained from Jan Van Wagtendonk (personal communication) and soil features at the same resolution from the Natural Resources Conservation Service (NRCS) Soil survey geographic (SSURGO) database for Yosemite National Park, California, USA at http://soildatamart.nrcs.usda.gov. The basin primarily consists of shallow soil and Tioga-age glacial till over impermeable granite and tolanite bedrock. Approximately 50% of basin area consists of outcropping bedrock. Soil water holding capacity to 200 cm in Yosemite National Park ranges from 32 to 342 mm (Lutz *et al*., 2010).

The meteorological station at Hetch Hetchy reservoir, (HTH), located approximately 3 km east and 370 m below Swamp Lake, receives an annual average precipitation of 89 cm (based on the period 1950-2006), with a standard deviation of 28 cm exhibiting the high interannual precipitation variability characteristic of the region (Lundquist *et al*. 2005) (Figure 3.2a). Local thunderstorms are the primary source summertime precipitation. Monthly snow water equivalencies (SWE, the volume of water stored in the extant snowpack) (Figure 3.2b) were obtained from the snowcourse at Bee Hive Meadows (BHV) located 6.5 km northeast and 446 m above Swamp Lake. Peak SWE occurs in March or April and quickly diminishes through June. SWE at Swamp Lake will be slightly lower and peak earlier than that at BHC due to a greater fraction of precipitation falling as rain at Swamp Lake's lower elevation. Average daily air temperatures (Figure 3.2c), obtained from the meteorological station at Buck Meadows (BKM) located 32 km southwest and 578 m below Swamp Lake, fluctuate above and below freezing between November and March. As temperatures at Swamp Lake would

be approximately 5ºC cooler due to the psuedoadiabatic lapse rate, we estimate that 25-40% of the days between November and March at Swamp Lake are below freezing. Summer temperatures at BKM are more stable and average 25ºC. Hydrographs of the Merced River discharge at Happy Isles are plotted in figure 3.3d to illustrate the significant interannual variability in runoff with total discharge for water year 2007 twice that from water year 2008. The precipitation, SWE, air temperature and discharge data described above were obtained from the California Department of Water Resources' California Data Exchange Center (CDEC) website, http://cdec.water.ca.gov/.

3.3.2 Annual lake level cycle

Following the method of Lundquist *et al*. (2003), two Solinst level loggers were deployed at Swamp Lake in October 2006, one in the seasonal inlet, and the other in the shallows along the lake's western bank, to capture lake level, inflow and water temperature. Both loggers were retrieved and redeployed in 2007, and the latter in 2008 and again in 2009. While the inlet stream proved too ephemeral to register pressures above background atmospheric noise, twice-hourly lake level fluctuations and water temperatures over water years 2007 and 2008 measured by the logger in the shallows (lake level data from 2009 water year was lost and Solinst devices have not yet been retrieved for 2010) (Figure 3.2e). The ~0.75 m annual lake level cycle can be characterized in four stages: 1) Swamp Lake levels begin to rise in mid December, likely due to surface and subsurface runoff and groundwater inflow from winter rains that fall as snow at higher elevations. The lake continues to fill through mid March, with rapid jumps in lake level likely due to early snow melt pulses or major storms. The lake reaches its peak in mid March, roughly a month in advance of maximum SWE at BHV

and two months ahead of peak discharge from the Merced River (Figure 3.2d). 2) Between mid March and mid June lake level begins to drop, as outflow exceeds inflow. 3) Lake level drop accelerates around mid June presumably due to increased evaporation rates, which have been documented to peak around mid July at slightly higher Sierra Nevada catchments (Leydecker & Melack, 2000). In July 2009 surface inflow and outflow appeared negligible, suggesting that evaporation may play dominant factor controlling lake level between June and September. Lake level drop over this period is consistent with daily lake surface and pan evaporation rates measured elsewhere in the Sierra Nevada (Kattelmann & Elder, 1991). Lake level drops steadily, reaching a minimum around mid October. 4) Levels remain at a steady state baseline until December, likely with minimal rates of inflow at and outflow. Lacking direct measurements of inflow and outflow rates, we are not equipped to make rigorous estimates of lake water balance. However, based on estimates of annual average precipitation, runoff, lake volume, soil holding capacity and knowledge of surface area for the Swamp Lake drainage basin, we estimate an average replacement time for the catchment of ~1.15 ± 0.56 (based on 1σ of annual HTH precipitation from 1910-2007). Based on the shallow soils over impermeable bedrock that cover the majority of the Swamp Lake drainage basin, we assume groundwater storage is minimal and gets flushed annually by wintertime precipitation and snowmelt, as documented at Sierra Nevada (Kattelmann & Elder, 1991; Huth *et al*., 2004).

Lake surface temperatures reach 4ºC in December and begin to rise again at the end of March, suggesting that the lake is monomictic, overturning in the fall and remaining isothermal throughout the winter (Figure 3.2f). Transient ice cover may protect

the lake from vigorous winter mixing, although air temperatures are not low enough to support permanent ice cover. The presence of unbioturbated sediments indicates that either oxygen is rapidly consumed once the hypolimnion becomes isolated from the atmosphere in the spring or that wintertime mixing is not efficient enough to oxygenate the benthos in the depocenter. Surface water temperatures begin to rise sharply in March, and reach a maximum of ~25ºC mid July, where they remain until declining steadily from mid September to December. The temperature profile in Figure 3.3 reveals a fully developed thermocline at approximately 4 m by July. The presence of a less-developed thermocline in May 2009 (J. Street, personal communication) indicates that thermal stratification begins in the spring. Dissolved oxygen is maximal at the base of the euphotic zone around 4 m and decreases to 12 m where conditions become dysoxic (dissolved oxygen concentrations < ~3 mg/L) (Figure 3.3).

3.3.3 Swamp Lake plant species diversity

The Swamp Lake catchment sits in the lower montane vegetation zone of the Sierra Nevada Mountains and hosts a diverse distribution of deciduous and coniferous trees and shrubs, riparian grasses and aquatic macrophytes. Common trees include ponderosa pine (*Pinus ponderosa*), black oak (*Quercus kelloggii*) and incense cedar (*Calocedrus decurrens*). A shrub fringe of white manzinita (*Arctostaphylos viscida*), western azalea (*Rhododendron occidentale*), deer brush (*Ceanthus integerrimus*), white alder (*Alnus rhombifolia*), willow (*Salix* sp.) and dogwood (*Cornus* sp.) surrounds the lake. Lakeshore sedge (*Carex lenticularis*), beaked sedge (*Carex utriculata*) and bog bean (*Dullichium arundinaceum*) are the dominant emergent plants. Swamp Lake is mesotrophic, supporting an abundant planktonic diatom community and numerous

emergent and submergent aquatic macrophytes in the shallow regions. Common emergent species include bog bean (*Menyathes trifoliata*), watershield (*Brasenia scherberi*) and another water lily of genus *Nuphar*. The submergent community is dominated by swaying bulrush (*Schoenoplectus subterminalis*) and pondweed (*Potamegeten robenseii*). Plant species identification was aided by Alison Colwell of the Yosemite National Park Service.

3.4 Methods

3.4.1 Sample collection and processing

We collected a total of 8 freeze cores and 6 Bolivia cores from Swamp Lake in the falls of 2006 and 2007 (Figure 3.1b). The freeze coring technique was employed to ensure preservation of the uppermost sedimentary layers deposited over the 20th century. This technique entailed freezing a ~1-1.5 cm thick sedimentary crust onto a hollow, weighted, aluminum wedge filled with a dry ice-ethanol slurry. The resulting hollow frozen sedimentary wedge was removed and stored in a cooler with solid CO2 for transport out of the field to permanent storage in a permanent -20ºC freezer. We also used a Bolivia corer, a more conventional device, to capture longer (~1.5 m) cores and thus older material. Bolivia cores were transported out of the field at room temperature and later stored in a 4ºC refrigerator at SIO. Metadata and descriptions of Swamp Lake cores can be found in Appendix B.

Lake water and vegetation samples were collected during a third field expedition in July 2009. Water samples were collected from the center of Swamp Lake at the surface and 2, 4, 5, 6, 8, 10, 12 and 14 m depth and stored in 50 mL HDPE bottles sealed with Parafilm to hinder evaporation. Bottles were capped and wrapped in aluminum foil to

prevent exposure to light. Snow that accumulated during six individual storm events between January and April 2010 was collected by Jim Roche (Yosemite National Park Service) at Hodgdon Meadow 5 m above and 17 km south of Swamp Lake. A 2' by 2' wooden board with a marker pole was placed on the ground prior to a storm following the procedure ascribed by the National Weather Service Forecast Office (2008). When precipitation ceased, snow was collected in a metal pot, with care taken to collect an equal amount of snow from all depths on the board. The sample was allowed to melt completely at room temperature, and an aliquot was transferred to an 8 mL glass vial allowing no headspace. Vials sealed with Parafilm wax, capped tightly and wrapped with Teflon tape to prevent evaporation and kept in the dark at room temperature until analysis.

Table 3.1 lists the species, type and location of 16 vegetation samples from Swamp Lake and its surroundings catchment. Approximately five to ten leaves, needles or blades of grass were collected from each species using clean scissors. Specimens were placed in Ziploc bags and transported frozen from the field in a cooler containing dry ice to permanent storage in a -20ºC freezer at the Scripps Institution of Oceanography where they remained until analysis.

3.4.2 Core logging and imaging

7 of 8 freeze cores and 5 of 6 Bolivia cores were logged at the Limnological Research Center at the University of Minnesota, Minneapolis (LRC) in the months following each expedition. In addition to basic core processing, high-resolution digital images of core surfaces were taken at the LRC using DMT CoreScan (at 100 pixels per cm resolution) and Geotek GeoScan-III (at 190-200 pixels per cm resolution) digital

linescan cameras for Bolivia and freeze cores respectively. Also at the LRC, subsamples of frozen sediment cores were embedded with Spurr's low viscosity epoxy resin and smear slides were taken along various depths in the Boliva cores for microscopic inspection. Once cured, embedded subsamples were cut on a rock saw and sent to San Diego Petrographic in Emmett ID where thin sections were made.

3.4.3 Water sample δD analysis

δD and $\delta^{18}O$ of Swamp Lake water samples and Hodgdon Meadow snow samples were measured in the lab of Alex Sessions at the California Institute of Technology in Pasadena, CA on a Los Gatos Research Liquid Water Analyzer 908-0008 following the instrument set up described in detail by Lis *et al*. (2008). Three replicate measurements for each precipitation sample and four for each lake water sample were carried out with six aliquots of 0.8 μl injected for every measurement. Samples were normalized to the SMOW/SLAP isotopic scale against a standard of known δD value, which was measured after every four unknowns. An additional sample of known isotopic value was analyzed in every cycle and treated as an unknown for quality control. The average precision for δD and $\delta^{18}O$ during the period of lake water sample measurement was 0.4‰ and 0.1‰ (1σ, N=48) respectively, with an accuracy of isotopic values reproducible within 0.5‰ and 0.18‰ based on replicate measurements of the quality control. For snow samples δD and $\delta^{18}O$ average precision was 0.8‰ and 0.1‰ (1σ, N=43) with an accuracy of isotopic values reproducible within 4.0‰ and 0.2‰. Poor δD accuracy for the snow samples may be due to slight evaporation of the quality control sample prior to and during analysis, shifting is its actual δD value slightly higher.

3.4.4 Sediment and plant sample preparation and lipid identification

Freeze core SL0601T was sampled in a -20ºC cold room with a sharp razor blade at annual to interannual resolution with the down core interval for each sample ranging from 1-3 mm. Care was taken to sample along laminations such that sampling was not always directly orthogonal to the down core axis (see Figure 3.4). Samples were placed into precombusted 20 ml glass vials and lyophilized. All chemical processing and analysis of sediment samples was carried out in the lab of Alex Sessions at the California Institute of Technology in Pasadena, CA. Lyophilized sediment samples were weighed, with masses ranging from 10-91 mg, and the solvent-soluble lipids extracted in 20 ml of the 9:1 dimethylchloride (DMC):methanol azeotrope in a Mars Express microwave-assisted solvent-extraction system (Mars 5, CEM corp.) for 30 min at 100ºC with stirring. Vegetation sub-samples were placed in precombusted 20 ml glass vials, lyophilized, and cut into approximately 1 cm x 1 cm pieces with solvent cleaned scissors. The solvent-soluble total lipid extract (TLE) by was extracted by sonicating in DCM for two 10-minute intervals.

Sediment and vegetation TLEs from all but one species (*A. viscida*) were separated into four organic fractions: hydrocarbons (*n*-alkanes), ketones, alcohols and fatty acids (*n*-acids) using solid phase extraction (SPE) procedure and elution schedule described in Sessions *et al*. (1999). Briefly, 8 ml glass syringe barrels were packed with 0.5 g of stationary phase bulk packing material (Supelco Discovery DSC-NH2). Hydrocarbons were eluted with 4 ml hexane, ketones with 7 ml 4:1 hexane:DCM, alcohols with 7ml 9:1 DCM:acetone and fatty acids with 8 ml 2% formic acid in DCM.

The fatty-acid fraction was derivatized to methyl esters by refluxing with boron trifluoride in methanol at 70ºC for 10 minutes.

3.4.5 δD Analysis of plant and sediment samples

The *n*-acid fraction was analyzed on a ThermoFinnigan Trace GC-DSQ quadrupole mass spectrometer equipped with a DB-5 column (30 m x 0.25 mm x 0.25μm) and PTV injector operated in splitless mode. The relative abundance of even carbon number *n*-acids C20-C32 was determined by integrating peak area using the Xcalibur software package. δD analyses of individual *n*-acids was carried out on a ThermoElectron Trace GC coupled to a Delta + XP IRMS via an Al_2O_3 pyrolysis chamber. All measurements took place in the lab of Alex Sessions at the California Institute of Technology in Pasadena, CA. δD values were determined relative to at least two reference peaks of CH_4 (C.P. grade) or H_2 gas co-injected during each GC-IRMS run and reported relative to VSMOW in per mil units. Two to three additional reference peaks were injected and treated as unknowns. To correct for H_3^+ interference with mass-3 (Sessions *et al*., 1999), the H_3^+ factor was calculated daily by measuring the mass 3/2 signal ratio of 10 peaks of H_2 reference gas with varying peak intensities covering the range of most H_2 peaks from analyzed sample compounds. The isotopic contribution of methylation reagents was corrected for by analyzing derivatized phthalic acid (dimethyl phthalate) of known δD (Sessions *et al*., 2002). An external standard containing 8 n-alkanes (F8) of known δD value determined independently offline was analyzed at the start and finish of every sample run and between every two to four samples. The mean precision for replicate measurements of the external standard was 5.16‰ (1σ, N=70) and the root-mean-square (RMS) error 4.63‰ during the period of analysis.

3.5 Determination of chronology

We used two independent methods to confirm the presence of annual laminations. We counted laminations from the sediment water interface to a thick charcoal band at ~5 cm depth following predetermined criteria for defining varves (Lamoreaux *et al*., 2001). Assuming each light-dark couplet equal to one year, we determined that this charcoal was deposited in 1996, the same year that the Ackerson Fire, one of the largest fires in Yosemite National Park history, which burned a 243 km^2 area that included the Swamp Lake drainage basin (Van Wagdendonk, personal communication). Light-dark couplets continue below this charcoal band, indicating that the presence of abundant charcoal is not a prerequisite for varve formation. We also examined thin sections under a microscope and observed that light couplets consist primarily of diatom frustules while dark couplets consist of charcoal, other organic material and clastic fragments. This seasonal cycle is characteristic of lakes in this region, where diatoms blooms occur in the spring and fall while terrigenous material is washed into the lake by winter and early spring runoff. An age model for SL0601T (Figure 3.4) was created by counting varves on high-resolution digital images on five separate occasions. The range of uncertainty was determined as the full range of the in number of years counted between clear marker lamina at each counting session. Spectral analysis of lightness, or L, in the L*a*b color space (see Appendix C for details).generates a clear peak at a 1-year periodicity according to the visually determined age-depth model, verifying the presence of annual laminations.

3.6 Results

3.6.1 Sediment and plant *n*-acid distributions

Relative abundance of *n*-acids C20-C32 was measured from all but one (*A. viscida*) of the 16 individual plant species listed in Table 1 (Figure 3.5). Average *n*-acid distributions of terrestrial (N=7), emergent (N=4) and submerged/floating plants (N=4) plants are shown in Figure 3.6. The large standard deviations reflect the significant variability within each plant group. C24 and C22 are the most abundant *n*-acids in the submerged/floating plants with relative abundances of 22 ± 7% and 21 ± 13% respectively. C24 alone is the most *n*-acids among emergent plants at 20 ± 3% relative abundance and C24 and C30 are most abundant *n*-acids for terrestrial plants with relative abundances of 21 ± 9% and 21 ± 11% respectively. On average the *n*-acid distribution of submerged/floating plants is weighted towards the shorter chain compounds while the *n*-acids of emergent and terrestrial plants are move evenly distributed. These *n*-acid distributions are generally consistent with those of same plant groups from vegetation collected at a series of lakes in East Africa (Ficken *et al*., 2000). C24 is on average the most abundant *n*-acid of the vascular plants sampled from the Swamp Lake watershed.

The average relative abundances of C20-C32 *n*-acids in the fatty acid fraction of sediment samples (N=72) are plotted in figure 3.7. Down core variability is low with C24 displaying the maximum relative abundance of 44 ± 5%. The distribution in figure 3.7 is typical of mesotrophic lake sediments (Meyers and Ishiwatari, 1993). We use simple mass balance in attempt to estimate relative contributions to sedimentary *n*-acids of submerged/floating versus emergent and terrestrial plants. Due to the large range in *n*-acid distribution between individual species within the same plant group, the relative uncertainty surrounding these estimates exceeds 100%. For example, based on the 10±1% relative abundance of C30 in modern sediment we calculate a 20±40%

contribution from submerged/floating plants. Although we cannot quantitatively estimate the contributions of these groups, qualitative comparison of sedimentary versus plant group distributions suggests a greater contribution from emergent and submerged/floating plants based on the low relative abundance of longer chain (C30 and C32) *n*-acids in the sediment. Therefore, while all three plant groups have similar relative abundances of C24, we assume that δD of sedimentary C24 n-acid primarily reflects that of submerged/floating and emergent plants.

3.6.2 Storm event, lake water and plant δD

δD of Hodgdon Meadow snow samples are listed in Table 3.2. δD of snow samples, which represent the integrated precipitation deposited over the course of a snow storm, range from -35.5‰ to -106.8‰ characteristic of the wide range of storm to storm isotopic variability in this region (Friedman *et al*., 1979; Berkelhammer *et al*., submitted). The amount-weighted average is estimated at -91‰, as only corresponding snow depth and not snow SWE was available. As Hodgdon Meadows is at the same elevation as Swamp Lake we assume that this isotopic value is representative of snow at Swamp Lake. Accounting for elevational differences (Friedman *et al*., 1979), this value is comparable to amount weighted average δD of April 1 snowpack, precipitation and stream flow from the surrounding region documented in several studies over the past few decades (Friedman *et al*., 1979; Kendall & Coplen, 2001; Huth *et al*., 2004; Unnikrishna *et al*., 2002; Berkelhammer *et al*., submitted).

Swamp Lake water δD from July 2009 is lowest in the upper 2 m at ~-78‰, and increases between 2 and 8m depth to ~-69‰ where it remains to 14 m, the deepest depth sampled (Figure 3.8). This transition roughly corresponds to the depth of the thermocline

(Figure 3.3). The presence of depleted surface water reflects inflow to the surface lake that occurred following the onset of thermal stratification in the spring, as observed in Pyramid Lake by Benson, (1994). The structure of this profile indicates that lake water exchange rates have dropped off by early summer allowing for the formation of a heterogeneous vertical δD profile. Assuming Swamp Lake is in isotopic steady state from year to year, which in reality is not likely as discussed below, and the δD of outflow is equivalent to that of well-mixed lake water, the roughly +10‰ offset between the δD of precipitation and δD of the deep lake requires that ~8% of annual inflow be evaporated, based on inflow δD of -90‰ and average δD of evaporation of -174‰. Summertime thermal stratification (Figure 3.3) and decoupling between the timing of inflow (winter and spring) and evaporation (summer and fall), results in a summertime epilimnion (the well-mixed upper ~4 m above the thermocline) that mimics a closed basin with minimal moisture inputs from summer storms and evaporation acting as the only moisture sink. As the epilimnion volume is only a fraction of total lake volume, evaporation can have a significant isotopic mass balance influence, shifting epilimnion values by 10s of ‰ over the course of the summer.

δD was measured for a subset of 4-6 plant species (Table 3.2). C24 δD values range from -123‰ to -189‰. Based on this small subset, δD does not appear to be a function of plant type, for example C24 values for terrestrial plants ranged from -126‰ to -195‰, although the δD from the two submerged/floating plants measured both have low C24 values of -182‰ and -195‰. We calculate net biological fractionations, reported here as the enrichment factors between wax lipids and water ($\varepsilon_{wax/w}$) in permil notation (Cohen *et al*., 2007) using the formula:

$$\varepsilon_{wax/w} = (\alpha_{wax/w} - 1) = \frac{\delta D_{wax} + 1}{\delta D_w + 1} - 1 \quad (3.2)$$

where the subscripts wax and w correspond to wax lipid and w respectively and $\alpha_{wax/w}$ is the fractionation factor between wax lipid and water. Based on weighted averages of the measured δD from C22-C28, and a water δD value of -78‰, equivalent to surface water measured at the time of plant sample collection, we estimate an overall net biological fractionation of -102 ± 19‰ (N = 6 species). Submergent/floating species have an average C24 net biological fractionation of -103 ± 10‰ (N = 2), and terrestrial species of -94 ± 32‰ (N = 4 species) although these small samples size may not be representative of the entire community.

3.6.3 Sediment *n*-acid δD

The δD of even carbon numbered n-acids C22-C28 was measured from 84 sediment samples spanning 1898-2006 (Figure 3.9). 72 samples were collected from SL0601T to create a 20th century time series, with replicate values from a sub-set of 21 samples measured months to years following original measurements. The average absolute offset between SL0601T C22-C28 replicates is 5.05 ± 1.57‰. Based on this offset and measurements of the F8 external standard we find that the δD of individual samples is reproducible within 7‰. Decadal scale δD variability over the 20th century is on the order of 30-50‰, with values ranging from -188‰ to -137‰ for C24. δD of C22-C28 covaries throughout the record. Average δD values for C24-C28 are the same within analytical uncertainty at -164‰ while average δD for C22 is slightly lower at -172‰. Of the four compounds analyzed, C24 yields the most complete record owing to its consistently large peak intensity and area and we therefore select the C24 δD time series

for further analysis. Based depth interval sampled, we use the varve chronology in figure 3.4 to assign a single "central" year to each C24 value. Four distinct, multi-decadal oscillations stand out in the 20th century C24 record (hereby referred to as "C24"), with decreasing magnitude going back in time. The highest values in the record occur during the late 1980s to mid 1990s. Values are also relatively elevated during the 1950s, early 1930s and around 1910. The lowest values occur between 2003 and 2006, the late 1970s, the mid 1940s, early 1920s and around the turn of the century. For each oscillation, low values are typically around -185‰ yet the high values get progressively higher with each cycle moving forward in time, resulting in an overall trend of ~20‰ between 1898 and 2006.

3.6.4 Comparison of modern δD to instrumental records

In order to examine the physical mechanisms responsible for driving interannual leaf wax lipid δD variability in Swamp Lake, we compare C24 to regional records of total annual precipitation, April 1st SWE and Palmer Drought Severity Index (PDSI) (Figure 3.10, series a-d). PDSI is a standardized indicator of regional aridity that uses autocorrelative techniques to account for cumulative impacts of sustained periods of water shortage (Palmer, 1965; Hayes, 2006). Precipitation, PDSI and temperature from California Climate Division 5 (Div5), which encompasses the San Joaquin Valley and the western Sierra Nevada Mountains, was obtained from the NOAA Earth System Research Laboratory (ESRL) monthly/season time series website: http://www.esrl.noaa.gov/psd/cgi-bin/data/timeseries/timeseries1.pl. April 1st SWE records are from the CDEC BHV and Donner Summit (DNS, 159 km north and 568 m above Swamp Lake) snow courses and were obtained from http://cdec.water.ca.gov.

Instrumental summertime (June-August) PDSI records from the 2.5º x 2.5º gridded North American Drought Atlas (NADA) grid squares 47 (gs47, centered on 37.5ºN, 120.0ºW) and 59 (gs59, centered on 37.5ºN, 117.5ºW) (Cook *et al*., 2004b) were obtained from http://www.ncdc.noaa.gov/paleo/pdsidata.html. Instrumental records were smoothed with a two-year running mean to mimic the time-integrating effects of the approximately biennial sampling resolution. Table 3.3 lists the coefficients of C24 correlation with all instrumental records analyzed at zero to three years lag. In order to avoid interpolation through missing δD values, smoothed instrumental records were resampled for those years containing a δD value, typically reducing the number of instrumental data points by approximately a factor of 2. Lagging the C24 record does not improve correlations with any of the records, nor does further smoothing of instrumental records. C24 exhibits negative correlation with all hydrologic indices with coefficients significant at the 95% confidence interval for all records except PDSI from NADA gs47. In other words, lower (higher) δD values correspond to greater (less) annual precipitation, more positive (more negative) values of PDSI and larger (smaller) April 1st SWE. The correlation with BHV April 1st SWE ($r = -0.53$, $p < 0.001$) is the strongest of all the climate records analyzed (Table 3.3). C24 shows no correlation with annual means of Div5 winter (NDJFM) or summer (MJJAS) average daily temperature (not shown). Table 3.4 lists correlation coefficients for annual comparison between each of the instrumental records examined. PDSI and precipitation are tightly linked ($r > 0.8$) while correlation of PDSI and precipitation with April 1st SWE is slightly less ($0.38 \leq r \leq 0.79$). Figure 3.11 illustrates that interannual C24 δD excursion can be matched to individual droughts and pluvial

episodes in the Sierra Nevada Mountains, such as the droughts in 1947, 1953, 1977 and 1988-1990 and pluvials in 1906, 1940, 1982, and 1986.

Having established a temporal relationship between δD and moisture availability at interannual time scales, we wish to determine whether this relationship extends to basin scale processes, specifically fluctuations in tropical Pacific SSTs. Tropical Pacific SSTs are thought to play a dynamical role in determining the origins, trajectory and amount of precipitation across the West, and were likely a factor in the occurrence modern and prehistoric droughts in this region (e.g. Seager *et al*., 2005a; Seager *et al*. 2005b; Seager *et al*., 2007; Seager *et al*., 2008; Rajagopalan *et al*., 2000; Cole *et al*., 2002; Hoerling & Kumar, 2003). Tropical-midlatitude atmospheric teleconnections that stem from the presence of anomalously cool SSTs in the eastern and central tropical Pacific (La Niña events), are linked to moisture deficits in the Sierra Nevada Mountains (Cayan *et al*., 1999). Monthly averaged SSTa from the NINO3.4 region (5ºN-5ºS, 150ºW-160ºE) were obtained from http://iridl.ldeo.columbia.edu/SOURCES/.Indices/.nino/.EXTENDED/.NINO34/. We observe a weak negative correlation between C24 and NINO3.4 SSTas (Figure 3.10 series e). This relationship is noticeable during the Dust Bowl Drought in the 1930s and again in the late 1980s when cool SSTa coincide with drought and elevated δD.

We can further examine the driving mechanisms of δD variability by comparing C24 with instrumental climate records at interdecadal frequencies (Figure 3.11). Between 1920 and 2006 20 year low pass filtered C24 tracks low pass filtered DNS April 1st SWE and NADA gp59 PDSI, however prior to 1920, we see C24 move out of phase with these indices. In order to assess the influence of basin-scale processes at interdecadal

frequencies, we also compare C24 with a 20 year low pass of the annually averaged Pacific Decadal Oscillation (PDO) index. PDO describes the dominant mode of multi-decadal warm-cold SST oscillations north of 20ºN in the Pacific basin (Latif & Barnett, 1994; Mantua *et al*., 1997; Zhang *et al*., 1997; Mantua & Hare, 2002), and has been active at decadal to multi-decadal frequencies over the past millennium (Biondi *et al*., 2001; Benson *et al*., 2003; Mantua & Hare, 2002; Geldolf & Smith, 2001; D'Arrigo *et al*., 2001; MacDonald & Case, 2005). The positive phase of PDO is associated with a wintertime deepening (strengthening) of Aleutian Low pressure system that results in wetter conditions in the American southwest and drier conditions in the Pacific Northwest, with precipitation anomalies of reverse sign documented during the negative phase of PDO (McCabe *et al*., 2004). Although the Sierra Nevada Mountains span the transition between this precipitation dipole, the location of Swamp Lake typically receives more precipitation when PDO is positive than when it is negative (McCabe *et al*., 2004; Stewart *et al*., 2005). The pattern of atmospheric circulation associated with the positive (negative) phase of PDO shifts mid latitude storms tracks to more southerly (northerly) latitudes that resemble those associated with shorter lived (interannual) El Niño (La Niña) events (Liu and Alexander, 2007). Therefore, in addition to influencing the amount of precipitation that falls at Swamp Lake, PDO also plays a role in determining the origins and trajectory of this precipitation. Monthly averaged PDO indices were obtained from http://jisao.washington.edu/pdo/PDO.latest. As observed with tropical Pacific SSTa at interannual frequencies, δD and PDO only covary when negative PDO corresponds to drought conditions, as during the 1930s.

We would expect any proxy for paleo-hydrologic conditions in the Sierra Nevada Mountains to also be correlated with hydrologic variability throughout the West, as droughts and pluvials in this region are experienced with a high degree of spatial coherency (Aguado, 1900; Cayan, 1996; Cayan *et al*., 1998). In order to test the spatial coherency of the negative correlation between δD and moisture availability, we compare C24 to records of April 1st SWE and PDSI throughout the Sierra Nevada and the West. We correlate annually interpolated (with the years of missing δD values excluded) C24 with April 1st SWE anomalies from 858 National Resources Conservation Service (NCRS) SNOwpack TELemetry (SNOTEL) and CDEC snow courses throughout the West (defined as 30-49ºN, 230-260ºE), including a subset of 204 snow courses in the Sierra Nevada Mountains (defined as 35-40ºN, 237-243ºE), provided by David Pierce (personal communication). We focus on the period 1948-2006 in order to maximize the number of stations with relatively complete records. April 1st SWE anomalies are smoothed with a two-year running mean as described above. C24 is negatively correlated with 99% of SWE records throughout the West, with 73% of these negative correlations significant at the 95% confidence interval (Figure 3.12a). None of the positive correlations are significant at the 95% confidence interval. 100% percent of Sierra Nevada correlations are less the 0, with 89% significant at the 95% confidence interval. (Figure 3.12c). In addition to the Sierra Nevada Mountains, negative correlations are strongest in the Central Rockies, and weakest in the Pacific Northwest and New Mexico. In order to remove any correlation driven monotonic trends in April 1st SWE over this time period, (Dettinger & Cayan, 1995; Stewart *et al*., 2005), we also correlate C24 and SWE records that have had a linear trend removed (Figure 3.12 b, d). Throughout the

West 96% of correlations between the detrended records are negative, with 67% significant. In the Sierra Nevada Mountains 100% are negative and 96% significant. Correlations with the majority of Pacific Northwest SWE weaken following detrending, with many switching to positive, although not statistically significant values. Strong negative correlations remain in the Sierra Nevada and the central Rockies of Colorado, southern Idaho and western Wyoming. The same correlation exercise was preformed for the gridded instrumental PDSI records in the NADA in the West (Figure 3.13) over the period 1900-2003. 96% of the 75 PDSI records are negatively correlated with C24, 71% of those significant at the 95% confidence interval.

We also examine the spatial patterns of April 1st SWE and summertime PDSI associated with high and low δD extremes in the C24 record. For SWE, the post-1948 C24 δD record was divided into quartiles, with years attached to δD values falling below the first quartile and above the third quartile referred to here as the low δD and high δD subsets respectively. Using the SWE data set presented above, composites of standardized April 1st SWE anomalies in the Sierra Nevada and the West were generated for these two subsets (not shown). Following the methodology of Huntington *et al*. (2004) and Knowles *et al*., (2006), we removed those snow courses missing more that 50% of annual observations over a ten year period. 79% of Sierra Nevada snow courses and 82% of snow courses across the West record positive April 1 SWE anomalies in the low δD composite with 27% and 27% of those anomalies, respectively, $\geq 0.5\sigma$. Composites for the high δD subset reveal the opposite pattern although not quite as strong, with composited SWE anomalies < 0 for 73% (1% $\leq -0.5\sigma$) of Sierra Nevada and 69% (3% $\leq -0.5\sigma$) of all snow courses in the West. For PDSI composites, low and high

δD quartile subsets were assigned in the same manner as above but over the period 1900-2003. Composites of gridded summertime instrumental PDSI from Cook *et al*. (2004b) were generated for these subsets in California and the West (Figure 3.14). 100% of grid squares in California (N=10) record positive PDSI in the low δD composite with PDSI in 10% of those ≥ 1 indicative of pluvial conditions. Across the West 91% of grid squares have composited PDSI > 0 for the low δD subset with 18% of those ≥ 1. The Pacific Northwest and is out of phase with the rest of the grid points, having composited PDSI < 1 for the low δD subset. The opposite pattern emerges in the high δD composite, with values < 0 throughout much of the West with the exception of the Pacific Northwest and the Texas-New Mexico Region. Overall 85% of grid squares record PDSI < 0 with 22% of those ≤ -1, indicative of drought conditions. In California, PDSI in 100% of grid squares is < 0, 10% of which are ≤ -1.

Using the low and high δD subsets, we can also investigate differences in the timing of snowmelt release for δD extremes. Even at the relatively low elevation of Swamp Lake, a significant fraction of winter precipitation is released to the catchment during spring snowmelt. The timing of snowmelt release, or the spring pulse timing, as detected in the rising limb of naturally flowing stream hydrographs, is a function of both SWE in the accumulated snowpack as well as springtime temperatures, with warmer temperatures and lower SWE resulting in earlier spring pulses (Cayan & Dettinger, 1995; Stewart *et al*., 2005). The isotopic signature of the spring pulse in the Sierra Nevada shows up as a pulse of depleted water in both snowmelt (Unnikrishna *et al*., 2002) and stream discharge (Huth *et al*., 2004). From discharge records in the USGS Hydro-Climate Data Network (HCDN), a dataset containing observations from rivers and river basins

with little anthropogenic influence on their natural flow (Slack & Landwehr 1992), we determine the difference in composited spring pulse timings for the post 1948 low δD and high δD subsets (Figure 3.15). Gauges were culled in the same manner as CDEC and SNOTEL snow courses. A total of 15 gauges in the Sierra Nevada and 102 throughout the west were selected. The difference in composited spring pulse timings for the low δD subset minus the high δD subset was +6.5 days on average across the west, and +12 days for the Sierra Nevada, meaning that on average the stream pulse in the Sierra Nevada arrives 12 days (> 1σ for Sierra Nevada gauges analyzed) later on average during years with low δD than those with high δD. Overall, 83% and 93% of pulse timings arrived later in the West and the Sierra Nevada respectively in the low δD subset with 83% of Sierra Nevada and 75% of West arrivals delayed by > 5 days.

Dividing C24 into quartiles also allows us to observe the patterns of atmospheric circulation associated with low and high δD. We create composites of NCEP/NCAR Reanalysis I 700mb height anomalies between 1948 and 2006 for the post 1948 low and high δD subsets using the plotting program on the ESRL website http://www.esrl.noaa.gov/psd/cgi-bin/data/composites/printpage.pl. Low δD values are associated with anomalous high pressure in the central north Pacific and anomalous low pressure centered over the Pacific North west (Figure 3.16a). This pattern, which results in cold moisture advected from the north Pacific (Cayan & Riddle, 1992), is similar to that corresponding to depleted precipitation in Southern California (Berkelhammer *et al*., submitted). It also closely resembles the pattern associated with the negative phase of the Pacific North America Pattern (PNA), one of several patterns associated with wet conditions and anomalously high precipitation (Cayan & Riddle, 1992) and April 1st

SWE (Cayan 1996) in the Sierra Nevada Mountains. The high δD composite displays a negative height anomaly in the central north Pacific, a feature associated with below average April 1st SWE and precipitation in California and other locations throughout the West (Cayan & Riddle, 1992; Cayan, 1996), and a ridge over the continental United States (Figure 3.16b). The presence of this ridge has been blamed for past droughts in the West and the Great Plains region, including the severe drought in 1988 (Trenberth, 1998; Seager *et al*., 2005a).

3.7 Discussion

The annually laminated, organic rich sediments of Swamp Lake allow for interannual measurement of sedimentary leaf wax lipid δD over the 20th century. The highly variable leaf wax lipid *n*-acid distributions among the submergent/floating, emergent and terrestrial plant groups (Figure 3.6) is consistent with observations from an earlier study of inter and intra species *n*-alkane and *n*-acid distributions (Sachse *et al*., 2006). Although this variability precludes robust constraint of plant sources to the sedimentary C22-C28 *n*-acids in Swamp Lake, we can infer from the low relative abundance of C30 in sediment samples compared to significant relative abundance in terrestrial plants that submergent/floating aquatic macrophytes and emergent plants are likely the dominant source of C22 and C24 over terrestrial plants, as documented in previous studies (Ficken *et al*., 2000; Meyers & Ishiwitari, 1986). Submerged/floating and emergent plants may also make a significant contribution to C26 and C28, although these compounds are traditionally thought to derive primarily from higher order terrestrial plants (Ficken *et al*., 2000). The slightly depleted long-term average of C22 δD relative to that of the other 3 compounds measured is consistent with a greater

contribution to sedimentary C22 from aquatic plants that do not transpire (Sachse *et al*., 2006). We therefore interpret the C24 δD record as having been primarily recorded by submerged/floating and emergent plants that draw on epilimnitic water for lipid biosynthesis.

C24 δD varies over the 20th century with a range of 30-50‰, an order of magnitude above analytical uncertainty (Figure 3.9) and exhibits significant negative correlation with records of regional precipitation, April 1st SWE and PDSI, such that higher δD values are associated with drier conditions and lower δD with wetter conditions. According to this negative correlation, Swamp Lake leaf wax lipid δD captures hydrologic variability in the Sierra Nevada Mountains on interannual time scales (Figure 3.10). Of the moisture availability indicators considered here, April 1st SWE is most strongly correlated with δD, suggesting that C24 δD may be particularly diagnostic of changes in alpine snowpack in the Sierra Nevada. Instrumental PDSI from NADA gs47 is the only hydrologic record with insignificant (albeit still negative) correlation to δD, even while PDSI from gs59 and Div5 exhibit a relatively strong correlation. Correlation weakness with gs47 may be due to the grid square's location over the Sierra Nevada crest. PDSI is known to poorly reflect moisture availability in snowmelt dominated catchments (Hayes, 2006), and may therefore be better suited as an indicator for hydrologic variability in the San Joaquin Valley (Div5) and Great Basin (gs59) than in the Sierra Nevada Mountains. This comparison of C24 δD with instrumental PDSI from NADA grid squares 47 and 59 is useful for assessing the paleohydrologic implications of down core δD variability, as the NADA includes gridded reconstructed PDSI records that extend back over 1000 years (Cook *et al*., 2004a). δD also tracks

moisture availability at interdecadal periodicities (Figure 3.11) although lack of negative correlation between δD and PDSI between 1898 and 1920 may reflect the influence of other processes in driving lower frequency δD variability.

Negative correlation of δD with interannual April 1st SWE and PDSI variability is upheld throughout the West (Figures 3.12-14). This coherency reflects the fact that anomalies in precipitation and SWE over much of the West is driven by similar patterns of atmospheric circulation, such that at any given time broad regions over multiple states will simultaneously experience anomalously wet or dry conditions (Aguado, 1990; Cayan, 1996; Dettinger *et al*., 1998; Cayan *et al*., 1998). As observed with the Sierra Nevada records, δD exhibits stronger correlation with April 1st SWE (Figure 3.12) than PDSI (Figure 3.13) throughout the West, but the spatial correlation patterns associated with the two properties are similar with negative correlations strongest in the Sierra Nevada Mountains and the central Rockies, and weakest or of reversed sign in the Pacific Northwest and eastern Southwest. This pattern may be due to the fact that April 1st SWE in the Sierras and Central Rockies exhibits strong positive correlation to wintertime precipitation and is relatively insensitive to winter or March temperatures, while April 1st SWE in the Pacific Northwest (Oregon) and New Mexico exhibits equivalent or stronger correlation March temperature as it does with winter precipitation (Cayan, 1996). Leaf wax lipid δD may therefore be better suited to record April 1st SWE in regions where survival of snowpack into the spring is more a function of the amount of precipitation than it is of winter and spring temperatures. The sensitivity of leaf wax lipid δD to snowpack is also reflected in the delay of spring pulse timing observed for the low δD subset relative to the high δD subset in the Sierra Nevada Mountains and the central

Rockies (Figure 3.15), as spring pulse timing in these ranges is strongly tied to April 1st SWE (Stewart *et al*., 2005).

The findings discussed above indicate that leaf wax lipid δD may be a diagnostic tracer of moisture availability in the Sierra Nevada Mountains on interannual to decadal time scales. However, interpretation of paleohydrologic δD records requires an understanding of the physical driving mechanisms that link these isotopic and hydrologic signals. We consider two possible end-member driving mechanisms: 1) the preformed isotopic content of precipitation deposited in the Swamp Lake and 2) post-depositional processes acting on the isotopic content of catchment water. On decadal timescales variability in the δD of precipitation along the western North American margin is influenced in part by the strength of the Aleutian Low (Berkelhammer *et al*., submitted; Field *et al*., 2010). The deep Aleutian low that prevails when PDO is in its positive phase shifts storm tracks to more southerly latitudes and facilitates meridional moisture advection from the subtropical North Pacific to the Sierra Nevada (Cayan *et al*., 1998), resulting in precipitation relatively enriched in δD (Berkelhammer *et al*., submitted). Therefore, were leaf wax lipid δD primarily recording variability in the preformed isotopic content of precipitation, we would expect to see a relationship on decadal scales with PDO (Berkelhammer & Stott, 2008). While the findings of Berkelhammer & Stott (2008) suggest that isotopic correlation with moisture availability is not a prerequisite for this model, we would expect any correlation that is observed between these records to be in positive, as, in general, the patterns of atmospheric circulation that result in drier conditions in the Sierra Nevada are also associated with more northerly shifted storm tracks (Cayan, 1996; Dettinger *et al*., 1998; Cayan *et al*., 1998) that transport relatively

cool air masses with moisture depleted in δD (Berkelhammer *et al*, submitted) while those associated with wetter conditions, including the warm, moisture intensive "Pineapple Express" storms (Dettinger, 2004), are associated with southerly shifted storm tracks that transport moisture originating from lower latitudes and enriched in δD (Berkelhammer *et al*., submitted). Not only do we observe the reverse correlation, we also find that the pattern of circulation composited from years recording the 25% highest δD between 1948-2006 (Figure 3.16a) resembles that associated with dry conditions in the Sierra Nevada Mountains (Cayan & Riddle, 1992; Cayan, 1996)

The negative correlation with moisture availability that we observe points instead towards the post-depositional isotopic mass balance between relatively depleted precipitation and evaporative enrichment in Swamp Lake and the surrounding catchment as the primary driving mechanism for sedimentary leaf wax lipid δD variability. Winters with heavy precipitation will result in greater flushing of residual water in the catchment with relatively depleted precipitation or snowmelt (Huth *et al*., 2004). As residual water has been exposed to evaporative enrichment during the previous summer, flushing reduces the δD value of the well of both lake and shallow ground water. Heavier winter precipitation also results in greater April 1st SWE and later spring pulse timing in the Sierra Nevada (Stewart *et al*., 2005). The presence of low salinity surface water in July 2009 (Figure 3.3) that is depleted in δD relative to the hypolimnion (the sub-thermocline portion of the lake) (Figure 3.8), likely reflects the presence of a snowmelt lens that entered the lake through surface runoff subsequent to the onset of thermal stratification in mid spring. Although we do not possess Swamp Lake isotopic profiles from additional years as a means for comparison, Benson (1994) observed that May surface water $\delta^{18}O$ in

Pyramid Lake in the northern Sierra Nevada Lake was depleted in ^{18}O by ~2‰ relative to the hypolimnitic water in the wet year of 1986 but had the same $\delta^{18}O$ value as the hypolimnion in may 1991, a dry year. Furthermore, studies of Sierra Nevada snowmelt and stream flow indicate that the most depleted water occurs during the peak of snowmelt (Unnikrishna *et al*, 2002; Huth *et al*., 2004; Rodhe, 1998). Years with heavier April 1st snowpack's will not only experience a greater pulse of depleted water, but this pulse will also occur later in the spring, establishing a lower epilimnion δD value at the start of the growing season. Therefore, winters with heavier precipitation and snow pack and delayed spring pulse timings foster more depleted surface water at the start of the growing season, which in turn lessens the mass balance influence of evaporative enrichment over the course of the summer. This mass balance driving mechanism is consistent with the relatively strong correlation between δD and April 1st SWE (Figure 3.12) and the delay in spring pulse timing observed for the low δD subset relative to the high δD subset in the Sierra Nevada Mountains (Figure 3.15). Because evaporation is only acting on epilimnion, variation in its mass balance influence has the potential to drive significant variability of the δD signature of epilimnitic water throughout the growing season. The δD recorded by floating/submerged aquatic macrophytes and emergent plants therefore primarily reflects the surface water mass balance partitioning between relatively depleted runoff and evaporative enrichment, such that plants undergoing lipid biosynthesis during growing seasons following drier winters will be exposed to water that with heavier isotopic values.

Although we are suggesting a primarily aquatic source to the C24 record, a similar mass balance partitioning mechanism could apply to terrestrial plants. Assuming

that the leaf wax *n*-acids faithfully capture δD of environmental water, the covariability among the four *n*-acids over the 20th century (Figure 3.9) is suggestive of three possibilities: 1) a small subset of plants contributes to the majority of leaf wax lipids preserved in Swamp Lake sediments, 2) all plants are drawing on the same source of environmental water for lipid biosynthesis or 3) post depositional catchment processes have similar effects on the isotopic content of water sources drawn upon by various plants. Possibilities 2 and 3, which are not mutually exclusive, are consistent with the small size and relatively short residence of water in the Swamp Lake catchment (Sachse, 2006) and *n*-acids C24-C28 sharing the same long term averages. Therefore, despite lack of robust constraint on plant source sedimentary *n*-acids, we can invoke the same mechanism to drive δD variability in plants that draw directly from Swamp Lake or from the surrounding groundwater. Varying degrees of wintertime flushing will result in relatively depleted or enriched shallow groundwater available during the growing season. Winters with lower precipitation will leave less residual groundwater in summer (Kattelmann & Elder, 1991), allowing evaporation to impart a greater mass balance impact on groundwater δD.

Why are shifts in water balance the dominant mechanism over fluctuations in the preformed in driving the δD of Swamp Lake leaf wax lipids? Due to Swamp Lake's estimated replacement time of 1-2 years, decadal shifts in the δD of precipitation should invoke corresponding shifts in the δD of the deep, well-mixed lake water. However, year to year standard deviation in $\delta^{18}O$ of precipitation is only on the order of ~0.5-0.75‰ in the Sierra Nevada (Vachon *et al*., 2007), which, based on a local meteoritic water line (LMWL) slope of 7.5 (Berkelhammer *et al*., submitted), translates to a δD range of ~4-

6‰. Because this already small range will be dampened by annual mixing of new and residual lake water, the role of variable precipitation δD should be minimal compared to that of the mass balance partitioning between depleted inflow and evaporative enrichment in determining the δD of water taken up by aquatic macrophytes. Larger magnitude changes in the isotopic content of precipitation occurring over multiple decades to centuries, (e.g. Berkelhammer & Stott, 2008; Field *et al*., 2010; Anderson *et al*., 2005), however, could to noticeably shift the baseline lake δD value and therefore the δD of summertime epilimnitic water. Therefore, Swamp Lake leaf wax lipid δD is a diagnostic tracer of moisture availability on interannual to decadal time scales but changes in the isotopic content of precipitation must be constrained in order to interpret lower frequency δD fluctuations in terms of moisture availability.

3.8 Conclusions

We have measured the δD of leaf wax lipid *n*-acids from Swamp Lake sediments at annual to biennial resolution over the 20th century. Comparison of plant and sedimentary *n*-acid distributions reveals that aquatic macrophytes and emergent grasses make a significant contribution to the sedimentary plant lipid pool and are the likely dominant source of the shorter carbon chain *n*-acids C22 and C24. δD of even carbon numbered sedimentary *n*-acids C22-C28 covaries over this period and varies at interannual to decadal time scales on the order of 30-50‰. Interannual C24 δD variability exhibits significant negative correlation with that of precipitation, April 1st SWE and PDSI from the Sierra Nevada. Of these records, April 1st SWE exhibits the strongest correlation with δD, with the record from BHV explaining ~25% of δD variability between 1932 and 2006. Negative correlations of leaf wax lipid δD with April

1st SWE and PDSI on interannual time scales are also observed throughout the West, a characteristic expected for a proxy that faithfully captures hydrologic variability in the Sierra Nevada Mountains. SWE correlations are strongest in the Sierra Nevada and the central Rockies where April 1st SWE is strongly tied to wintertime precipitation, reflecting the sensitivity of δD to moisture availability. PDSI correlations are strongest in southern California, the Great Basin and the Rocky Mountains. Relative weakness of the PDSI-δD negative correlation in the Sierra Nevada may reflect issues of PDSI as an indicator of wet or dry conditions in snow melt dominated catchments (Hayes, 2006). The ~15 day delay of spring pulse timing in Sierra Nevada streams for the low δD subset relative to the high δD subset is consistent with sensitivity to April 1st SWE, which is strongly correlated to spring pulse timing in the Sierra Nevada Mountains (Stewart *et al*., 2005). Finally, composites of 700 mb geopotential height anomalies display opposite patterns of atmospheric circulation for the low and high δD subsets consistent with the negative relationship between δD and moisture availability in the Sierra Nevada and throughout the West.

These comparisons with instrumental records indicate that Swamp Lake leaf wax lipid δD is a diagnostic tracer of moisture availability. However we observe little to no relationship between δD and tropical or north Pacific SSTa fluctuations, represented at interannual and decadal time scales by the ENSO and PDO climate indices respectively. Because these SSTa fluctuations invoke latitudinal shifts in moisture source and trajectory that in turn influence the performed δD of precipitation, lack of relationship with ENSO and PDO makes preformed δD an unlikely driving mechanism for leaf wax

lipid δD. Negative correlation with moisture availability is also inconsistent with this potential driving mechanism. Instead, we propose that catchment water balance facilitates a causal relationship between amount of precipitation and leaf wax lipid δD. The isotopic mass balance portioning of relatively depleted lake inflow derived from wintertime precipitation and snowmelt with summertime evaporative enrichment of the epilimnion determines the δD of lake surface water drawn upon by aquatic macrophytes and emergent plants for lipid biosynthesis during the growing season. Winters with heavier precipitation result in more voluminous inflow that extends later into the spring and establishes lower surface water δD at the start of the growing season that offsets the mass balance impact of evaporative enrichment over the course of the summer. Of the sources of lake inflow, the spring snowmelt pulse carries the most depleted δD signature (Unnikrishna *et al*., 2002; Huth *et al*., 2004) that will further offset this impact, a fact which explains the particular sensitivity of δD with April 1st SWE and the significant delay in spring pulse timing for years with low δD relative to those with high δD.

Although the above model explains the opposing relationship between moisture availability and leaf wax lipid δD variability, it highlights the fact that different proxies capture hydrologic information through fundamentally different mechanisms. For example, variability in $\delta^{18}O$ of tree ring cellulose just east of the Sierra Nevada records shifts in the preformed δD of precipitation, and shows little relationship to moisture availability (Berkelhammer & Stott, 2008). Therefore, only by combining multiple independent proxy records can we ascertain a comprehensive understanding of past hydrologic variability. This study of temporal δD variability, which complements the

spatial investigations of Hou *et al*. (2008) and Feakins & Sessions (2010), demonstrates that the δD of sedimentary leaf wax lipids reflects that of a single source environmental water over multiple decades, and may prove a useful addition to existing suite of paleohydrologic proxies. Constraint of catchment water balance and vegetative contribution to the sedimentary *n*-acid pool, however, is crucial to interpretation of this proxy. We suggest thorough investigation of these properties, in greater detail than presented in this study, prior to down core investigations. With appropriate constraint, leaf wax lipid δD in Sierra Nevada lake sediments can be used to capture interannual to decadal scale hydrologic variability, and may reveal further insight into the impact of previously documented droughts and pluvials over the last millennium on hydroclimate of the Sierra Nevada Mountains.

Chapter 3:, in part, is being prepared for submission for publication. Roach, L.D., Sessions, A.L., Cayan D.R., Charles, C.D., R.S. Anderson. The dissertation author was the primary investigator and author of this paper.

Table 3.1 List of plant species collected at Swamp Lake.

Species	Common Name	Group
Potamogeton robbinsii	Robbin's Pondweed	Submergent
Schoenoplectus subterminalis	Swaying Bulrush	Submergent
Brasenia schreberi	Watershield	Floating
Nuphar polysepala	unknown	Floating
Dulichium arundinaceum	Threeway Sedge	Emergent
Carex lenticularis	Lakeshore Sedge	Emergent
Carex utriculata	Beaked Sedge	Emergent
Menyathes trifoliate	Bog Bean	Emergent
Ceanothus integerrimus	Deer Brush	Terrestrial
Arctostaphylos viscida	White Manzanita	Terrestrial
Rhodoendron occidentale	Western Azalea	Terrestrial
Quercus kelloggii	Black Oak	Terrestrial
Pinus ponderosa	Ponderosa Pine	Terrestrial
Calcocedrus deccurrens	Incense Cedar	Terrestrial
Pseudtosuga menziesii	Douglas Fir	Terrestrial
Alnus rhombifolia	While Alder	Terrestrial

Table 3.2 δD of Plant collected at Swamp Lake, July 2009 and snow samples collected at Hodgdon Meadow, winter 2010.

	δD (‰)			
Swamp Lake Plant Species	C22	C24	C26	C28
Schoenoplectus subterminalis	-206	-195	na	na
Brasenia schreberi	na	-182	na	na
Ceanothus integerrimus	-140	-161	-142	-154
Rhodoendron occidentale	na	-126	-137	-147
Pseudtosuga menziesii	-170	-176	-165	-166
Pinus ponderosa	-196	-195	na	na
Hodgdon Meadow Snow (dates of storm, 2010)	δD (‰)			
January 18 - January 22	-92 ± 1			
March 3 - March 4	-93 ± 3			
March 8 - March 9	-36 ± 2			
March 25 – March 26	-61 ± 2			
March 31	-53 ± 1			
April 4 – April 5	-107 ± 2			

Table 3.3 Correlation coefficients of C24 δD with instrumental records at 0 to -3 years lag. Instrumental records smoothed with a 2-year running average. Bold signifies significance at the 95% confidence interval, italics at the 99% confidence interval.

Record	Time Period	r, lag			
		0	-1 year	-2 years	-3 years
HTH precip	1911-2006	***-0.36***	-0.24	-0.04	0.06
Div5 precip	1898-2006	**-0.30**	-0.20	-0.04	0.05
BHV SWE	1933-2006	***-0.53***	-0.15	-0.06	-0.03
DNS SWE	1913-2006	***-0.35***	-0.17	-0.11	-0.03
Div5 PDSI	1898-2006	***-0.35***	-0.15	-0.01	-0.12
gs47 PDSI	1901-2003	-0.20	-0.16	-0.07	-0.04
ps59 PDSI	1901-2003	**-0.32**	**-0.28**	**-0.26**	-0.21
Div5 win temp	1898-2006	-0.06	-0.08	-0.03	0.05
Div5 sum temp	1898-2006	0.08	-0.04	-0.07	-0.05
NINO3.4 SSTa	1898-2006	-0.17	-0.08	0.01	0.12

Table 3.4 Correlation coefficients between instrumental records. Coefficients in bold are significant at the 95% confidence interval, those in italics at the 99% confidence interval.

	HTH precip	Div5 precip	BHV SWE	DNS SWE	Div5 PDSI	gs47 PDSI	ps59 PDSI	Div5 summer temp	Div5 winter temp
HTH precip	-	-	-	-	-	-	-	-	-
Div5 precip	***0.89***	-	-	-	-	-	-	-	-
BHV SWE	***0.62***	***0.69***	-	-	-	-	-	-	-
DNS SWE	***0.70***	***0.79***	***0.84***	-	-	-	-	-	-
Div5 PDSI	***0.80***	***0.87***	***0.66***	***0.71***	-	-	-	-	-
gs47 PDSI	***0.63***	***0.80***	***0.64***	***0.64***	***0.82***	-	-	-	-
ps59 PDSI	***0.65***	***0.73***	***0.69***	***0.64***	***0.72***	***0.82***	-	-	-
Div5 sum temp	0.13	**-0.22**	0.00	0.15	***-0.25***	0.00	-0.02	-	-
Div5 win temp	0.00	0.00	0.10	0.00	0.00	0.10	0.08	0.08	-
NINO 3.4 SSTa	0.01	**0.23**	**0.24**	0.09	**0.22**	***0.28***	**0.21**	-0.04	***0.29***

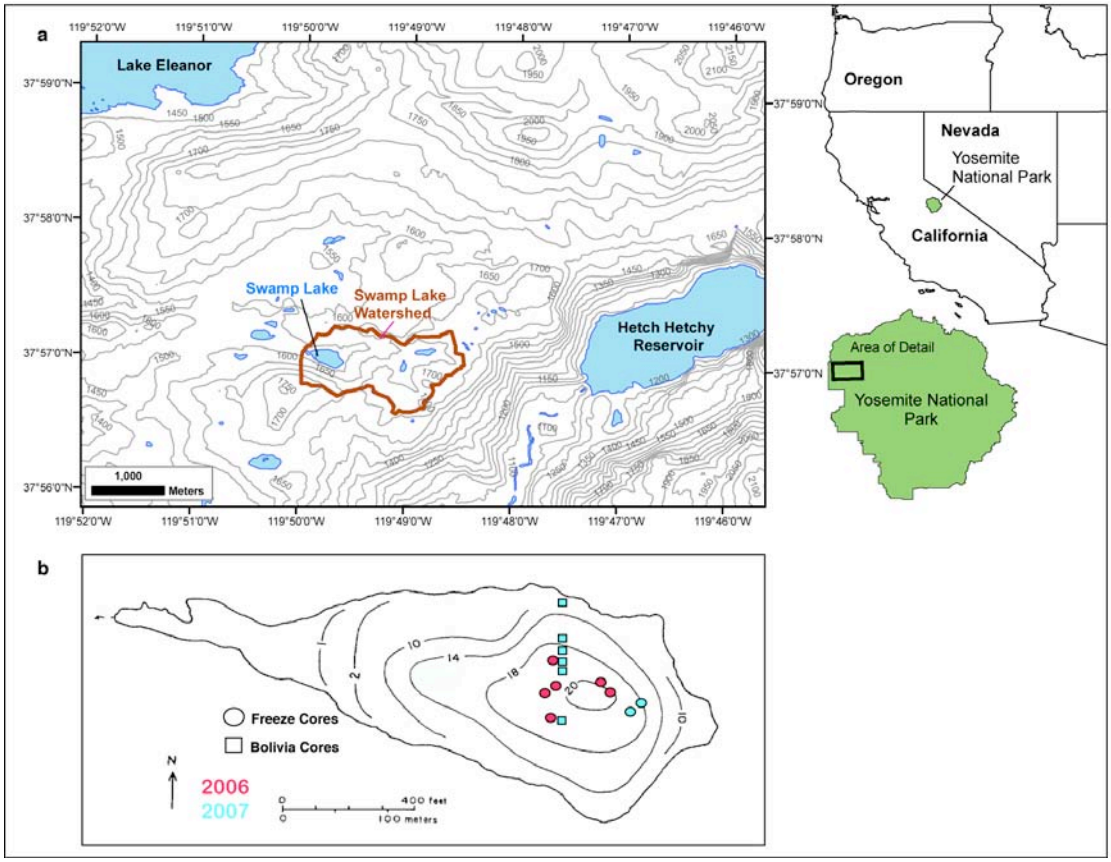


Figure 3.1 Map showing location of the Swamp Lake drainage basin in the northwest corner of Yosemite National Park along the western slope of the Sierra Nevada Mountains in California (a) and bathymetric map of Swamp Lake indicating locations of Bolivia cores (squares) and Freeze cores (circles) collected in October 2006 (red symbols) and September 2007 (blue symbols). Bathymetric map from Smith & Anderson (1992).

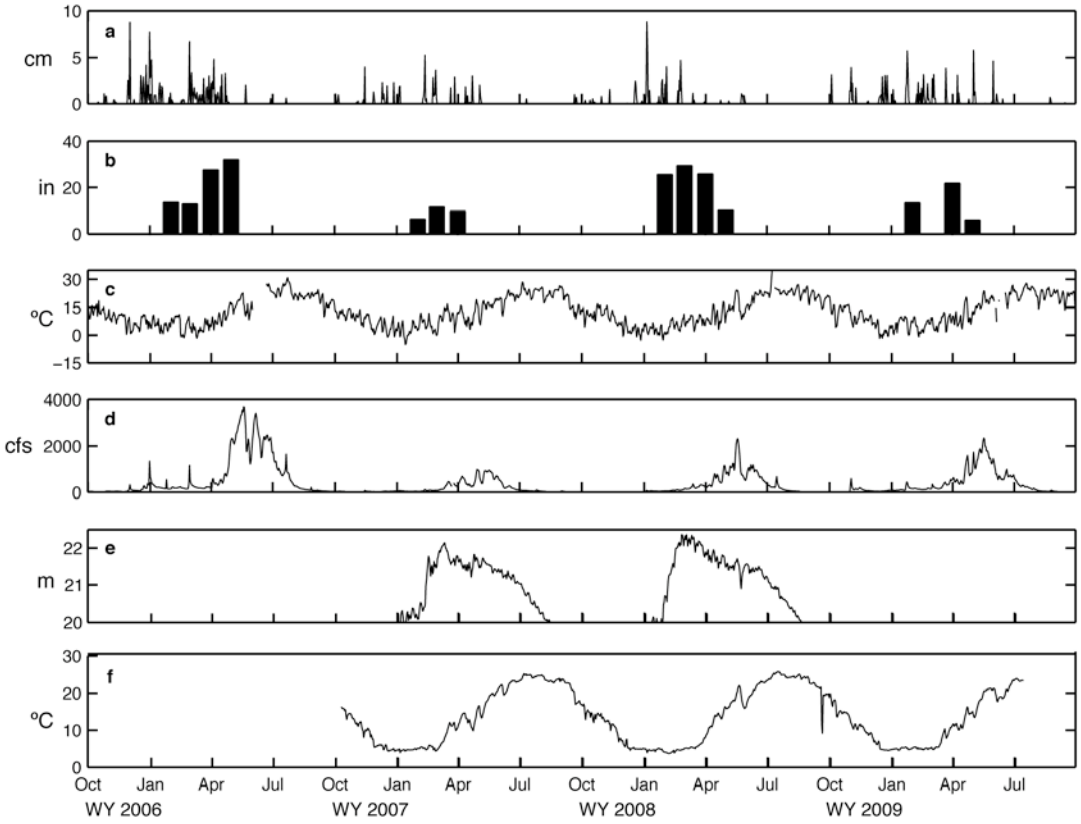


Figure 3.2 Total daily precipitation from HTH-3 km east and 370 m below Swamp Lake (a), total monthly SWE from BHV-6.5 km northeast and 446 m above Swamp Lake (b), daily average air temperature from BKM-32km southwest and 578m below Swamp Lake (c), total daily discharge of the Merced Rivers at the Happy Isles gauge (d), Swamp Lake level (e) and surface water temperature (f).

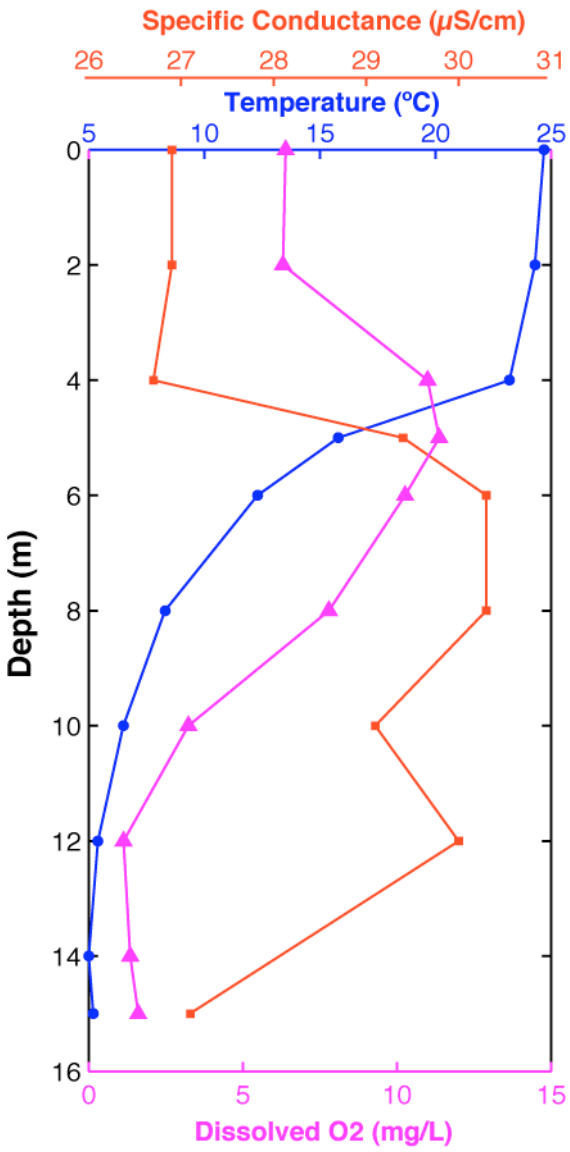


Figure 3.3 Temperature (blue), dissolved oxygen (pink) and specific conductance (red) profiles from the center of Swamp Lake, measured July 2009.

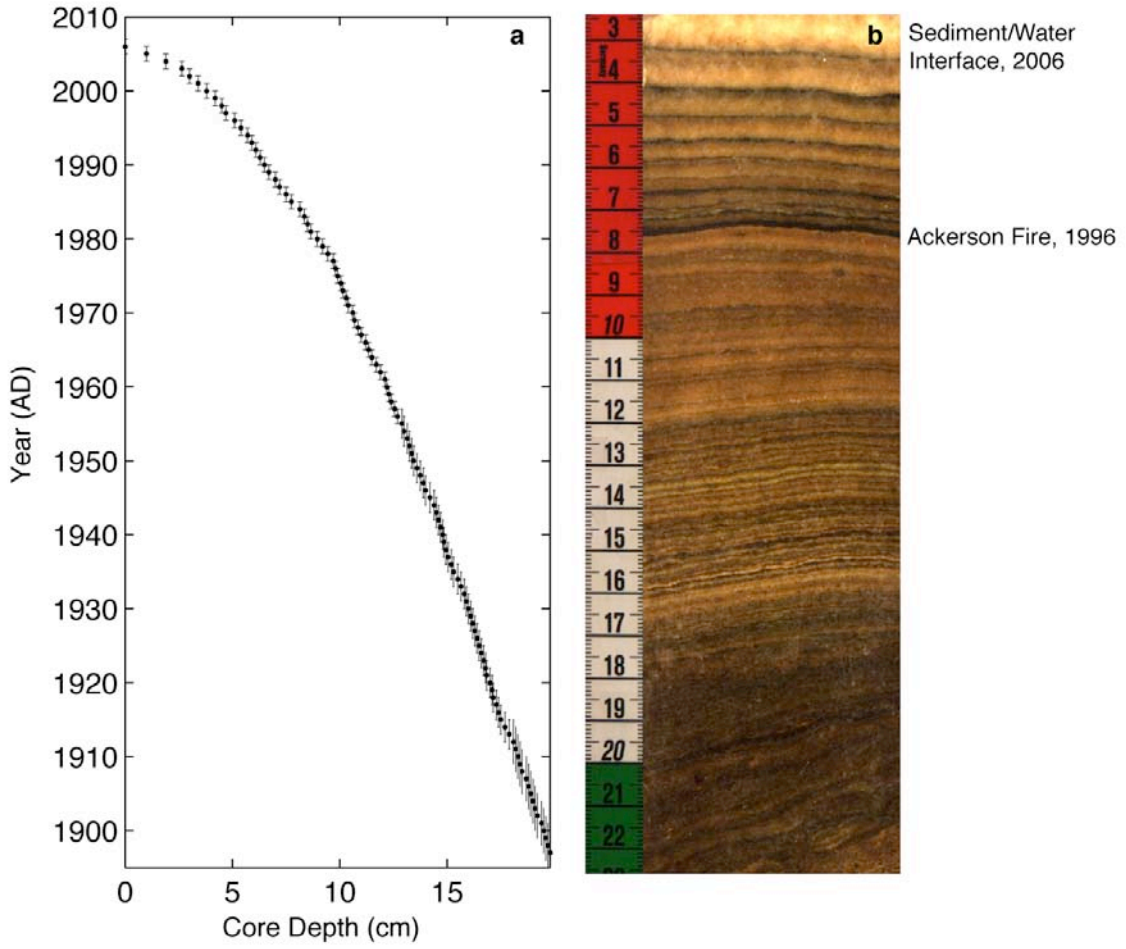


Figure 3.4 Age-depth model for SL0601T (a), with error bars reflecting uncertainty in years in varve chronology, and digital image of SL0601T (b) indicating the location of the sediment water interface and the depth of the charcoal layer deposited during the 1996 Ackerson Fire. The sediment water interface (core depth = 0 cm) starts at 2.5 cm on the image ruler.

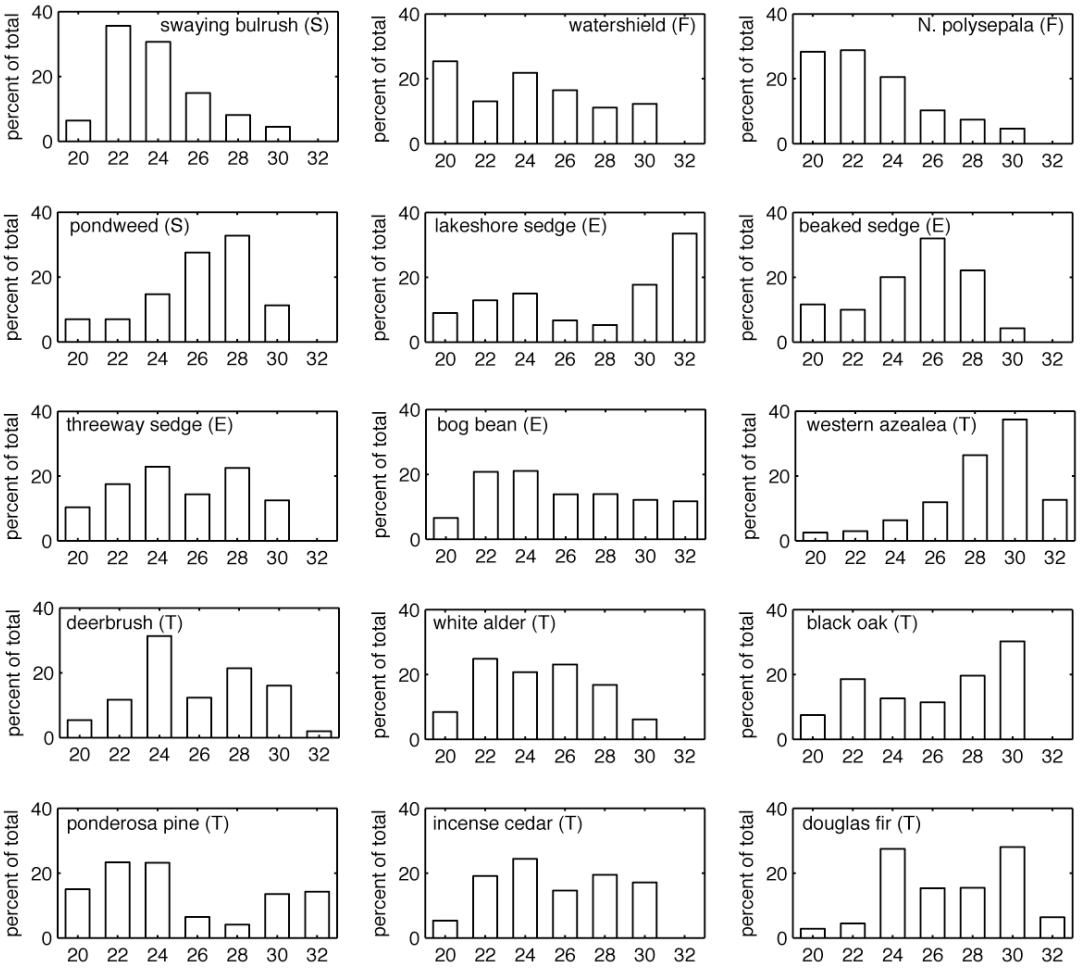


Figure 3.5 *n*-acid distribution from 15 plant species collected from in and around Swamp Lake July 2009. (S), (F), (E) and (T) refer to plant groups submerged, floating, emergent and terrestrial respectively. X-axis labels refer to carbon number.

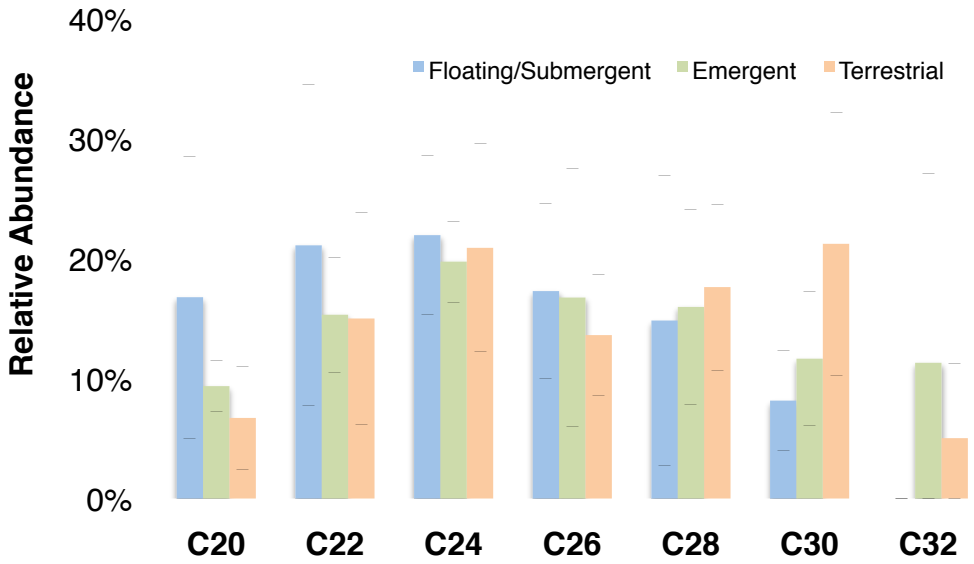


Figure 3.6 Average *n*-acid distribution for floating/submergent (blue), emergent (green) and terrestrial (orange) plants from the 15 individual species. Error bars represent 1σ. X-axis labels refer to carbon number.

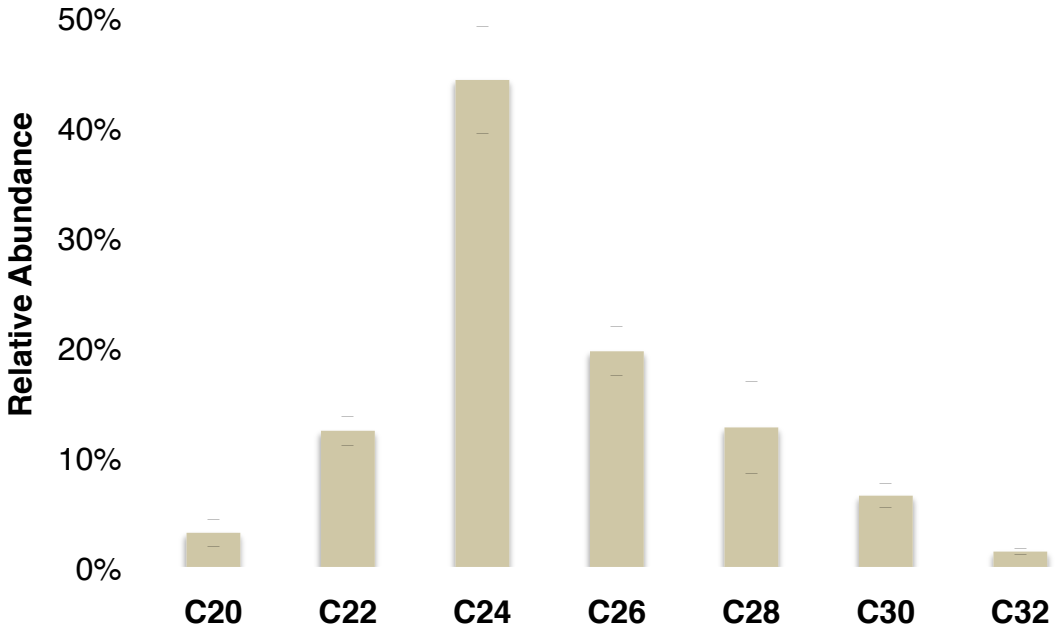


Figure 3.7 Average *n*-acid distribution from SL0601T sediment samples. Error bars represent 1σ. Axis labels as in figures 3.5 and 3.6.

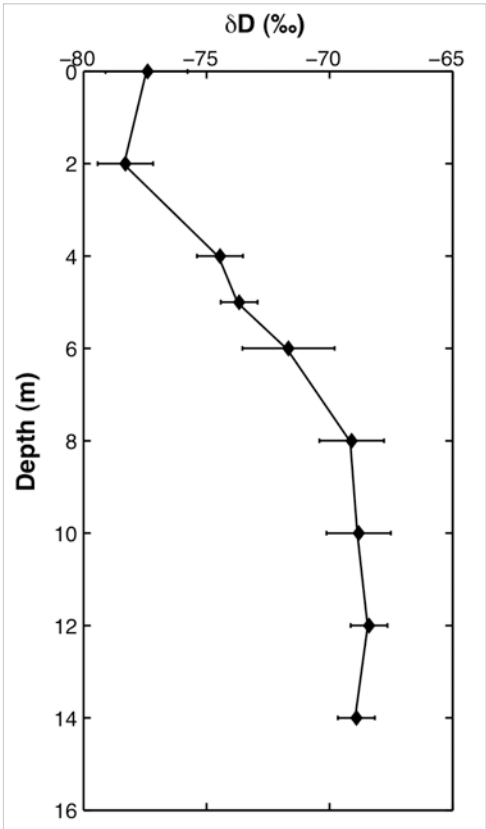


Figure 3.8 Lake water δD profile from the center of Swamp Lake, July 2009. Error bars represent 1σ of 3 replicate measurements.

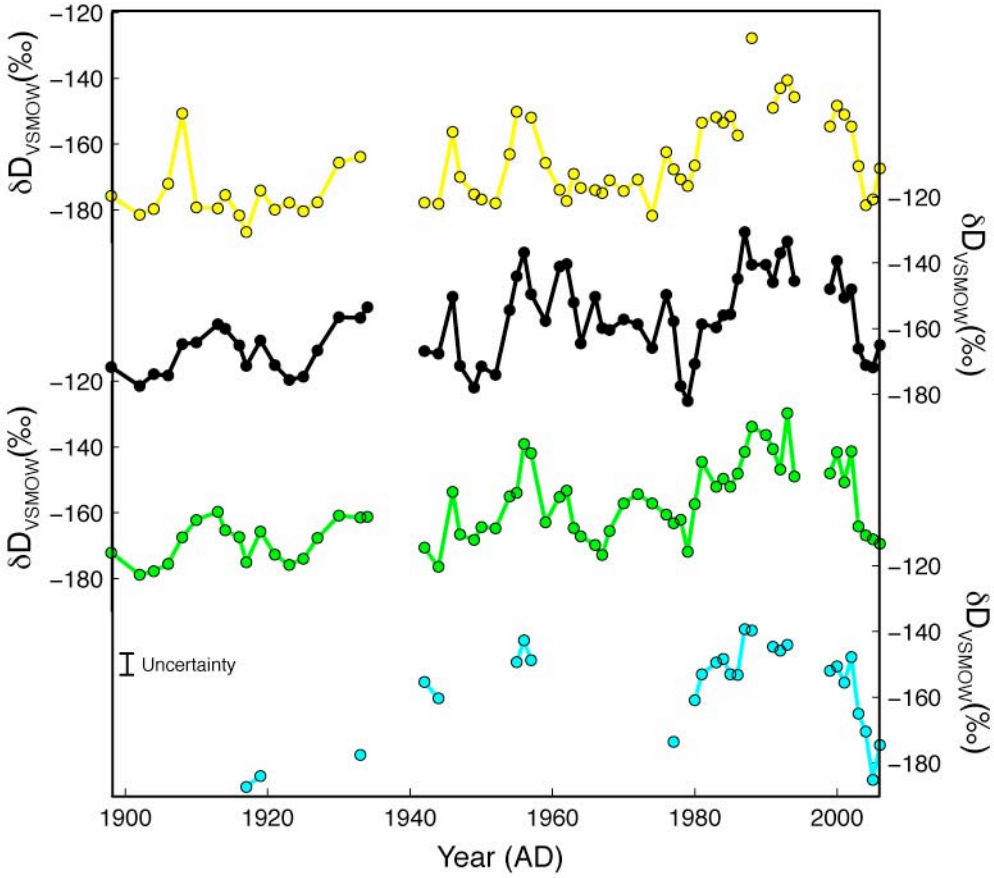


Figure 3.9 SL0601T *n*-acid δD for C22 (yellow), C24 (solid black), C26 (green) and C28 (cyan). Dashed black line is C24 δD from SL0606T.

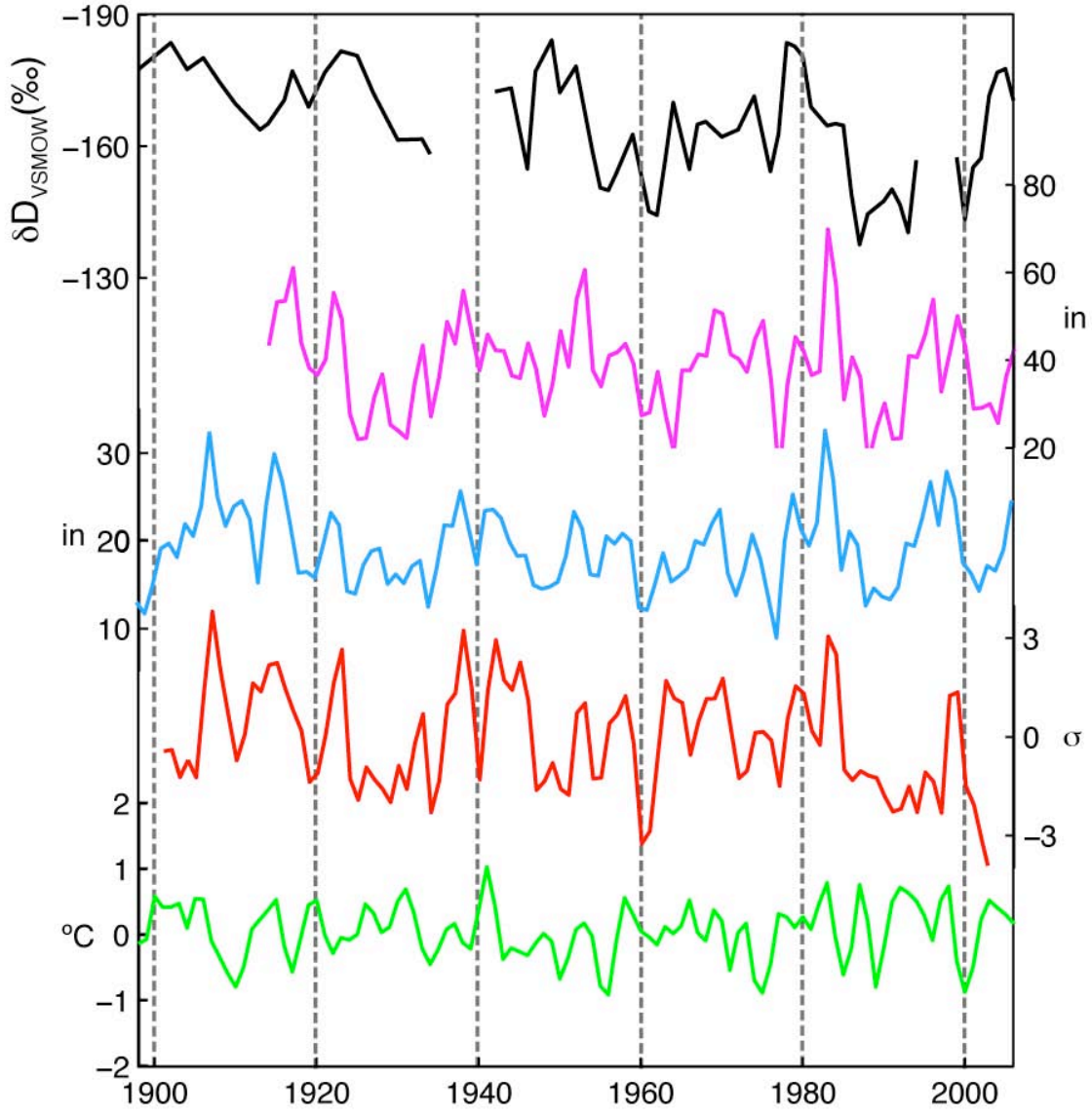


Figure 3.10 Comparison of C24 δD (black line) with, BHV April 1st SWE (pink), Div5 total annual precipitation (blue), gs59 PDSI (red) and NINO 3.4 SSTa (green). Instrumental records have been smoothed with a two-year running mean.

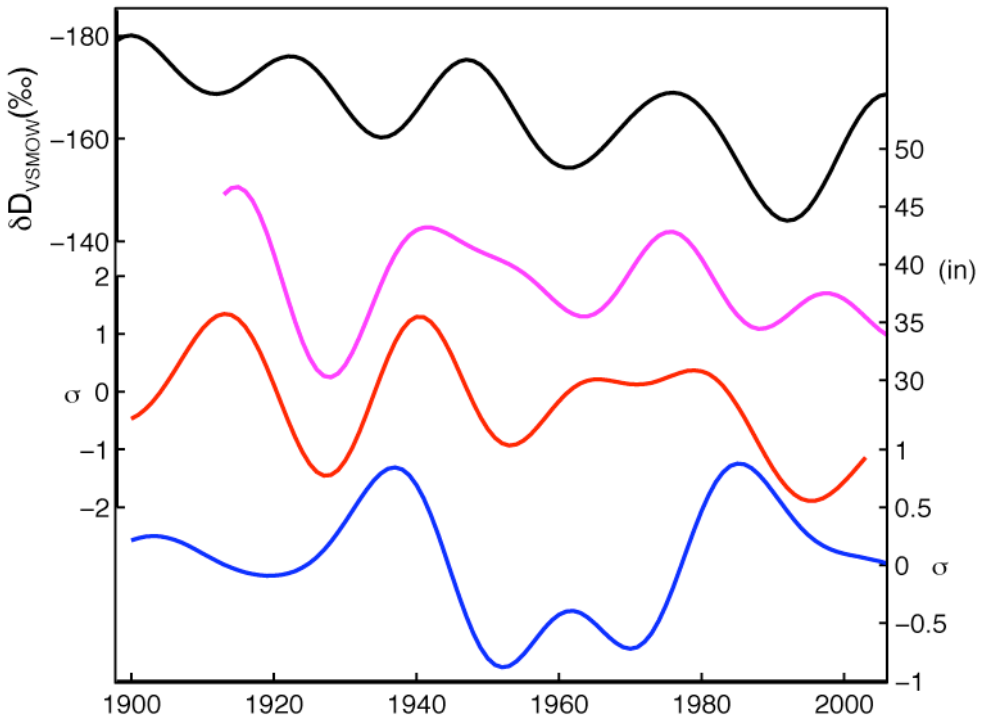


Figure 3.11 20-year low pass filtered C24 δD (black), BHV April 1st SWE (pink), gs59 PDSI (ref) and PDO (blue) (Mantua *et al*., 1997).

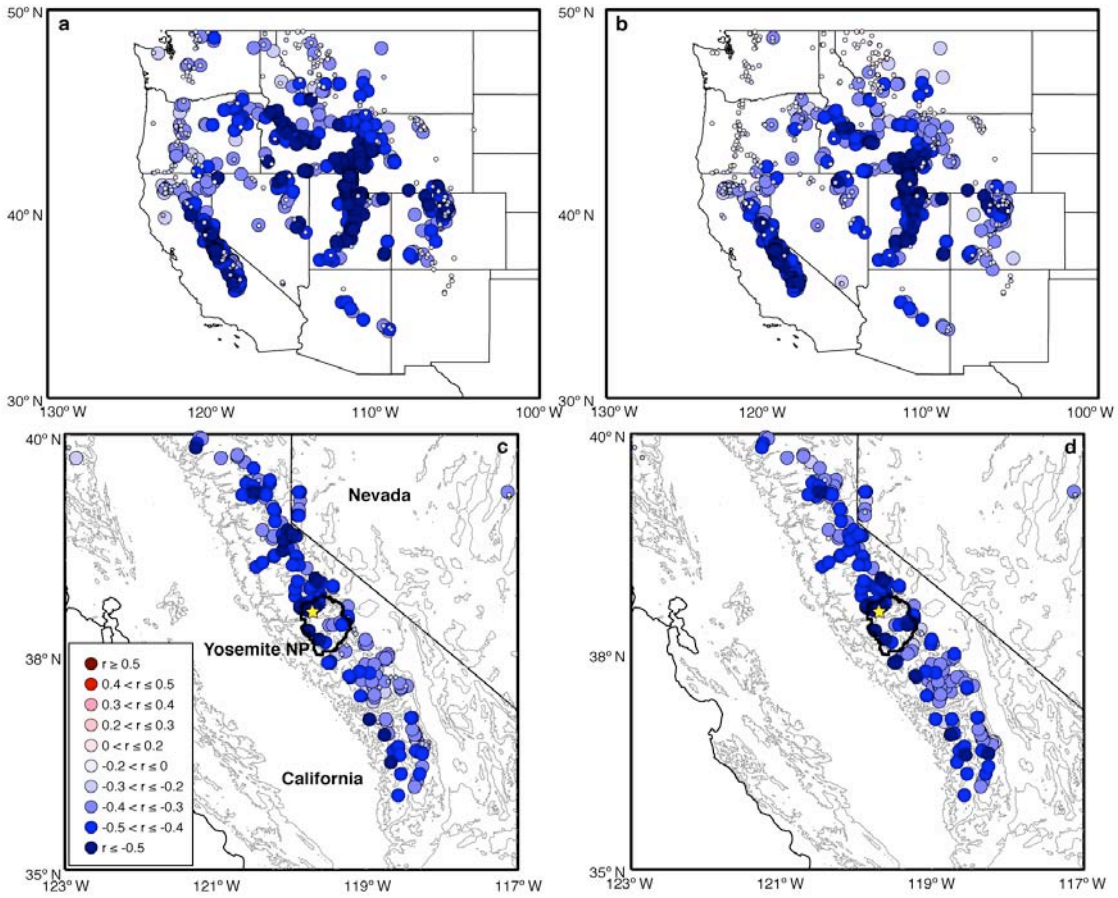


Figure 3.12 Correlation of C24 δD with April 1st SWE from CDEC and SNOTEL stations throughout the west (a, b) and in the Sierra Nevada Mountains (c, d) over the period 1949-2006. δD and SWE records have had a linear trend removed in b and d. All SWE records smoothed with a 2-year running mean. Large symbols indicate correlations significant at the 95% confidence interval. The outline of Yosemite National Park is demarked by a thick black line in c and d, with the location of Swamp Lake indicated by the yellow star. Contours in c and d at 500, 1000, 2000 and 3000, meters. Symbols as indicated in (c).

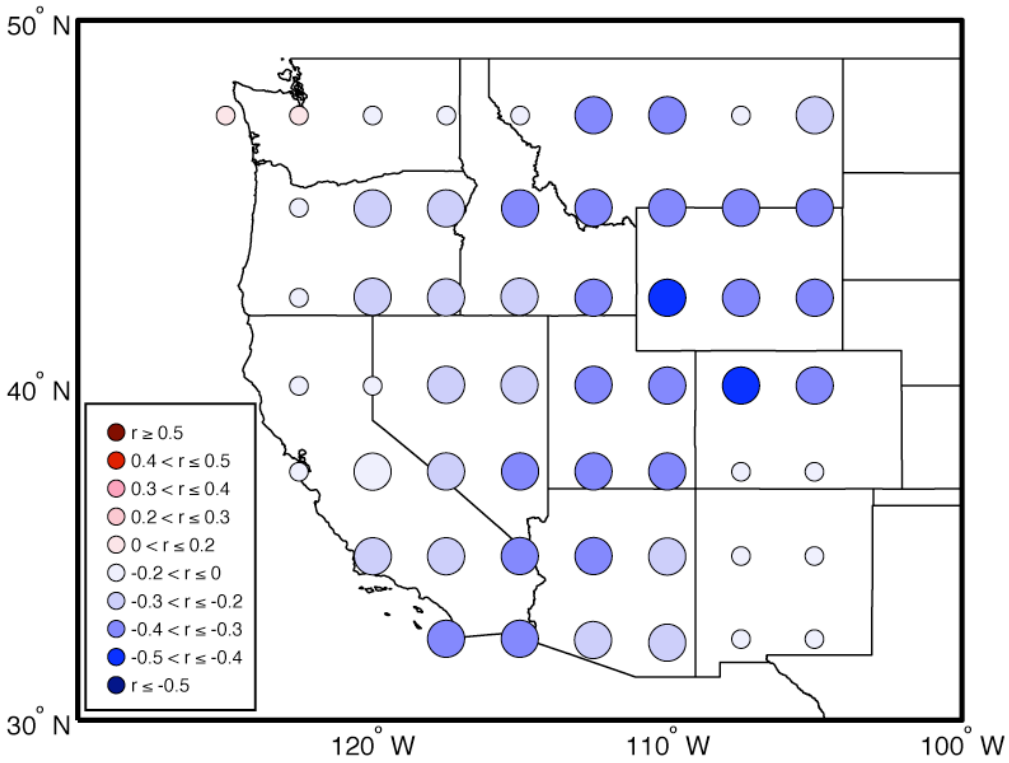


Figure 3.13 Correlation of C24 δD with gridded instrumental PDSI from the NADA 1901-2003. PDSI records have been smoothed with a two-year running mean. Large symbols indicate significance at the 95% confidence interval.

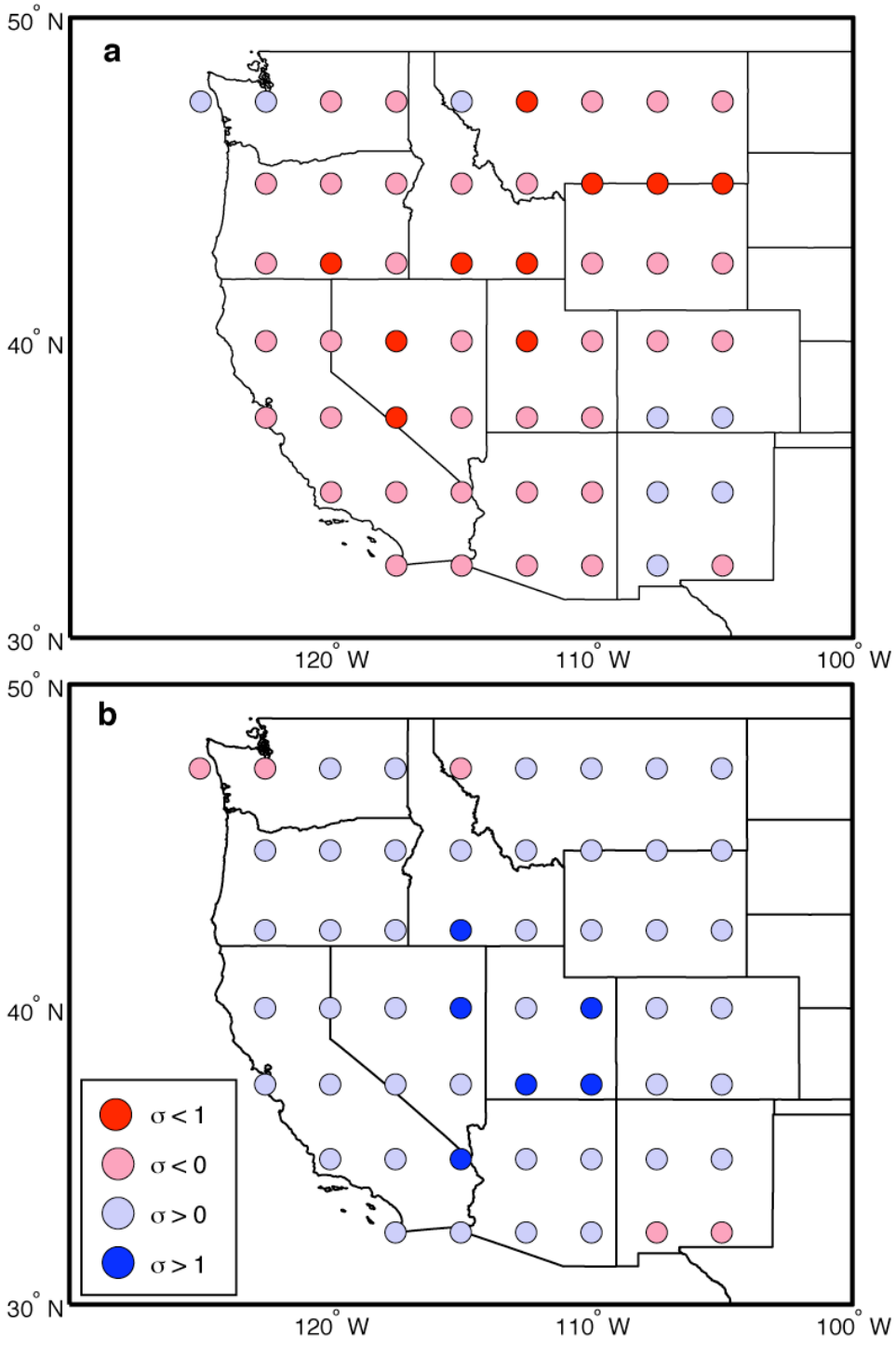


Figure 3.14 Gridded composites of instrumental NADA PDSI for the high δD subset (δD < 3rd quartile) (a) and low δD subset (δD < 1st quartile) (b).

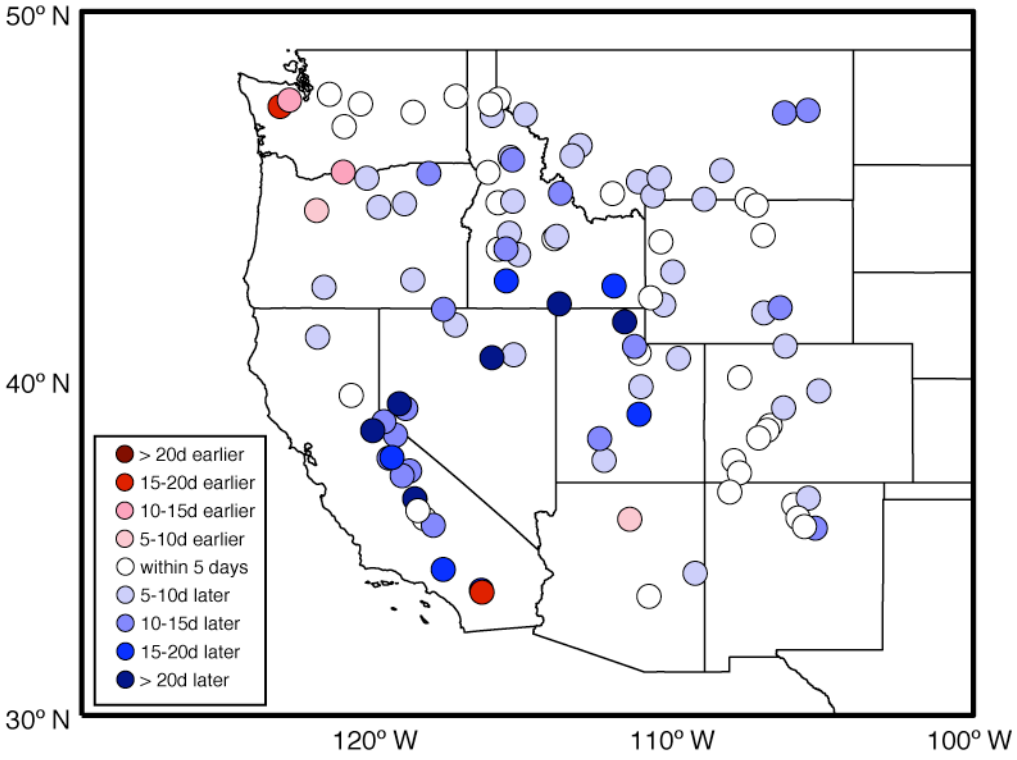


Figure 3.15 Difference in spring pulse timing in days for the low δD subset minus the high δD subset.

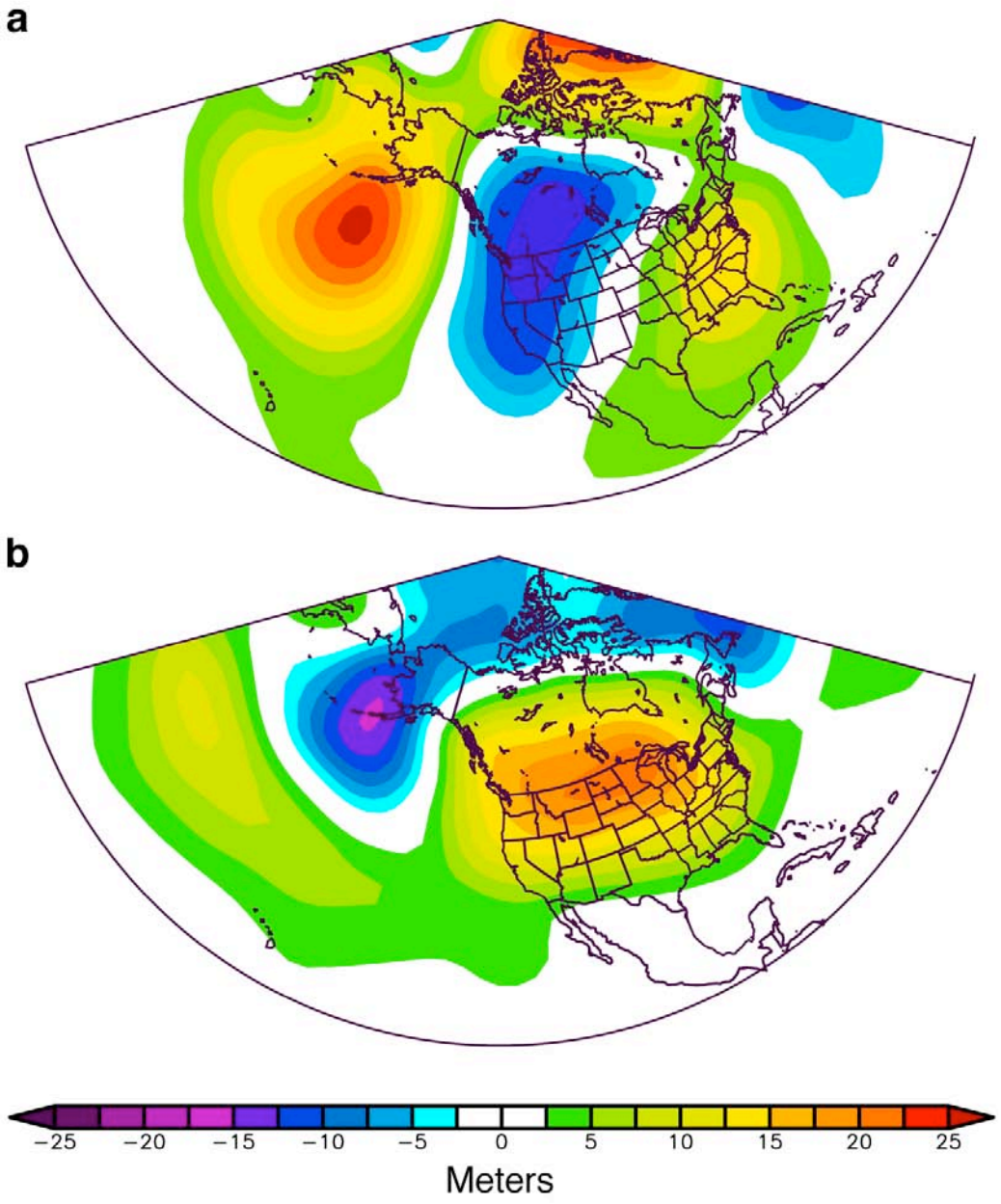


Figure 3.16 Composited NCEP Reanalysis I 700mb height anomalies from the high δD (a) and low δD (b) subsets. Figures generated using the Earth System Research Laboratory Montly/Seasonal Climate Composites page (http:www.esrl.noaa.gov/psd/cgi-gin/data/composites/printpage.pl)

3.9 References

Aguado, E. (1990) Elevation and latitudinal patterns of snow accumulation departures from normal in the Sierra Nevada. *Theor. Appl. Climatol.* 42:177-185.

Barnes, C. J. and J. V. Turner, 1998. Isotopic exchange in soil water. in: *Isotope Tracers in Catchment Hydrology*. Kendall C. and J. J. McDonnell eds. Elsevier 137-162.

Barnett, T. P., Pierce, D. W., Hidalgo, H. G., Bonfils, C., Santer, B. D., *et al.* (2008) Human-induced changes in the hydrology of the western United States. *Science* 319:1080-1083.

Benson, L. and Kleiforth, H. (1989) Stable isotopes in precipitation and ground water in the Yucca Mountain region, southern Nevada: paleocliamtic implications. *Geophys. Monograph* p 18.

Benson, L. V., (1994) Stable isotopes of oxygen and hydrogen in the Truckee River-Pyramid Lake surface-water system. 1. Data analysis and extraction of paleoclimatic information. *Limnol. Oceanogr.* 39:344-355.

Benson, L., Linsley, B., Smoot, J., Mensing, S., Lund, S., Stine, S., and Sarna-Wojcicki, A., (2003) Influence of the Pacific Decadal Oscillation on the climate of the Sierra Nevada, California and Nevada. *Quat. Res* 59:151-159.

Berkelhammer, M. B., Stott, L. D. (2008) Recent and dramatic changes in Pacific storm trajectories recorded in d18O from Bristlecone Pine tree ring celluslose. *Geochem Geophys Geosys* 9:doi:10.1029/2007GC001803.

Berkelhammer, M. B., Stott, L. D., Yoshimura, K., Johnson, K., and Sinha, A., (submitted). Synoptic and mesoscale controls on the isotopic composition of precipitation in the southwestern United States.

Cayan, D. R. (1996) Interannual climate variability and snowpack in the western United States. *J. Climate* 9:928-948,

Cayan, D. R., Dettinger, M. D., Diaz, H. F., and Graham, N. E. (1998) Decadal variability of precipitation over western North America. *J. Climate* 11:3148-3166.

Cayan, D.R., Kammerdiener, S.A., Dettinger, M.D., Caprio, J.M. and Peterson D.H. (2001) Changes in the Onset of Spring in the Western United States. *Bull. Am. Met. Soc.* 82:399-415

Cayan, D. R., Redmond, K. T., and Riddle, L. G. (1999) ENSO and hydrologic extremes in the western United States. *J. Climate* 12:2881-2893.

Cayan, D. R., and Riddle, L. (1992) Atmospheric circulation and precipitation in the Sierra Neveda. Managing Water Resources During Global Change, American Water Resources Association. p. 711-719.

Cohen, E.R., Cvitas, T., Frey, J.G., Homlstrom, B., Kuchitsu, K., Marquard, R., Mills, I., Pavese, R., Quack, M., Stohner, J., Strauss H. L., Takami, M., and Thor, A.J. (Eds) (2007) Quantities, Units and Symbols in Physical Chemistry, 3rd edition. Royal Society of Chemistry Publishing, Cambridge, UK, 265 pp.

Cook, E. R., Woodhouse, C.A., Eakin, C.M., Meko, D.M., and Stahle, D.W. (2004a) Long-term aridity changes in the western United States. *Science* 306:1015-1018.

Cook, E. R., Meko, D.M., Stahle, D.W. and Cleaveland, M.K. (1999) Drought reconstructions for the continental United States. *J. Climate* 12:1145-1162.

Cook, E.R. and coauthors (2004b) North American Summer PDSI Reconstructions. IGBP PAGES/World Data Center for Paleoclimatology, Data Contribution Series # 2004-045. NOAA/NGDC Paleoclimatology Program, Boulder CO, USA.

Craig, H., (1961) Isotopic variations in meteoric waters. *Science* 133:1702-1703.

Dansgaard, W., (1964) Stable isotopes in precipitation. *Tellus* 16:436-468.

Dettinger, M.D. (2004) Fifty-two years of "Pineapple-express" storms across the west coast of North America, *in* United States Geological Survery, S.I.O., ed., California Energy Comission, PIER Energy Related Environmental Research.

Dettinger, M. D., and Cayan, D. R. (1994) Large-Scale Atmospheric Forcing of Recent Trends toward Early Snowmelt Runoff in California. *J Climate* 8:606-622.

Dettinger, M. D., Cayan, D. R., Diaz, H. F., and Meko, D. M. (1998) North-south precipitation patterns in western North America on interannual-to-decadal timescales. *J. Climate* 11:3095-3111.

Eglinton G. and Hamilton R. (1967) Leaf epicuticular waxes. *Science*. 156:1322.

Ehhalt, D., Knott, K., Nagel, J.F. and Vogel, J.C. (1963) Deuterium and oxygen-18 in rain water. *J. Geophys. Res*. 68:3774-3780.

Feakins, S.J. and Sessions, A.L. (2010) Controls on the D/H ratios of plant leaf waxes in an arid ecosystem. *Geochim. Cosmochim. Acta* 74:2128-2141.

Friedman I., Machta, L., and Soller, R. (1962) Water vapor exchange between a water droplet and its environment. *J. Geophys. Res*. 67:2761-2766.

Friedman I., Redfield, A.C., Schoen, B. and Harris, J. (1964) The Variation of the Deuterium Content of Natural Waters in the Hydrologic Cycle. *Rev. Geophys*. 2:177-224.

Friedman, I. and G. I. Smith (1970) Deuterium content of snow cores from the Sierra Nevada area. *Science* 169:467-470.

Gat, J. R., (1996) Oxygen and hydrogen in the hydrologic cycle. *Ann. Rev. Earth Pl. Sc.* 24:225-262.

Graumlich L. J. (1993) A 1000-year record of temperature and precipitation in the Sierra Nevada. *Quat. Res.* 39:249-255.

Hayes, M. J., Drought Indices. National Drought Mitigation Center. www.drought.unl.edu/whatis/indices.htm#pdsi, 2006. Accessed June 1, 2006.

Herweijer, C., Cook, E.R., and Emile-Geay, J. (2007) North American droughts of the last millennium from a gridded network of tree-ring data. *J. Climate* 20:1353-1376.

Hou, J., D'Andrea, W.J., and Huang, Y. (2008) Can sedimentary leaf waxes record D/H ratios of continental precipitation? Field, model and experimental assessments. *Geochim. Cosmochim. Acta* 72:3503-3517.

Hou, J., D'Andrea, W.J., MacDonald, D. and Huang, Y. (2007) Hydrogen isotopic variability in leaf waxes among terrestrial and aquatic plants around Blood Pond, Masachusetts (USA). *Org. Geochem.* 38:977-984.

Hou, J., Huang, Y., Wang Y., Shuman, B., Oswald, W.W., Faison, E. and Foster, D.R. (2006) Postglacial climate reconstruction based on compound-specific D/H ratios of fatty acids from Blood Pond, New England. *Geochem. Geophys. Geosys.* 7:doi: 10.1029/2005GC001076.

Howat, I. M., and S. Tulaczyk (2005), Climate sensitivity of spring snowpack in the Sierra Nevada, *J. Geophys. Res.*, *110*, F04021, doi:10.1029/2005JF000356

Huang , Y.S., Lockheart, M.J., Collister, J.W. and Eglington, G. (1995) Molecular and isotopic biogeochemistry of the Miocene Clarkia Formation: hydrocarbons and alcohols. *Org. Geochem.* 23:785-801.

Huang, J. H. Shuman, B., Wang, Y. and Webb III, T. (2002) Hydrogen isotope ratios of palmitic acid in lacustrine sediments record late Quaternary climate variations. *Geology* 30:1103-1106.

Huang, J.H., Shuman, B., Wang, Y. and Webb III, T. (2004) Hydrogen isotope ratios of individual lipids in lake sediments as novel tracers of climatic and environmental change: A surface sediment test. *J. Paleolimnol.* 31:363-375.

Huth A. K., Leydecker, A., Sickman, J. O., Bales, R. C. (2004) A two-component hydrograph separtion for three high-elevation catchments in the Sierra Nevada, California. *Hydro. Proc.* 18:1721-1733.

Ingraham, N. L. and Taylor, B. E. (1986). Hydrogen isotope study of large-scale meteoric water transport in northern California and Nevada. *J. Hydrol.* 85;183-197.

Ingraham, N. L. and Taylor, B. E. (1991) Light stable isotope systematics of large-scale hydrologic regimes in California and Nevada. *Water Resour. Res.* 27:77-90.

Kattelmann, R., and Elder, K., (1991) Hydrologic characteristics and water balance of an alpine basin the Sierra Nevada. *Water Resour. Res.* 27:1553-1562.

Knowles, N., Detinger, M.D. and Cayan, D.R. (2006) Trends in snowfall versus rainfall in the western United States. *J. Climate* 19:4545-4559.

Leydecker, A. and Melack, J. M. (2000) Estimating evaporation in seasonally snow-covered catchments in the Sierra Nevada, California. *J. Hydrol.* 236:121-138.

Lis, G., Wassenaar, L.I. and Hendry, M.J. (2008) High-precision laser spectroscopy D/H and $^{18}O/^{16}O$ measurements of microliter natural water samples. *Anal. Chem.* 80:287-293.

Lundquist, J. D., Cayan, D. R., and Dettinger, M. D., (2003). Meteorology and hydrology in Yosemite National Park: A Sensor Network Application, in *Information Processing in Sensor Networks: Second International Workshop, IPSN 2003* (F. Zhao and L. Guibas eds), 518-528, Springer, New York.

Lundquist, J. D., Dettinger, M. D., and Cayan, D. R., (2005) Snow-fed Stream flow Timing at Different Basin Scales: Case Study of the Tuolumne River above Hetch Hetchy, Yosemite, California. *Water Resour. Res.* 41:W07005.

Lutz, J. A., van Wagtendonk, J. W., and Franklin, J. F. (2010) Climatic water deficit, tree species ranges, and climate change in Yosemite National Park. *J. Biogeogr.* 37:936-950.

Majzoub, M., (1971). Fractionnement en oxygene-18 et en deuterium entre l'eau et sa vapeur. *J. Chem. Phys.* 68:1423-1436.

Markham, C. G., (1970) Seasonality of Precipitation in the United States. *Ann. Assoc. Am. Geogr.* 60:593-597.

McCabe G. J., Palecki, M. A., and Betancourt, J. L. (2004) Pacific and Atlantic Ocean influences on multidecadal drought frequency in the United States. *Proc. Natl. Acad. Sci* 101:4136-4141.

Meko, D. M., Therrell, M. D., Baisan, C. H., and Hughes, M. K. (2001) Sacramento River flow reconstructed to A.D. 869 from tree rings. *J. Amer. Water Res. Assoc.* 37: 1029-1039.

Meko, D. M., and Woodhouse, C. A. (2005) Tree-ring footprint of joint hydrologic drought in Sacramento and Upper Colorado river basin, western USA. *J. Hydrol.* 308:196-213.

Meyers, P. A. and R. Ishiwatari, 1993. Lacustrine organic geochemistry—An overview of indicators of organic matter sources and diagenesis in lake sediments. *Org. Geochem.* 20:867-900.

Millar, C. I., King, J.C., Westfall, R.D., Alden, H.A., and Delany, D.L. (2006) Late Holocene forest dynamics, volcanism, and climate change at Whitewing Mountain and San Joaquin Ridge, Mono County, Sierra Nevada, CA, USA. *Quat. Res.* 66:273-287.

Mote, P. W., Hamlet, A.F., Clark, M.P. and Lettenmaier, D.P. (2005) Declining mountain snowpack in western North America. *Bull. Am. Meteorol. Soc.* 86:39-49.

Overpeck, J., Udall, B. (2010) Dry Times Ahead. *Science* 328:1624-1643.

Palmer, W. C. (1965) Meteorological drought. Research Paper No. 45, US. Weather Bureau, p 58.

Regonda, S., Clark, M.P., Rajagopalan, B., and Pitlick, J. (2005): Seasonal cycle shifts in Hydroclimatology over the western United States. *J. Climate*, 18:372-384.

Rodhe, A. (1998). Snowmelt-dominated systems. in *Isotope Tracers in Catchment Hydrology*. Kendall C. and J. J. McDonnell eds. Elsevier 137-162.

Roos, M., (1991) A Trend of Decreasing Snowmelt Runoff in Northern California. *Proc. 59th Western Snow Conference*, Juneau, AK, 29-36.

Sachse, D., Radke, J. and Gleixner, G. (2004) Hydrogen isotope ratios of recent lacustrine sedimentary *n*-alkanes record modern climate variability. *Geochim. Cosmochim. Acta* 68:4877-4889.

Sachse, D., Radke, J. and Gleixner, G. (2006) δD values of individual n-alkanes from terrestrial plants along a climatic gradient—Implications for the sedimentary biomarker record. *Org. Geochem.* 37:469-483.

Sauer, P.E. Eglinton, T.I., Hayes, J.M., Schimmelmann, A. and Sessions, A.L. (2001) Compound-specific D/H ratios of lipid biomarkers from sediments as a proxy for environmental and climatic conditions. *Geochim. Cosmochim. Acta* 65:213-222.

Schimmelman A. Sessions, A.L. and Mastalerz, M. (2006) Hydrogen isotopic (D/H) composition of organic material during diagenesis and thermal maturation. *Annu. Rev. Earth Pl. Sc.* 34:501-533.

Seager, R., Burgman, R., Kushner, Y., Clement, A., Cook, E.R., Niak, N. and Miller, J. (2008) Tropical Pacific forcing of North American medieval megadroughts: Testing the concept with an atmospheric model forced by coral-reconstructed SSTs. *J. Climate* 21:6175-6190.

Seager, R., Harnik, N., Robinson, W.A., Kushnir, Y., Ting, M., Huang, H.P. and Velez, J. (2005a) Mechanisms of ENSO-forcing of hemispherically symmetric precipitation variability. *Q. J. R. Meteorol. Soc.* 131:1501-1527.

Seager, R. Kushnir, Y., Herweijer, C., Naik, N., and Velez, J. (2005b) Modeling of tropical forcing of persistent droughts and pluvials over western North America: 1856-2000. *J. Climate* 18:4065-4088.

Sieh, K. and Bursik, M. (1986) Most recent eruption of the Mono Craters, eastern central California. *J. Geophys Res.* 91:12,539-12,571.

Sessions, A. L. (2006) Seasonal changes in D/H fractionation accompanying lipid biosynthesis in *Spartina alterniflora*. *Geochim et Cosmochim Acta* 70:2153-2162.

Sessions, A.L., Burgoyne, T.W., Schimmelmann, A., and Hayes, J.M. (1999) Fractionation of hydrogen isotopes in lipid biosynthesis. *Org. Geochem.* 30:1193-1200.

Sessions, A.L., Jahnke, L.L., Schimmelmann, A. and Hayes, J.M. (2002) Hydrogen isotope fractionation in lipids of the method-oxidizing bacterium *Methylococcus capsulatus*. *Geochim. Cosmochim. Acta* 66:3955-3969.

Smith, G.I., Friedman, I., Kleiforth, H., and Hardcastle, K. (1979) Areal distribution of deuterium in eastern California precipitation, 1968-1969. *Journal Appl. Meteorol.* 18:172-188.

Stewart I.T., Cayan, D.R., and Dettinger, M.D. (2005) Changes toward earlier streamflow timing across Western North America. *J. Climate* 18:1136-1155.

Stine, S. (1994) Extreme and persistent drought in California and Patagonia during mediaeval time. *Nature* 369:546-549.

The National Weather Service Forecast Office (2008). Snow measurement guidelines for National Weather Service snow spotter. Wakefield, Virginia.

Unnikrishna, P. V., McDonnell, J. J., and Kendall, C. (2002) Isotope variations in a Sierra Nevada snowpack and their relation to meltwater. *J. Hydrol* 260:38-57.

Wood, S. H., (1977) Distribution, correlation, and radiocarbon dating of late Holocene tephra, Mono and Inyo craters, eastern California. *Geol. Soc. of Amer Bull* 88:89-95.

Woodhouse, C.A. and Overpeck, J.T. (1998). 2000 years of drought variability in the central United States. *Bull. Am. Meteorol. Soc.* 79:2693-2714.

Yang, H. and Huang, Y. (2003) Preservation of lipid hydrogen isotope ratios in Miocene lacustrine sediments and plant fossils at Clarkia, northern Idaho, USA. *Org. Geochem.* 34:413-423.

Yuan, F. Linsley, B.K., Lund, S.P., and McGeehin, J.P. (2004) A 1200 year record of hydrologic variability in the Sierra Nevada from sediments in Walker Lake, Nevada. *Geochem. Geophys. Geosys.* 5:doi:10.1029/2003GC000652

Zhang, Y., Wallace, J.M. and Battisti, D.S. (1997) ENSO-like interdecadal variability: 1900-93. *J. Climate* 10:1004-1020.

Chapter 4. Hydroclimate of the Sierra Nevada Mountains during the late medieval period (1160-1432 A.D.) as captured by sedimentary leaf wax lipid hydrogen isotope ratios.

Abstract

Persistent drought is among the greatest risks of climate change facing the western United States. This risk is accentuated by paleohydrologic reconstructions during the medieval period (~900-1300 A.D.) that suggest this region was witness to droughts of greater duration than any experienced in recorded history. Here we apply the stable hydrogen isotope ratios (δD) of plant leaf wax lipid compounds preserved in lake sediments to reconstruct past hydroclimate variability in the Sierra Nevada Mountains. Previous studies establish that the δD values of these compounds capture that of lake water and/or shallow ground water and comparison of 20th century leaf wax lipid δD measurements with instrumental climate records demonstrates a clear relationship between this tracer and moisture availability in the Sierra Nevada Mountains. Leaf wax fatty acids were extracted from lake sediments in Yosemite National Park, along the western slope of the Sierra Nevada, and their δD measured at interannual resolution over the period 1160-1432 A.D., the "late medieval" period. Late medieval δD variability correlates with coeval regional tree ring derived PDSI reconstructions at multidecadal frequencies. The reconstruction does suggest at least one drought of greater duration than any witnessed in the Sierra Nevada during the last 100 years. However, complete analysis of late medieval drought frequency and severity—including comparisons to the 20th

century--requires further constraint on the driving mechanisms for leaf wax lipid δD variability on longer (centennial) timescales.

4.1 Introduction

Prolonged drought in southern California has the potential for devastating environmental and socioeconomic impacts. Such impacts were felt when severe aridity plagued the state during the late 1920's to mid 1930's (the "Dust Bowl" drought) in 1976-1977, in 1987-1992, and most recently from 1999-2004. Future drought related impacts in California may be inevitable as projected climate warming over the coming decades to centuries will likely increase water stress across the western United States (henceforth "the West") (Barnett *et al*., 2008; Overpeck and Udall, 2010; Seager *et al*. 2007a). Southern California is at particular risk to future water stress as it draws a significant percentage of its year-round fresh water supply from snow pack in the Sierra Nevada mountains (e.g. California Climate Change Center, 2006), a resource that is highly sensitive to climate warming and may already be showing signs of demise at lower elevation catchments (Roos, 1991; Dettinger & Cayan, 1994; Cayan et al. 2001; Regonda et al. 2005; Stewart et al. 2005; Barnett *et al*., 2008; Mote et al 2005; Howat and Tulaczyk 2005).

Further highlighting the need for water resources preparedness is evidence from paleohydrologic archives including submerged tree stumps (Stine, 1994), tree rings (Douglas, 1929; Meko *et al*., 2001; Stahle *et al*., 2007), gridded tree ring networks (Cook *et al*., 1999, 2004a) and lake sediments (Li *et al*., 2000; Woodhouse & Overpeck, 1998; Yuan *et al*., 2003) that historical droughts in the West may have been limited in severity and duration compared to those over the last millennium, particularly during the medieval period (~900-1300 A.D.). Early evidence for anomalous aridity in the West during the

13th century emerged in the form of anomalously thin tree ring widths (Douglas, 1929) and paucity of bison bones (Dillehay, 1974). More recently, relict tree stumps submerged in several present-day water bodies in central California provided some of the first evidence for the occurrence of severe and protracted droughts throughout the medieval period (Stine, 1994). Radiocarbon dates from the outermost growth ring of these stumps cluster in two groups, one around 1100 A.D. and another around 1350 A.D., suggesting that dry conditions in the decades prior to those years drove lake levels low enough to support stands of mature pine trees. Cook *et al*. (2004a) expanded upon this evidence with a North America-wide network of tree ring chronologies that reconstruct the Palmer Drought Severity Index (PDSI), a regional index of moisture availability and aridity (Palmer, 1965; Hayes, 2006). Detailed analysis of these PDSI reconstructions by Herweijer *et al*. (2007) revealed that the medieval droughts were of comparable magnitude and spatial expression as many 19th and 20th century droughts, but had unprecedented persistence (multiple decades as opposed to years).

Evidence from several isolated hydrologic proxy records indicates that the Sierra Nevada Mountains did not escape prolonged drought during the medieval period (Graumlich, 1993; Meko *et al*., 2001; Yuan *et al*., 2003). However, the persistence and severity of these droughts relative to those of the 20th century remains unclear. For example, tree-ring widths measured by Graumlich suggest that although the Sierra Nevada experienced aridity in ~20-year intervals, these were no longer or more severe than those at later times over the last millennium. Tree-ring reconstructed discharge of the Sacramento River, which drains part of the Sierra Nevada Mountains, reveals high and low flow anomalies between 869 and 1440 A.D. with persistence unmatched over the

historical record (Meko *et al*., 2001). However, the authors acknowledge that these anomalies were recorded in the earliest and therefore least accurate part of the tree ring reconstruction. Indeed, hydrologic data from the Sierra Nevada and throughout the West is relatively scarce before ~1600 A.D. (Cook *et al*., 2004a; Woodhouse *et al*., 2009). Additional independent proxy records are needed to constrain the persistence and severity of droughts in the Sierra Nevada Mountains during the medieval period, and to place these droughts within the greater framework of hydrologic variability throughout the West over the last millennium.

Sedimentary leaf wax lipid δD shows promise as one such paleohydrologic proxy. In Chapter 3 of this dissertation, building upon discoveries that the δD of leaf wax lipids tracks that of environmental water along a variety of temperature and moisture gradients (Sachse *et al*., 2004, 2006; Hou *et al*., 2008; Feakins & Sessions, 2010), I demonstrate the sensitivity of this proxy to moisture availability on interannual to decadal time scales in the Sierra Nevada Mountains over the 20th century. I propose that winters with low precipitation and snowpack result in a reduced input of water relatively depleted in deuterium (D) to the Swamp Lake catchment that allows evaporative enrichment to impart a greater isotopic mass balance impact on lake surface water and shallow ground water during the growing season when lipid biosynthesis occurs. This driving mechanism explains the significant negative correlations of leaf wax lipid δD variability with instrumentally recorded PDSI and April 1st snow water equivalencies (SWE) both in the Sierra Nevada Mountains and throughout the West. In this study, I have measured leaf wax lipid hydrogen isotope ratios (δD) from sediments deposited in Swamp Lake, western Sierra Nevada Mountains, over the period 1160-1432 A.D. (referred to here as

the “late medieval” period) at interannual (~3 year) resolution. Comparison to existing paleohydrologic reconstructions from the Sierra Nevada and the West facilitates further investigation of the driving mechanisms of multidecadal to centennial scale δD variability. Based on these comparisons and my findings in Chapter 3, I interpret the resulting δD record in terms of its implications for the duration and severity of droughts in the Sierra Nevada Mountains during the late medieval period.

4.2 Study site

Swamp Lake is located at (37°57’N, 119°46’W) at 1535 m on the western slope of the Sierra Nevada (Chapter 3, Figure 3.1), where is receives the full brunt of the frontal, wintertime storms that bring ~80% of annual precipitation in the region (Markham, 1970). Annual precipitation in the region of Swamp Lake is ~89 cm but exhibits high year to year variability with amounts in a given year 50-200% of the long-term average not uncommon (Lundquist *et al*., 2005). Chapter 3 describes in detail the climatology of region surround the Swamp Lake catchment and the seasonal lake level and temperature cycles in Swamp Lake. The lake, approximately 8 ha in surface area, sits in a relatively small 1.6 km^2 catchment of primarily granite bedrock that is exposed in numerous outcrops and otherwise overlain by shallow, unconsolidated soils, with an exception being the thicker, Tioga age glacial till on the steep slope to the south of Swamp Lake. Based on measurements of lake level and meteorological observations from nearby stations, we estimate an average residence time of water in the catchment of ~1.5 years, consistent with comprehensive measurements of water catchment scale water balance from drainage basins of similar size elsewhere in the Sierra Nevada (Kattelmann & Elder, 1991; Huth *et al*., 2004).

4.3 Methods

Details of lake sediment collection, processing and sampling as well as compound specific *n*-acid δD measurement are described in detail in Chapter 3. Briefly, frozen sediment slabs, or freeze cores, were collected from Swamp Lake in the falls of 2006 and 2007 (Please refer to Appendix B for Swamp Lake core details). Core SL0708 was sampled at 2 mm intervals in a -20ºC cold room with a sharp razor blade, with care taken to follow annual laminations. Frozen samples were placed in precombusted glass vials and lyophilized. Extraction, separation, identification and isotopic measurement of leaf wax lipids were carried out at the lab of Alex Sessions at the California Institute of Technology. Sediment samples were weighed, with dry masses ranging from 55 to 533 mg and the solvent soluble lipids extracted in 20 ml of the 9:1 dimethylchloride (DMC):methanol azeotrope in a Mars Express microwave-assisted solvent-extraction system (Mars 5, CEM corp.) for 30 min at 100ºC with stirring. The resulting total lipid extracts (TLEs) were separated into four organic fractions: hydrocarbons (*n*-alkanes), ketones, alcohols and fatty acids (*n*-acids) using solid phase extraction (SPE) procedure and elution schedule described in Sessions *et al*. (1999) and Chapter 3. *n*-acids were derivatized to methyl esters by refluxing with boron trifluoride in methanol at 70ºC for 10 minutes.

The *n*-acid fraction was analyzed on a ThermoFinnigan Trace GC-DSQ quadrupole mass spectrometer equipped with a DB-5 column (30 m x 0.25 mm x 0.25 μm) and PTV injector operated in splitless mode. The relative abundance of even carbon number *n*-acids C20-C32 was determined by integrating peak area. δD analyses of individual *n*-acids was carried out on a ThermoElectron Trace GC coupled to a Delta +

XP IRMS via an Al_2O_3 pyrolysis chamber. Determination of the H_3^+ factor (Sessions *et al*., 1999), analytical uncertainty and isotopic correction for the added methyl group was carried out as described in Chapter 3. The mean precision for replicate measurements of the external F8 standard was 4.12‰ (1σ, N=143) and the root-mean-square (RMS) error 5.13‰ during the period of analysis. In total the δD of C22-C28 *n*-acids was analyzed in 89 sediment samples, with 69-70 run in duplicate.

4.4 Determination of chronology

The SL0708b age model (Figure 4.1a) was generated using a combination of tephranalysis and digital image analysis. Microscopic examination of thin sections prepared from Bolivia Cores SL0702 and SL0703 revealed three tephra layers. 6 samples, one from each of the three matching tephra layers in SL0702 and SL0703, were geochemically analyzed by Elmira Wan (USGS) at the Menlo Park Tephrachronology Lab. Distinct marker layers were used to cross correlate the Bolivia cores with SL0708, and the shallowest of the three tephras (labeled T1) was identified at 17.0 cm (22.4 cm depth on the image ruler) (Figure 4.1 b-c). Comparison of tephra geochemistry with that from a library of previously analyzed tephra samples confirmed that T1 was likely generated from the eruption of the Mono Craters in the mid 14th century first documented by Wood (1977) (Wan, personal communication). Sieh & Bursik (1986) used radiocarbon dating, dendrochronology and stratigraphy to determine an upper limit of 1368 A.D. for this eruption, which they further constrained to have occurred within a few months to 2 years after the latest eruption of the Inyo craters. In a more recent study, this Inyo eruption was dated at exactly 1350 A.D. using dendrochronology and death dates (Millar *et al*., 2006). We therefore fix the depth of T1 at 1350 A.D. This timing is

consistent with the Bolivia core depths of the next deepest tephra (T2), which a close geochemical the "Tephra I" eruption of Wood (1977) dated at ~1190 years ^{14}C years b.p. The deepest tephra (T3) has poor geochemical constraint, but due to its close proximity (within 10 cm) to T2 suggests that it may have been generated by an eruption ~1250 year bp associated with that of Wood's Tephra 1 (Bursik, personal communication).

Although clearly visible (Figure 4.1c), the varves on SL0708 are too thin to count accurately with the human eye. A comparison of periodograms from years counted by eye and those chosen by the computerized varve selection program (Appendix C) indicated that the program identified light dark transitions with greater fidelity, as shown by the sharp peak generated at a period of 1 year (Figure 4.1 d-f). We took the average sedimentation rate of 630 μm/yr derived from varve assignments by the program from one digital image of SL0708t and two overlapping images of SL0708b, and used this rate to assign ages above and below T1 to generate the age model in (Figure 4.1a). Visual inspection of a ~25 cm long massive unit in the digital images of all freeze cores revealed grading of sediment from course sand and small pebbles on the bottom to a fine clay cap at the top (Figure B1). This grading indicates that this section was formed from a bank failure rather than oxygenation of the lake bottom waters. Furthermore, on all cores counted, the clay cap fell within ten varve years of 1872, the date of the powerful Owens Valley earthquake, which was documented to have been strongly felt in Yosemite Valley by John Muir himself and to have generated a similar slump in Owens Lake (Li *et al*. 2000). We therefore assume that the massive section was instantaneously deposited at the time of the Owens Valley earthquake. As an independent check, we extrapolated the estimated sedimentation rate to the depth of T1 and arrived at an age of 1344 A.D.,

within 6 years of T1. Based on this offset the relative tight age constraint for the timing of deposition for tephra T1, we assign a chronological uncertainty to the age model in figure 4.1a of ~±10 years.

As a second check, the SL0708b age model was compared to one generated for a suite of much longer Swamp Lake cores collected by R. Scott Anderson in 1987 and 1991 that extend through the Holocene (Smith & Anderson 1992). Cross correlation between the Bolivia cores and SL0708 with SL-02-05, one of these longer cores, was preformed by comparison of digital images and alignment of clearly identifiable tephra bands. The estimated sediment rate of 630 μm/year is equivalent to the ~0.06 cm/yr rate in the SL-02-05 age model at corresponding depths (Hallett, personal communication).

4.5 Results

Values of δD for the C22-C28 *n*-acids covary across the entire record (Figure 4.2). δD varies on the order of 25‰ at interdecadal frequencies with a full range of -200‰ to -160‰. Back to back duplicate measurements were made for the majority of samples, and averages taken as the final value. A single value is used in the absence of duplicate measurements. Average absolute offset between duplicate measurements of the four compounds was 4.6‰, 3.8‰, 3.4‰, and 2.3‰ for C22, C24, C26 and C28 (N= 70, 69, 69, 70) respectively. As observed in 20th century sediment (Chapter 3), the long-term averages of the C24-C28 (-181‰, -176‰ and -180‰ respectively) are indiscernible within the 5-6‰ analytical error while that for C22 (-187‰) is slightly lower. Due to its high sedimentary abundance, C24 provides to most complete δD record, and is therefore chosen for further examination.

Figure 4.3a depicts the annually interpolated C24 record run through a low pass Gaussian filter to maximize >10 year periodicities. In this time series, we identify 9 multidecadal excursions towards higher δD values centered on A.D. 1186, 1215, 1236, 1256, 1296, 1319, 1346, and 1393, which, based on our 20th century findings (Chapter 3), we interpret as shifts towards drier conditions, with lower wintertime precipitation and snowpack. The excursion centered on 1296 A.D. is the most pronounced and δD at this date in the annually interpolated record (-160‰) is the highest of the time series. Excursions centered on 1186 and 1236 are the 2nd and 3rd highest respectively. Although not among the top three elevated δD excursions in terms of absolute value, the excursion centered on 1393 is nearly as dramatic in relative increase as that centered on 1296 and is the most persistent of the 9 dry periods.

In order to interpret isotopic variability within the framework of previously documented hydrologic conditions in the Sierra Nevada, we compare the C24 δD record in figure 4.3a to regional tree ring width summertime (June-August) PDSI reconstructions from the NADA processed with the same low pass filter. Summertime PDSI is found to have the closest relationship with tree ring widths (Cook *et al*., 1999) and reflects wintertime aridity through the autoregressive nature of the PDSI index (Palmer, 1965). Individual grid square NADA PDSI reconstructions were obtained from Cook & Krusic (2004) (updated version available online at http://www.ncdc.noaa.gov/paleo/pdsi_ts.html; NOAA National Climatic Data Center 2008). Table 4.1 lists correlation coefficients of low pass filtered C24 with PDSI reconstructions from the five most proximal 2.5º x 2.5º NADA grid squares (gs46, gs47, gs48, gs59 and gs60). C24 is negatively correlated with all 5 PDSI reconstructions, with

the strongest correlation observed with gs60 ($r = -0.47$, $p < 0.001$). gs47 exhibits one of the weaker correlations with δD despite it's being situated directly over the location of Swamp Lake in Sierra Nevada Mountains. In Chapter 3 I hypothesize that strength of correlation with gs59 relative to that with gs47, situated directly over Swamp Lake, may be due to issues of PDSI as an indicator of aridity in snowpack dominated catchments. The PDSI reconstructions may therefore better reflect hydrologic conditions in the Great Basin (gs59) and southern California (gs60) than over the Sierra Nevada crest (gs47). It should be noted that all PDSI reconstructions are derived from heavily overlapping sets of individual tree ring chronologies (Cook, personal communication) (Figure D1). Differences in the reconstructions are therefore based on variable spatial weighting of chronologies among the 5 grid squares, as described in Cook *et al*. (1999), and the addition or subtraction of a handful of individual chronologies (Figure D1). The number of chronologies available for PDSI reconstructions in the five grid squares considered here increases by a factor of 1.6-2.1 from 1160 to 1432 with the majority of new chronologies added after 1300 A.D. (Figure D2). Of the 5 grid squares considered, gs47 and gs59 include the largest number of individual chronologies, 13 to 24 and 18 to 30 respectively, and are in closest proximity to Swamp Lake (see figure D1 for grid square perimeters relative to the location of Swamp Lake) and we therefore choose them for further comparison with the C24 δD record. 8 and 7 of the 9 high δD excursions in figure 4.3a correspond to multidecadal decreases in PDSI at gs59 (Figure 4.3b) gs47 PDSI (Figure 4.3c) respectively. In contrast to this general correspondence between δD and reconstructed PDSI over multiple decades, we observe little relationship on centennial time scales. δD increases as PDSI decreases between ~1170 and 1240 A.D.,

and decreases as PDSI increases from 1240 to 1320. However, after 1320 δD continues to decrease while PDSI declines.

While comparison to the gs47 and gs59 PDSI reconstructions facilitates assessment of δD variability in terms of regional drought, that with the DAI time series (Cook *et al*., 2004a) (Figure 4.3d) allows us to assess the covariance of hydrologic conditions in the Sierra Nevada with those across the West as a whole. DAI values were obtained from Cook & Krusic (2004). DAI is strongly correlated to gridded NADA PDSI reconstructions throughout the West, with a bulls eye-like spatial pattern of correlation centered on Utah and the four corners region (Figure D3a). Correlation with reconstructed Sierra Nevada PDSI from 1150-1450 ranges from -0.6 to -0.8 (Figure D3b). We find that the multidecadal elevated δD excursions centered on A.D. 1186, 1215, 1236, 1256, 1319, 1346 and 1393 correspond to multidecadal increases in DAI. The dramatic excursion centered on 1296 A.D., however, is not reflected in the DAI time series. Centennial variability of gs47 and gs59 generally follows that of DAI, although DAI fluctuations are of greater relative magnitude. These centennial fluctuations are not matched by those in C24 δD with the exception of the trend towards higher δD and drier conditions between 1170 and 1250 A.D.

In order to examine the driving mechanisms behind multidecadal to centennial scale leaf wax lipid δD fluctuations during the late medieval, we compare C24 δD to a reconstruction of the Pacific Decadal Oscillation (PDO, Mantua *et al*., 1997) index (MacDonald & Case, 2005) (Figure 4.3e) complied from tree-ring chronologies sampled at the opposing N/S dipoles of PDO's precipitation influence along the western North American margin (MacDonald & Case, 2005). Reconstructed PDO exhibits weak but

significant positive correlation with gs47 ($r = 0.18$, $p < 0.01$) and gs59 ($r = 0.24$, $p < 0.001$) PDSI at multidecadal frequencies over the period 1150-1450, such that more negative values of PDO correspond to more negative values of PDSI, consistent with the observed influence of PDO on western Sierra Nevada precipitation over the 20th century (McCabe *et al*., 2004) and the argument of MacDonald & Case (2005) that a protracted negative phase of PDO in the medieval period contributed to aridity in the West. Two of the high δD excursions correspond to lower PDO values (1186 and 1296), three with higher values (1236, 1319 and 1346) and four with near average (relative to the 1150-1450 time period) values, (1215, 1256, 1269 and 1393). Overall, the correlation of multidecadal δD and reconstructed PDO variability is significantly negative ($r = -0.39$, $p<0.001$). However, centennial scale PDO fluctuations show little relationship to those of C24 δD, with the exception of more negative PDO corresponding to elevated δD between ~1270-1320 A.D. and 1370-1470 A.D.

In Figure 4.4 we compare late medieval C24 δD (series a) to that measured from the 20th century, along with corresponding reconstructed and instrumental PDSI from gs59 (series b), DAI (series c) and PDO (series d) derived from tree-ring widths (MacDonald & Case, 2005) and instrumental SST observations (Mantua *et al*., 1997; Zhang *et al*., 1997). Instrumental PDO values were obtained from http://jisao.washington.edu/data_sets/pdo and instrumental PDSI values from (Cook *et al*., 2004b) Multidecadal variability in reconstructed PDSI and drought area is high over both periods, but according to these records both the Sierra Nevada and the West were slightly wetter in the 20th century that during the late medieval. 20th century averages of PDSI and drought area are 0.59σ higher and 9.3% lower respectively than late medieval

averages, both differences significant at the 95% confidence interval based on a two-tailed student's t-test. 20th century averages of reconstructed and instrumental PDSI are identical. The 20th century average of reconstructed PDO (0.18) is 0.48, or just over one half the millennium-long standard deviation, higher than the -0.30 average from 1160-1432 A.D., a difference also significant at the 95% confidence interval. The 20th century instrumental PDO average is slightly lower than the reconstructed average, but still significantly higher than the 1160-1432 A.D. reconstructed average. Average C24 δD in the 20th century is 17‰ higher than that during the late medieval, equivalent to >2σ of the variability in both records. This increase is heavily weighted by the ~20‰ increasing δD trend over the 20th century, as δD in the early 20th century are within 1σ of the late medieval average.

4.6 Discussion

Nearly all of the multidecadal δD fluctuations in figure 4.3a track those of reconstructed PDSI from gs47 and gs59 with elevated δD corresponding to more negative PDSI, i.e. drier conditions. This negative correlation is consistent with that observed between Swamp Lake leaf wax lipid δD and PDSI over the 20th century (Chapter 3) and suggests that this proxy reflects moisture availability on multidecadal timescales in the Sierra Nevada during the late medieval as well. As discussed in Chapter 3, patterns of atmospheric circulation, such as those associated with PDO, can influence the isotopic content of precipitation and consequently play a role in driving this δD variability (Berkelhammer & Stott, 2008; Berkelhammer *et al*., submitted). However, the negative correlation between δD and PDO observed here is in the opposite direction as that expected under this mechanistic scenario. Instead, the results here points towards

catchment-scale isotopic mass balance as the primary mechanism driving leaf wax lipid δD variability during the late medieval. In Chapter 3, we argue that this mechanism is responsible for linking leaf wax lipid δD to moisture availability and explains its particular sensitivity to April 1st snow water equivalence (SWE). The results here therefore suggest that the same processes were responsible for driving δD variability during the 20th century and the late medieval period.

The relationship between C24 δD and moisture availability during the late medieval is further evident through comparison with additional paleohydrologic records besides the NADA PDSI reconstructions of Cook *et al*. (2004). The dramatic δD excursion at the turn of the 14th century corresponds to two of the lowest 20 year periods of tree-ring reconstructed Sacramento River flow, which ended in A.D. 1311 and 1312 (Meko *et al*., 2001). High δD excursions centered on A.D. 1215, 1236, 1256 and 1269 also correspond to low 20-year averaged Sacramento River flow. Flow is consistently below the long term average between 1350 and 1400 A.D., potentially corresponding to the elevated δD between ~1375 and 1410 A.D. Low δD excursions centered on 1174, 1200 and 1283 A.D. correspond to elevated flow, although relatively high flows between 1325 and 1350 are not matched with below average δD. Multidecadal C24 δD variability also corresponds to that observed in wintertime precipitation reconstructed by Graumlich (1993) from tree ring chronologies obtained east of the Sierra Nevada crest. Graumlich (1993) observes that prolonged (> 20 year) droughts appear to have been a regular feature of the Sierra Nevada Mountains throughout the last millennium, although they may have been more common during the medieval period, with 3 of the 5 most negative reconstructed 50-year mean precipitation anomalies falling between 1000 and 1300 A.D.

The lowest of these anomalies occurs between 1250-1299 A.D., and another between 1315-1364 A.D., corresponding, within chronological uncertainty, to high δD excursions centered on A.D. 1296, 1312, 1332 and 1368. The turn of the 14th century drought appears to have been dramatic and widespread throughout the Sierra Nevada, as it is documented in several additional hydrologic reconstructions, including precipitation in Nevada Climate Division 3, which neighbors the eastern Sierra Nevada (Hughes & Graumlich, 1996), and water levels of Walker Lake, located in Nevada just east of the Sierra Nevada Mountains (Yuan *et al*., 2003). Despite its prevalence in the Sierra Nevada region, this drought may not have been widespread throughout the West as evidenced by its absence in the DAI record. Instead, while conditions in the first half of the 13th century had begun to transition from drought to pluvial across the majority of the West by the turn of the 14th century (Cook *et al*., 2004), the Sierra Nevada experienced a decades-long return to drought conditions that lasted until ~1330 A.D.

Having established that Swamp Lake leaf wax lipid δD variability reflects changes in moisture availability on multidecadal time scales, we consider the implications of the δD record for the persistence and severity of droughts in the Sierra Nevada Mountains during the late medieval period relative to those over the 20th century. The late medieval δD record contains 2 >20 year periods when δD falls above the record-long average, one in the mid 13th century and another in the late 14th century, indicating that between 1160 and 1432 A.D. the Sierra Nevada may have witnessed multiple decades when low wintertime precipitation and snowpack enhanced the catchment isotopic mass balance impact of evaporative enrichment. The 20th century record contains no such intervals of persistently elevated δD (Figure 4.4). This finding is consistent with

those of Meko *et al*., (2001) and Graumlich (1993)--that periods of protracted aridity in the Sierra Nevada were concentrated before 1400 A.D. They are also consistent with the widely believed hypothesis that medieval droughts were of greater duration than those on historical record (Herweijer *et al*., 2007).

The shift to higher overall mean δD in the 20th century compared to the late medieval--despite generally wetter 20th century conditions (Figure 4.4)--complicates assessment of relative drought severity between these periods. This shift highlights the disparity between the driving mechanism of interannual to multidecadal δD variability, which we have determined to be catchment-scale isotopic mass balance related to moisture availability, and that of longer term (centennial scale) variability. One potential cause for this shift is a change in the aquatic and terrestrial flora of the Swamp Lake community that altered the isotopic composition of the integrated sedimentary *n*-acid pool (please refer to Chapter 3 for a discussion on net biological fractionations among differing plant types and species). Compared to that from the 20th century (Figure 3.7), the late medieval sedimentary *n*-acid distribution (Figure D4) contains a greater relative abundance of C26 and C28, which may be due to a larger overall contribution from terrestrial plants (Cranwell, 1982; Ficken *et al*., 2000; Meyers & Ishiwatari, 1993). Because the net biological fractionations of terrestrial plants are typically smaller than those of aquatic plants due to transpirative enrichment (Sachse *et al*., 2004, 2006) we would expect this increased terrestrial contribution to raise, not lower, sedimentary leaf wax lipid δD relative to the modern period, where aquatic plants are the dominant source of leaf wax lipids to the Swamp Lake sediments (Chapter 3). Furthermore, based on the findings of Feakins & Sessions (2010), variability in net biological fractionation may be

random and not specific to individual plant species or groups of plants, although this study did not consider aquatic plants. A more thorough investigation of the *n*-acid distributions and δD variability in the plants surrounding Swamp Lake, akin to that of Hou *et al*. (2007), is necessary to further constrain the aspect of δD variability.

Although ruled out as the primary driving mechanism for multidecadal δD fluctuations, changes in the preformed isotopic composition of precipitation could also play a role in causing long-term δD shifts. During the cool phases of PDO and the El Niño Southern Oscillation (ENSO), north Pacific storm tracks are shifted to more northerly latitudes (Cayan *et al*., 1998) and the contribution of moisture from the tropical and subtropical Pacific to central California storms is diminished relative to that from the central and subpolar north Pacific (Berkelhammer *et al*., 2009) resulting in precipitation comparatively depleted in deuterium to fall in the Sierra Nevada (Berkelhammer *et al*., submitted; Berkelhammer & Stott, 2008). Therefore, the hypothesized medieval occurrence of a protracted La Niña or absence of El Niño in the eastern tropical Pacific, (Cobb *et al*., 2003; Seager *et al*., 2007b, 2008) and negative phase of the PDO (Mac Donald *et al*., 2005) could have driven the isotopic content of water in the Swamp Lake catchment towards a lower mean than observed in the 20th century. However, central tropical Pacific SSTs have only varied within a narrow, <1ºC temperature range (Cobb *et al*., 2003) on centennial scales throughout the last millennium. Only since 1970 have temperatures increased by ~0.8ºC (McPhaden & Zhang, 2002). Similarly, it would be difficult for the 0.48 increase in reconstructed PDO (Mac Donald & Case, 2005) during the 20th century relative to the late medieval to force the 17‰ increase in leaf wax lipid δD when this proxy appears impervious to much larger multidecadal swings in PDO

despite the relatively short ~1.5 year estimate for replacement time of the Swamp Lake catchment (Chapter 3).

We have ruled out changes in sedimentary plant lipid distribution and isotopic composition of precipitation as the primary driving mechanisms behind the long term shifts in δD such as that observed between the late medieval and the 20th century. However, lacking a continuous δD record, we cannot further constrain these mechanisms beyond recognizing that they are not the same as those responsible for driving interannual to multidecadal scale δD fluctuations. We can surmise that if hydrologic conditions in the Sierra Nevada Mountains during the late medieval were drier on the whole than those during the 20th century, these mechanisms must be influential enough to overprint the isotopic effects of a prolonged reduction in moisture availability. Another possibility is that despite the occurrence of droughts with greater persistence than those during the modern period, hydrologic variability in the Sierra Nevada did not fluctuate around a significantly drier mean in the late medieval than it has over the last 100 years. It is also worth noting that elevated δD values in the latter half of the 20th century heavily weight the increase in overall average. Only by filling in the record can we determine whether the ~+20‰ 20th century trend and these elevated values are unique to the last 100 years.

4.7 Conclusions

We have measured δD of leaf wax *n*-acids C22-C28 from Swamp Lake, Sierra Nevada Mountains at interannual resolution over the late medieval period. Isotopic covariability is observed among all *n*-acid compounds. Multidecadal fluctuations in C24 δD track those of regional reconstructed PDSI (Cook *et al*., 2004; Cook & Krusic, 2004) such that higher values of δD correspond to drier conditions. This relationship between

leaf wax lipid δD and moisture availability is consistent with that observed over the 20th century and indicates that the same catchment-scale processes played a dominant role in driving δD variability during both periods. One of the most pronounced multidecadal droughts captured in the δD record occurs at turn of the 14th century. This drought is a prominent feature among paleohydrologic records from the Sierra Nevada (Meko *et al*., 2001, Yuan *et al*., 2003; Graumlich *et al*., 1993; Hughes & Graumlich, 1996), but may have been unique to the Sierra Nevada Mountains, occurring at a time when the majority of the West was transitioning to wetter conditions (Cook *et al*., 2004). The dramatic increase in δD at this time suggests that, although hydrologic conditions in the two regions are coupled (e.g. Cayan, 1996), the Sierra Nevada can experience prolonged reductions in winter precipitation and snowpack even in the absence of systemic drought throughout the West.

We observe 2 > 20 year periods of dry conditions during the late medieval while such periods are absent in the 20th century, suggesting that the Sierra Nevada, like much of the West (Cook *et al*., 2004; Meko *et al*., 2001; Herweijer *et al*., 2007; Woodhouse & Overpeck, 1998; Woodhouse *et al*., 2009), experienced droughts during the late medieval period of unprecedented persistence relative to those on historical record. The implications of the δD record for late medieval versus modern drought severity, however, is compounded by a >2σ shift towards higher isotopic values in the 20th century, the opposite direction expected based on relatively the wetter modern conditions (Cook *et al*., 2004). This shift highlights the disparity between the driving mechanism of multidecadal δD fluctuations (i.e. moisture availability) and those occurring over longer, centennial to mulitcentennial time periods. Although we rule out changes in the floral community of

the Swamp Lake catchment and the isotopic content of precipitation as influenced by the PDO and ENSO modes of climate variability as causing this shift, further constraint of its driving mechanisms requires a continuous record. A continuous record would also allow us to determine whether the pronounced increasing δD trend over the 20th century is unique to this time period, or if such centennial trends occur at other times over the last millennium.

Chapter 4:, in part, is being prepared for submission for publication Roach, L.D., Sessions, A.L., Cayan D.R., Charles, C.D., R. S Anderson. The dissertation author was the primary investigator and author of this material.

Table 4.1 Correlation of annually interpolated C24 δD with reconstructed PDSI records from the five most proximal grid squares in the NADA (Cook & Krusic 2004; NOAA National Climatic Data Center, 2008a) to the location of Swamp Lake

NADA grid square #	Center coordinates	r
46	40.0ºN, 120.0ºW	-0.31
47	37.5ºN, 117.5ºW	-0.36
48	35.0ºN, 117.5ºW	-0.37
59	37.5ºN, 120.0ºW	-0.39
60	35.0ºN, 120.0ºW	-0.47

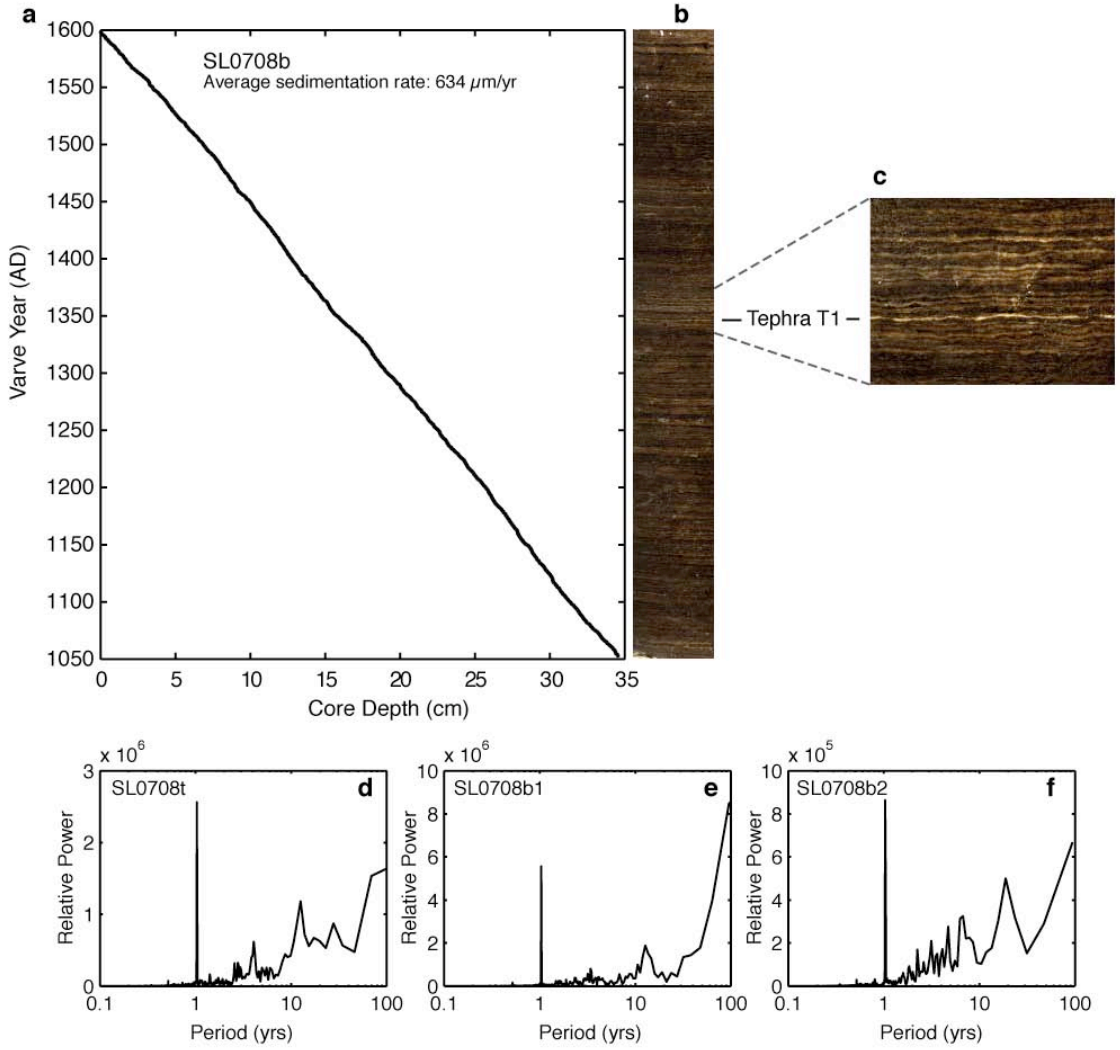


Figure 4.1 Age model of freeze core SL0708b (a) pictured in (b). A blown up image of the portion of the core containing Tephra T1 (see text for details) is shown in (c). Periodograms from cores SL0708t (d) and SL0708b (e-f) (image for SL0708b divided into sections 1 and 2 for ease of compuing) generated from the digital analysis techique use to assinging laminations (Appendix C) with peak at 1 year periodicity. Average sedimentation rate for SL0708b was derived as the averaged of sedimentation rates based on lamination assignments in SL0708b1 and SL0708b2.

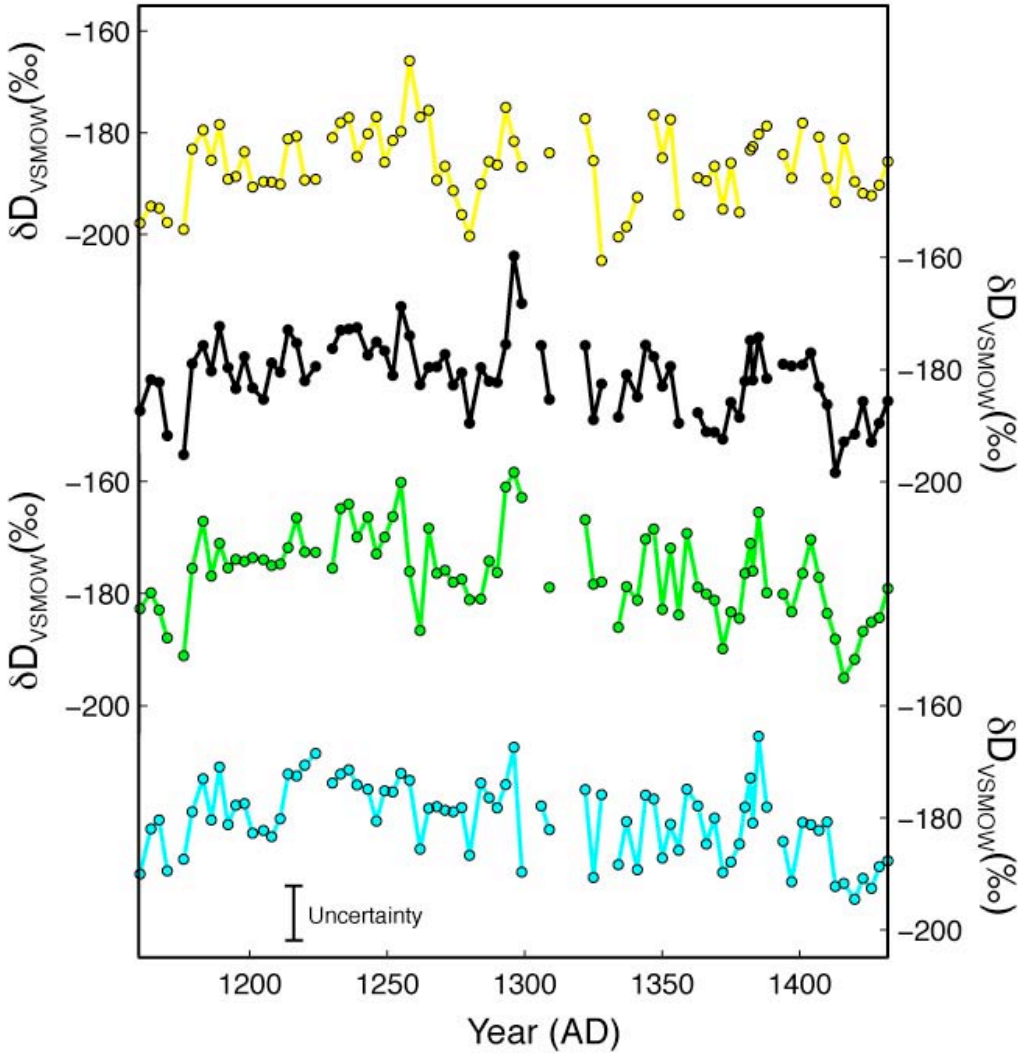


Figure 4.2 Measured δD for *n*-acids C22 (yellow), C24 (black), C26 (green) and C28 (blue).

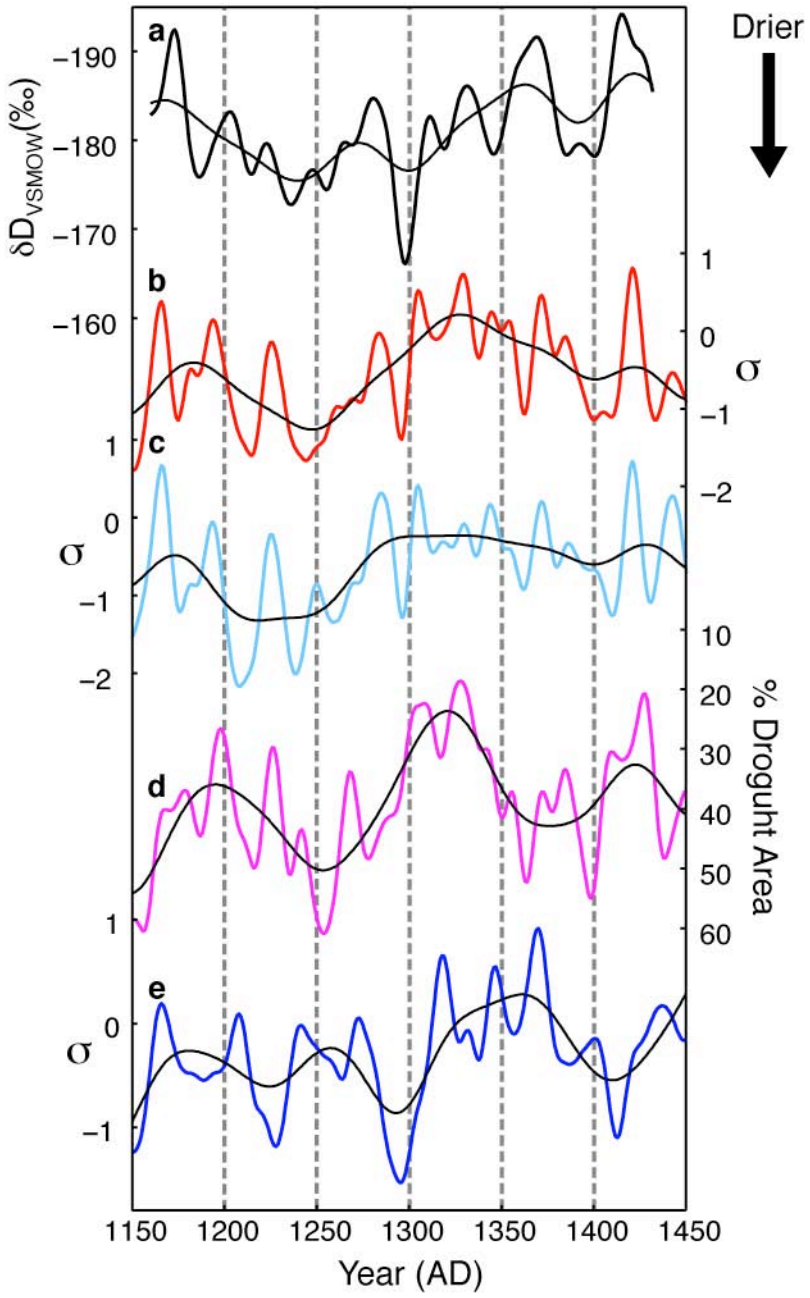


Figure 4.3 Comparison of multidecadal late medieval δD record (a) with reconstructed PDSI from NADA gs59 (b) and gs47 (c) (Cook *et al*., 2004, Cook & Krusic, 2004), the DAI (d) (Cook *et al*., 2004) and reconstructed PDO (e) (MacDonald & Case, 2005). All records have been passed through a low pass Gaussian filter to maximize >10 year periodicities. Vertical dashed lines correspond to the 9 high δD excursions.

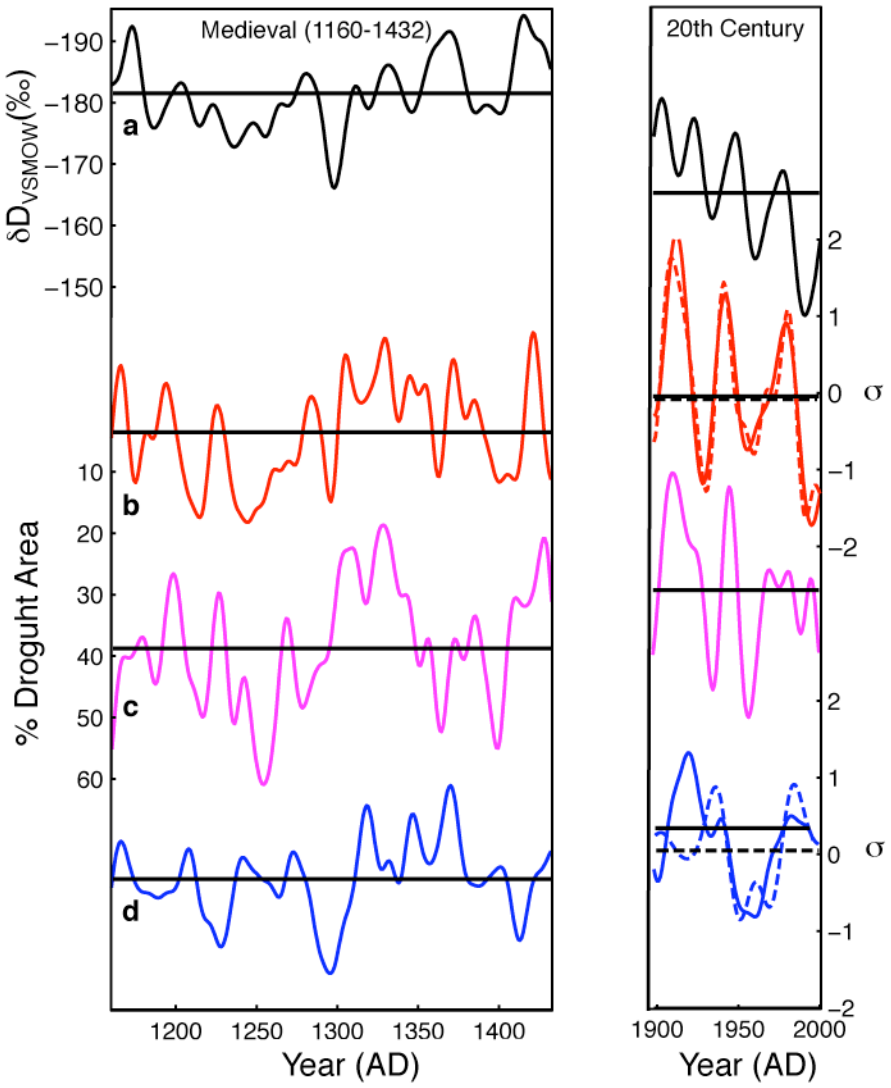


Figure 4.4 Comparison of late medieval and 20th century leaf wax lipid δD (a), gs59 PDSI (b) (Cook *et al*., 2004; Cook & Krusic, 2004), DAI (c) (Cook *et al*., 2004) and PDO (d) (MacDonald & Case, 2005). For PDSI and PDO solid lines denote reconstructed values and dashed lines denote instrumental values. Insturmental PDO from Mantua *et al*. (1997). Horizontal black lines depict long term averages of each record over the respecitve time periods, with dashed and solid denoting instrumental and reconstructed respectively where two records are present.

4.8 References

Barnett, T. P., Pierce, D. W., Hidalgo, H. G., Bonfils, C., Santer, B. D., *et al*. (2008) Human-induced changes in the hydrology of the western United States. *Science* 319:1080-1083.

Berkelhammer, M. B., Stott, L. D. (2008) Recent and dramatic changes in Pacific storm trajectories recorded in d18O from Bristlecone Pine tree ring celluslose. *Geochem Geophys Geosys* 9:doi:10.1029/2007GC001803.

Berkelhammer, M.B., Stott, L.D., and Yoshimura, K. (2009) Anomalous export of tropical water to western North America during the current decade. *Eos. Trans. AGU* 90(52), Fall Meet. Suppl., Abstract PP12C-05.

Berkelhammer, M. B., Stott, L. D., Yoshimura, K., Johnson, K., and Sinha, A., (submitted). Synoptic and mesoscale controls on the isotopic composition of precipitation in the southwestern United States.

California Climate Change Center (2006) Our Changing Climate Assessing Risks to California 16 pp. [Available online at meteora.ucsd.edu/cap/pdffiles/CA_climate_ Scenarios.pdf]

Cayan, D. R. (1996) Interannual climate variability and snowpack in the western United States. *J. Climate* 9:928-948,

Cayan, D.R., Dettinger, M.D., Diaz, H.F. and Graham, N.E. (1998) Decadal variability of precipitation over western North America. *J. Climate* 11:3148-3166.

Cayan, D.R., Kammerdiener, S.A, Dettinger, M.D., Caprio, J.M. and Peterson, D.H. (2001) Changes in the Onset of Spring in the Western United States. *Bull. Am. Met. Soc*. 82:399-415

Cobb, K.M., Charles, C.D., Cheng, H. and Edwards, R.L. (2003) El Niño/Southern Oscillation and tropical Pacific climate during the last millennium. *Nature* 407:271-276.

Cook, E.R. and Krusic, P.J. 2004. The North American Drought Atlas. Lamont-Doherty Earth Observatory and the National Science Foundation. http://iridl.ldeo.columbia.edu/SOURCES/.LDEO/.TRL/.NADA2004/.pdsi-atlas.html

Cook, E. R., Meko, D.M., Stahle, D.W. and Cleaveland, M.K. (1999) Drought reconstructions for the continental United States. *J. Climate* 12:1145-1162.

Cook, E. R., Woodhouse, C.A., Eakin, C.M., Meko, D.M., and Stahle, D.W. (2004a) Long-term aridity changes in the western United States. *Science* 306:1015-1018.

Cook, E.R. and coauthors (2004b) North American Summer PDSI Reconstructions. IGBP PAGES/World Data Center for Paleoclimatology, Data Contribution Series # 2004-045. NOAA/NGDC Paleoclimatology Program, Boulder CO, USA.

Cranwell, P.A. (1982) Lipids of aquatic sediments and sedimenting particulates. *Prog. Lipid Res.* 21:271-308.

Dettinger, M. D., and Cayan, D. R. (1994) Large-Scale Atmospheric Forcing of Recent Trends toward Early Snowmelt Runoff in California. *J Climate* 8:606-622.

Dillehay, T.D. (1974) Late Quaternary bison population changes in the southern plains. *Plains Anthropologist* 19:180-196.

Douglas, A.E. (1929) The secrets of the Southwest solved by talkative tree rings. *National Geographic* 54:737-770.

Feakins, S.J. and Sessions, A.L. (2010) Controls on the D/H ratios of plant leaf waxes in an arid ecosystem. *Geochim. Cosmochim. Acta* 74:2128-2141.

Ficken, K.J., Li, B., Swain, D.L. and Eglinton, G. (2000) An *n*-alkane proxy for the sedimentary input of submerged/floating freshwater aquatic macrophytes. *Org. Geochem* 31:745-749.

Graumlich L. J. (1993) A 1000-year record of temperature and precipitation in the Sierra Nevada. *Quat. Res.* 39:249-255.

Hayes, M. J., Drought Indices. National Drought Mitigation Center. www.drought.unl.edu/whatis/indices.htm#pdsi, 2006. Accessed June 1, 2006.

Herweijer, C., Cook, E.R., and Emile-Geay, J. (2007) North American droughts of the last millennium from a gridded network of tree-ring data. *J. Climate* 20:1353-1376.

Hou, J., D'Andrea, W.J., and Huang, Y. (2008) Can sedimentary leaf waxes record D/H ratios of continental precipitation? Field, model and experimental assessments. *Geochim. Cosmochim. Acta* 72:3503-3517.

Hou, J., D'Andrea, W.J., MacDonald, D. and Huang, Y. (2007) Hydrogen isotopic variability in leaf waxes among terrestrial and aquatic plants around Blood Pond, Masachusetts (USA). *Org. Geochem.* 38:977-984.

Howat, I. M., and S. Tulaczyk (2005), Climate sensitivity of spring snowpack in the Sierra Nevada, *J. Geophys. Res.*, *110*, F04021, doi:10.1029/2005JF000356

Huth A. K., Leydecker, A., Sickman, J. O., Bales, R. C. (2004) A two-component hydrograph separtion for three high-elevation catchments in the Sierra Nevada, California. *Hydro. Proc.* 18:1721-1733.

Howat, I.M., and Tulaczyk, S. (2005) Climate sensitivity of spring snowpack in the Sierra Nevada. *J Geophys Res*. 110:doi:10.1029/2005JF000356.

Hughes, M.K. and Graumlich, L.J. (1996) Multimillennial dendroclimatic studies from the western United States, in *Climatic Variations and Forcing Mechanisms of the Last 2000 Years* J. Jouzel ed. Springer-Verlag, New York. pp. 109-124.

Kattelmann, R., and Elder, K., (1991) Hydrologic characteristics and water balance of an alpine basin the Sierra Nevada. *Water Resources Res*. 27:1553-1562.

Li, H., Bischoff, J.L., Ku, T., Lund, S.P. and Stott, L.D. (2000) Climate variability in east-central California during the past 1000 years reflected by high-resolution geochemical and isotopic records from Owens Lake sediments. *Quat Res* 54:189-197.

Lundquist, J. D., Dettinger, M. D., and Cayan, D. R., (2005) Snow-fed Stream flow Timing at Different Basin Scales: Case Study of the Tuolumne River above Hetch Hetchy, Yosemite, California. *Water Resour. Res*. 41:W07005.

MacDonald, G.M. and Case, R.A. (2005) Variations in the Pacific Decadal Oscillation over the past millennium. *Geophys. Res. Lett*. 32:doi:10.1029/2005GL022478.

Mantua, N.J., Hare, S.R., Zhang, Y., Wallace, J.M., and Francis, R.C. (1997) A Pacific interdecadal climate oscillation with impacts on salmon productions. *Bull. Amer. Met. Soc*. 78:1069-1079.

Markham, C. G., (1970) Seasonality of Precipitation in the United States. *Ann. Assoc. Am. Geogr*. 60:593-597.

McCabe G. J., Palecki, M. A., and Betancourt, J. L. (2004) Pacific and Atlantic Ocean influences on multidecadal drought frequency in the United States. *Proc. Natl. Acad. Sci* 101:4136-4141.

McPhaden, M.J. and Zhang, D.X. (2002) Slowdown of the meridional overturning circulation of the upper Pacific Ocean. *Nature* 415:603-608.

Meko, D. M., Therrell, M. D., Baisan, C. H., and Hughes, M. K. (2001) Sacramento River flow reconstructed to A.D. 869 from tree rings. *J. Amer. Water Res. Assoc*. 37: 1029-1039.

Meyers, P. A. and R. Ishiwatari, 1993. Lacustrine organic geochemistry—An overview of indicators of organic matter sources and diagenesis in lake sediments. *Org. Geochem*. 20:867-900.

Millar, C. I., King, J.C., Westfall, R.D., Alden, H.A., and Delany, D.L. (2006) Late Holocene forest dynamics, volcanism, and climate change at Whitewing Mountain and San Joaquin Ridge, Mono County, Sierra Nevada, CA, USA. *Quat. Res*. 66:273-287.

Mote, P. W., Hamlet, A.F., Clark, M.P. and Lettenmaier, D.P. (2005) Declining mountain snowpack in western North America. *Bull. Am. Meteorol. Soc*. 86:39-49.

Overpeck, J., Udall, B. (2010) Dry Times Ahead. *Science* 328:1624-1643.

Palmer, W. C. (1965) Meteorological drought. Research Paper No. 45, US. Weather Bureau, p 58.

Regonda, S., Clark, M.P., Rajagopalan, B., and Pitlick, J. (2005): Seasonal cycle shifts in Hydroclimatology over the western United States. *J. Climate*, 18:372-384.

Roos, M., (1991) A Trend of Decreasing Snowmelt Runoff in Northern California. *Proc. 59th Western Snow Conference*, Juneau, AK, 29-36.

Sachse, D., Radke, J. and Gleixner, G. (2004) Hydrogen isotope ratios of recent lacustrine sedimentary *n*-alkanes record modern climate variability. *Geochim. Cosmochim. Acta* 68:4877-4889.

Sachse, D., Radke, J. and Gleixner, G. (2006) δD values of individual n-alkanes from terrestrial plants along a climatic gradient—Implications for the sedimentary biomarker record. *Org. Geochem*. 37:469-483.

Seager R. and coauthors (2007a) Model projections of an imminent transitions to a more arid climate in southwestern North America. *Science* 312:1181-1184.

Seager, R., Graham, N., Herwijer, C., Gordon, A.L., Kushnir, Y. and Cook, E. (2007b) Blueprints for Medieval hydroclimate. *Quat. Sci. Rev*. 26:2322-2336.

Seager, R., Burgman, R., Kushner, Y., Clement, A., Cook, E.R., Niak, N. and Miller, J. (2008) Tropical Pacific forcing of North American medieval megadroughts: Testing the concept with an atmospheric model forced by coral-reconstructed SSTs. *J. Climate* 21:6175-6190.

Seager, R. Kushnir, Y., Herweijer, C., Naik, N., and Velez, J. (2005) Modeling of tropical forcing of persistant droughts and pluvials over western North America: 1856-2000. *J. Climate* 18:4065-4088.

Sessions, A.L., Burgoyne, T.W., Schimmelmann, A., and Hayes, J.M. (1999). Fractionation of hydrogen isotopes in lipid biosynthesis. *Org. Geochem*. 30:1193-1200.

Sieh, K. and Bursik, M. (1986) Most recent eruption of the Mono Craters, eastern central California. *J. Geophys Res*. 91:12,539-12,571.

Smith, S.J. and Anderson, R.S. (1992) Late Wisconsin paleoecological record from Swamp Lake, Yosemite National Park, California. *Quat. Res*. 38:91-102.

Stahle, D.W., Fye, F.K., Cook, E.R. and Griffin, R.D. (2007) Tree-ring reconstructed megadroughts over North America since A.D. 1300. *Climatic Change* 83:133-149.

Stewart I.T., Cayan, D.R., and Dettinger, M.D. (2005) Changes toward earlier streamflow timing across Western North America. *J. Climate* 18:1136-1155.

Stine, S. (1994) Extreme and persistent drought in California and Patagonia during mediaeval time. *Nature* 369:546-549.

Wood, S. H., (1977) Distribution, correlation, and radiocarbon dating of late Holocene tephra, Mono and Inyo craters, eastern California. *Geol. Soc. Am. Bull.* 88:89-95.

Woodhouse, C.A. and Overpeck, J.T. (1998). 2000 years of drought variability in the central United States. *Bull. Am. Meteorol. Soc.* 79:2693-2714.

Woodhouse, C.A., Russell, J.L. and Cook, E.R. (2009) Two modes of North American drought from instrumental and paleoclimate data. *J. Climate* 22:4336-4347.

Yuan, F. Linsley, B.K., Lund, S.P., and McGeehin, J.P. (2003) A 1200 year record of hydrologic variability in the Sierra Nevada from sediments in Walker Lake, Nevada. *Geochem. Geophys. Geosys.* 5:doi:10.1029/2003GC000652

Zhang, Y., Wallace, J.M. and Battisti, D.S. (1997) ENSO-like interdecadal variability: 1900-93. *J. Climate* 10:1004-1020

Appendix A. Benthic Foraminiferal Faunal Reference List

for:

Chapter 1. Radiocarbon as a tracer for decadal scale sub-thermocline variability along the Southern California margin

and

Chapter 2. Benthic foraminiferal community distribution in the bathyal Santa Barbara Basin since 1744 A.D.

Bolivina advena Cushman

Bolivina argentea Cushman

Bolivina seminuda Cushman

Buliminella tenuata Cushman

Cassidulinoides cornuta (Cushman) = *Fursenkoina cornuta* (Cushman) = *Virgulina cornuta* Cushman

Chilostomella ovoidea Reuss

Loxostomum pseudobeyrichi (Cushman) = *Bolivina pseudobeyrichi* (Cushman)

Nonionella sp. cf. *N. globosa* Ishiwada

Nonionella stella Cushman and Moyer

Suggrunda eckisi Natlan

Appendix B. Swamp Lake Core Descriptions and Metadata

for:

Chapter 3. High-resolution measurements of sedimentary leaf wax lipid hydrogen isotope ratios capture interannual to decadal scale variability in wintertime precipitation and snowmelt in the Sierra Nevada Mountains

and

Chapter 4. Hydroclimate of the Sierra Nevada Mountains during the late medieval period (1160-1432 A.D.) as captured by sedimentary leaf wax lipid hydrogen isotope ratios.

A total of 8 freeze cores and 6 Bolivia cores were collected from Swamp Lake between over two coring expeditions in October 2006 and September 2007. Because of their brittle nature, the freeze cores, essentially frozen slabs of sediment, almost always broke orthogonal to the down core during initial processing. This breaking resulted in two separate cores, labeled with "T" of "B" to denote the top or bottom piece. Often slabs were purposefully broken in a ~25 cm long massive section captured in all cores to avoid breaking within laminated sections. Once separated, these pieces were treated as separate cores, and hence retained their unique Core ID. Table B1 lists the Core IDs, core type, date collected, water depth and length of the full suite of Swamp Lake sediment cores collected as part of this dissertation. High resolution images of all freeze core surfaces

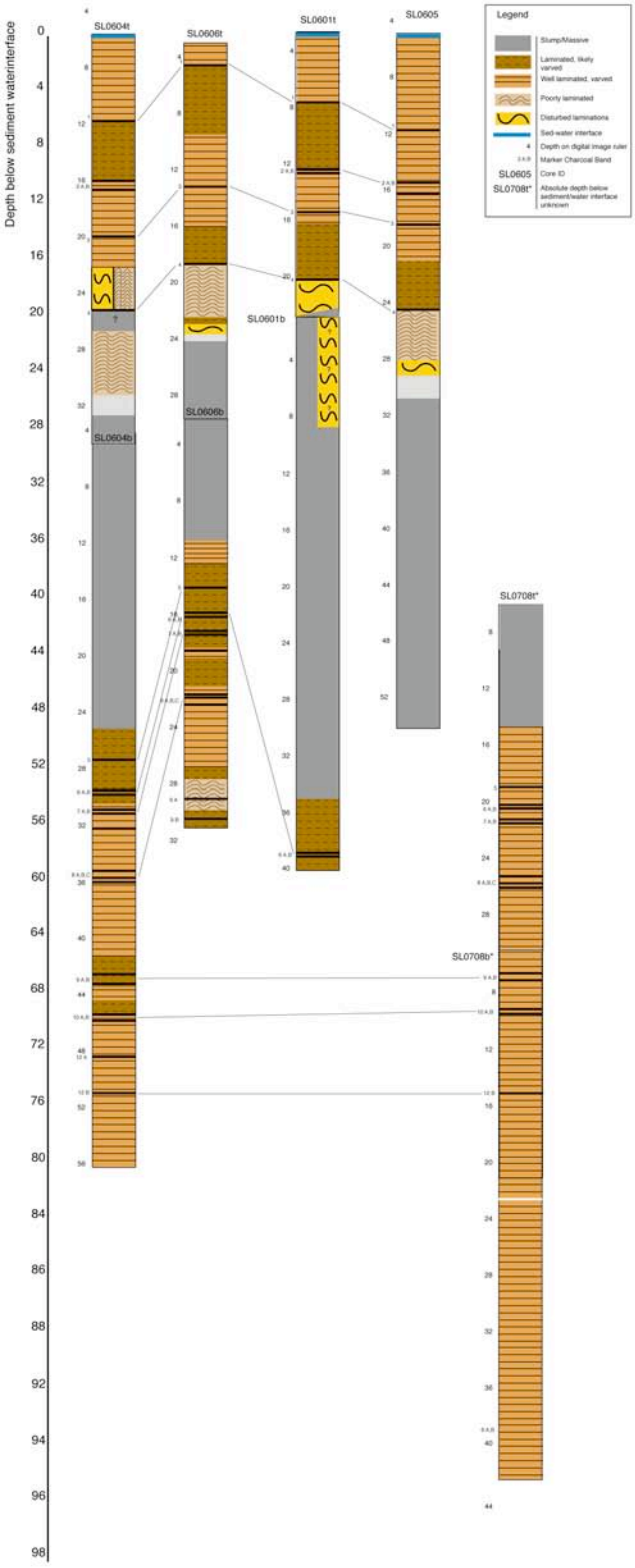
were carried out at the Limnological Research Center (LRC) at the University of Minnesota, Minneapolis using a Geotek GeoScan-III digital linescan camera at 200 pixels/cm (~500 dpi). Lithological core descriptions were based on examination of these images for freeze cores (Figure B1).

Also at the LRC, Bolivia Cores were logged with GeoTek multi-sensor core logger and split into a working and archive group. The exposed surface of working group halves was cleaned and imaged on a DMT CoreScan digital linescan camera at 100 pixels/cm (~254 dpi). ~7-10 Smear slides were created per cores to examine microscopic sediment composition at routine depth horizons as well at interesting features such as anomalously light bands. For example, using smear slides I confirmed the presence of the three tephra layers T1-T3 by observing silica shards with elongated trapped air bubbles. Lithological core descriptions were made based on examination of images, exposed core surfaces, and contents of smear slides (Figure B2).

Table B1 Locations and information of Swamp Lake sediment Freeze and Bolivia cores

Core ID[a]	Type	Date Collected	Depth (m)	Length (cm)
SL0601T	Freeze	October 6, 2006	19	22.0
SL0601B	Freeze	October 6, 2006	19	37.0
SL0602T	Freeze	October 6, 2006	19	11.5
SL0602B	Freeze	October 6, 2006	19	42.5
SL0604T	Freeze	October 6, 2006	20	33.5
SL0604B	Freeze	October 6, 2006	20	49.5
SL0605	Freeze	October 6, 2006	19	54.0
SL0606T	Freeze	October 6, 2006	19	56.5
SL0606B	Freeze	October 6, 2006	19	10.0
SL0701	Bolivia	September 23, 2007	19	139.0
SL0702	Bolivia	September 23, 2007	19	149.0
SL0703	Bolivia	September 23, 2007	19	149.0
SL0704	Bolivia	September 23, 2007	12	123.0
SL0705	Bolivia	September 23, 2007	18	nm
SL0706	Bolivia	September 23, 2007	19	147.5
SL0707	Freeze	September 24, 2007	18	nm
SL0708T	Freeze	September 24, 2007	18	26.5
SL0708B	Freeze	September 24, 2007	18	36.7

Figure B1 Lithological core descriptions of freeze cores SL0601(T and B), SL0604(T and B), SL0606(T and B), SL0605 and SL0708(T and B). The absolute depth below the sediment water interface of SL0708 and SL0606T are not known as the sediment water interface was not captured for these cores. Marker layers, typically charcoal, used for cross correlation are indicated


Depth below sediment waterinterface
SL0604t
SL0606t
SL0601t
SL0605
SL0601b
SL0606b
SL0604b
SL0708t*
SL0708b*
Legend
Stump/Massive
Laminated, likely varved
Well laminated, varved
Poorly laminated
Disturbed laminations
Sed-water interface
Depth on digital image ruler
Marker Charcoal Band
SL0605 Core ID
SL0708t* Absolute depth below sediment/water interface unknown

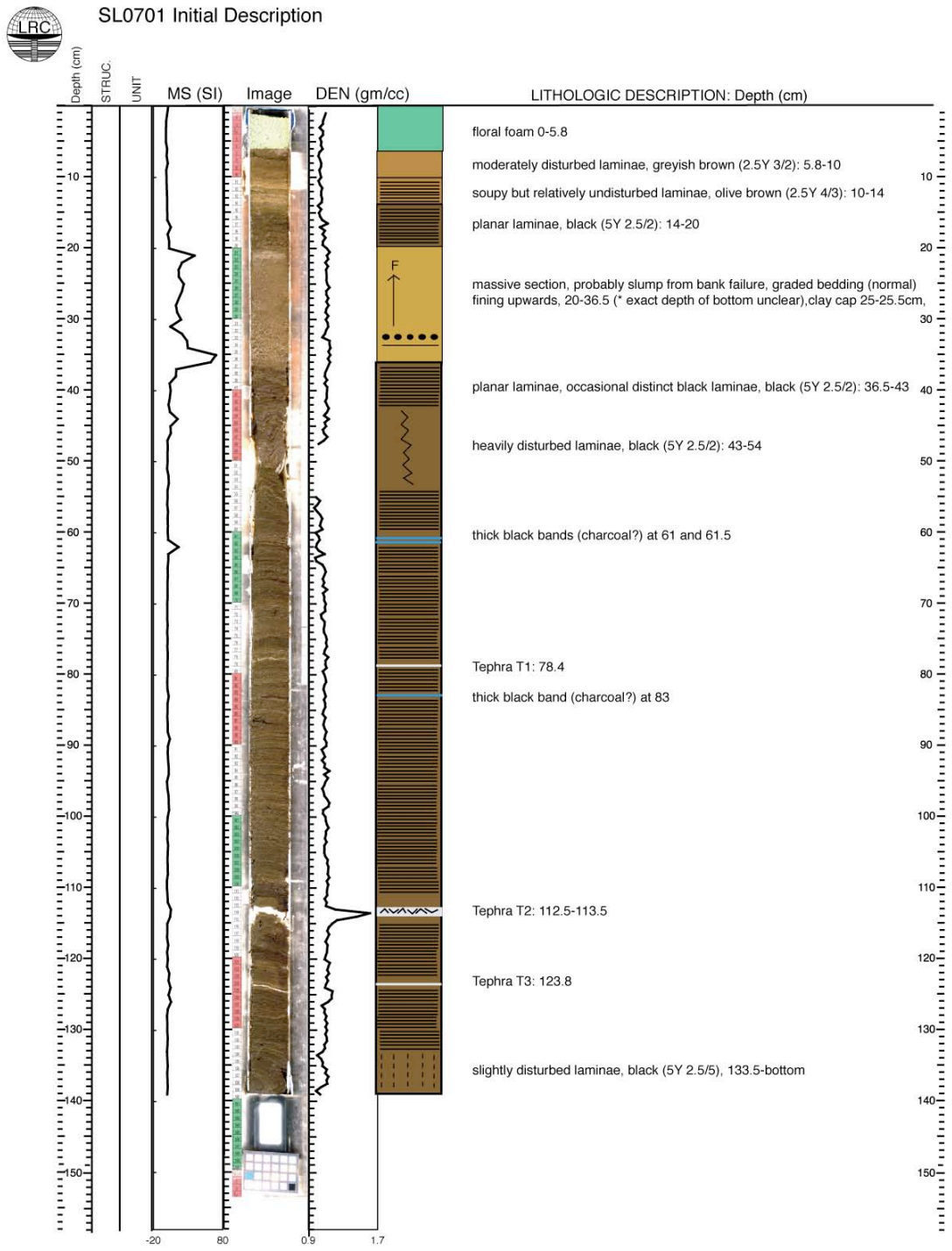


Figure B2 Digital images and initial core descriptions of Bolivia cores SL0701 (a), SL0702 (b), SL0703 (c), SL0704 (d) and SL0706 (e). Core SL0705 was not processed.

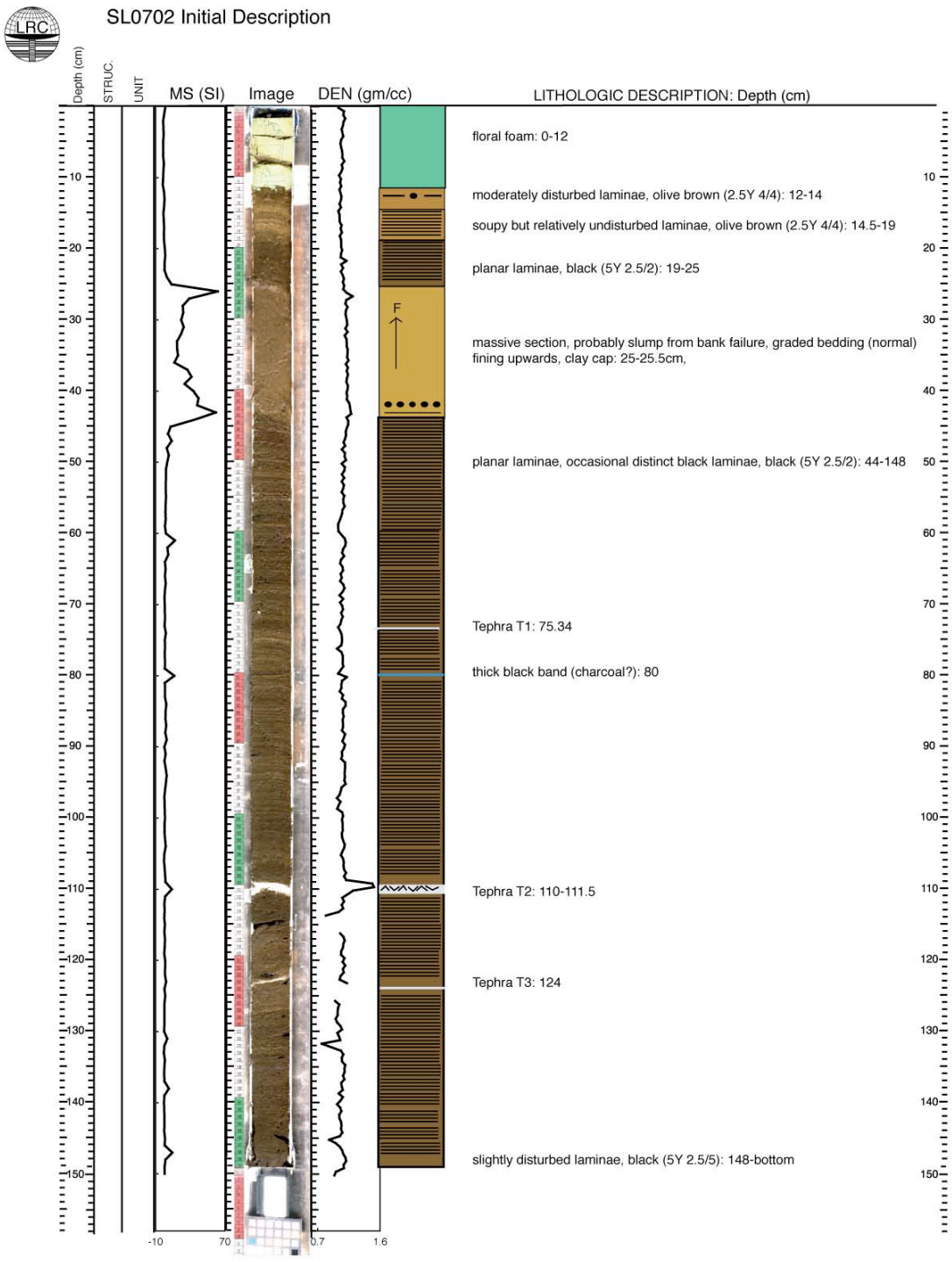


Figure B2 Boliva core initial digital images and initial description, Continued

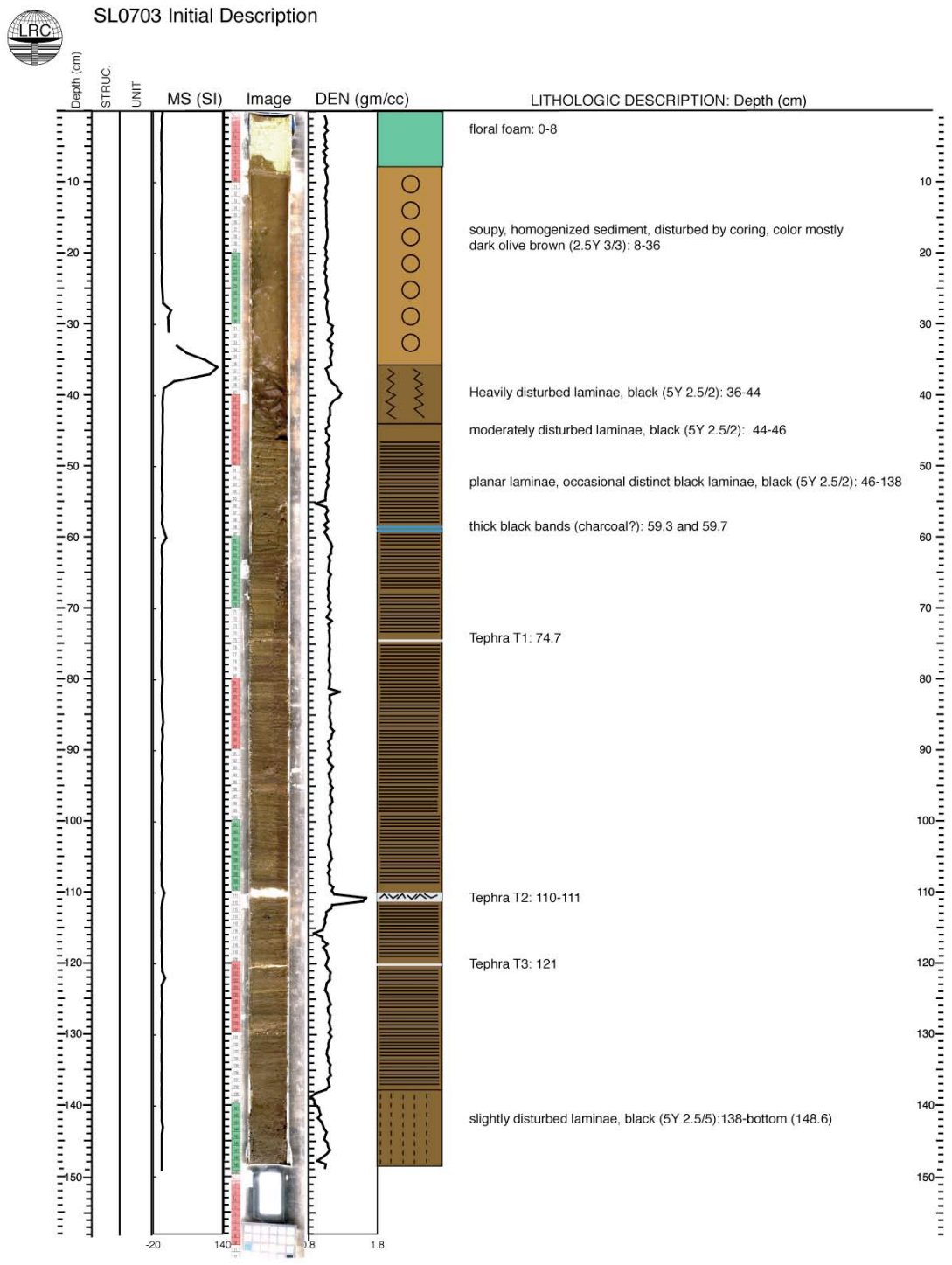


Figure B2 Boliva core initial digital images and initial description, Continued

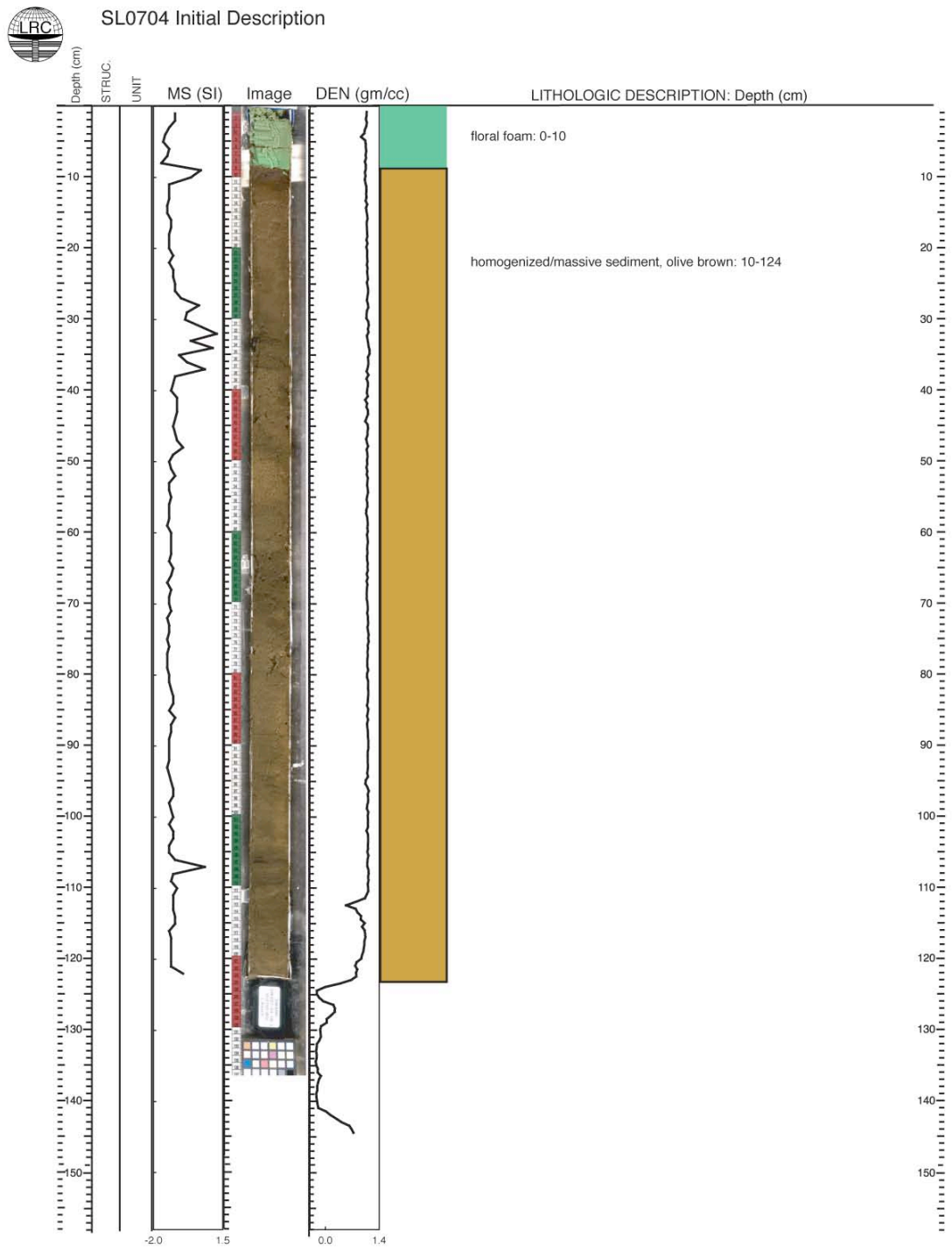


Figure B2 Boliva core initial digital images and initial description, Continued

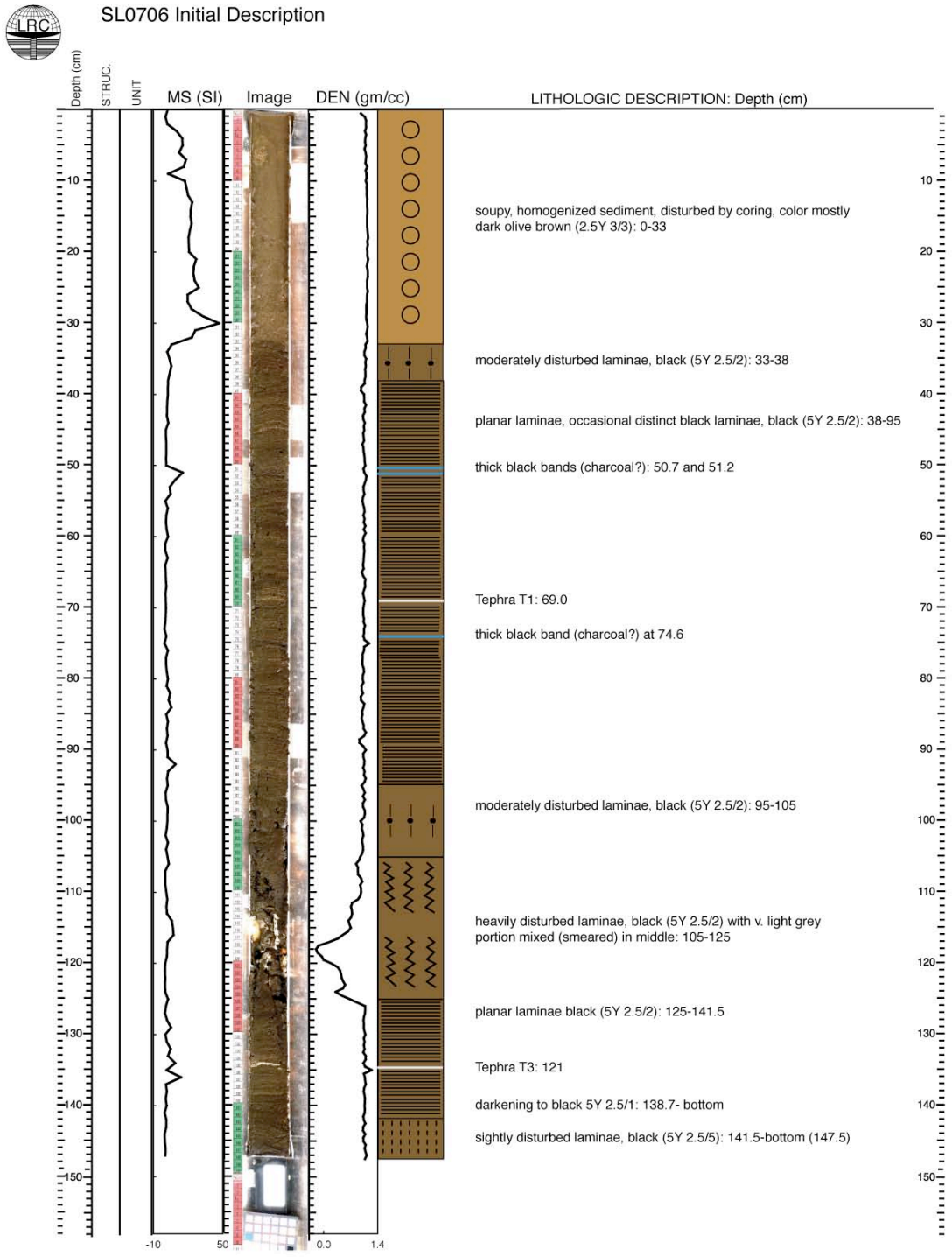


Figure B2 Boliva core initial digital images and initial description, Continued

Appendix C. The Varve Selection Program: A Computerized Technique for Identifying Sub-millimeter Varves in Digital Images of Swamp Lake Freeze Cores

as referred to in :

Chapter 3. High-resolution measurements of sedimentary leaf wax lipid hydrogen isotope ratios capture interannual to decadal scale variability in wintertime precipitation and snowmelt in the Sierra Nevada Mountains

and

Chapter 4. Hydroclimate of the Sierra Nevada Mountains during the late medieval period (1160-1432 A.D.) as captured by sedimentary leaf wax lipid hydrogen isotope ratios.

The presence of annual laminations in the upper 100 cm of Swamp Lake was confirmed through microscopic inspection of thin sections and counting of layers following a distinct charcoal band deposited in 1996 during the massive Ackerson Fire in Yosemite National Park (Von Wagdendonk, personal communication). However, in freeze core SL0708, upon which the isotopic measurements presented in Chapter 4 were preformed, the combined thickness of the light-dark couplets that comprise each annual lamination (varve) is submillimeter (~600 μm on average), making varves difficult to count accurately with the human eye, even on the high resolution (200 pixels/cm, ~500 dpi) digital images preformed at the Limnological Research Center (LRC). I therefore

developed a computerized method, the varve selection program, which identifies the transitions between light and dark varve couplets in high resolution (≥ 200 pixels/cm) digital images. This method consists of a series of 4 MATLAB scripts. The first script, rgb2lab, imports digital images into MATLAB, converts pixilated color and lightness information to the appropriate color scheme, and creates down core lightness and color curves, the second, v_spline, smoothes lightness curves with a cubic spline and finds inflection points, or light dark transitions, of smoothed lightness curve, the third, v_thick, enumerates the number of varves, and therefore years, identified in the smoothed curve, and measures the thickness of those varves and the fourth, v_chron, carries out temporal spectral analysis of down core lightness or color curves. Inherent to this program is the identification of inflections points as transitions between light and dark couplets of a varve. Existing software packages employ this method to distinguish annual banding in tree rings (e.g. DendroScan) and corals (e.g. CoralXDS). Attempts to apply these programs to Swamp Lake freeze core images indicated that the nature of Swamp Lake varve morphology necessitated a customized approach. Below I describe the varve selection program, using analysis of freeze core SL0708b as an example.

Prior to image analysis with the varve selection program, the levels of images may need to be adjusted in order to enhance the light-dark contrast (this can be easily achieved using image software such as Adobe Photoshop or The National Institutes of Health's ImageJ). Levels adjustment in the RGB color scheme used in these programs, involves removing the darkest color information and redistributing the remaining information over the 0 to 255 RGB grey scale (please refer to Nederbragt *et al*., 2004a for more detail on the subject of levels adjustment). However, when dealing multiple images

from the same, originally unbroken, freeze core such as those of SL0708t and SL0708b, levels must be redistributed over the same range. Also prior to image analysis, freeze core images are oriented horizontally, such that up (shallower core depths) faces to the left, and cropped such that the entire image captures the core surface without any surroundings, steps that also can be easily carried out in the image software listed above.

Following levels adjustment and image orientation and cropping, the first step in digital image analysis with the varve selection program is to import a digital image into MATLAB. Large images such may need to be divided into two smaller, overlapping images for computing ease. MATLAB recognizes the image as a unit8 unsigned integer data file, which can be converted to a double-precision array. Following the orientation, the double-precision array will have dimensions [m n p] where m equals the core width in pixels, n equals the core length in pixels and p equals 3. The 3 m x n matrices contain color information for the R, G, and B channels. In the rgb2lab script, these numerical RGB color space values are linearly translated into the Commission Internationale de l'Éclairage (CIE) L*a*b (henceforth Lab) color space following the steps outlined by Nederbradgt *et al*. (2004a). The L channel contains light/dark information, the a channel contains red/green information and the b channel contains blue/yellow information. The Lab color scheme is used in the varve selection program over RGB because the L channel more closely resembles the human eye's perception of lightness than grey scale RGB or CMYK and it is thus better suited for image analysis of sedimentary surfaces (Nederbradgt *et al*., 2004b).

Following conversion to Lab, the L, a and b values within a 40-60 pixel-wide swath parallel to the longitudinal core axis, typically of length n pixels (although shorter

subsections of core can be used) (Figure C1), are averaged to create down core lightness, red/green and blue/yellow curves. Because we are interested in identifying varves, we will focus on the lightness curve. Lightness extremes in the Lab color scheme range from 0 (black) and 100 (white), although in SL0708b fluctuate across a smaller range (Figure C2). The 40-60 pixel-wide swath is selected based on inspection of digital images to avoid anomalous features or imperfections. Averaging over 40-60 pixels was found to minimize noise while avoiding any canceling of lightness or darkness information caused by laminations that are not perfectly orthogonal to the down core axis. Care must be taken to ensure that the first and last pixels in the lightness curve correspond to those at the start and end of the core, or section of core, chosen for analysis. Knowledge of the annual sediment cycle is also necessary. In Swamp Lake, the transition between light and dark couplets occurs in the late fall, when precipitation and runoff begin to wash allochthonous matter into the lake, and the transition from dark to light occurs in the late spring when this runoff ceases and autochthonous material, primarily diatom frustules, rain down from the euphotic zone. I therefore select the first pixel at the top of the first light couplet, and the last pixel at the bottom of the last dark couplet, such that the record starts and ends in the fall, and years roughly correspond to water years (October-September).

The next steps, carried out in the v_spline script, involve smoothing the lightness curve with a cubic spine and taking the second derivative of that spline (Figure C3a). In the lightness curve (e.g. Figure C2), x values are monotonically increasing pixel numbers and y values are lightness values. MATLAB will find the pixels at which the second derivative equals zero. The resulting output is a 1 x u matrix, known as the zeros matrix,

where each data point marks the pixel at which an inflection point in the lightness curve occurs (Figure C3b). Since I purposefully started the lightness curve at the top of a light couplet, every data point in the zeros matrix with an odd numbered index (i.e. 1, 3, 5…u-1.) corresponds to the beginning of a light couplet. The pixels associated with these odd numbered zeros therefore mark the beginning of each water year, and the number of varve years in the section of core analyzed is equivalent to u/2. However, the number of inflection points, and thus varves identified, is highly sensitive to the extent of smoothing, a notable limitation of the varve selection program. Selection of the smoothing factor must therefore be carried out empirically by comparing the smoothed lightness curves with sections of core containing easily identifiable varves, such as those pictured in figure C3c. Over smoothing will cause the program to miss true transitions between light and dark couplets, while under smoothing will cause the program to assign transitions within individual light or dark couplets where true transitions do not actually exist. Once a smoothing factor is selected and the cubic spline generated, locating the inflection points simply requires finding the zeros of the second derivative of the spline, which can be preformed in a single line of code in MATLAB. Each zero represents the down core pixel number at which a transition between light and dark occurs, such that there are two zeros per varve.

Using the v_thick script, conversion from pixel to depth is a simple matter of dividing pixel number by the image resolution (200 pixels/cm). Although this conversion facilitates the measurement of varve thickness, the fidelity of varve assignment in this method has not been tested rigorously enough to confirm its use for accurate varve thickness measurement. Instead, year assignments are used to investigate temporal

periodicities of the lightness curve, which in turn can confirm the presence of annual laminations and generate an estimate of sedimentation rate. In order to convert the lightness curve to frequency space, the number of data points, or pixels between each year must be the same. Since in reality this number varies considerably—it ranges from 2 to 11 in SL0708b--lightness values between each year must be interpolated such that the number of pixels in every year is equivalent to the highest number of pixels (max N) actually measured for a given year. This interpolation can be carried out with a for loop in MATLAB. With an even sampling scale in place, periodograms are created using Fast Fourier Transform with segmented Hanning windows. The x values are years, with the interval between years equivalent to 1/max N and y values are unsmoothed and interpolated lightness values. If the method has identified true light dark couplets, the resulting periodograms should contain a sharp peak at periodicities of 1 year as seen in figure C4a-b. It should be noted that the assignment of years to individual pixels will result in a 1-year peak even in the smoothed lightness curve of unlaminated (massive) sediment and that generated with randomly assigned values, as evident in the periodograms in figure C4c and C4d respectively. The lightness curve analyzed for figure C4c was generated from 50-pixel wide section of the image for freeze core SL0601b, which captures the sediment slump that most likely occurred during the 1872 Owens Valley earthquake (see Chapter 4). However, the 1-year peak in figure C4a-b clearly dominants over the relatively subtle 1-year peaks in figures C4c and C4d. In particular, the peak from varved sediment (Figure C4a-b) has greater magnitude that the lower-frequency peaks, which is not the case for the peak from massive sediment (Figure C4c).

The creation of the SL0708b age model in Figure 4.1 was in part generated using the varve selection program. SL0708b contains a tephra layer, labeled as Tephra T1, that is a close geochemical match the tephra generated by the eruption of the Mono Craters documented at Tephra I by Wood (1977) (Wan, personal communication). This tephra was later dated to have occurred within months to a few years before a subsequent eruption of the Inyo Craters and no later than 1368 A.D. (Sieh and Bursik, 1986). Finally, Millar *et al*. (2006) use dendrochronology to constrain the timing of this Inyo eruption at 1350 A.D. I therefore assign an absolute age of 1350 A.D. to Tephra T1 and use the varve selection program to estimate a sedimentation rate that I then apply above and below this absolute age to generate an age model for SL0708b. RGB grey level values 0-135 were redistributed over the 0-255 scale. Because of its size, the digital image for SL0708b was divided into two subimages, SL0708b1 and SL0708b2 to ease computing. In both subimages L values were averaged over a 50 pixel-wide band (Figure C1). Two bands adjoining bands were used for SL0708b1 and two for SL0708b2 to avoid imperfections in the freeze core surface that would distort the lightness curve. A smoothing factor of 0.068 was found to generate the largest peak at 1 year periodicities and provided the most accurate varve assignments when compared to a section of clearly defined varves (Figure C3c). The image for SL0708t was also analyzed, and a smoothing factor of 0.05 generated the largest 1-year peak in the periodogram (Figure C4a).

The average sedimentation rates for SL0708t, SL0708b1 and SL0708b2 (611 μm/yr, 646 μm/yr and 634 μm/yr respectively) were calculated by dividing the number of years identified by the depth covered in each core or core subimage in the case of SL0708b. The overall average sedimentation rate of 630 μm/yr was calculated as the

mean of these three rates. To check that varve selection program did not dramatically over or under assign varves, this sedimentation rate was applied down core from the bottom of the 1872 Owens Valley earthquake slump. Following this exercise, the date of Tephra T1 was found to be 1344 A.D., just 6 years before its assigned date of 1350A.D. Having independently arrived close to the correct age of Tephra T1 using the sedimentation rate derived from the varve selection program, I used this rate to extrapolate ages above and below the depth of Tephra T1, thereby creating the SL0708b age model in figure 5.1.

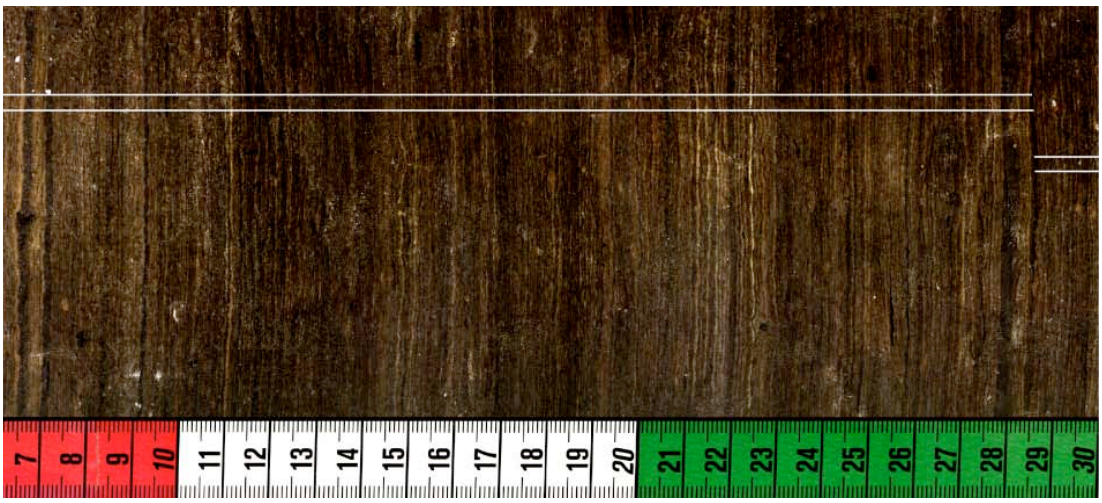


Figure C1 Digital image SL0708b1 (the upper subimage from the image for freeze core SL0708b). The two 50-pixel wide swaths from which the lightness curve was generated are marked by the parallel white lines.

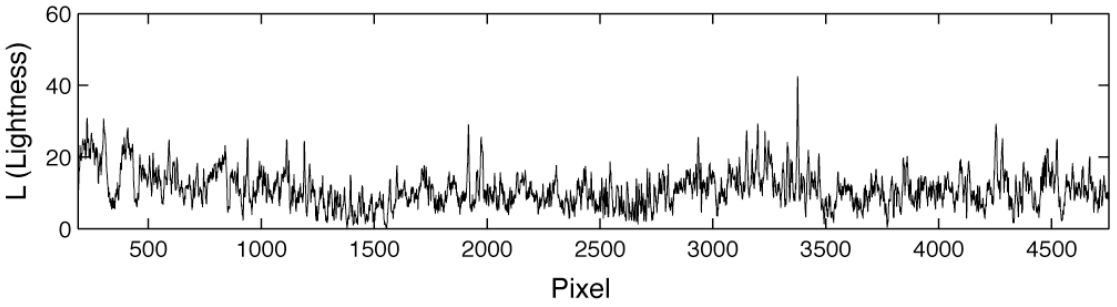


Figure C2 Lightness curve for image SL0708b1 created in the rgb2lab script.

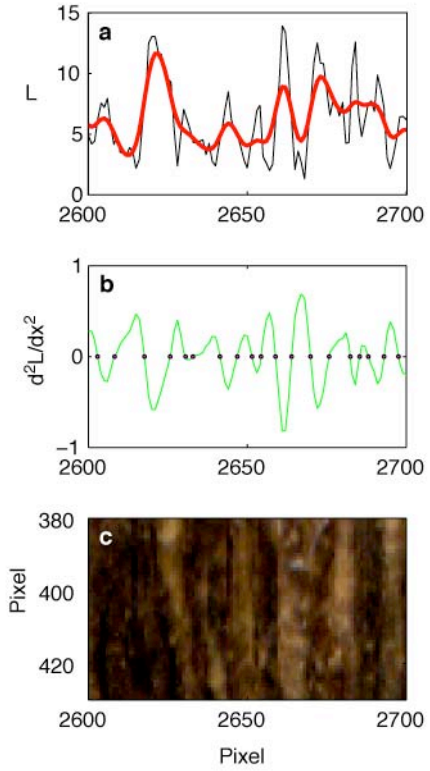


Figure C3 Identification of lightness curve inflections points using the v_spline script. (a) Raw lightness curve (black line) and smoothed curve (red line). (b) Second derivative of smoothed lightness curve (d2L/dx2, where x corresponds to pixel number) (green line)

with zeros marked with black dots. (c) Corresponding SL0708b1 image.

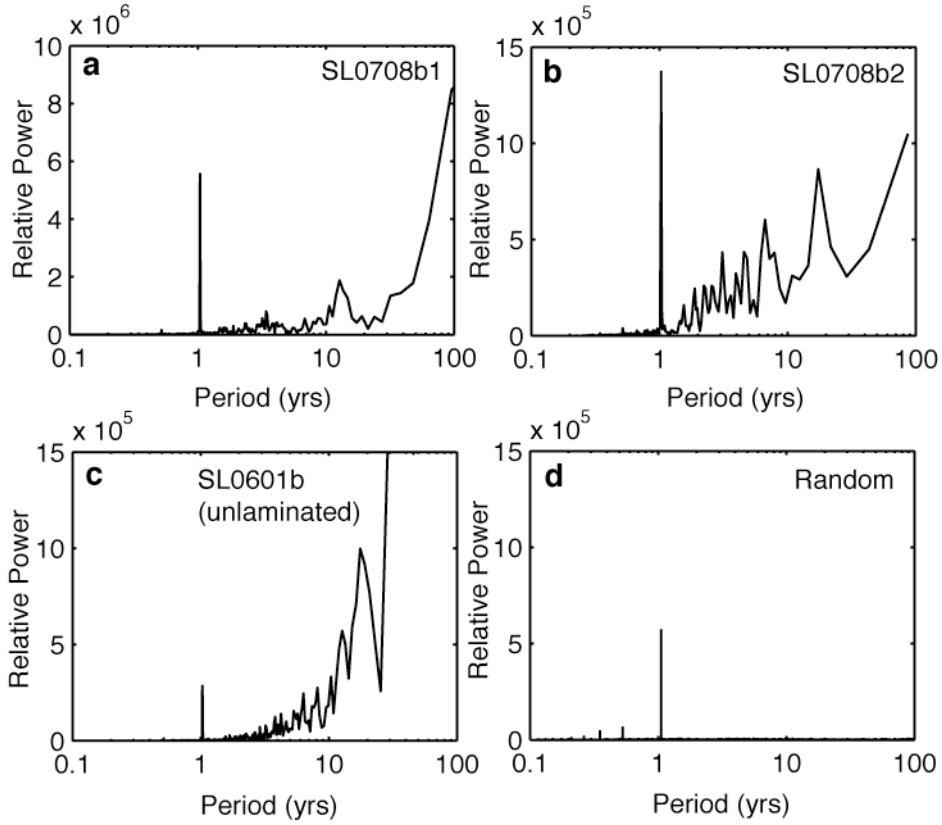


Figure C4 Periodograms for freeze core images SL0708b1 (a) and SL0708b1 (b), SL0601b (unlaminated sediment from the Owens Valley earthquake slump) (c) and randomly assigned lightness values (d) created using the v_chron script. Note the different y-axis in (a).

References for Appendix C

Millar, C. I., King, J.C., Westfall, R.D., Alden, H.A., and Delany, D.L. (2006) Late Holocene forest dynamics, volcanism, and climate change at Whitewing Mountain and San Joaquin Ridge, Mono County, Sierra Nevada, CA, USA. *Quat. Res*. 66:273-287.

Nederbragt, A.J., Francus, P., Bollmann, J., and Soreghan, M.J. (2004a) Image calibration, filtering and processing, In: Francus, P. (ed.) *Image Analysis, Sediments and Paleoenvironments*. Kluwer Academic Publishers, Dordrecht, Norwell, MA. 35-58 pp.

Nederbragt, A.J. and Thurow, J.W. (2004b) Digital sediment colour analysis as a method to obtain high resolution climate proxy records, In: Francus, P. (ed.) *Image Analysis, Sediments and Paleoenvironments*. Kluwer Academic Publishers, Dordrecht, Norwell, MA. 105-124 pp.

Sieh, K. and Bursik, M. (1986) Most recent eruption of the Mono Craters, eastern central California. *J. Geophys. Res*. 91:12,539-12,571.

Wood, S. H., (1977) Distribution, correlation, and radiocarbon dating of late Holocene tephra, Mono and Inyo craters, eastern California. *Geol. Soc. Am. Bull*. 88:89-95

Appendix D. Supplementary Text and Figures

for:

Chapter 4. Hydroclimate of the Sierra Nevada Mountains during the late medieval period (1160-1432 A.D.) as captured by sedimentary leaf wax lipid hydrogen isotope ratios.

The location and number of tree ring chronologies from grids squares 36, 47, 48, 59, and 60 of the North American Drought Atlas (NADA) PDSI reconstructions (Cook *et al*., 2004; Cook & Krusic 2004) are discussed in Chapter 4. Figures D1 and D2 respectively depict the location and number of individual chronologies used for each of these grid squares during the late medieval period (1160-1432 A.D.)

Chapter 4 also discusses the correlation of the Drought Area Index (DAI, Cook *et al*., 2004), which quantifies on an annual basis the percentage of NADA grid squares in the West that have a reconstructed PDSI value ≤ -1, to the gridded PDSI reconstructions of the NADA. Figure D3 depicts the spatial pattern of this correlation during the late medieval as well as over the entire record (800-2000 A.D.)

When examining the possible causes for the +17‰ increase in the average δD over the 20th century relative to that over the late medieval period, we consider changes in the relative contribution of terrestrial versus aquatic plants to the sedimentary *n*-acid pool. To further investigate this possibility, we compare sedimentary *n*-acid distributions from the two time periods. Figure D4 depicts this distribution for the late medieval period, and is analogous to Figure 3.7.

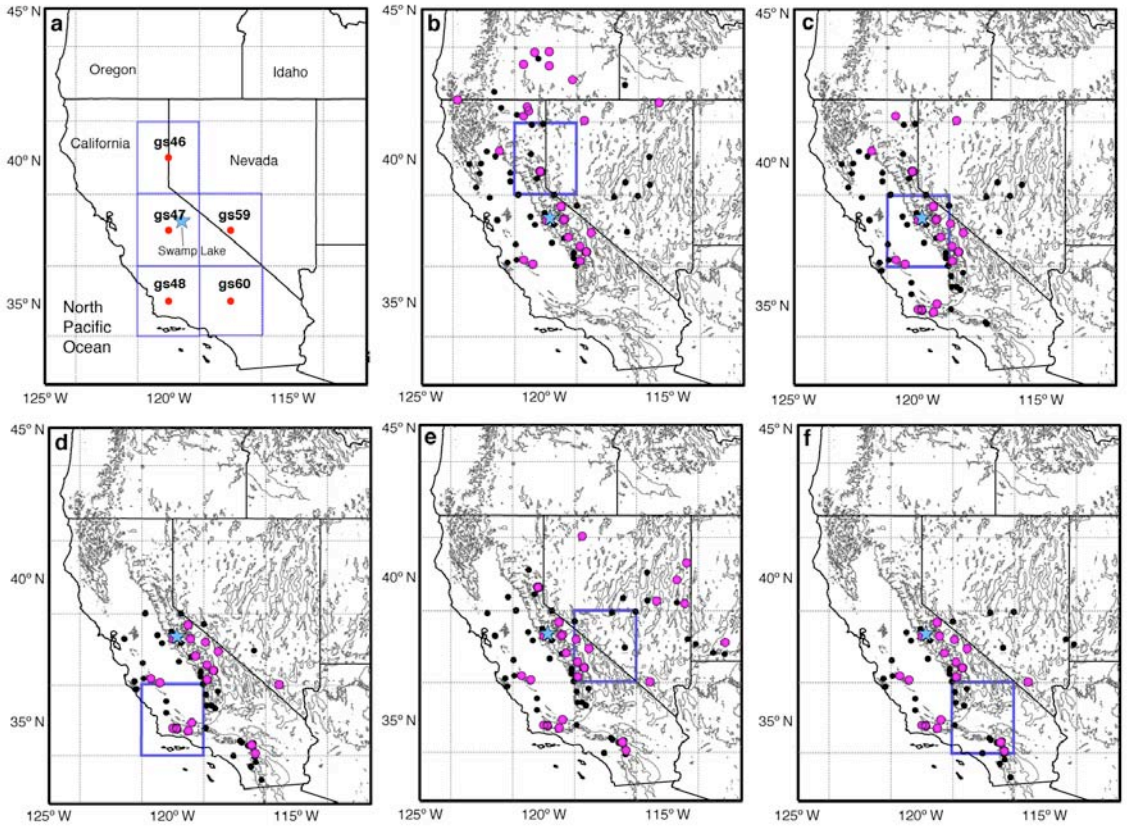


Figure D1 Location and perimeter of grid squares 46, 47, 47, 59 and 60 (a) and location of individual tree ring chronologies for used in PDSI reconstructions from grid squares 46 (b), 47 (c), 48 (d), 59 (e) and 60 (f) that begin before 1450 A.D (pick circles). Black circles represent chronologies that begin after 1450 A.D. Blue stars denote the location of Swamp Lake, and dashed lines outline the perimeters of NADA grid squares, with the thick blue line outlining the grid square for which chronologies are plotted. Contours at 1000 m intervals. Locations and start dates of individual chronologies provided by Cook (personal communication).

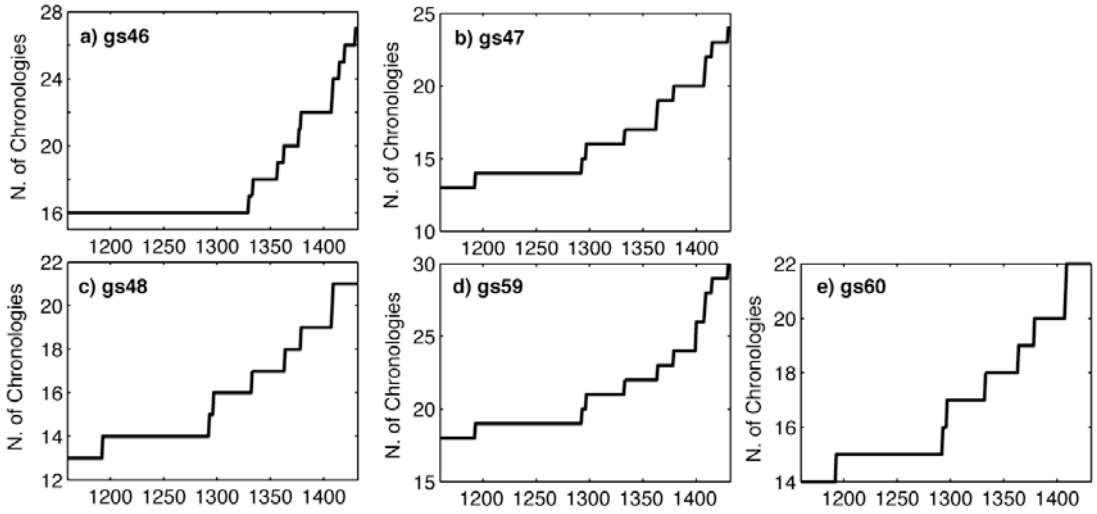


Figure D2. Number of individual tree ring chronologies incorporated into the NADA PDSI reconstructions (Cook *et al*., 2004; Cook & Krusic, 2004) for grid squares 46 (a), 47 (b), 48 (c), 59 (d) and 60 (e) between 1150 and 1450 A.D.

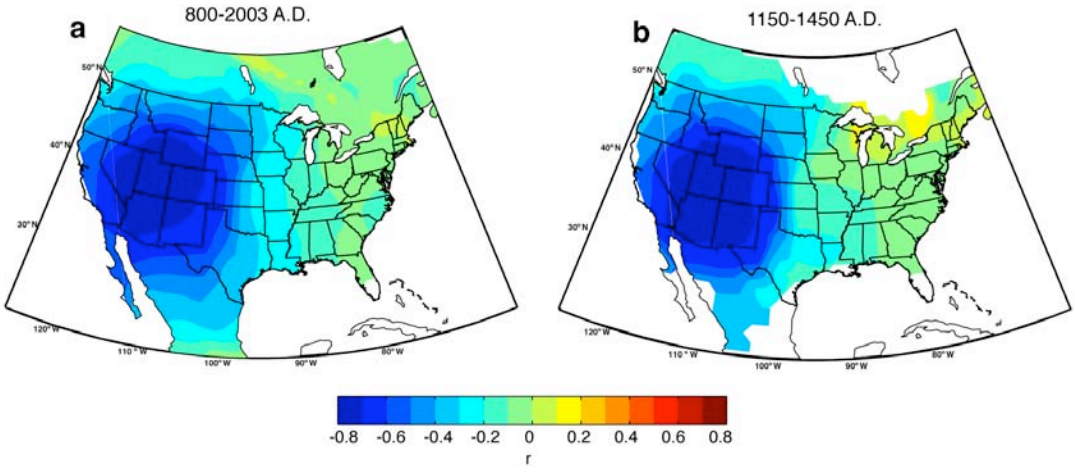


Figure D3 Spatial pattern of DAI (Cook *et al*., 2004) correlation, r, with gridded NADA PDSI reconstructions (Cook *et al*., 2004; Cook & Krusic, 2004) over the last millennium (800-2003 A.D.) (a) and from 1150-1450 A.D. (b). Over the entire millennium DAI correlation with reconstructed PDSI is centered on Utah, but is strong throughout the West. A highly similar pattern is evident between 1150 and 1450 A.D., although the "bulls eye" of correlation is shifted slightly southeast over the four corners region.

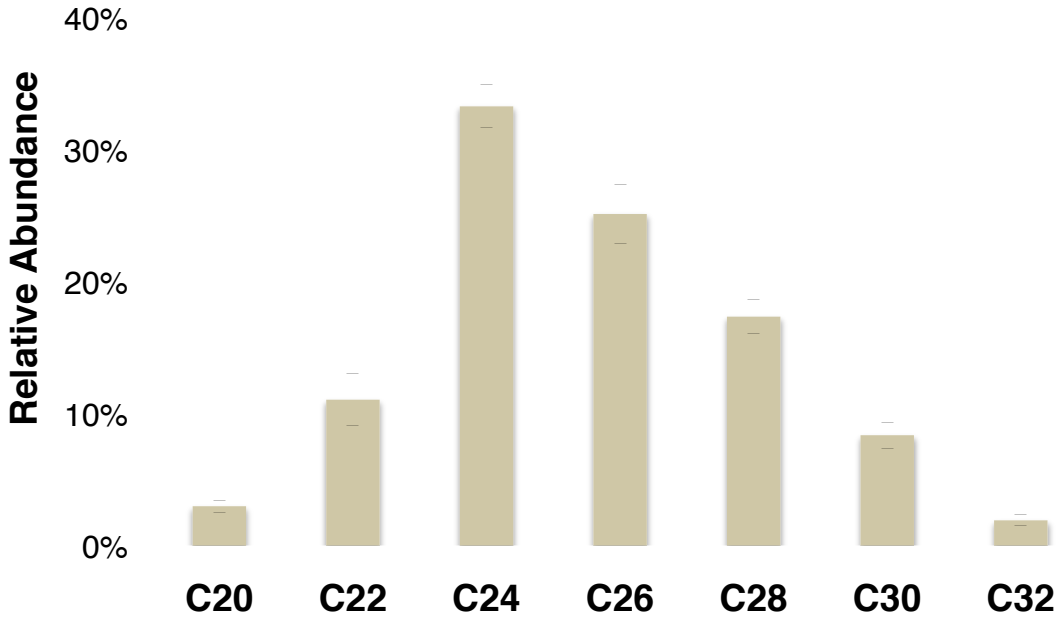


Figure D4 Average *n*-acid distribution from SL0708b sediment samples. Error bars represent 1σ. Axis labels as in figures 3.5 and 3.6.

References for Appendix D

Cook, E. R., Woodhouse, C.A., Eakin, C.M., Meko, D.M., and Stahle, D.W. (2004) Long-term aridity changes in the western United States. *Science* 306:1015-1018.

Cook, E.R. and P.J. Krusic. 2004. The North American Drought Atlas. Lamont-Doherty Earth Observatory and the National Science Foundation. http://iridl.ldeo.columbia.edu/SOURCES/.LDEO/.TRL/.NADA2004/.pdsi-atlas.html